INFORMATION TO USERS

This manuscript has been reproduced from the microfilm master. UMI films the text directly from the original or copy submitted. Thus, some thesis and dissertation copies are in typewriter face, while others may be from any type of computer printer.

The quality of this reproduction is dependent upon the quality of the copy submitted. Broken or indistinct print, colored or poor quality illustrations and photographs, print bleedthrough, substandard margins, and improper alignment can adversely affect reproduction.

In the unlikely event that the author did not send UMI a complete manuscript and there are missing pages, these will be noted. Also, if unauthorized copyright material had to be removed, a note will indicate the deletion.

Oversize materials (e.g., maps, drawings, charts) are reproduced by sectioning the original, beginning at the upper left-hand corner and continuing from left to right in equal sections with small overlaps.

Photographs included in the original manuscript have been reproduced xerographically in this copy. Higher quality 6" x 9" black and white photographic prints are available for any photographs or illustrations appearing in this copy for an additional charge. Contact UMI directly to order.

Bell & Howell Information and Learning
300 North Zeeb Road, Ann Arbor, MI 48106-1346 USA

UMI®
800-521-0600

Synthesis, Structural and Solid-State, Multinuclear Magnetic Resonance Studies of Some Manganese and Nickel Complexes Containing Silicon, Tin, Lead and Phosphorus Ligands

by

Dharamdat Christendat

A thesis submitted to the Faculty of Graduate Studies and Research of McGill University in partial fulfillment of the requirements for the Degree of Doctor of Philosophy.

March 1998

Department of Chemistry

McGill University

Montreal, Quebec, Canada

Dedicated to my parents, three loving sisters and brother for their support and encouragement throughout the course of my education.

ABSTRACT

A number of organometallic complexes involving manganese, bonded to silicon, tin, lead and phosphorus ligands, and nickel, bonded to various trialkylphosphine ligands, has been synthesized and their crystal structures, vibrational, and multinuclear magnetic resonance spectra have been obtained. The FT–IR and FT–Raman spectra of the manganese carbonyl compounds in the carbonyl region (2200-1850 cm^{-1}) have been assigned. Solid-state, CP-MAS, ^{13}C, ^{29}Si, ^{31}P, ^{117}Sn, ^{119}Sn and ^{207}Pb NMR spectra of substituted pentacarbonylmanganese(I) and tetracarbonylmanganese(I) complexes feature asymmetric sextets, whereas those containing a group 14 (IVA) element bridging two pentacarbonylmanganese(I) moieties show asymmetric undecets. The uneven splitting arises from spin-spin coupling and second-order quadrupole-dipole effects, which are not eliminated by magic angle spinning. The solid-state NMR spectra of the manganese complexes have been analyzed to give the isotropic chemical shifts, the chemical shift tensors, one-bond spin-spin coupling constants, ^{55}Mn nuclear quadrupole coupling constants, effective dipolar coupling constants and the anisotropies in the spin-spin coupling for each complex. The results provide new insights into the relationship between spin-spin coupling and quadrupolar coupling in bimetallic complexes involving a quadrupole transition-metal and a spin-1/2 nucleus.

For the *para*-substituted triaryltin complexes, the ^{13}C, ^{55}Mn and ^{119}Sn chemical shifts and one-bond spin-spin constants in solution show excellent correlations with pairs of substituent constants (σ_I, σ_R). However, there is no correlation of the chemical shifts or spin-spin coupling with either Hammett (σ_p) or Taft (σ_p°) constants or the Mn-Sn bond lengths, r_{Mn-Sn}. The results obtained from dual substituent parameter (DSP) analysis

indicate that both resonance effects (σ_R) and inductive effects (σ_I) are important in determining the NMR parameters.

Crystal structures and high-resolution solution and solid-state ^{31}P NMR spectra were obtained for several dihalobis(trialkylphosphine)nickel(II) complexes. The crystal structures and NMR results indicate that these complexes are *trans* square-planar in the solid-state. The chemical shifts and shift tensors were obtained and found to vary with the electronic properties of the halogens. The ^{31}P isotropic chemical shifts in the solution spectra of dibromo- and diiodiobis(tribenzylphosphine)nickel(II) are very different from those found for the solid-state, and chemical exchange effects were observed in all spectra. The mechanism of exchange appears to involve the formation of dimers with bridging halides.

RÉSUMÉ

Une variété de complexes organométalliques impliquant une liaison entre un atome demanganèse et des ligands de silicone, d'étain, de plomb et de phosphore ainsi qu'entre le nickel et des ligands trialkylphosphines variés ont été synthétisés et leur structure cristalline ont été obtemes, de même que leur spectre vibrationnel et de résonance magnétique. Les spectres IR-FT Raman-FT et des composés de manganèse carbonylés ont été assignés dans la région carbonyle (2200-1850 cm^{-1}). Les spectres d'état solide, CP-MAS, ^{13}C, ^{29}Si, ^{31}P, ^{117}Sn, ^{119}Sn et ^{207}Pb RMN des complexes substitués de pentacarbonylmanganèse(I) et de tétracarbonylmanganèse(I) présentent des "sextets" asymétriques alors que les complexes des éléments du Groupe 14 (IVA) comportant deux unités pontées de pentacarbonylmanganèse(I) présentent des "undecets" asymétriques. Cette différence provient du couplage spin-spin et des effets quadrupôle-dipôle de second-ordre qui ne sont pas éliminés par la rotation à angle magique. Les spectres haute-résolution à l'état solide des complexes de manganèse ont été analysés afin de déterminer le déplacement chimique isotropique, les tenseurs de déplacement chimique, la constante de couplage spin-spin à travers un lien, la constante de couplage quadrupolaire nucléaire du ^{55}Mn, la constante de couplage dipolaire effective et l'anisotropie du couplage spin-spin pour chacun des complexes. Ces résultats apportent de nouvelles connaissances sur la relation existant entre le couplage spin-spin et le couplage quadrupolaire dans les complexes bimétalliques impliquant un métal de transition avec quadrupôle et un noyau de spin-1/2.

Les déplacements chimiques en ^{13}C, ^{55}Mn et ^{119}Sn et les constantes spin-spin à travers un lien d'une molecule en solution, pour les complexes *para*-substitués de triarylétain, démontrent une excellente corrélation avec les paires de constantes de substituants (σ_I, σ_R). Par contre, il n'existe pas de corrélation entre le déplacement chimique ou la constante de couplage spin-spin avec la constante de Hammett (σ_P) ou celle de Taft (σ_P°), ni avec la longueur de liaison Mn-Sn, r_{Mn-Sn}. Les résultats obtenus de l'analyse de paramètres de substituants doubles (DSP) indique que les effets de résonance (σ_R) et inductifs (σ_I) sont tous deux importants lors de la détermination des paramètres de RMN.

Les structures cristallines et les spectres haute-résolutions en solution et à l'état solide de la RMN du ^{31}P ont également été obtenus pour plusieurs complexes dihalobis(trialkylphosphine)nickel(II). Les structures cristallines et les résultats de RMN indiquent que ces complexes sont *trans*, plan carré, à l'état solide. Les déplacement chimiques et les tenseurs de déplacement ont été obtenus et varient avec les propriétés électroniques des halogènes. Les déplacements chimiques isotropiques du ^{31}P dans les spectres en solution du dibromo- et du diiodobis(tribenzylphosphine)nickel(II) son très différents de ceux trouvés à l'état solide, et des effets provenant de l'échange chimique ont été observés dans tous les spectres. Le mécanisme d'échange semble impliquer la formation de dimères avec halogénures pontés.

ACKNOWLEDGEMENTS

I am extremely grateful to my supervisors, Dr. D. F. R. Gilson and Dr. I. S. Butler, for their guidance, patience and support throughout the course of this work.

I would like to express my deepest gratitude to Dr. F. G. Morin, who has obtained some very exotic NMR spectra during this work, for his assistance and helpful discussions.

I would also like to thank:

McGill University and the Department of Chemistry for financial support in the form of teaching and research assistantships;

The post graduate student society (P.G.S.S.) for financial support in the form a travel award to present my work at the 80th CSC Conference and Exhibition in Windsor, Ontario, June 1997;

Dr. R. D. Markwell for assisting me in the synthesis of the acyl- and alkyl-manganese(I) complexes and many wonderful and enjoyable discussions;

Dr. I. Wharf for his assistance and helpful discussions on the synthesis of triaryltin halides;

Dr. B. A. Arndtsen for his advice concerning the work on ^{31}P NMR spectroscopy of mixed nickel(II) halides studied in solution;

Drs. R. Hynes and A. M. Lebuis for the X-ray structures;

Miss Virginie Guillemette and Mr. Danny Lafrance for their help in translating the abstract into French;

Jordan H. Wosnick for many wonderful discussions of matters other than chemistry;

The office staff, in particular, Ms. R. Charron, C. Brown and C. Marotte, for their assistance when needed;

and all my colleagues, past and present, for their generous cooperation.

Finally, I wish to express my deepest gratitude to my mother for her love and understanding. Without her, this mission would have been impossible to accomplish.

NOTES ON UNITS

The following units have been used in this thesis for historical reasons. Their definitions and SI equivalents are given below:

Physical quantity	Symbol	SI unit	Unit used in this work
Bond length	r	m	Å (= 10^{-10} m)
Mass	m	kg	g (= 10^{-3} kg)
volume	V	m^3	cm^3 or ml (= 10^{-6} m^3)
Temperature	K	K	°C (= K - 273)
Wavenumber	ν	m^{-1}	cm^{-1} (= 100 m^{-1})

LIST OF SYMBOLS AND ABBREVIATIONS

R	Alkyl-
Bu	*n*-Butyl-
Bz	Benzyl-
Cy	Cyclohexyl-
CyMe	Cyclohexylmethyl-
dppe	Bis(diphenylphosphino)ethane
dppey	*Cis*-1,2-bis(diphenylphosphino)ethylene
Et	*n*-Ethyl-
Cp^*	Pentamethylcyclopentadiene
Me	Methyl-
Mes	2,4,6-Trimethylbenzyl-
CP-MAS	Cross-polarization and magic-angle spinning
CSA or $\Delta\delta$	Chemical shift anisotropy
η_C	Chemical shift asymmetry parameter
δ_{iso}	Isotropic chemical shift
δ_{ii}	Chemical shift tensors
D	Dipolar coupling
D″ or D´	Effective dipolar coupling
d	Effective dipolar-quadrupolar coupling
EFG	Electric field gradient

FT	Fourier transform
FID	Free induction decay
B_o	Magnetic field strength of spectrometer
γ	Magnetogyric ratio
N.A.	Natural abundance
Q	Nuclear electric quadrupole moment
χ	Nuclear quadrupole coupling constant
PAS	Principal axis system
η_Q	Quadrupole asymmetry parameter
K_{IS}	Reduced spin-spin coupling constant
ΔJ_{IS}	Spin-spin anisotropy
J_{IS}	Spin-spin coupling constant

TABLE OF CONTENTS

LIST OF TABLES

CHAPTER 1

CHAPTER 2

CHAPTER 4

CHAPTER 5

CHAPTER 6

CHAPTER 7

CHAPTER 8

CHAPTER 9

LIST OF FIGURES

CHAPTER 3

CHAPTER 4

CHAPTER 5

CHAPTER 6

CHAPTER 8

CHAPTER 9

Suggestions for Future Work

Chapter 1

General Introduction

Organometallic chemists use a variety of spectroscopic techniques to characterize and study the complexes they create, to follow reactions, and to understand the nature of bonding interactions at the molecular level. Over the past few decades, however, the rate of progress in evaluating the results of chemical reactions by spectroscopic techniques has been such that a single spectroscopist or synthetic chemist cannot possibly keep track of all new developments. This situation results in increasing specialization and segregation into a number of independent disciplines. Even the field of inorganic chemistry has been drastically sub-divided into specific areas, such as organometallic and physical inorganic chemistry, inorganic polymers, materials science and a host of branches of spectroscopy, including vibrational (infrared and Raman), multinuclear NMR, X-ray diffraction studies, and other methods. However, the field of solid-state NMR spectroscopy, especially where it involves the ^{31}P nucleus, has been left relatively unexplored by organometallic and inorganic chemists.[1-3]

For many years, coordination chemists have used a variety of tertiary phosphine ligands in the development of homogeneous transition metal catalysts for several significant industrial processes. Despite the increasing number of these phosphine-metal catalysts, relatively few research groups have routinely employed solid-state ^{31}P NMR spectroscopy in their work as a method of characterization and investigation of bonding and reactivity. The ^{31}P nucleus has proven to be an excellent NMR probe, with a wide chemical shift range (>300 ppm), 100% natural abundance, high sensitivity, and large

spin-spin interactions with transition metals. In addition, commonly seen features in homogeneous catalytic systems, such as changes in the coordination number and oxidation state of the metal and *cis-trans* isomerization of the ligands within the coordination sphere, can all be conveniently followed by ^{31}P NMR spectroscopy because of the large changes in chemical shift. However, despite the excellent NMR properties of the ^{31}P nucleus, Table 1.1, structures of phosphine-containing transition metal complexes have traditionally been determined by vibrational techniques and/or X-ray crystallography. One must bear in mind that both of these tools require high purity plus the added necessity of a single-crystal requirement for X-ray crystallography, whereas solution and solid-state NMR measurements require only pure bulk material.

The purpose of this thesis is to examine the application of both solution and solid-state multinuclear NMR spectroscopy to a variety of transition metal complexes. The chemical shift is the most significant NMR parameter used for structure elucidation in solution. This quantity is represented by a second-rank tensor which, because of rapid molecular tumbling in solution, is averaged to an isotropic value given by the trace of the tensor. In the solid state, however, molecular motion is restricted and the three principal components of the chemical shift tensor are observed in the static spectrum, or can be determined from spinning sideband intensities. The tensor values have the potential of revealing a greater amount of information about the bonding interactions and structure in the local environment of the probe nucleus than does the isotropic value of the chemical shift. The thesis work presented also includes studies by vibrational and solution NMR spectroscopy, and single-crystal X-ray diffraction measurements.

Table 1.1. Properties of the NMR isotopes examined in this thesis

Isotope	Spin	N.A. (%)	Relative Receptivity (*vs.* ^{1}H)[a]	γ ($\times 10^7$ rad T^{-1} s^{-1})	Q ($\times 10^{-28}$ m^2)
^{1}H	1/2	99.99	1.00	26.75	---
^{13}C	1/2	1.11	1.8×10^{-4}	6.73	---
^{29}Si	1/2	4.7	3.7×10^{-4}	-5.31	---
^{31}P	1/2	100	6.6×10^{-2}	10.84	---
^{55}Mn	5/2	100	1.8×10^{-1}	6.64	0.50
^{61}Ni	3/2	1.19	4.3×10^{-5}	-2.39	0.16
^{117}Sn	1/2	7.6	3.5×10^{-3}	-9.59	---
^{119}Sn	1/2	8.6	4.5×10^{-3}	-10.00	---
^{207}Pb	1/2	22.6	2.1×10^{-3}	5.62	---

[a]Relative receptivity is the sensitivity divided by the % natural abundance.

The thesis is divided into three sections. The first section is devoted mainly to X-ray diffraction and solid-state, CP-MAS, ^{31}P NMR studies of tertiary phosphine substituted alkyl- and acyl(tetracarbonyl)manganese(I) complexes. The NMR studies in particular are facilitated by the 100%-abundant, spin-1/2 probe (^{31}P) being directly bonded to a 100%-abundant quadrupolar nucleus (^{55}Mn). Nuclear quadrupole resonance has been used for many years to probe electronic distributions in solids and has found many useful applications in the understanding of chemical reactivity, such as in the study of the π-bonding interactions in chloro derivatives of nitrogen hetrocycles[4] and the

relative electronegativities of sulfur and carbon atoms.[5-6] The nuclear quadrupole coupling constants for manganese complexes are notoriously difficult to determine by NQR, but can be determined from solid-state NMR experiments. The results obtained from multinuclear solution measurements are also briefly discussed in terms of bonding interactions and hybridization.

Section II of this thesis describes the investigation of covalent bimetallic complexes containing the pentacarbonylmanganese(I) fragment and group 14 (IVA) elements. Each of the group 14 elements has NMR-active spin-1/2 isotopes in usable abundance, with the exception of Ge (spin-9/2), and so all are excellent candidates for NMR studies. However, the solid-state NMR spectroscopy of bimetallic complexes is a relatively unexplored area. To our knowledge, no NMR-based investigation of covalent metal-metal bonding has appeared in the literature. The main focus of this section was to investigate the effects of *para* substituents on the aryl ring in a series of (*para*-$XC_6H_4)_3SnMn(CO)_5$ [X = H, F, Cl, CH_3, OCH_3, SCH_3 and $S(O)_2CH_3$] derivatives on the structure and bonding of these complexes by using single-crystal X-ray diffraction and multinuclear magnetic resonance studies. The specific parameters under investigation were the Mn-Sn bond distances, chemical shifts, spin-spin coupling constants, the shielding and spin-spin anisotropies and the nuclear quadrupole coupling constants of these compounds. The solid-state ^{29}Si, ^{119}Sn and ^{207}Pb NMR spectra of triphenylsilyl, diphenyltin, tricyclohexyltin, triphenyllead and diphenyllead complexes were also investigated. The results obtained from solution NMR measurements are explained in terms of resonance (σ_R) and inductive (σ_I) parameters.

In Section III of this thesis, the ^{31}P shielding tensors of a number of *trans*-dihalobis(trialkylphosphine)nickel(II) complexes are interpreted in terms of the structural and bonding interactions involved. Nickel(II) is known to form a wide range of complexes with tertiary phosphine ligands. Some general discussions about solution-solid state effects, *cis-trans* isomerization, chemical exchange and dimerization with bridging halides are presented.

The three different sections of this thesis are logically linked together from an NMR point of view. The first section deals with a 100%-abundant spin-1/2 NMR probe bonded to a 100%-abundant quadrupolar nucleus. The second section investigates low abundance (<25%) spin-1/2 nuclei bonded to one or two of the same, 100%-abundant, quadrupolar nuclei, whereas the final section deals with 100%-abundant spin-1/2 probes bonded to a very low abundance spin-3/2 nucleus (^{61}Ni, 1.2%). Table 1.1. summarizes the NMR properties of the nuclei under investigation, while Table 1.2 lists the complexes studied in this thesis.

Table 1.2. Transition-metal complexes synthesized and studied in this thesis

Section I

$BzMn(CO)_5$ **(I)**

$MesCH_2Mn(CO)_5$ **(II)**

cis-$BzC(O)Mn(CO)_4(PPh_3)$ **(III)**

cis-$MesCH_2C(O)Mn(CO)_4(PPh_3)$ **(IV)**

cis-$BzC(O)Mn(CO)_4(PCy_3)$ **(V)**

cis-$MesCH_2C(O)Mn(CO)_4(PCy_3)$ **(VI)**

cis-$BzMn(CO)_4(PPh_3)$ **(VII)**

cis-$BzMn(CO)_4(P(tolyl_3)$ **(VIII)**

cis-$BzMn(CO)_4(P(p\text{-}FC_6H_4)_3)$ **(IX)**

cis-$BzMn(CO)_4(PCy_3)$ **(X)**

Section II

$Ph_3SiMn(CO)_5$ **(XI)**

$Ph_3SnMn(CO)_5$ **(XII)**

$Ph_3PbMn(CO)_5$ **(XIII)**

$Cy_3SnMn(CO)_5$ **(XIV)**

$[(CO)_5Mn]_2SnPh_2$ **(XV)**

$[(CO)_5Mn]_2PbPh_2$ **(XVI)**

trans-$Ph_3SnMn(CO)_4PPh_3$ **(XVII)**

(p-$CH_3C_6H_4$)$SnMn(CO)_5$ **(XVIII)**

(p-$CH_3OC_6H_4$)$SnMn(CO)_5$ **(XIX)**

(p-$CH_3SC_6H_4$)$SnMn(CO)_5$ **(XX)**

(p-$CH_3S(O)_2C_6H_4$)$SnMn(CO)_5$ **(XXI)**

(p-FC_6H_4)$SnMn(CO)_5$ **(XXII)**

(p-ClC_6H_4)$SnMn(CO)_5$ **(XXIII)**

Section III

trans-$(Bz_3P)_2NiCl_2$ **(XXIV)**

trans-$(Bz_3P)_2NiBr_2$ **(XXV)**

trans-$(Bz_3P)_2NiI_2$ **(XXVI)**

trans-$(Bz_3P)_2Ni(SCN)_2$ **(XXVII)**

trans-$((CyCH_2)_3P)_2NiCl_2$ **(XXVIII)**

trans-$((CyCH_2)_3P)_2NiBr_2$ **(XXIX)**

trans-$((CyCH_2)_3P)_2NiI_2$ **(XXX)**

trans-$(Cy_3P)_2NiCl_2$ **(XXXI)**

trans-$(Cy_3P)_2NiBr_2$ **(XXXII)**

trans-$(Cy_3P)_2NiI_2$ **(XXXIII)**

References

(1) R. V. Parish, *NMR, NQR, EPR and Mössbauer Spectroscopy in Inorganic Chemistry*, Ellis Horwood Ltd., London, England, 1990.

(2) C. A. Fyfe, *Solid State NMR for Chemists*, C.F.C. Press, Guelph, Ontario, 1983.

(3) M. Gielen, R. Willem and B. Wrackmeyer, *Advanced Applications of NMR to Organometallic Chemistry*, John Wiley & Sons Ltd., London, England, 1996.

(4) M. Dewar and E. A. C. Lucken, *J. Chem. Soc.* 2653 (1958).

(5) M. Dewar and E. A. C. Lucken, *J. Chem. Soc.* 426 (1958).

(6) E. A. C. Lucken, *Nuclear Quadrupole Coupling Constants*, Academic Press, New York, New York, 1969.

Chapter 2

Experimental

General

A dry nitrogen atmosphere was used for all reactions involving air- and moisture-sensitive compounds. An inert atmosphere was also employed while performing alkyl migration and carbon monoxide displacement reactions. All glassware was dried at 120 ± 5 °C and was flushed with dry nitrogen for 5-10 min before use. Spectroscopic grade solvents were used as received, except acetonitrile, which was stored over molecular sieves before use, while tetrahydrofuran (THF) and hexane were dried over sodium with a benzophenone indicator immediately prior to use.

2.1 Preparation of Alkyl- and Acylmanganese(I) Complexes

The starting materials, benzyl chloride, 2,4,6-trimethylbenzyl chloride, dimanganese decacarbonyl, triphenylphosphine, tricyclohexylphosphine, tris(*p*-fluorophenyl)phosphine and tris(*p*-tolylphosphine), were obtained from Aldrich Chemical Co., and were used without further purification.

2.1.1 Synthesis of Alkyl(pentacarbonyl)manganese(I) Complexes

The solid organomanganese(I) complexes, $BzMn(CO)_5$ (I) and $MesCH_2Mn(CO)_5$ (II), were prepared and purified by methods based on those described previously by Drew *et al.*[1] and Cotton *et al.*[2] Benzyl- and 2,4,6-trimethylbenzyl(pentacarbonyl)manganese(I) were prepared by reductive cleavage of $Mn_2(CO)_{10}$ with sodium amalgam in THF yielding $Na[Mn(CO)_5]$, which in turn was treated with benzyl chloride or 2,4,6-trimethylbenzyl chloride, at room temperature, to form the alkyl product in 70-80% yield.

Single crystals of $BzMn(CO)_5$ and $MesCH_2Mn(CO)_5$ were obtained from hexane and ethanol, respectively, by slow evaporation at -10 to -15°C. The purity of these crystals was established by the absence of any impurity peaks in their IR, Raman, and ^1H, ^{13}C and ^{55}Mn NMR spectra.

2.1.2 Synthesis of Tertiary Phosphine Substituted Alkyl- and Acyl(tetracarbonyl)-Manganese(I) Complexes

The solid organomanganese(I) complexes, *cis*-$BzC(O)Mn(CO)_4(PPh_3)$ **(III)**, *cis*-$MesCH_2C(O)Mn(CO)_4(PPh_3)$ **(IV)**, *cis*-$BzC(O)Mn(CO)_4(PCy_3)$ **(V)**, *cis*-$MesCH_2$-$C(O)Mn(CO)_4(PCy_3)$ **(VI)**, *cis*-$BzMn(CO)_4(PPh_3)$ **(VII)**, *cis*-$BzMn(CO)_4[P(p\text{-Tol})_3]$ **(VIII)** and *cis*-$BzMn(CO)_4[P(p\text{-F-Ph})_3]$ **(IX)**, were synthesized by methods similar to those described previously by Cotton *et al.*[2,3] Reactions of **I** and **II** with triphenylphosphine and tricyclohexylphosphine at 5-10 °C in acetonitrile yielded the solid acyl complexes, **III** and **IV**, and **V** and **VI**, respectively, in 50-65 % yield. Attempts to prepare acyl complexes of tris(*p*-fluorophenyl)phosphine and tris(*p*-tolylphosphine) resulted in dark brown oils, which decomposed into black solids when exposed in air, presumably MnO_2. The *cis*-benzyl(triarylphosphine)manganese(I) complexes, **VII-IX**, were prepared by thermal decarbonylation at 65 °C of the respective acyl complexes in acetonitrile. Attempts to synthesize the 2,4,6-trimethylbenzyl and benzyl(tricyclohexylphosphine) analogues were unsuccessful. However, slow evaporation over a period of 4 to 5 days of a benzene/octane solution of compound **V** resulted in 95 % decomposition with a few single-crystals of *cis*-$BzMn(CO)_4(PCy_3)$ **(X)** being formed. Compound **X** was first characterized by FT-IR spectroscopy, by the absence of the acyl vibration, $\nu_{C=O}$, in the 1800-1600 cm^{-1} region,

followed by single-crystal X-ray diffraction measurements. Compounds **III-IX** were characterized by their FT-IR, FT-Raman, and solution ^{1}H, ^{13}C, ^{31}P, and ^{55}Mn NMR spectra and the similarity of some of these spectra to those in the literature.[1-4]

2.1.3 Characterization of Tertiary Phosphine Manganese(I) Complexes

cis-BzC(O)Mn(CO)$_4$(PPh$_3$). A yellow compound was precipitated out of the reaction mixture and was washed with acetonitrile at 10 °C. ^{1}H NMR ($CDCl_3$) δ (ppm): 4.0 (s, 2H, CH_2), 7.0 (m, 5H, phenyl), 7.5 (m, 15H, phenylphosphine). ^{13}C NMR δ (ppm): 71.2 (s, CH_2), 130 (m, phenyl), 213.4 (d, $^{2}J_{PC}$ 12.1 Hz, CO *trans* to P), 214.1 (d, $^{2}J_{PC}$ 20.1 Hz, CO *trans* to CO), 216.7 (d, $^{2}J_{PC}$ 6.0 Hz, CO *trans* to CH_2) 267.9 (d, $^{2}J_{PC}$ 16.3 Hz, C=O). ^{31}P NMR δ (ppm): 50.6 (s). ^{55}Mn NMR δ (ppm): -1682.5 (s, $\Delta\nu_{1/2}$ 2146 Hz). IR (Nujol mull on KBr plates): [ν(CO) region, a_1^2, b_1, a_1^1, b_2, acyl] 2059, 1992, 1965, 1953, 1622 cm^{-1}. Raman (powder in sample cup): [ν(CO) region, a_1^2, b_1, a_1^1, b_2, acyl] 2060, 1995, 1954, 1935, 1626 cm^{-1}.

cis-MesCH$_2$C(O)Mn(CO)$_4$(PPh$_3$). A yellow powder was precipitated out of the reaction mixture and was washed with acetonitrile at 25 °C. ^{1}H NMR ($CDCl_3$) δ (ppm): 2.0 (s, , 6H *o*-CH_3), 2.2 (s, 3H, *p*-CH_3), 4.0 (s, 2H, CH_2), 6.8 (s, 2H, phenyl), 7.5 (m, 15H, phenylphosphine). ^{13}C NMR δ (ppm): 20.2 (s, *o*-CH_3), 20.8 (s, *p*-CH_3), 67.2 (s, CH_2), 130 (m, phenyl), 213.1 (d, $^{2}J_{PC}$ 12.3 Hz, CO *trans* to P), 215.0 (d, $^{2}J_{PC}$ 21.3 Hz, CO *trans* to CO), 217.7 (d, $^{2}J_{PC}$ 5.2 Hz, CO *trans* to CH_2), 264.3 (d, $^{2}J_{PC}$ 14.3 Hz, C=O). ^{31}P NMR δ (ppm): 51.2 (s). ^{55}Mn NMR δ (ppm): -1693.5 (s, $\Delta\nu_{1/2}$ 2960 Hz). IR (Nujol mull on KBr plates): [ν(CO) region, a_1^2, b_1, a_1^1, b_2, acyl] 2058, 1992,1965, 1946, 1634 cm^{-1}. Raman

(powder in sample cup): [ν(CO) region, a_1^2, b_1, a_1^1, b_2, acyl] 2059, 1986, 1943, 1918, 1636 cm^{-1}.

cis-BzC(O)Mn(CO)$_4$[P(C$_6$H$_{11}$)$_3$]. The yellow compound was first dissolved in dichloromethane and was then precipitated out by the slow addition of acetonitrile at 10 °C. ^{1}H NMR ($CDCl_3$) δ (ppm): 1.7 (m, 33H, tricyclohexylphosphine), 4.26 (s, 2H, CH_2), 7.1 (m, 5H, phenyl). ^{13}C NMR δ (ppm): 28.7 (m, tricyclohexyl), 71.1 (s, CH_2), 128 (m, phenyl), 214.2 (d, $^2J_{PC}$ 14.9 Hz, CO *trans* to P), 216.6 (d, $^2J_{PC}$ 19.4 Hz, CO *trans* to CO), 217.2 (d, $^2J_{PC}$ 5.1 Hz, CO *trans* to CH_2), 267.3 (d, $^2J_{PC}$ 13.1 Hz, C=O). ^{31}P NMR δ (ppm): 53.4. ^{55}Mn NMR δ (ppm): -1802 (s, $\Delta\nu_{1/2}$ 3330 Hz). IR (Nujol mull on KBr) plates: [ν(CO) region, a_1^2, b_1, a_1^1, b_2, acyl] 2048, 1989, 1980, 1944, 1629 cm^{-1}. Raman (powder in sample cup): [ν(CO) region, a_1^2, b_1, a_1^1, b_2, acyl] 2050, 1970, 1955, 1927, 1632 cm^{-1}.

cis-MesCH$_2$C(O)Mn(CO)$_4$[P(C$_6$H$_{11}$)$_3$]. The yellow compound was first dissolved in dichloromethane and was then precipitated out by the slow addition of acetonitrile at 20 °C. ^{1}H NMR ($CDCl_3$) δ (ppm): 1.7 (m, 33H, tricyclohexylphosphine), 2.1 (s, 6H, *o*-CH_3), 2.2 (s, 3H, *p*-CH_3), 4.4 (s, 2H, CH_2), 6.8 (m, 2H, phenyl). ^{13}C NMR δ (ppm): 28.7 (m, tricyclohexyl), 66.7 (s, CH_2), 130 (m, phenyl), 214.3 (d, $^2J_{PC}$ 16.7 Hz, CO *trans* to P), 217.6 (d, $^2J_{PC}$ 19.7 Hz, CO *trans* to CO), 218.1 (d, $^2J_{PC}$ 3.1 Hz, CO *trans* to CH_2), 267.3 (d, $^2J_{PC}$ 11.5 Hz, C=O). ^{31}P NMR δ (ppm): 54.7 (s). ^{55}Mn NMR δ (ppm): -1774 (s, $\Delta\nu_{1/2}$ 3404 Hz). IR (Nujol mull on KBr plates): [ν(CO) region, a_1^2, b_1, a_1^1, b_2, acyl] 2045, 1961, 1946, 1930, 1643 cm^{-1}. Raman (powder in sample cup): [ν(CO) region, a_1^2, b_1, a_1^1, b_2, acyl] 2045, 1968, 1957, 1930, 1644 cm^{-1}.

cis-BzMn(CO)$_4$(PPh$_3$). The crude sample was recrystallized from a hexane-ethanol mixture and then washed with 95% ethanol. Yellow crystals were obtained by slow evaporation from a 1:1 mixture of benzene and cyclohexane. ^{1}H NMR ($CDCl_3$) δ (ppm): 1.7 (d, 2H, $^3J_{PH}$ 6.0 Hz, CH_2), 7.0 (m, 5H, phenyl), 7.6 (m, 15H, phenylphosphine). ^{13}C NMR δ (ppm): 17.1 (d, $^2J_{PC}$ 8.4 Hz, CH_2), 128 (m, phenyl), 216.1 (d $^2J_{PC}$ 21.1 Hz, CO *trans* to P), 217.1 (d, $^2J_{PC}$ 10.1 Hz, CO *trans* to CH_2), 219.8 (d, $^2J_{PC}$ 20.3 Hz, CO *trans* to CO). ^{31}P NMR δ (ppm): 61.4 (s). ^{55}Mn NMR δ (ppm): -1819.3 (d, $^1J_{Mn-P}$ 256.9 Hz, peak width at half-height ($\Delta\nu_{1/2}$) 178 Hz). IR (Nujol mull on KBr plates) : [ν(CO) region, a_1^2, b_1, a_1^1, b_2] 2048, 1987, 1962, 1931 cm^{-1}. Raman (powder in sample cup): [ν(CO) region, a_1^2, b_1, a_1^1, b_2] 2050, 1973, 1961, 1917 cm^{-1}.

cis-BzMn(CO)$_4$[P(tolyl)$_3$]. The sample was recrystallized from a hexane-ethanol mixture and then washed with 95% ethanol. Yellow crystals were obtained by slow evaporation from a 2:1 mixture of benzene and ethanol over a period of 2 days. ^{1}H NMR ($CDCl_3$) δ (ppm): 1.7 (d, 2H, $^3J_{PH}$ 6.3 Hz, CH_2), 2.41 (s, CH_3), 7.0 (m, 5H, phenyl), 7.4 (m, 12H, phenylphosphine). ^{13}C NMR δ (ppm): 17.4 (d, $^2J_{PC}$ 8.5 Hz, CH_2), 21.3 (s, CH_3), 133 (m, phenyl), 215.8(d, $^2J_{PC}$ 21.4 Hz, CO *trans* to P), 216.4 (d, $^2J_{PC}$ 9.3 Hz, CO *trans* to CH_2), 219.6 (d $^2J_{PC}$ 22.7 Hz, CO *trans* to CO). ^{31}P NMR δ (ppm): 69.0 (s). ^{55}Mn NMR δ (ppm): -1819.2 (d, $^1J_{Mn-P}$ 252.2 Hz, $\Delta\nu_{1/2}$ 148 Hz). IR (Nujol mull on KBr plates): [ν(CO) region, a_1^2, b_1, a_1^1, b_2] 2049, 1976, 1971, 1917 cm^{-1}. Raman (powder in sample cup): [ν(CO) region, a_1^2, b_1, a_1^1, b_2] 2046, 1775,1971, 1919 cm^{-1}.

cis-BzMn(CO)$_4$[P(p-fluorophenyl)$_3$]. The sample was recrystallized from a dichloromethane-ethanol mixture and then washed with 95% ethanol. Golden yellow

crystals were obtained by slow evaporation from a 2:1 mixture of dichloromethane and ethanol over a period of 16 h. ^{1}H NMR ($CDCl_3$) δ (ppm): 1.7 (d, 2H, $^3J_{PH}$ 5.3 Hz, CH_2), 7.2 (m, 17H, phenyl). ^{13}C NMR δ (ppm): 17.4 (d, $^2J_{PC}$ 8.1 Hz, CH_2), 138 (m, phenyl), 216.4 (d, $^2J_{PC}$ 19.7 Hz, CO *trans* to P), 217.3 (d, $^2J_{PC}$ 8.3 Hz, CO *trans* to CH_2), 220.1 (d, $^2J_{PC}$ 21.3 Hz, CO *trans* to CO). ^{31}P NMR δ (ppm): 61.1 (s). ^{55}Mn NMR δ (ppm): -1822.5 (d, $^1J_{Mn-P}$ 254.8 Hz, $\Delta\nu_{1/2}$ 222 Hz). IR (Nujol mull on KBr plates): [ν(CO) region, a_1^2, b_1, a_1^1, b_2] 2050, 1977, 1967, 1929 cm^{-1}. Raman (powder in sample cup): [ν(CO) region, a_1^2, b_1, a_1^1, b_2] 2050, 1982, 1963, 1918 cm^{-1}.

2.2 Preparation of $Ph_{4-n}E[Mn(CO)_5]_n$, (E = Si, Sn, Pb; n = 1,2)

The starting materials, diphenylsilane, triphenylsilane, diphenylsilyl dichloride, diphenyltin dichloride and triphenyltin chloride were obtained from Aldrich Chemical Co.; diphenyllead diacetate and triphenyllead acetate were purchased from Alfa Products, and dimanganese decacarbonyl was purchased from Strem Chemical Co. All the chemicals were used as received.

The white, solid complexes, $(CO)_5MnSnPh_3$ and $[(CO)_5Mn]_2SnPh_2$, were synthesized by the procedure developed by Gorsich,[5] from the reaction of $Na[Mn(CO)_5$ with Ph_3SnCl and Ph_3SnCl_2, respectively, whereas the white $(CO)_5MnSiPh_3$ compound was prepared by the method described previously by Jetz *et al.*[6], from the reaction of $Mn_2(CO)_{10}$ and Ph_3SiH in an evacuated tube at 250 °C. Attempts to prepare $[(CO)_5Mn]_2SiPh_2$ by the methods of Gorsich[5] and Jetz *et al.*[6] resulted in no reaction and the formation of an insoluble black solid, presumably MnO_2. The corresponding lead

compounds, $(CO)_5MnPbPh_3$ and $[(CO)_5Mn]_2PbPh_2$, were conveniently prepared for the first time by similar procedures from the reaction of $Na[Mn(CO)_5]$ with $Ph_3Pb(OC(O)CH_3)$ or excess $Ph_2Pb(OC(O)CH_3)_2$ in THF.

Dimanganese decacarbonyl (4.0 g, 10 mmol) in 35 ml THF was added to excess sodium amalgam (1.0 g Na, 43 mmol/10 g Hg) and was stirred under nitrogen for 35-40 min until the yellow color dissipated. The unreacted amalgam was drained from the reaction vessel and the THF solution was washed twice with mercury (2×5 ml). A solution of diphenyllead diacetate (4.8 g, 10 mmol) or triphenyllead acetate (12.4 g, 25 mmol) in 10 ml THF was added to the reaction mixture and the resulting solution was stirred at room temperature for 30 min. The volume of the reaction mixture was reduced to about 20 ml by means of simple distillation and poured into 80 ml of cooled, distilled water. The pale yellow solids produced were filtered and extracted three times with 50 ml of *n*-hexane. The combined extracts were concentrated to approximately 15 ml and, on cooling, light yellow or light orange crystals were obtained in 65-78 % yield. Single crystals of $(CO)_5MnPbPh_3$ and $[(CO)_5Mn]_2PbPh_2$ were then obtained by slow evaporation of benzene/octane or octane and *n*-hexane solutions, over a period of 3 days, respectively.

2.3 Preparation of *para*-Substituted Triaryltin(pentacarbonyl)manganese(I) Complexes

The starting materials, tin tetrachloride (Strem Chemical Co.), *para*-substituted bromobenzenes (Aldrich) and dimanganese decacarbonyl (Strem) were used without further purification.

Tetraaryltin compounds were prepared by reacting the appropriate Grignard reagent with tin tetrachloride in ether or THF.[7] The *para*-substituted triaryltin chlorides were synthesized by the Kocheshkov redistribution reaction[8] of the corresponding tetraaryltin and tin tetrachloride, and were characterized by the methods described by Wharf.[9] However, attempted syntheses of the *para*-CF_3 and -$N(CH_3)_2$ substituted triaryltin halides were unsuccessful.

2.3.1 Synthesis of $(p\text{-}CF_3C_6H_4)_4Sn$ and $(p\text{-}(CH_3)_2N)C_6H_4)_4Sn$

These two complexes, $(p\text{-}CF_3C_6H_4)_4Sn$ and $(p\text{-}(CH_3)_2NC_6H_4)_4Sn$, were prepared from the reaction of the respective lithium reagents with tin(IV) chloride.[10] Fine shavings of lithium were placed in absolute ether (dried over CaH_2) and stirred vigorously, while 4-trifluoromethylbromobenzene or *p*-bromodimethylaniline in dry ether was added. To start the reaction, a few small crystals of iodine were added and the mixture was heated for a few minutes until the iodine was completely reacted. The bromo compound in ether was then added at a rate sufficient to keep the mixture refluxing. After the addition of bromo starting material, the mixture was heated for an additional 30 min to complete the reaction and the resulting solution was siphoned out into a 2-neck round-bottom flask connected to a dropping funnel filled with tin(IV) chloride in benzene under nitrogen. The benzene solution was added dropwise to a slight excess of the lithium reagent over a period of 20 min. The reaction mixture was decomposed with water, the ether layer was separated and was then evaporated to dryness. The solid residues were purified by recrystallization from hexane; yield 45-60 %.

2.3.2 Attempted Synthesis of $(p\text{-}CF_3C_6H_4)_3SnX$ (X = Cl, I)

First attempt. Tin(IV) chloride was added to tetrakis(4-trifluoromethylphenyl)-tin(IV) (6.30g, 9 mmol) in a ratio of 1:3 and stirred at 190-200 °C for 2 h. After cooling, the solid cake was crushed in 75 ml methanol. The methanolic solution was filtered and concentrated under reduced pressure to about 10 ml. The solution was stored at -10 °C, but no precipitation resulted. The solid obtained from the filtrate was found to be tetrakis(4-trifluoromethylphenyl)tin(IV) (4.3 g).

Second attempt. 10 mmol of iodine in 50 ml of toluene was added to a slight excess of tetrakis(4-trifluoromethylphenyl)tin(IV) (7.7 g, 11 mmol) and refluxed overnight. The unreacted iodine was destroyed with a solution of Na_2SO_3 and the resulting organic solution was evaporated to dryness under reduced pressure. The ^1H, ^{13}C and ^{119}Sn NMR spectra of the solid residue indicated that no reaction had occurred.

Third attempt. The attempted synthesis of tris(4-trifluoromethylphenyl)tin(IV) bromide was carried out following the procedure of Becker *et al.*[11] for triaryltin bromides. A solution of 4-trifluoro-methylbromobenzene (22.8 g, 0.10 mol) in 100 ml of dry ether was added dropwise to 2.0 g of finely cut lithium ribbon. After addition, the reaction mixture was heated to reflux for one hour. The solution was then cooled and siphoned under an inert atmosphere of nitrogen into a 2-neck round-bottom flask containing a slight excess of mercuric bromide (54.1 g, 0.15 mol) in 20 ml ether. The resulting mixture was heated to reflux overnight, after which a solution of KBr (8.5 g) dissolved in 50 ml 1% aqueous HBr was added dropwise with stirring at 0°C. The solution was filtered, and the ether layer was separated from the aqueous layer, washed several times with saturated NaCl

solution and dried over anhydrous sodium sulfate. The ether solution was evaporated to dryness, and the resulting solids were recrystallized twice from a 1:1 mixture of benzene and ethanol to give a white fluffy solid, m.p 265-268°; yield 52% (22.4 g, 0.052 mol).

Fourth attempt. To a mixture of excess powdered tin (25.0 g, 0.45 mol) and 12.6 g of (4-trifluoromethylphenyl)mercury(II) bromide (0.030 mol) was added 55 ml of xylene in a 2-neck flask equipped with a stirring bar and a reflux condenser. The mixture was then refluxed for a period of 2 days under an inert atmosphere. The resulting solution was filtered by hot gravity filtration into a 150-ml round-bottom flask. The xylene solution was evaporated to dryness under reduced pressure leaving an oily residue, from which 10.8 g of yellow solids were obtained by slow addition of 50 ml of ethanol. The solids were recrystallized from a benzene/ethanol mixture to give 7.5 g of white solid. The solid was found to be the starting material, (4-trifluoromethyl-phenyl)mercury(II) bromide. This was also confirmed by the absence of any signal in the solution ^{119}Sn NMR spectrum.

2.3.3 Attempted Synthesis of $(p\text{-}(CH_3)_2N)C_6H_4)_3SnX$ (X = Cl, I)

First attempt. Tin(IV) tetrachloride (0.78 g, 9 mmol), without solvent, was added to solid tetrakis(*p*-dimethylaminophenyl)tin (6.00 g, 10 mmol) and the mixture was stirred at 190-200 °C for 2 h. The oily mixture was cooled and 50 ml of methanol was added, resulting in a dark purple solution. The solution was filtered and washed with an addition 10 ml of methanol. The resulting filtrate was evaporated to dryness producing a dark blue solid in 20 % yield. The solid has a strong and obnoxious smell, and was considered to be toxic. No further reaction was possible due to low yield and possible toxicity.

Second attempt. A solution of iodine (6 mmol) in 30 ml of benzene was added to a slight excess of tetrakis(*p*-dimethylaminophenyl)tin(IV) (4.30 g, 7 mmol) in 20 ml of benzene. The iodine rapidly disappeared upon addition resulting in a yellow mixture. After the addition of the iodine solution, the mixture was stirred for an additional one-half hour and the solution was filtered in a 100-ml round bottom flask. The filtrate was then evaporated to dryness resulting in a yellow solid; yield 35 %. The solid was stored overnight, yielding a dark blue solid. Attempts to recrystallize this dark blue solid were unsuccessful. This solid has the same characteristics as the chloro analog.

2.3.4 Synthesis of *para*-Substituted Triaryltin(pentacarbonyl)manganese(I) Complexes

The *para*-substituted triaryltin(pentacarbonyl)manganese(I) complexes, with the exception of the sulphone compound, were synthesized by a method similar to that described previously for triphenyltin(pentacarbonyl)manganese(I).[5] Dimanganese decacarbonyl (3 g, 7.5 mmol) in 35 ml of dry THF was added to sodium amalgam (0.95 g, 41 mmol/10 ml Hg) and the mixture was stirred under nitrogen for 30-40 min at room temperature. The amalgam was drained from the reaction vessel and washed twice with 5 ml of mercury. Subsequently, 15.5 mmol of triaryltin chloride was added and the reaction mixture was stirred for 40 min. The volume of the reaction mixture was then reduced to about 20 ml by simple distillation and poured onto 75-100 g of crushed ice. The pale green solids produced were filtered off and extracted several times with refluxing hexane. The combined extracts were concentrated under reduced pressure until colorless or pale yellow crystals appeared. The resulting mixture was cooled and the crystallized solids

were filtered off and dried by suction filtration to give 65-85% yields of triaryltin-(pentacarbonyl)manganese(I). The final products were recrystallized from mixed solvents and the melting points were determined (Table 2.1).

Table 2.1. Physical properties of $Ar_3SnMn(CO)_5$ (Ar = *para*-XC_6H_4)

X	Solvent[a]	Yield (%)	Melting point (°C)	Color
H[b]	hexane	85	150-152	white
CH_3	dichloromethane/hexane	67	137-138	white
OCH_3	hexane	75	146-148	white
SCH_3	dichloromethane/hexane	74	126-128	pale yellow
F	benzene/heptane	70	128-130	white
Cl	dichloromethane/butanol	73	143-145	white
$S(O)_2CH_3$	dichloromethane/benzene	65	260-264[c]	off-white

[a]Solvent used for obtaining single crystals.
[b]R. D. Gorsich, *J. Am. Chem. Soc.*, **84**, 2486 (1964).
[c]Melts with decomposition.

Tris(*p*-methylsulphonylphenyl)tin(pentacarbonyl)manganese(I) was prepared by the oxidation of tris(*p*-thioanisyl)tin(pentacarbonyl)manganese(I) at -10 °C, using *meta*-chloroperbenzoic acid (MCPBA) as the oxidizing agent. A slurry of MCPBA (85%, 15.50g) and 50 ml CH_2Cl_2 was added slowly to a well-stirred CH_2Cl_2 (50 ml) solution of tris(*p*-thioanisyl)tin(pentacarbonyl)manganese(I) over a period of 2 h at -10 °C. Additional CH_2Cl_2 (60 ml) was added and the mixture was allowed to warm to room

temperature. The suspension was gravity-filtered and then washed with a 1:1 CH_2Cl_2-ether (150 ml) mixture. The resulting filtrate was refiltered and the product was precipitated as an off-white powder by the addition of 125 ml ether to the clear filtrate. The product was purified by dissolution in a minimum amount of CH_2Cl_2 followed by precipitation by slow addition of benzene. The product was vacuum-filtered and dried overnight under vacuum (yield 73%). Single crystals of (*para*-$XC_6H_4)_3Sn(CO)_5Mn$(I) were obtained by slow evaporation of the appropriate solutions (Table 2.1) over a period of 2-4 days in the dark. However, it was not possible to obtain crystals of the sulphone compound suitable for X-ray diffraction studies.

2.3.5 Attempted Synthesis of (p-$XC_6H_4)_3SnMn(CO)_5$ (X = CF_3 and $N(CH_3)_2$)

The starting material, $Br_3SnMn(CO)_5$, was prepared from the reaction of $Ph_3SnMn(CO)_5$ with excess bromine in carbon tetrachloride.[5] Attempts to prepare (p-$XC_6H_4)_3SnMn(CO)_5$ (X = CF_3 and $N(CH_3)_2$) by the reaction of $Br_3SnMn(CO)_5$ with excess lithium reagent, p-$(CH_3)_2NC_6H_4Li$ and p-$CF_3C_6H_4Li$, in absolute ether were unsuccessful. The material recovered after the reaction consisted of MnO_2 and less than 30 % of $Br_3SnMn(CO)_5$ (starting material).

2.4 Preparation of *trans*-$Ph_3SnMn(CO)_4PPh_3$

This complex was prepared from the reaction of triphenylphosphine and triphenyltin(pentacarbonyl)manganese(I).[5] A mixture of triphenylphosphine (2.0 g, 7.7 mmol) and 7.5 mmol (4.11 g) triphenyltin(pentacarbonyl)manganese(I) was added to a 100-ml round-bottom flask, and heated at 195 °C for 4 h. The resulting solid cake was

dissolved in 25 ml of benzene and slowly precipitated by addition of 95 % ethanol. The white powder obtained was recrystallized from a 1:1 mixture of benzene and absolute ethanol; yield 78 %, m.p. 225-227 °C (Lit: 228-230 °C).

2.5 Preparation of Dihalobis(trialkylphosphine)nickel(II) Complexes

The starting materials, nickel(II) chloride and nickel(II) bromide (Aldrich), were crushed and heated at 260 °C for 2 days to remove water of crystallization, and were stored in a dessicator prior to use. The solution of nickel(II) iodide was prepared by the reaction of sodium iodide in boiling ethanol with a stoichiometric amount of nickel nitrate in hot ethanol, subsequent cooling, and decantation to produce NiI_2 in ethanol. The tertiary phosphine ligands, tricyclohexylphosphine and tris(cyclohexylmethyl)phosphine, were used as received (Aldrich), whereas tribenzylphosphine was prepared from the reaction of benzylmagnesium(II) chloride with phosphorus trichloride.[12]

2.5.1 Synthesis of Tribenzylphosphine

A solution of benzylmagnesium(II) chloride was prepared by the addition of benzyl chloride (12.66 g, 100 mmol) in 25 ml benzene to a stirred suspension of excess magnesium turnings (2.5 g) in 50 ml dry ether at a rate sufficient to maintain gentle reflux. The mixture was boiled for an additional 30 min, cooled, stirred and treated in turn with dropwise addition of phosphorus chloride (4.12 g, 30 mmol) in 50 ml benzene. The resulting white mixture was refluxed for 45 min and cooled in an ice bath while being treated with saturated, degassed ammonium chloride solution (5.0 g in 300 ml H_2O). The

organic layer was separated under nitrogen and dried with anhydrous sodium sulphate, Na_2SO_4. The solvents were removed under reduced pressure, resulting in an off-white powder in 80-85 % yield. The complex was characterized by ^{1}H, ^{13}C and ^{31}P NMR spectroscopy. Tribenzylphosphine oxide was also prepared by passing air through a solution of tribenzylphosphine in ethanol, the oxide readily separating as a crystalline power. This was done to test for the presence of any phosphine oxide in the final product.

2.5.2 Synthesis of Dihalobis(trialkylphosphine)nickel(II) Complexes

The nickel complexes were prepared by the addition of a boiling ethanolic solution under nitrogen of the alkylphosphine to the appropriate nickel(II) halides.[13] The complexes crystallized on cooling and were recrystallized from *n*-butanol. The physical properties of the ten nickel(II) compounds are given in Table 2.2.

2.6 Infrared and Raman Spectroscopy

Mid-IR spectra were acquired on a Bruker IFS-48 FT-IR spectrometer equipped with a A-590 microscope, a CCD-IRIS color video camera and a nitrogen-cooled MCT-B detector. Spectra were obtained for hexane solutions (1.0 mg sample/ml of *n*-hexane) in a0.5-mm KBr solution cell and/or from Nujol mulls on KBr plates at a resolution of 2 cm^{-1}. The numbers of transients acquired were 128 and 64 for solution and solid-state spectra, respectively.

FT-Raman spectra were recorded at room temperature on a Bruker IFS-88 FT-IR spectrometer equipped with a CaF_2 beamsplitter, a FRA-106 FT-Raman module and a

Table 2.2. Physical properties of trialkylphosphine complexes of nickel(II)

Complex	Colour	Yield (%)	Melting point (°C)
$(Bz_3P)_2Ni(SCN)_2$	pepper red	83	185-187
$(Bz_3P)_2NiCl_2$	dark red	78	123-125
$(Bz_3P)_2NiBr_2$	brown	75	130-133
$(Bz_3P)_2NiI_2$	dark brown	78	132-134
$(Cy_3P)_2NiCl_2$	rose	68	225-227[a]
$(Cy_3P)_2NiBr_2$	greenish yellow	72	230-232[a]
$(Cy_3P)_2NiI_2$	aqua	55	235-238[a]
$[(CyCH_2)_3P]_2NiCl_2$	pepper red	75	157-159
$[(CyCH_2)_3P]_2NiBr_2$	brown	73	166-169
$[(CyCH_2)_3P]_2NiI_2$	brownish yellow	74	121-123

[a]Decomposition point.

liquid nitrogen-cooled proprietary detector. The instrument was interfaced to a Dell 486-DX microcomputer and the NIR output at 1064.1 nm of an air-cooled, Nd^{3+}:YAG laser was used to excite the sample at the highest power possible (*ca.* 250 mW). The 180° backscattered Raman light was collected by a short focal length quartz lens at a resolution of 2.6 cm^{-1}. Typical sample preparation involved packing a few milligrams of sample into the 2-mm central hole of a 10-mm outer diameter aluminum cup and placing this cup into the sample compartment located in the Raman module. The spectra thus obtained were of excellent quality from about 128-256 transients.

2.7 Solution and Solid-State Multinuclear NMR Spectroscopy

The solution ^{1}H, ^{13}C, ^{29}Si, ^{31}P, ^{55}Mn, ^{119}Sn and ^{207}Pb NMR spectra of the manganese-containing compounds studied were recorded at room temperature from concentrated solutions in $CDCl_3$ and THF-d_8 using a Varian XL-300 MHz spectrometer operating at 7.05 T. The ^{1}H, ^{13}C and ^{31}P NMR spectra of the nickel-containing compounds were obtained at variable temperature and concentration for CD_2Cl_2, benzene-d_6 and toluene-d_8 solutions. The ^{1}H, ^{13}C and ^{29}Si chemical shifts were referenced to an external sample of tetramethylsilane and the ^{119}Sn and ^{207}Pb shifts were referenced to external tetramethyltin and tetramethyllead, respectively. The ^{31}P chemical shifts were referenced to an external sample of 85 % phosphoric acid and the ^{55}Mn chemical shifts to an external sample of $KMnO_4$ in D_2O. The complex tris(acetylacetonato)chromium(III), $Cr(acac)_3$, was added to the NMR solution of $(CO)_5MnSiPh_3$ as a relaxation agent, prior to recording the ^{1}H, ^{13}C, ^{29}Si and ^{55}Mn spectra, to avoid spin saturation of the energy levels.

The solid-state, CP-MAS, ^{13}C, ^{29}Si, ^{31}P, ^{117}Sn, ^{119}Sn and ^{207}Pb spectra were measured at 7.05 T and, in some cases, at 2.35 T, using Chemagnetics CMX-300 and CMX-100 spectrometers, respectively. Spectra were acquired with high-power proton decoupling. The ^{13}C, ^{29}Si, ^{31}P, ^{117}Sn, ^{119}Sn and ^{207}Pb chemical shifts were referenced to the same standard used in the solution experiments. However, external secondary chemical shift references of hexamethylbenzene (17.35 ppm, ^{13}C), 2,2-dimethyl-2-silapentane-5-sulfonate (0.80 ppm, ^{29}Si), (2R, 3R)-(+)-bis(diphenylphosphino)butane (-13.0 ppm, ^{31}P), tetracyclohexyltin (-97.0 ppm, ^{117}Sn and ^{119}Sn) and tetraphenyllead (-136.0 ppm, ^{207}Pb) were used for solid-state measurements. The CP-MAS spectra were obtained from

approximately 250-300 mg of sample packed into zirconia pencil-type rotors. Contact times of 1-3 ms were used. The pulse delays, numbers of transients and spinning rates are given in the figure captions where necessary. No line broadening was applied to the ^{13}C, ^{29}Si and ^{31}P NMR spectra, but line broadenings of 10-50 Hz were applied to the rest of the spectra. The FIDs were zero-filled to 4 K and 8 K data points on the CMX-100 and CMX-300 instruments, respectively, before transformation. Curve fitting procedures were performed on the centre and spinning sidebands by using the program Peakfit (Jandel Scientific *ver. 2*). Calculation of the shielding tensors was performed with the aid of computational packages developed by Wasylishen *et al.*[14]

2.8 X-Ray Crystallography

X-ray diffraction measurements were conducted on a Rigaku AFC6S diffractrometer at 20 °C using graphite-monochromated Cu-Kα (λ_{max} = 1.5418 Å) or Mo-Kα (λ_{max} = 0.7107 Å) and a ω-2θ scan technique. In all cases, selected crystals were mounted on glass fibers. The structures for the two nickel complexes were solved by the direct methods and were refined by full-matrix least-squares using the SHELX program.[15] All other structures were solved by direct methods using SHELXS-86[16] and were refined on F^2 by full-matrix least-squares calculations for independent reflections using SHELX-93 crystallographic software.[17] Additional crystallographic data are given in Appendices **I-III**. Atomic scattering factors and anomalous scattering terms were obtained from standard sources.[18] In every case, all non-hydrogen atoms in the structures

were refined anisotropically and hydrogen atoms were placed in fixed calculated positions.

References

(1) D. Drew, M. Y. Darensbourg and D. J. Darensbourg, *J. Organomet. Chem.*, **85**, 73 (1975).

(2) J. D. Cotton and R. D. Markwell, *J. Organomet. Chem.*, **388**, 123 (1989).

(3) J. D. Cotton and R. D. Markwell, *Inorg. Chim. Acta*, **175**, 187 (1990).

(4) P. DeShong, G. A. Slough, D. R. Sidler, P. J. Rybczynski, W. Philipsborn, R. W. Kunz, B. E. Bursten and T. W. Clayton Jr., *Organometallics*, **8**, 1381 (1989).

(5) R. D. Gorsich, *J. Am. Chem. Soc.*, **84**, 2486 (1962).

(6) W. Jetz, P. B. Simons, J. A. J. Thompson and W. A. G. Graham, *Inorg. Chem.*, **5**, 2217 (1966).

(7) E. Krause and R. Becker, *Chem. Ber.*, **53**, 173 (1920).

(8) K. A. Kocheskov, M. M. Nadi and A. P. Aleksandrov, *Chem. Ber.*, **67**, 1348 (1920).

(9) I. Wharf, *Inorg. Chim. Acta*, **159**, 41 (1989).

(10) P. R. Austin, *J. Am. Chem. Soc.*, **54**, 3727 (1932).

(11) A. Stern and E. I. Becker, *J. Org. Chem.*, **29**, 3221 (1964).

(12) R. C. Hinton and F. G. Mann, *J. Chem. Soc.*, 2835 (1959).

(13) M. C. Browning, J. R. Mellor, D. J. Morgan S. A. Pratt, L. E. Sutton and L. M. Venanzi, *J. Chem. Soc.*, 693 (1962).

(14) A. P. Kengens, W. Power, R. E. Wasylishen, *HBLQFIT, Sideband analysis, version 2.2*, Dalhousie University: Halifax, Nova Scotia, Canada, 1991.

(15) G. M. Sheldrick, *SHELX, Programme for Structure Determination*, University of Cambridge, England (1976).

(16) G. M. Sheldrick, *SHELXS-86, Programme for the Solution of Crystal Structures,* University of Göttingen, Germany (1985).

(17) G. M. Sheldrick, *SHELXL-93, Programme for Structure Refinement,* University of Göttingen, Germany (1993).

(18) In *International Tables for Crystallography*, Dordrecht: Kluwer Academic Publishers, Vol. C Table 4.2.6. (1992).

Chapter 3

Solution and Solid-state Multinuclear NMR Spectroscopy

3.1 Introduction

The history of nuclear magnetic resonance spectroscopy is one of the most important and fascinating discoveries in science. At the end of the last century, Zeeman observed that closely spaced doublets appeared in the absorption and emission spectra of certain atoms when subjected to the influence of a strong magnetic field.[1] As spectral resolution improved and spectra of additional species were studied, further smaller splittings (hyperfine structure) were observed. In 1925, Uhlenbeck and Goudsmit[2] introduced the concept of a spinning electron, with quantized angular momentum ($-h/4\pi$) and a magnetic dipole moment associated with the spinning charge. The concept of a spinning electron was grafted onto the old Bohr theory and later onto the Schrödinger/Heisenberg formulation of quantum mechanics to account for the strange interactions observed by Zeeman, but this failed to explained the hyperfine splitting observed in some species. Meanwhile, anomalies in the heat capacity of hydrogen led Dennison[3] to propose that protons have an angular momentum of $-h/4\pi$. Molecular hydrogen, H_2, then would consist of two proton spins oriented parallel or antiparallel to each other. This concept completely accounted for the heat capacity results. In fact, Pauli[4] had already postulated that certain nuclei behave as spinning particles and therefore have a quantized momentum together with an associated quantized magnetic moments, μ, which accounts for the hyperfine splittings. Pauli's concept of proton spin came before the idea of electron spin had been formulated and was based on the widespread

misconception that the nucleus consisted of only protons and electrons. This misconception was due to the fact that the neutron had not been discovered at that time (the discovery came in 1932). The first real "NMR" signal was observed some 15 years later by the Rabi group at Columbia University,[4] by the use of elegant molecular beam experiments, for which Rabi received the Nobel Prize in Physics in 1944. However, the real beginning of NMR spectroscopy developed from the work of two groups of physicists at Harvard University[5] (Purcell, Torrey and Pound) and at Stanford University[6] (Bloch, Hansen and Packard), where they independently observed the resonance of protons in bulk water and paraffin materials, respectively. This discovery led to the awarding of the 1952 Nobel Prize in Physics to Bloch and Purcell.[7] The birth of this branch of spectroscopy has led to several major and exciting new developments and discoveries in every branch of science, such as chemistry, biochemistry, biomedical research and materials science. Continued progress has led to another Nobel Prize in Chemistry, awarded to the Swiss physical chemist Ernst in 1991 for his outstanding contributions to the developments of Fourier transformation and experimental NMR techniques.[8]

The physical foundation of NMR spectroscopy lies in the magnetic properties of atomic nuclei. Many nuclei have spin angular momenta, since proton and neutrons themselves have this property, represented by the spin quantum number, I, which can be half-integral or integral, depending on the nucleus. Nuclei which have either an odd number of protons or an odd number of neutrons, but not both, exhibit half-integral spin I, whereas nuclei which possess an odd number of protons and an odd of number neutrons have integral spin quantum numbers. Nuclei in which both the number of protons and

neutrons are even, such as ^{12}C, ^{16}O, ^{28}Si, possess no angular momentum (I = 0) and exhibit no magnetic properties. The interaction of the nuclear magnetic moment with an external magnetic field, B_o, leads to 2I + 1 allowed orientations with different energy levels, Fig 3.1. The states are separated by an energy, ΔE, which depends on the strength of the interaction between the nucleus and the magnetic field. ΔE can be measured by applying electromagnetic radiation of frequency, ν, which causes transition between the nuclear spin states, provided the resonance condition $\Delta E = h\nu$ is satisfied.

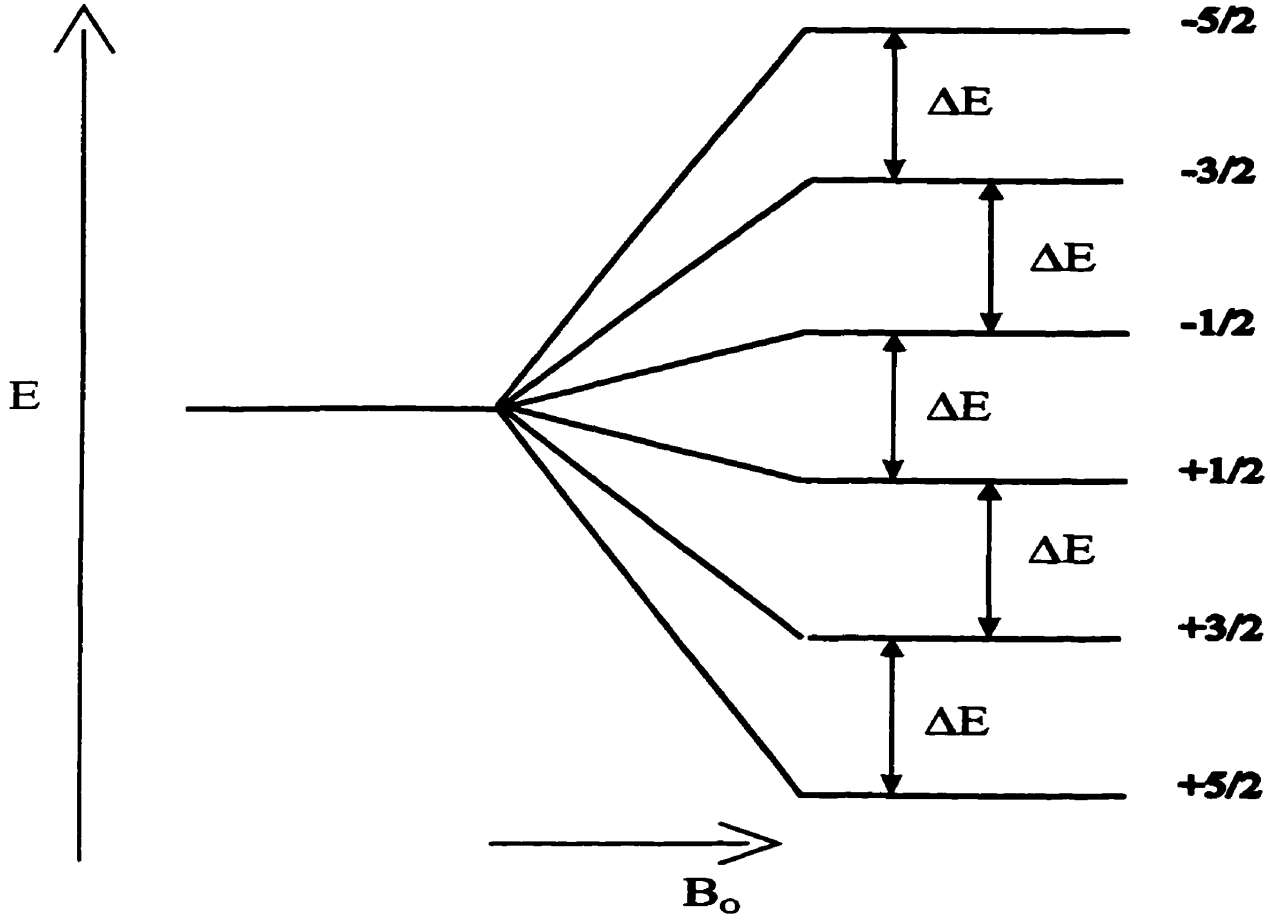

Figure 3.1 Energy-level diagram for a spin-5/2 system.

3.2 Nuclear Interactions in Solutions and Solids

The high-resolution NMR spectroscopy of non-viscous solutions or liquids has provided valuable structural information in all branches of chemistry, since the discovery of the chemical shift and spin-spin interaction in the late 1940s, but, while solid-state NMR spectroscopy has been known for the same time period of time, it is only over the past two decades that its potential applications have been realized. The major difference between the NMR spectra of liquids and solids lies in the linewidths of the observed resonances. The spectra of solution samples generally have linewidths of less than a few Hertz, which permit the observation of chemical shifts and coupling constants, whereas the spectra of solid materials typically have linewidths of tens of kHz and the loss of valuable information. This difference is due to rapid molecular tumbling motions in solution which lead to isotropic interactions, whereas in the solid-state all interactions are anisotropic. The characteristics of solid-state NMR spectra are therefore much more complex and contain orientation-dependent terms, which may ultimately yield more important information than the corresponding solution-state spectra. The nuclear spin Hamiltonian operators, together with the approximate magnitudes, for both cases can be defined by the following expressions:

$$h^{-1}H = (H_Z + H_{CS} + H_J + H_D + H_Q)h^{-1} \quad [3.2.1]$$

solution (Hz)	10^6-10^9	10^3-10^5	10-10^4	0	0
solid (Hz)	10^6-10^9	10^3-10^5	10-10^4	0-10^5	10^5-10^9

where the subscripts denote the relevant interactions: Z, the Zeeman interaction with the magnetic field; CS, magnetic shielding by the surrounding electrons giving the chemical

shifts; J, spin-spin couplings to other nuclei; D, direct dipole-dipole interactions with other nuclei; Q, quadrupolar interactions with nuclei of spin > 1/2.

Zeeman Interaction, H_Z

The Zeeman interaction occurs for all nuclei possessing spin ≥ 1/2, between the nuclear magnetic moment, μ, of the nucleus and the applied magnetic field, $\boldsymbol{B}_0$, yielding 2I +1 equally spaced energy levels (Fig. 3.1). The Hamiltonian for this interaction is given by

$$H_Z = -(\gamma h / 2\pi)\, \mathbf{B}_0.\mathbf{I} \qquad [3.2.2]$$

where γ is the magnetogyric ratio of the nucleus. The eigenvalue of this term, Eq. [3.2.2], is

$$E = -(\gamma h / 2\pi)\, m_I \times B_0 \qquad [3.2.3]$$

where m_I is the magnetic quantum number and has 2I + 1 values in integral steps between -I and +I. In the absence of other interactions, this would generate a line spectrum at frequency

$$\nu = \gamma B_0 / 2\pi \qquad [3.2.4]$$

Chemical Shift Interaction, H_{CS}

The chemical shift interaction is due to the local magnetic fields generated at the nucleus by the circulation of the surrounding electrons induced by the applied magnetic field and is described by

$$H_{CS} = (h / 2\pi)\, \gamma\, \mathbf{I}.\sigma.\mathbf{B}_0 \qquad [3.2.5]$$

where σ is a dimensionless second rank tensor with a non-zero trace. Unlike other interactions (see below), the chemical shielding interaction and Zeeman interaction are field-dependent.

Indirect Spin-Spin Interaction, H_J

The spin-spin interaction involves coupling between pairs of spins I and S, mediated by the electronic environment between the nuclei rather than behaving as a dipolar through-space interaction, and is given as

$$H_J = (h / 2\pi)\ \mathbf{I}.\mathbf{J}_{IS}.\mathbf{S} \qquad [3.2.6]$$

where $\mathbf{J}_{IS}$ is the electron-coupling nuclear spin interaction tensor, which describes the variation in the spin-spin coupling with the orientation of the molecules in the magnetic field. This interaction is usually small compared with the other interactions and is field-independent.

Magnetic Dipolar Coupling, H_D

The dipolar coupling term arises from direct, through-space, dipole-dipole interactions between the nuclei. The dipolar interaction between an isolated unlike spin pair, I and S, can be written as

$$H_D = \gamma_I\gamma_S(h / 2\pi r^3)\ \mathbf{I}.\mathbf{D}_{IS}.\mathbf{S} \qquad [3.2.7]$$

where γ_I and γ_S are the magnetogyric ratios of spin I and S, respectively, **D** is the dipolar coupling tensor with a trace of zero, and r is the internuclear distance between the two nuclei I and S.

Quadrupolar Interactions, H_Q

All nuclei with spin greater than 1/2 possess a non-spherically symmetric charge distribution, resulting in a quadrupole moment, eQ. In general, the charge distribution of nuclear spheroids can be either prolate, $Q > 0$ (elongated, football shape) or oblate, $Q < 0$ (contracted, disk shape). The quadrupolar interaction arises from the interaction of the nuclear electric quadrupole moment with the non-spherical electric field gradient around the nucleus. It is also magnetic field-independent and is given by

$$H_Q = \mathbf{I.Q.I} \qquad [3.2.8]$$

where Q is the quadrupole coupling tensor, defined as $[2\pi e^2Q / 2hI(2I-1)]$ **V** and **V** is the electric field gradient tensor at the nuclear site.

In solution, rapid molecular tumbling occurs reducing the dipolar and quadrupolar terms to zero due to the fact that the traces of the dipolar and quadrupolar tensors, **D** and Q, are zero. However, the chemical shift and spin-spin interactions are averaged to their isotropic values and are the dominating factors in solution-state spectroscopy.

In a solid, all of the above interactions are anisotropic and severe line-broadening of resonance signals is observed, usually resulting in featureless spectra. In order to obtain high-resolution spectra with reasonably narrow resonance lines, three difficulties are encountered which must be overcome. The first arises from the magnetic coupling between nuclear dipoles I and S. Where the spin I is usually that of protons and the spin S represents the nucleus investigated, such as ^{13}C, ^{29}Si, ^{31}P, ^{119}Sn or ^{207}Pb. For ^{13}C, dipolar coupling between like spins (^{13}C-^{13}C) and other NMR-active nuclei are negligible because

of the very low natural abundance of ^{13}C (1.1%) or 100% natural abundant nuclei that are widely seperated in the solid, reduced D, resulting in so-call "dilute niclei". Second is the orientation-dependence of the shielding constants in a static magnetic field, which gives rise to a distribution of chemical shifts, known as a powder pattern, and results in further line broadening. Third is the low sensitivity and long spin-lattice relaxation times in solids, particularly in the case of low abundance nuclei, such as ^{13}C, ^{29}Si and ^{207}Pb, leading to weak signals in repetitive pulse experiment. These goals can be successfully achieved by means of three sophisticated experimental techniques: *high-power proton decoupling, magic angle spinning (MAS) and cross-polarization (CP).*

3.2.1 High-Power Proton Decoupling

The major line broadening effect in solid-state NMR spectroscopy is due to dipolar interactions between the nuclei. In the case of the interaction between protons and other nuclei, this type of heteronuclear interaction can be reduced to near zero values by the application of a very strong high-power decoupling field at the proton resonance frequency. It is analogous to proton decoupling in solution-state experiments, but in solid-state experiments, much higher decoupling powers are needed in order to reduce the interactions with protons where the dipolar coupling is of the order of kHz.

3.2.2 Magic Angle Spinning (MAS)

Solid polycrystalline or amorphous materials contain molecular groupings which are oriented in all possible directions with respect to an applied magnetic field in an NMR experiment. This give rise to a spectrum consisting of a diffuse peak known as a "powder

pattern", Fig 3.2. Several techniques have been proposed and applied to suppress this anisotropic broadening, including complicated pulse sequences, but with limited success.

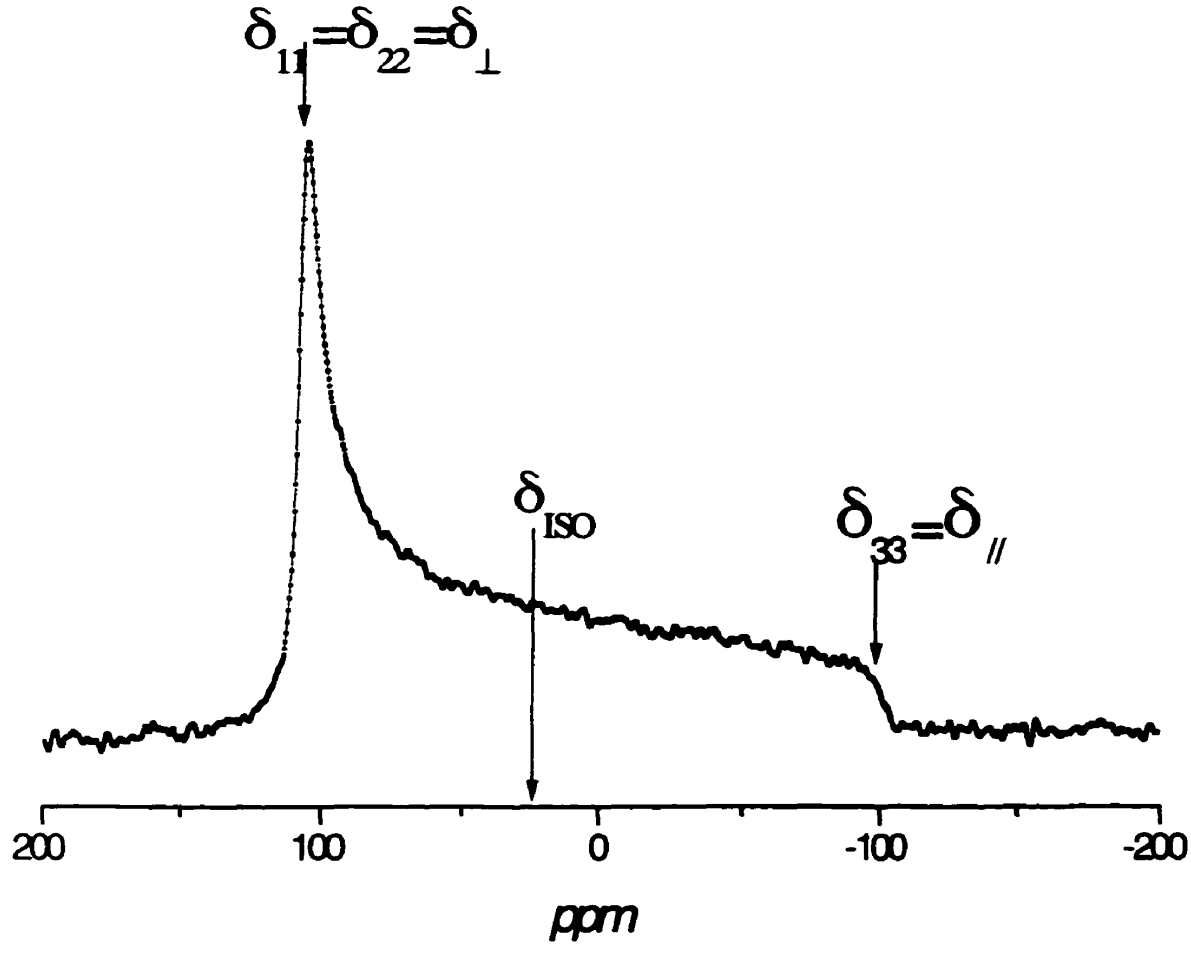

Figure 3.2. Chemical shift powder pattern for tribenzylphosphine oxide showing axial symmetry

The dipolar interactions contain the angular term $(3\cos^2\theta - 1)$ and one way of reducing the dipolar interaction to zero is by making this angular term vanish. This can be accomplished by rapid rotation of the sample about an axis inclined at an angle θ =

54.73° with respect to the magnetic field. In addition to the removal of dipolar interactions, the chemical shift anisotropy, the spin-spin anisotropy and the first-order electric quadrupole interactions are also reduced to zero since the $(3\cos^2\theta - 1)$ factor appears in the mathematical description of these interactions. This 54.73° angle is termed the "magic angle" and the technique is known as Magic Angle Spinning or MAS, however, the more appropriate term should be Andrew-Lowe angle spinning due to the fact that this technique was developed by Andrew and Lowe[9] in the late 1960s.

3.2.3 Cross-Polarization

The cross-polarization technique, in conjunction with MAS, has been widely applied in solid-state NMR studies. One of the major problems when recording NMR spectra of solids is that the spin-lattice relaxation time, T_1, may be extremely long for low abundant nuclei such as ^{13}C and ^{29}Si and makes signal detection a difficult and lengthy process. The cross-polarization, CP, experiment, first reported by Hartmann and Hahn in 1962,[10] provides a way of circumventing this problem. This technique was combined ten years later with the high-power decoupling experiment by Pines, Gibby and Waugh.[11] The object of the experiment is to make use of the strong polarization of abundant proton nuclei to enhance inherently weak spin polarization of dilute nuclei with long longitudinal relaxation times, Fig 3.3.

The CP experiment in the solid is easily understood in terms of thermodynamic language. Consider two reservoirs; I, which is a large proton reservoir with a high heat capacity or low-spin temperature, and S, which is a small probe reservoir with a low heat capacity or high-spin temperature. The high heat capacity reservoir of magnetization

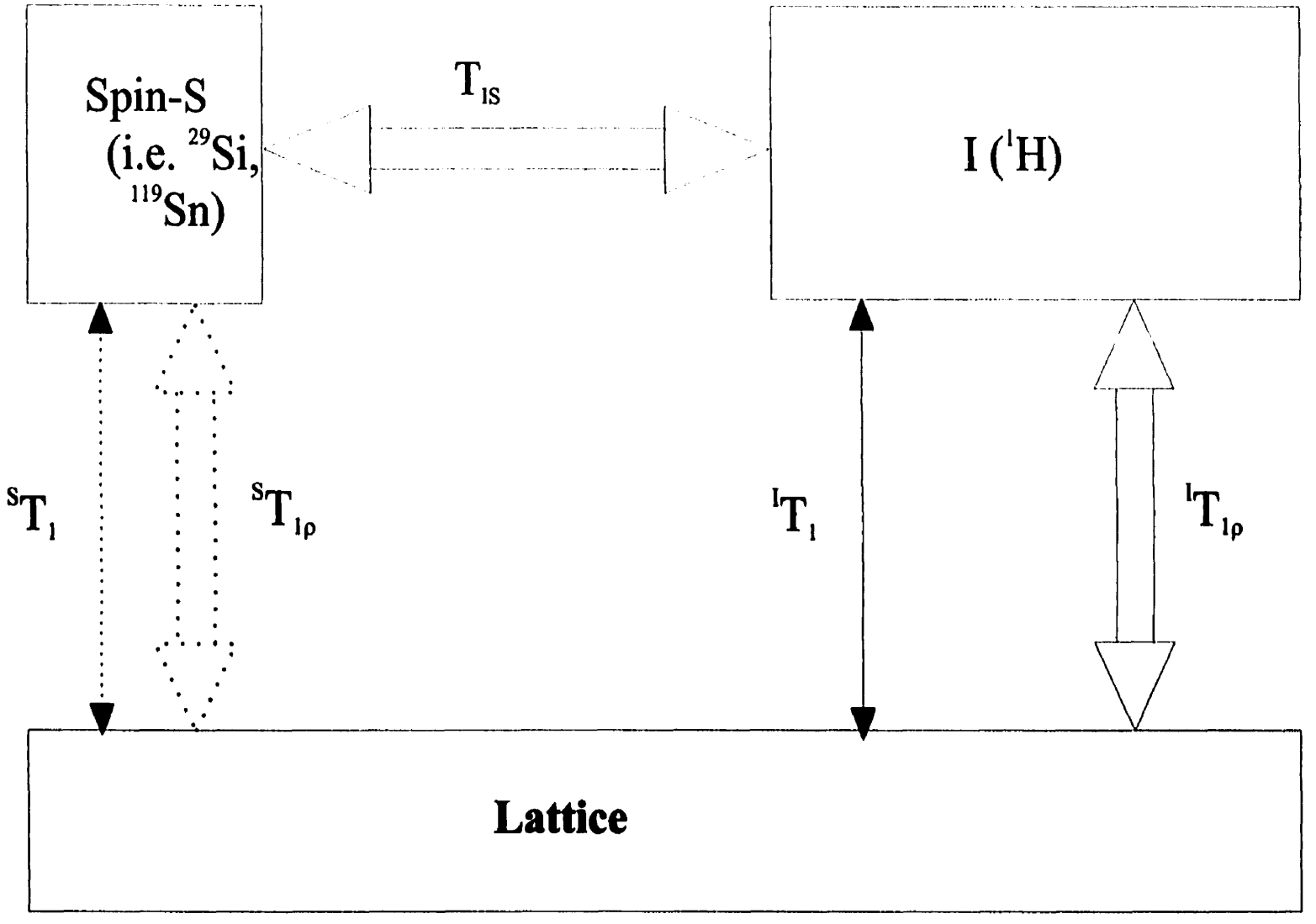

Figure 3.3. Thermodynamic representation of I and S spin reservoirs. Arrows indicate transfer routes among the various reservoirs by cross-polarization or spin-lattice relaxation.

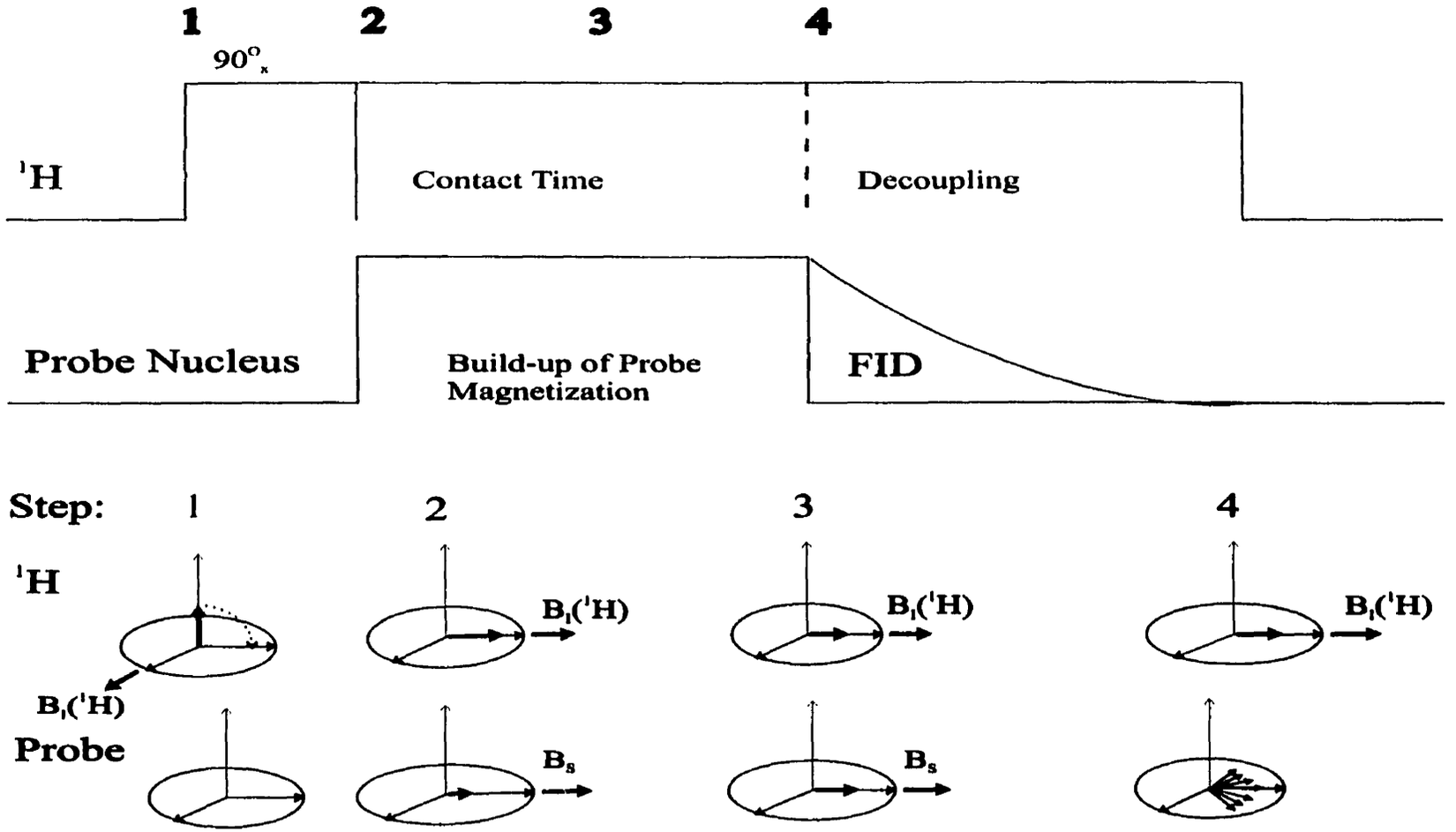

Figure 3.4. The spin-lock cross-polarization transfer experiment, showing the behaviour of the ^1H and spin-S magnetization.

could provide a means of cooling the probe reservoir without significantly reducing the heat capacity of the proton reservoir. This is accomplished by allowing both the I and S spins to precess in their respective rotating frames at some common frequency. This common frequency is that in which the Hartmann-Hahn condition is satisfied, Eq [3.2.9]

$$\gamma_I B_I = \gamma_S B_S \qquad [3.2.9]$$

Under this condition, the Zeeman levels in the rotating frame are matched and effective transfer of energy between the two reservoirs is accomplished *via* dipolar coupling. The sequence of events for establishing contact between the two spins and observing the S spin is summarized in Figures 3.3 and 3.4.

3.3 Chemical Shift and Chemical Shift Anisotropy

The fundamental equation of NMR spectroscopy, Eq. [3.2.4], tell us that if every nucleus in a sample was subjected to an external magnetic field, B_0, then the NMR spectrum of that sample would be composed of resonance lines of identical frequency, the Zeeman frequency. This is only true if all the nuclei in the sample were stripped of all their electrons. However, as this is never the case, each non-equivalent nucleus will resonate with a characteristic frequency due to the shielding effects of electrons. These nuclear shielding effects originate from the circulation of electrons within their atomic and molecular orbitals and around the nucleus, induced by an external magnetic field. The circulation of these surrounding electrons will generate a small magnetic field with a magnitude proportional to the applied field, and which may be parallel or antiparallel to

B_o depending on the electron distribution around the nucleus. This situation will result from shielding or deshielding of the nucleus by it surrounding electrons, Eq. [3.3.1]

$$\nu = \gamma B_o(1 - \sigma) / 2\pi \qquad [3.3.1]$$

where σ is referred to as the shielding or screening constant and a typical value is of the order 10^{-4}-10^{-6}. In principle, the magnetic shielding of a given nucleus depends on the molecular orientation with respect to B_o and is, therefore, represented by a tensor quantity, a 3×3 matrix, which depends upon the electronic structure of the molecule. By a suitable choice of coordinate system, the "principal axis system" PAS, the chemical shift tensor matrix can be diagonalized such that all the off-diagonal elements are zero, Fig. 3.5. The chemical shift tensor can, therefore, be described in term of the three principal values, σ_{11}, σ_{22} and σ_{33}, and three angles specifying the orientation of the PAS with respect to the molecular axis. The values of these three tensor components are absolute values with respect to the bare nucleus.[12]

$$\begin{bmatrix} \sigma_{xx} & \sigma_{xy} & \sigma_{xz} \\ \sigma_{yx} & \sigma_{yy} & \sigma_{yz} \\ \sigma_{zx} & \sigma_{zy} & \sigma_{zz} \end{bmatrix} \xrightarrow{\text{diagonalization}} \begin{bmatrix} \sigma_{11} & 0 & 0 \\ 0 & \sigma_{22} & 0 \\ 0 & 0 & \sigma_{33} \end{bmatrix}$$

Figure 3.5. Diagonalization of the chemical shift tensor in the laboratory frame to the principal axis frame.

In NMR spectroscopy, the shielding constant σ is an inconvenient measure of the chemical shift. Due to the fact that absolute shifts are very seldom needed and extremely

difficult to determine, it is common practice to define the chemical shift in term of the difference in resonance frequencies between the nucleus under investigation and a reference signal by means of a dimensionless parameter δ:

$$\delta = [(\nu_s - \nu_{ref}) / \nu_{ref}] \times 10^6 \qquad [3.3.2]$$

where ν_s and ν_{ref} are the resonance frequencies of the sample and reference, respectively. The principal components of the chemical shielding tensor can also be expressed as chemical shifts.

$$\delta = [(\sigma_{ref} - \sigma) / (1 - \sigma_{ref})] \times 10^6 \qquad [3.3.3]$$

It should be noted that an increase in σ (greater shielding) leads to a decrease in δ, so that δ is thus a deshielding parameter.

The convention chosen and used in this thesis for the shielding components is that proposed by Haeberlen,[13] and is the convention used today by many NMR chemists.

$$|\delta_{33}-\delta_{iso}| \geq |\delta_{11}-\delta_{iso}| \geq |\delta_{22}-\delta_{iso}| \qquad [3.3.4]$$

$$|\sigma_{33}-\sigma_{iso}| \geq |\sigma_{11}-\sigma_{iso}| \geq |\sigma_{22}-\sigma_{iso}| \qquad [3.3.5]$$

It is conventional to choose the magnetic field direction to be the Z direction in the laboratory coordinate system.[14] In this laboratory frame, the NMR experiment measures σ_{ZZ}, and the observed chemical shift Eq [3.3.1] becomes

$$\nu = \gamma B_0(1 - \sigma_{ZZ}) / 2\pi \qquad [3.3.6]$$

An expression for σ_{ZZ} in terms of the principal values of the shielding tensors and some arbitrary orientation B_0 relative to the PAS axes can be expressed in terms of the three principal components:[15]

$$\sigma_{ZZ} = \sigma_{11}\cos^2\theta_{11} + \sigma_{22}\cos^2\theta_{22} + \sigma_{33}\cos^2\theta_{33} \qquad [3.3.7]$$

where σ_{ii} are the three principal values along its principal axes, and θ_{ii} are the three angles made between each of these axes and the direction of B_O. For rapid and random rotation, each angle in Eq [3.3.7] varies randomly, so that the value of σ_{ZZ}, which is now δ, is given by

$$\delta_{iso} = 1/3\ (\delta_{11} + \delta_{22} + \delta_{33}) \qquad [3.3.8]$$

since the average values of each $\cos^2\theta_{ii}$ is 1/3, and the isotropic value is obtained. This is the mechanism that occurs in gaseous or solution measurements.

In solid samples, however, the molecules are not free to rotate or tumble and different nuclear sites will have different values for the angle in Eq. [3.3.8]. This will result in a distribution of local fields and, hence, a broadened line from which the three principal tensor values can be obtained. These tensor values contain potential information in three dimensions regarding the structure and bonding interactions of the compound under investigation. Therefore, they can be three times more informative than the isotropic value obtained from a gas or solution experiment.

Other important solid-state parameters are the chemical shift anisotropy, CSA, ($\Delta\delta$) and the asymmetry parameter, η_C, which defines the departure from axial symmetry at the probe site and lies in the 0 to 1 range.

$$\Delta\delta = \delta_{33} - 1/2(\delta_{11} + \delta_{22}) \qquad [3.3.9]$$

$$\eta_C = |\ (\delta_{22} - \delta_{11}) / (\delta_{33} - \delta_{iso})| \qquad [3.3.10]$$

For an axially symmetric tensor, such as that of tribenzylphosphine oxide, the value of η_C is zero, but the CSA is not zero. For spherical symmetric molecules, such as

tetraphenyllead, both the asymmetry parameter and the chemical shift anisotropy are very close to zero.

It is often practically impossible to calculate the exact value for the screening constant due to the complexity of the mechanisms which give rise to it, but the chemical shifts can be understood empirically by a combination of several types of interaction, Eq. [3.3.11].[16]

$$\sigma_l = \sigma_d + \sigma_p + \Sigma\sigma^{AB}_{Inter} + \sigma' \qquad [3.3.11]$$

Diamagnetic term, σ_d

The diamagnetic currents arise from the circulation of electrons, induced by the applied magnetic field, in spherically symmetrical atomic or molecular orbitals around the nucleus. The current so induced generates a small magnetic field B´ in the opposite direction to B_O, and the nucleus is thus shielded from the applied field. The magnitude of this current is determined by the ground state electronic wavefunction and can be described in terms of the mean distance from the nucleus and the charge of the electrons, Eq [3.3.12], but it can generally be related to the electron density on the probe nucleus.[17]

$$\sigma_d = (\mu_o/4\pi)\ (e^2/2m)\ \Sigma\langle 1/r_i\rangle \qquad [3.3.12]$$

where $\langle 1/r_i\rangle$ is the mean inverse distance of the electron from the nucleus and the summation is made only over electrons of that atom. The diamagnetic shielding is fairly easily to calculate for atoms and depends strongly on the number of electrons surrounding the nucleus.

Paramagnetic term, σ_p

The paramagnetic term takes into account deviations of the electron distribution from spherical symmetry (for all electrons except those in s orbitals) and has absolutely nothing to do with the effect of unpaired electrons. In the case of a hydrogen atom, the paramagnetic term does not contribute to the chemical shift since s electrons have no effect on this term. For this reason, the range of chemical shifts is small in comparison to other nuclei. The contribution of the paramagnetic term is extremely difficult to determine but can be loosely described by[17,18]

$$\sigma_p = -(\mu_o/4\pi)\,[e^2h^2L(L+1)/(3m^2\Delta E)]\,\langle 1/r^{-3}\rangle_{n,l} \qquad [3.3.13]$$

where $h^2L(L+1)$ is the square of the magnitude of the total angular momentum of all electrons in the n^{th} shell with individual angular momentum quantum number 1, and ΔE is the average excitation energy and represents an approximation to a summation of energy differences between the ground state and the various excited states of the atoms. A decrease in ΔE leads to a decrease in nuclear shielding, however, it is not readily calculated and its role in determining chemical shifts is still not well defined. It is often assumed to be a constant for structurally related series of complexes.[16]

Interatomic contribution, $\Sigma\sigma^{AB}_{Inter}$

This term represents the interatomic contribution due to local magnetic fields generated at a given nucleus by the anisotropy of neighbouring groups, such as the ring

current effect induced in aromatic rings. Another important example is the extreme low-field shifts found for aldehyde protons due to the anisotropy of the carbonyl group.

Other sources of shielding, σ'

The final part of Eq [3.3.11] is used to consider collectively all other interactions which can contribute to the chemical shifts. This includes electric field shifts, hydrogen bonding, unpaired electrons and solvent effects.[19]

3.4 Indirect Spin-Spin Coupling Constant

In section 3.3, the impression was given that the appearance of NMR spectra is determined solely by chemical shifts. In fact, there is another extremely valuable source of information encoded is most solution and solid-state spectra, the magnetic spin-spin interactions or indirect J-coupling between NMR-active nuclei. This type of coupling is produced by an indirect interaction of valence electrons of the molecules between spins of neighbouring nuclei.

It is well recognized that the spin-spin coupling constants depend on orbital hybridization, the electronegativity of substituents, and the geometry of the coupling path. This makes them an invaluable tool in structural studies of the bonding interactions and electron distributions within chemical bonds of both inorganic and organic complexes. The indirect spin-spin coupling is a tensor quantity and its three principal tensor parameters are extremely difficult to measure by high-resolution NMR

spectroscopy. Frequently, measurements are carried out in an isotropic phase (solution or rapid spinning of solids at the magic angle), and in such conditions, much information associated with this tensors is lost. However, with the development of experimental and theoretical techniques, a notable increase in the experimental determination of anisotropies of J coupling tensors have been reported for single crystals[20-25] and powder samples (section 3.5).[26-28] Recently, theoretical calculation of the isotropic CLOPPA (Contribution from Localized Orbital within the Polarization Propagator Approach) formulation[29] using semiemperical ground-state wave functions was extended to include the second-rank character of the spin-spin coupling tensor and it was applied to analyze ^{1}J coupling tensors in $(CH_3)_3E$-^{19}F and $(CH_3)_3E$-^{35}Cl (E = ^{13}C, ^{29}Si, ^{119}Sn, ^{207}Pb) compounds.[30] The results obtained were compared to experimental ΔJ values, whenever possible, and were found to be smaller than the experimental values by more than 40%. Due to mathematical complexity and problems encountered in the theoretical calculation of spin-spin coupling constants and their tensors, we have decided to focus only on the major contributions.

There are four contributions to the mechanism of indirect spin-spin interactions based on Ramsey's formulations.[31] Ramsey described the interaction by means of the Hamiltonian, H_J, where:

$$H_J = H_{FC} + H_{SD} + H_{PSO} + H_{DSO} \qquad [3.4.1]$$

The first term corresponds to the fully isotropic Fermi contact interaction and the other three anisotropic terms correspond to the spin-dipolar interaction, the paramagnetic spin-orbital interaction and the diamagnetic spin-orbital interaction. If the Fermi contact term

is the dominant mechanism of isotropic spin-spin coupling, then the $^1J_{X-Y}$ coupling values will increase as the *s* bonding character increases (Eq. [3.4.2]):[32]

$$J_{XY} \propto \gamma_X \gamma_Y \, |n_X S(o)|^2 \, |n_Y S(o)|^2 \, \alpha^2_X \alpha^2_Y \, (\Delta E)^{-1} \qquad [3.4.2]$$

where γ is the nuclear magnetogyric ratio, $|nS(o)|^2$ are the electron densities at the nuclear sites, α^2 is the *s*-character of the hybrid used in the bonding orbital and ΔE is the average excitation energy. In this thesis, the anisotropic contributions will not be discussed. For a detailed analysis of both the isotropic and anisotropic spin-spin interactions, the reader is encourage to consider references 24, 29-30.

It was shown earlier by Gilson that a relationship exists between the isotropic, one-bond, carbon-hydrogen, spin-spin coupling constants, $^1J_{C-H}$, and halogen nuclear quadrupole coupling constants in mono, di, and trihalogenated methanes.[33] According to the theory of nuclear quadrupole coupling of Townes and Dailey, as the s bonding character increases the field gradient at the nucleus decreases (Eq. [3.4.3]):[34]

$$q_{zz} = (1 - s - I - \pi) \, q_{at} \qquad [3.4.3]$$

where q_{zz} is the largest component of the electric field gradient, q_{at} is the atomic field gradient, and s, I and π are the s, ionic, and double bond characters, respectively. Thus, the field gradient decreases with increased *s*-character.

3.5 Second-Order Quadrupole-Dipole Effects in Solid-State, CP-MAS, NMR Spectra of Spin-1/2 Nuclei

In recent years, the effect of directly bonded quadrupolar nuclei on the solid-state, CP-MAS, NMR spectra of a spin-1/2 probe nucleus has received enormous

attention.[26,35-43] This is mainly due to the fact that the existence of quadrupole coupling constants, $\chi = e^2Qq_{ZZ}/h$, which are in excess of a few MHz in most cases, interferes with the ability of the MAS experiment to suppress the dipolar interactions between the probe and quadrupolar nuclei and, hence, the term "quadrupole-dipole" interactions. Angular terms in the Hamiltonian involving geometric factors other than $(3\cos^2\theta - 1)$, such as $\sin\theta \cos\theta$ and $\sin^2\theta$ become relevant and cannot be eliminated by the MAS technique, however, it does scale them down.

Full theoretical treatments to account for this quadrupolar effect are well documented in the literature,[37,44-46] but are rather complicated. Recently a first-order perturbation treatment has been proposed,[26,47-49] which results in a simple expression for the second-order shift of the resonance frequencies, provided that the ratio of the quadrupole coupling constant to Zeeman frequency for the quadrupolar nucleus is small, $\chi/[4S(2S-1)\nu_S] < 1$, leading to the expression

$$\Delta\nu_m = -mJ + (3\chi D''/20\nu_S)\,[\{S\,(S+1) - 3m^2\}\,/\,\{\,S\,(2S-1)\}] \qquad [3.5.1]$$

where $\Delta\nu_m$ is the shift produced by the m eigenstates of the quadrupolar nucleus (relative to the unperturbed isotropic shift frequency, δ_{iso}), J is the isotropic I-S spin-spin coupling constant, ν_S is the resonance frequency of the quadrupolar nucleus, χ is the quadrupolar coupling constant (e^2qQ/h), and D″ is the effective dipolar coupling constant, including the anisotropy in the spin-spin coupling (ΔJ) (Eq. [3.5.2]):

$$D'' = 3(D\cos^2\beta^D - (\Delta J/3)\cos^2\beta^J) - (D - \Delta J/3) +$$
$$\eta_Q\,(D\sin^2\beta^D\cos 2\alpha^D - (\Delta J/3)\sin^2\beta^J\cos 2\alpha^J) \qquad [3.5.2]$$

where D is the I-S direct dipolar coupling constant, Eq [3.4.3], and η_Q is the asymmetry in the electric field gradient q.

$$D = (\mu_o/4\pi)\,\gamma_I\,\gamma_S\,\hbar/\,(4\pi^2\,(r_{I\text{-}S})^3) \qquad [3.5.3]$$

The angular terms α^D and β^D, and α^J and β^J describe the orientation of the internuclear dipole vector $\mathbf{r}_{I\text{-}S}$ and the indirect coupling tensor J, respectively, in the principal-axis system of the electric field gradient tensor q, Fig. 3.6. However, these angular terms are notoriously difficult to determine and it is reasonable to assume that the J tensors are collinear with the internuclear dipole vector. This assumption results in a much simplified expression for D″, Eq [3.5.4]

$$D'' = (D - \Delta J/3)\,(3\cos^2\beta - 1 + \eta\sin^2\beta\cos 2\alpha) \qquad [3.5.4]$$

A schematic representation of one of the two possible cases for a spin-1/2 nucleus coupled to a spin-5/2 nucleus is depicted in Fig. 3.7, provided that first-order perturbation theory is valid. In the second case, where $\chi D''/\nu_S$ is positive, the bunching of peaks will occur at low-field and would result in a mirror image of Fig. 3.7.

The effective dipolar coupling constants, D″, and the quadrupole coupling constants cannot be determined separately from the effective dipolar-quadrupolar couplings, unless one of these quantities is known. The quadrupole coupling constants can be obtained experimentally from either NQR measurements or single-crystal NMR studies, but are remarkably difficult to determine for transition-metal complexes. Recently, it was shown by Gobetto *et al.*[49] that the effective dipolar coupling constant can be obtained for axially symmetric molecules from an analysis of spinning sideband manifolds (Eq. [3.5.5]).

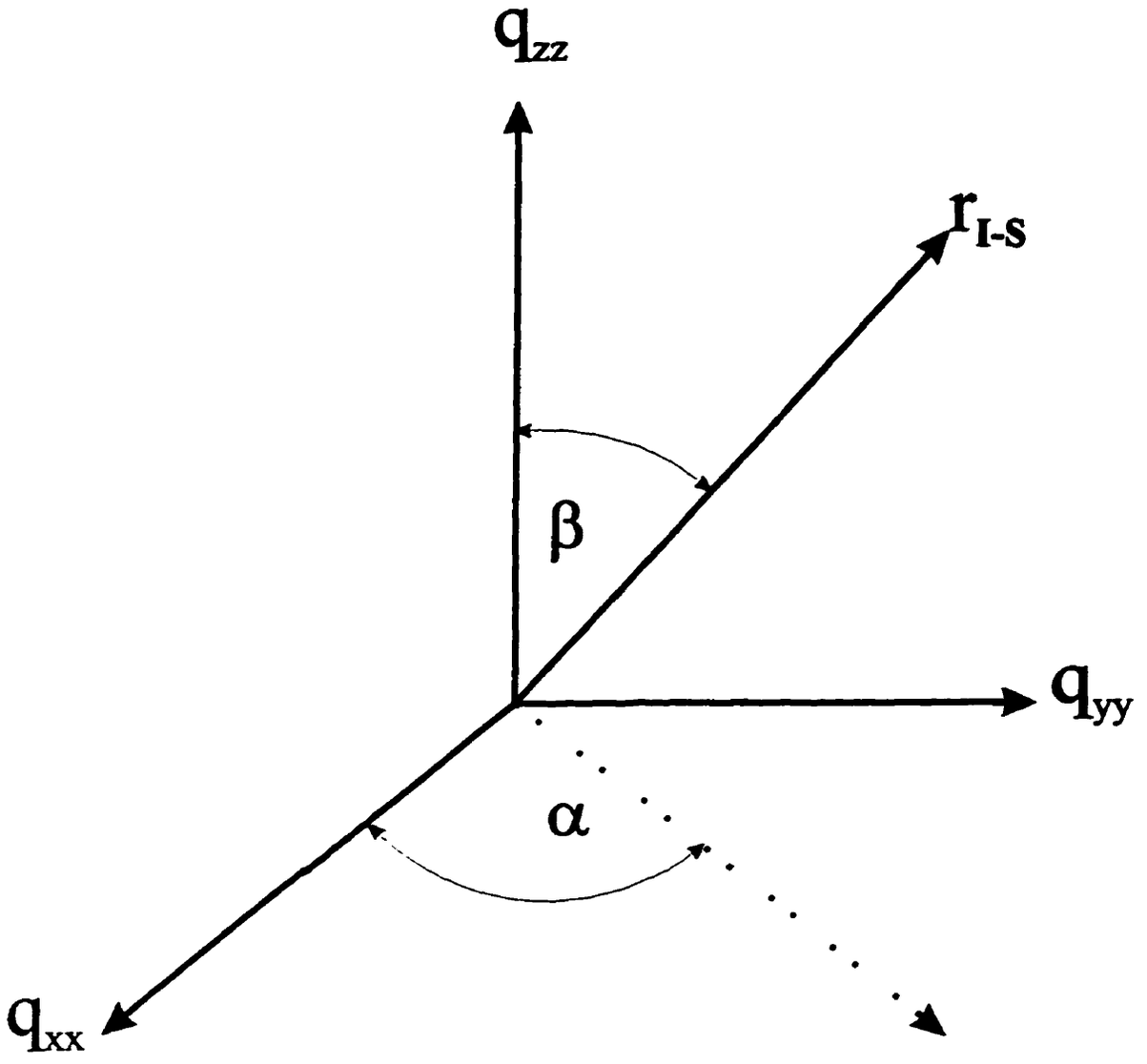

Figure 3.6. The orientation of the dipolar vector, r_{IS}, with respect to the PAS of the EFG tensor is defined by the polar angles, α and β.

$$\Delta\delta_{mI} = \Delta\delta_I - [2(D - \Delta J/3) / \nu_I]m_S \qquad [3.5.5]$$

where $\Delta\delta_I$ is the shielding anisotropy of the I nucleus, $\Delta\delta_{mI}$ is the shielding anisotropy of the I spin for the m eigenstate of the S nucleus, and ν_I is the resonance frequency of the probe nucleus. The values of D", Eq.[3.5.4], can be obtained from a regression plot of m

vs. $\Delta\delta_{ml}$, where the slope of the plot is equal to $-2(D - \Delta J/3)/\nu_S$ and the intercept equals $\Delta\delta_I$. Thus, it is possible, in principle, to obtain the dipolar coupling constant, the anisotropy in the chemical shift, the anisotropy in $J_{I\text{-}S}$, and the nuclear quadrupole coupling constant from a combination of single-crystal X-ray diffraction studies and solid-state, CP-MAS, NMR experiments.

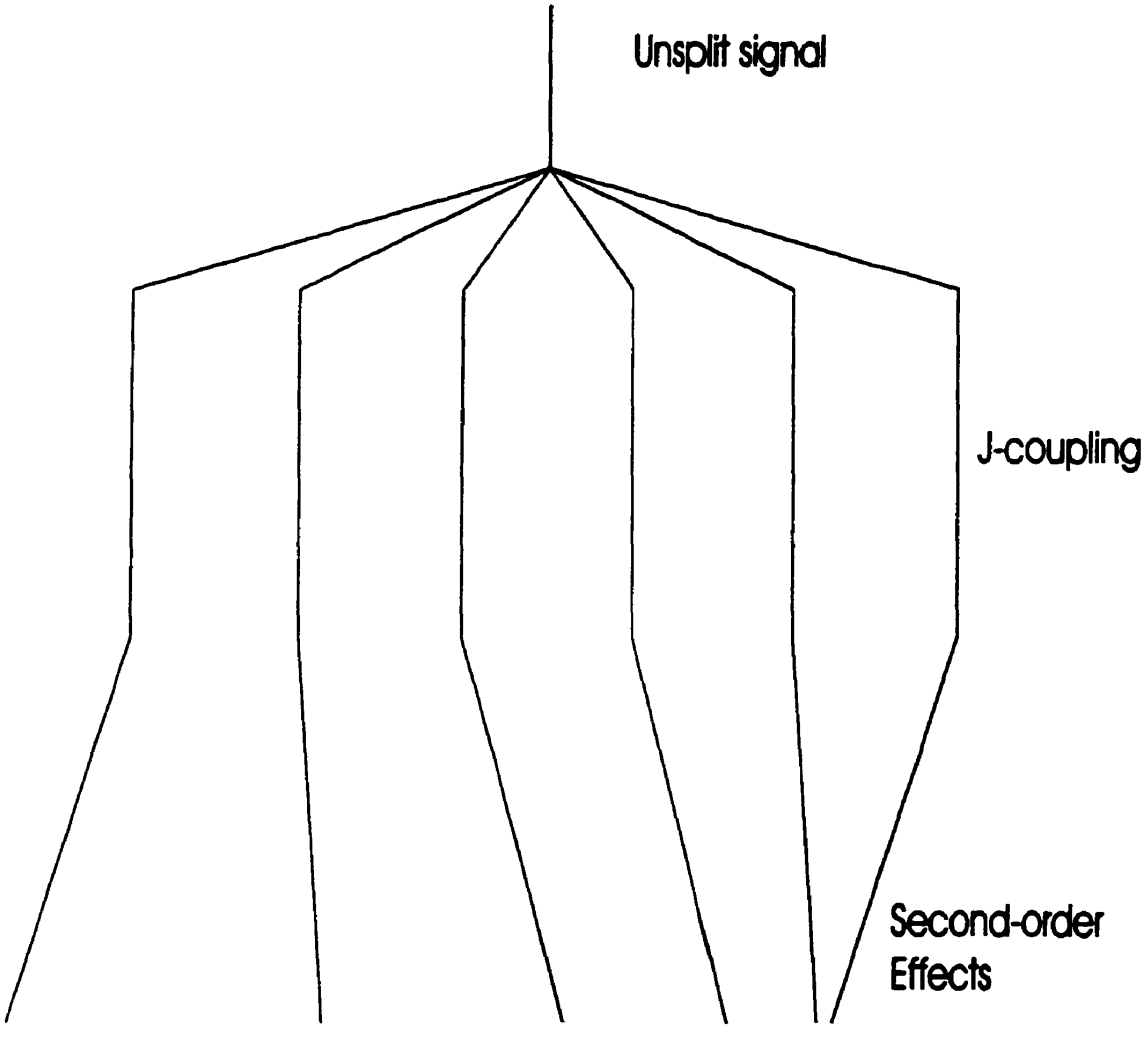

Figure 3.7. Schematic representation of the CP-MAS spectrum of ^{119}Sn coupled to a single ^{55}Mn nucleus. Spin-spin coupling results in six equally spaced lines. First-order perturbation on the ^{119}Sn spectra arising from coupling to a quadrupolar nucleus, ^{55}Mn (S = 5/2), as a function of the parameter $\chi D''/\nu_S$.

In cases where the quadrupole coupling constants are comparable to the Zeeman frequency of the quadrupolar nucleus S (i.e., when $\chi/[4S(2S-1)\nu_S] < 1$ is not fulfilled but χ is not much larger than ν_S), the use of first-order perturbation treatment is no longer valid. Therefore, the Zeeman-quadrupole eigenstates of S have to be calculated more exactly, usually by complicated time-consuming numerical methods.[43, 47-50] This involves a full Hamiltonian diagonalization for thousands of orientations in space in order to obtain the corresponding eigenstate of S, and will not be discussed here. However, this time consuming procedure can be avoided by either going to higher or lower magnetic field. The latter case is usually more accessible, in which case $\chi/[4S(2S-1)\nu_S] > 1$ and inverse perturbation can be used.[51-52] When the quadrupole coupling constant is usually large $\chi/[4S(2S-1)\nu_S] \gg 1$, fast quadrupole relaxation is able to induce a "self-decoupling" of the type described by Spiess *et al.*[53] for the case in *trans*-diiodoethylene. However, if this is not the case, the highest possible field must be used.

References

(1) E. D. Becker, C. L. Fisk and C. L. Khetrapal, " *The Development of NMR* " in *Encyclopedia of nuclear Magnetic Resonance*, D. M. Grant and R. K. Harris, Eds. (John Wiley and Sons, Chichester, England), 1, 1 (1996).

(2) G. E. Uhlenbeck and S. Goudsmith, *Naturwissenschaften*, 13, 953 (1925).

(3) W. Pauli, *Naturwissenschaften*, 12, 741 (1924).

(4) I. I. Rabi, J. R. Zacharias, S. Millaman and P. Kusch, *Phys. Rev.*, 53, 318 (1938).

(5) E. M Purcell, H. C. Torrey and R. V. Pound, *Phys. Rev.*, 69, 37 (1946).

(6) F. Bloch, W. W. Hansen and M. Packard, *Phys. Rev.*, 69, 127 (1946).

(7) E. D. Becker, *Appl. Spectrosc*, 50, 16a (1996).

(8) H. Günther, *NMR Spectroscopy, Basic Principles, Concepts, and Applications in Chemistry*, Second Edition, John Wiley & Sons, Inc., New York, 1995.

(9) (a) E. R. Andrew, A. Bradbury and R. G. Eades, *Nature*, 183, 1802 (1959).
(b) I. J. Lowe, *Phys. Rev. Lett.*, 2, 285 (1959).

(10) S. R. Hartmann and E. L. Hahn, *Phys. Rev.*, 128, 2042 (1962).

(11) A. Pines, M. G. Gibby and J. S. Waugh, *J. Chem. Phys.*, 59, 1776 (1972).

(12) W. P. Power and R. E. Wasylishen, in *Annual Reports on NMR Spectroscopy*, Vol.23, (G. A. Webb, ed.), Academic Press, New York, 1991, p. 1.

(13) U. Haeberien, *Adv. Magn. Reson., Suppl.* 1 (1976).

(14) B. C. Gerstein and C. R. Dybowski, *Transient Techniques in NMR of Solids, An Introduction to Theory and Practice*, Academic Press, New York, 1985.

(15) E. O. Stejskal and J. D. Memory, *High Resolution NMR in the Solid State*, Oxford University Press Inc., New York, 1994.

(16) D. J. Craik, in *Annual Report on NMR Spectroscopy*, Vol.15, (G. A. Webb, ed.), Academic Press, New York, 1983, p. 1.

(17) C. J. Jameson and J. Mason, in *Multinuclear NMR*, Plenum Press, New York, 1987, Chap. 3.

(18) K. Hallenga and A. I. Popov, in *Modern NMR Techniques and Their Application in Chemistry*, Marcel Dekker Inc., New York, 1991, Chap. 1.

(19) M. Witanowski, L. Stefaniak and G. A. Webb, in *Annual Report on NMR Spectroscopy*, Vol. 7, (G. A. Webb, ed.), Academic Press, New York, 1977, p. 117.

(20) J. Lounila and J. Jokisaari, *Prog. NMR Spectrosc.*, **15**, 249 (1982).

(21) J. Jokisaari, Y. Hiltunen and J. Lounila, *J. Chem. Phys.*, **85**, 3189 (1986) and references therein.

(22) C. J. Jameson and J. Mason, in *Multinuclear NMR*, Plenum Press, New York, 1987, Chap. 4.

(23) D. C. Apperley, H. Bai, and R. K. Harris, *Mol. Phys.*, **68**, 1277 (1989).

(24) C. J. Jameson and J. Mason, in *Multinuclear NMR*, Plenum Press, New York, 1987, Chap. 4.

(25) K. Eichele, R. E. Wasylishen, K. Maitra, J. H. Nelson and J. F. Britten, *Inorg. Chem.*, **36**, 3539 (1997).

(26) R. K. Harris and A. C. Olivieri, *Prog. Nucl. Magn. Reson. Spectrosc.*, **24**, 435 (1992) and references therein.

(27) K. Eichele and R. E. Wasylishen, *J. Magn. Reson.*, **106**, 46 (1994) .

(28) C. W. Kirby, M. D. Lumsden and R. E. Wasylishen, *Can. J. Chem.*, **73**, 604 (1995) and references therein.

(29) A. C. Diz, C. G. Giribet, M. C. Ruiz de Azúa and R. H. Contreras, *Int. J. Quantum chem.*, **37**, 663 (1990).

(30) J. A. González, G. A. Aucar, M. C. Ruiz de Azúa and R. H. Contreras, *Int. J. Quantum Chem.*, **61**, 823 (1997).

(31) N. F. Ramsey, *Phys. Rev.*, **91**, 303 (1953).

(32) C. Juan and H. S. Gutowsky, *J. Chem. Phys.*, **37**, 2198 (1962).

(33) D. F. R. Gilson, *J. Chem. Phys.*, **43**, 312 (1965).

(34) B. P. Dailey and C. H. Townes, *J. Chem. Phys.*, **23**, 118 (1955).

(35) K. Eichele and R. E. Wasylishen, *Angew. Chem. Int. Ed. Engl.*, **31**, 1222 (1992).

(36) S.H. Alarcón, A. C. Olivieri and R. K. Harris, *Solid State Nucl. Magn. Reson.*, **2**, 325 (1993).

(37) P. Grondona and A. C. Olivieri, *Concepts in Magn. Reson.*, **5**, 319 (1993).

(38) V. C Gibson, R. Gobetto, R. K. Harris, C. Langdale-Brown and U. Siemeling, *J. Organomet. Chem.*, **479**, 207 (1994).

(39) K. Eichele and R. E. Wasylishen, *Inorg. Chem.*, **33**, 2766 (1994).

(40) H. Li, I. S. Butler D. F. R. Gilson, J. F. Harrod, and F. G. Morin, *J. Phys. Chem.*, **99**, 8490 (1995).

(41) N. A. Davies, R. K. Harris and A. C. Olivieri, *Mol. Phys.*, **87**, 669 (1996).

(42) D. Christendat, R. D. Markwell, D. F. R. Gilson, I. S. Butler and J. D. Cotton, *Inorg. Chem.*, **36**, 230 (1997).

(43) E. M. Menger and W. S. Veeman, *J. Magn. Reson.*, **46**, 257 (1982).

(44) A. Naito, S. Ganapathy and C. A. McDowell, *J. Chem. Phys.*, **74**, 5393 (1981).

(45) N. Zumbulyadis, P. M. Henrichs and R. H. Young, *J. Chem. Phys.*, **75**, 1603 (1981).

(46) J. G. Hexem, M. H. Frey and S. J. Opella, *J. Chem. Phys.*, **77**, 3847 (1982).

(47) A. C. Olivieri, *J. Magn. Reson.*, **81**, 201 (1989).

(48) A. C. Olivieri, *J. Magn. Reson.*, **82**, 342 (1989).

(49) R. Gobetto, R. K. Harris and D. C. Apperley, *J. Magn. Reson.*, **96**, 119 (1992).

(50) J. Böhm, D. Fenkze and H. Pfeifer, *J. Magn. Reson.*, **55**, 197 (1983).

(51) A. C. Olivieri, *J. Magn. Reson. Series A*, **101**, 313 (1993).

(52) S. H. Alarcon, A. C. Olivieri, S. A. Carss and R. K. Harris, *Magn. Reson. Chem.*, **33**, 603 (1995).

(53) H. W. Spiess, U. Haeberlen and H. Zimmermann, *J. Magn. Reson.*, **25**, 55 (1977).

Chapter 4

Solid-State, Phosphorus-31, CP-MAS, NMR Studies of Tertiary Phosphine Substituted Alkyl- and Acyl(tetracarbonyl)manganese(I) Complexes

4.1 Introduction

The wide chemical shift range, 100% natural abundance, high sensitivity, and large spin-spin interactions make the ^{31}P nucleus an ideal NMR probe for the study of chemical structures, bonding interactions, and molecular dynamics. When a phosphorus ligand is coordinated to a metal centre, the ^{31}P chemical shift is influenced by such factors as the metal atom, the bonding interaction between the phosphorus and the metal atom, and the oxidation state and coordination number of the metal. The influence of the *cis* and *trans* ligands, and the position of the phosphorus ligand within the coordination sphere can also have a large effect on the chemical shifts. Most of the theoretical and experimental work on transition metal-tertiary phosphine complexes has involved studies of isotropic chemical shifts in solution.[1-3] A change in the molecular structure may lead to small changes in the isotropic shift and spin-spin coupling but to significant differences in their tensor components. Therefore, the anisotropy of these shifts can be more informative than are the isotropic values and this information can be obtained from solid-state ^{31}P NMR spectra.

We report in this section of the thesis the results of an analysis of the solid-state, CP-MAS, ^{31}P NMR spectra of a series of tertiary phosphine substituted alkyl-, phenylacyl- and (2,4,6-trimethylphenyl)acyl(tetracarbonyl)manganese(I) complexes,

Table 1.2. These types of complexes have received considerable attention for the past 25 years due to their mechanistic importance in homogeneous hydroformylation reactions and other catalytic processes that involve alkyl migration, carbonyl insertion, or carbonyl elimination reactions.[4-6]

The first alkyl- and acylmanganese(I) phosphine complexes were prepared in the early 1960s by Kraihanzel and Maples[7] by the reaction of methyl(pentacarbonyl)-manganese(I) with triphenylphosphine and the *cis* and *trans* isomers of $CH_3Mn(CO)_4(PPh_3)$ and $CH_3C(O)Mn(CO)_4(PPh_3)$ were identified. Subsequent X-ray structural analysis of these complexes revealed that the crystal structures are disordered and confirmed the presence of the *cis* and *trans* isomers.[8,9] These results led to speculation that both the methyl and/or the carbonyl groups can migrate. It was 10 years later that Flood *et al.*[10], by using ^{13}CO, and Cotton *et al.*[11-13], by using large alkyl groups, established that the alkyl group migrates onto a carbonyl group and that the carbonyl group does not insert into the metal-alkyl bond. In our work, we also decided to study these complexes by FT-IR, FT-Raman and solution NMR spectroscopy, and single-crystal X-ray diffraction to test for the presence of *cis-trans* isomers and to detect the differences in the magnetic properties of the alkyl and acyl complexes.

The electric quadrupole moment of ^{55}Mn is large but direct nuclear quadrupole resonance measurements have been reported for only a few manganese carbonyl compounds. If quadrupolar relaxation is dominant, then the NMR line widths, i.e. $1/T_1$, of the ^{55}Mn resonances in solution are proportional to the square of the NQR coupling constant. Brown *et al.*[14] have shown that such a relationship exists for several manganese

complexes in tetrahydrofuran solution. Thus, the NQR coupling constants can be estimated from ^{55}Mn solution NMR linewidths and such data are also reported in this section of the thesis.

4.2 Result and Discussion

The ^{31}P NMR spectra of all the alkyl- and acylmanganese(I) complexes in solution exhibited only sharp singlets in the 50-62 ppm range, indicating the presence of a single isomer. The ^{13}C NMR solution spectra in the carbonyl region contained three sets of doublets confirming the presence of three different carbons each coupled to phosphorus. The two-bond, carbon-phosphorus, spin-spin coupling constants, $^2J_{C\text{-}P}$, for the acyl, alkyl and carbonyl groups are given in Table 4.1. The $^2J_{C\text{-}P}$ values for the carbonyl groups *trans* to another carbonyl ligand lie in the range 19-23 Hz and showed little or no variation for the series of complexes studied. The values are about 10 Hz larger for the carbonyl group *trans* to an acyl or alkyl group, and similar values were obtained for the CO ligand *trans* to the tertiary phosphine substituent in the alkyl complexes. It was observed that the $^2J_{C\text{-}P}$ values for the acyl groups are larger than are those of the alkyl compounds, and the $^2J_{C\text{-}P}$ values for the CO group *trans* to the acyl groups are about 3 Hz smaller compared to those for the alkyl complexes. These effects can be attributed to a Fermi contact mechanism [3.4.2] because the acyl carbons are sp^2 hybridized while those of the alkyl groups are sp^3 hybridized.

The FT-IR and FT-Raman spectra exhibited four vibrational modes in the 2250-1850 cm^{-1} carbonyl region (Fig. 4.1). Group theory for an octahedral $RMn(CO)_4L$ species, with C_{4v} symmetry, predicts two IR-active ($a_1 + e$) and three Raman-active ($a_1 + b_1 + e$)

Table 4.1. $^2J_{P-C}$ Coupling constants for compounds III-IX[a]

compound	C^b (Hz)	$^{\alpha}CO^c$ (Hz)	$^{\beta}CO^d$ (Hz)	$^{\gamma}CO^e$ (Hz)
$PhCH_2C(O)Mn(CO)_4(PPh_3)$ (III)	16.3	12.3	6.0	20.1
$MesCH_2C(O)Mn(CO)_4(PPh_3)$ (IV)	14.3	12.3	5.2	21.3
$PhCH_2C(O)Mn(CO)_4[P(C_6H_{11})_3]$ (V)	13.1	14.9	5.1	19.4
$MesCH_2C(O)Mn(CO)_4[P(C_6H_{11})_3]$ (VI)	11.5	16.7	3.1	19.7
$PhCH_2Mn(CO)_4(PPh_3)$ (VII)	8.4	21.1	10.1	20.3
$PhCH_2Mn(CO)_4[P(Tolyl)_3]$ (VIII)	8.5	21.4	9.3	22.7
$PhCH_2Mn(CO)_4[P(PhF)_3]$ (IX)	8.1	19.7	8.3	21.3

[a]Data from solution ^{13}C NMR spectra with an uncertainty of ± 0.5 Hz.
[b]Acyl or alkyl group.
[c]CO *trans* to tertiary phosphine.
[d]CO *trans* to alkyl or acyl group.
[e]CO *trans* to CO.

vibrational modes for the *trans* isomer, but four IR-active and four Raman-active ($2a_1 + b_1 + b_2$) vibrational modes for the C_{2v} *cis* isomer. The solution ^{31}P NMR, FT-IR and FT-Raman spectra therefore indicate *cis* geometry for all the alkyl and acyl complexes studied, which is in agreement with previous reports for *cis*-$R'Mn(CO)_4(PR_3)$ complexes.[10-13] From these results, the possible mechanistic pathways are alkyl or carbonyl group migration but not a combination of both processes. The latter would result

in a mixture of *cis* and *trans* isomers for the alkyl and acyl complexes, and this was not observed. Introduction of a bulky group, 2,4,6-trimethylbenzyl, did not lead to carbonyl elimination for the acyl complexes. This may due to the steric crowding of the methyl groups on the phenyl ring, which hinders the alkyl group from re-migrating. If the reactions proceed by carbonyl migration, it should then be possible for the acyl CO group located between the metal and the alkyl group to be eliminated, affording a metal-alkyl bond, but this was not observed and it was concluded that the reactions proceeded by alkyl migration and not by carbonyl migration, in agreement with earlier studies.[10-13]

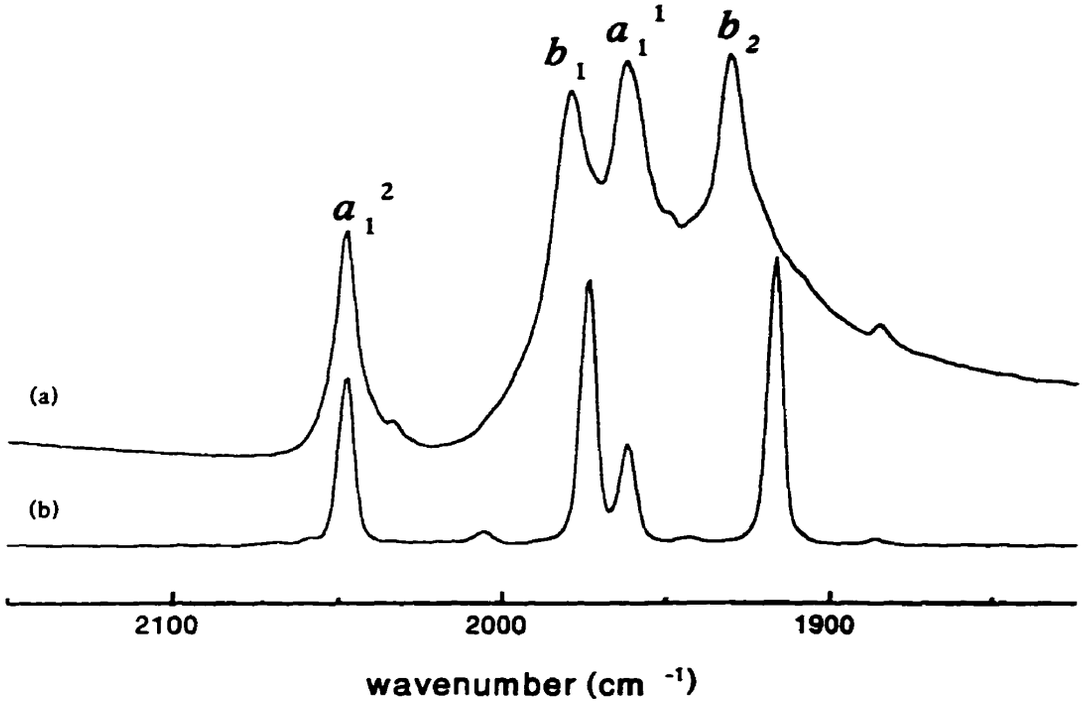

Figure 4.1. (a) FT-IR and (b) FT-Raman spectra of *cis*-$PhCH_2Mn(CO)_4(PPh_3)$ in the carbonyl region showing the four vibrational modes, a_1^2, b_1, a_1^1, and b_2 in decreasing wavenumber.

The crystals for the structure determination of benzyl(tetracarbonyl)(triarylphosphine)manganese(I) **VII-IX** and benzyl(tetracarbonyl)(tricyclohexylphosphine)-manganese(I) **X** were obtained by slow evaporation of the appropriate solvent (see Chapter 2), and it was found that only the *cis* isomer was present in each case (Appendix I). The structures of these alkyl complexes also strongly indicate that the only mechanism operative is alkyl migration. However, single crystals of the acyl product suitable for X-ray structure determination could not be obtained.

Table 4.2. Solution and solid-state ^{31}P NMR isotropic chemical shifts and coupling constants of compounds **III-IX**

Compound	δ_{iso} (soln)[a]	δ_{iso} (solid)[a]	J_{Mn-P} (solid) (Hz)	d[b] (Hz)
$BzC(O)Mn(CO)_4(PPh_3)$ **(III)**	50.6	54.1	216 (4)	109 (1)
$MesCH_2C(O)Mn(CO)_4(PPh_3)$ **(IV)**	51.2	53.2	233 (2)	112 (1)
$BzC(O)Mn(CO)_4[P(C_6H_{11})_3]$ **(V)**	53.2	55.4	220(2)	108(3)
$MesCH_2C(O)Mn(CO)_4[P(C_6H_{11})_3]$ **(VI)**	54.7	54.4	232(2)	97(3)
$BzMn(CO)_4(PPh_3)$ **(VII)**	61.4	68.0	202 (2)	110 (2)
$BzMn(CO)_4[P(Tolyl)_3]$ **(VIII)**	59.0	65.6	196 (3)	103 (2)
$BzMn(CO)_4[P(PhF)_3]$ **(IX)**	61.1	66.1	204 (1)	114 (3)

[a]Uncertainties are ± 0.2 and ± 0.5 ppm for the solution and solid-state ^{31}P NMR spectra, respectively.
[b]$d = 3\chi D'/10\nu_S$.

The measured ^{31}P chemical shifts of compounds **III-IX** in solution and the solid state are given in Table 4.2. The isotropic chemical shifts, δ_{iso}, in the solid state are close to the values obtained for the solutions indicating that the structures are the same in the solid-state and in solution. The chemical shifts for the alkyl complexes are more deshielded than are those for the acyl compounds. This may be due to the greater shielding effects of the acyl group *cis* to the tertiary phosphine ligand. The spin-spin coupling between phosphorus and manganese, $^1J_{Mn-P}$, cannot be determined from the solution ^{31}P NMR spectra because of fast quadrupolar relaxation processes. However, it could be observed in the solution ^{55}Mn NMR spectra for the alkyl complexes, **VI-IX**, and in the solid-state ^{31}P NMR spectra for both the acyl and alkyl compounds. The $^1J_{Mn-P}$ values obtained from the solution ^{55}Mn NMR spectra were ~50 Hz larger than were those obtained from the ^{31}P solid-state NMR spectra for the alkyl complexes. This may be due to changes in torsion angle of the aryl rings which, in this case, are found to increase the $^1J_{Mn-P}$ coupling. The ^{55}Mn NMR chemical shift for compound **VII** was determined previously by Cotton *et al.*[13], DeShong *et al.*[15] and Rehder[16] to be -1819 ppm with a $^1J_{Mn-P}$ value of 260 ± 8 Hz. These values are in excellent agreement with those obtained in this study, -1819 ppm and $^1J_{Mn-P}$ = 257 ± 2 Hz. The value reported by Torocheshniknov *et al.*,[17] δ_{Mn} -1939 ppm ($\Delta\nu_{1/2}$ = 22,000 Hz), appears to belong to the *trans* isomer with no $^1J_{Mn-P}$ coupling. The solution ^{55}Mn NMR spectra for the acyl compounds were very broad with $\Delta\nu_{1/2}$ = 2100-3400 Hz and no $^1J_{Mn-P}$ splitting was observed. The absence of spin-spin coupling of the acyl compounds **III-VI** in the solution ^{55}Mn spectra may be due to a much faster quadrupolar relaxation than those of the alkyl complexes, **VII-IX**.

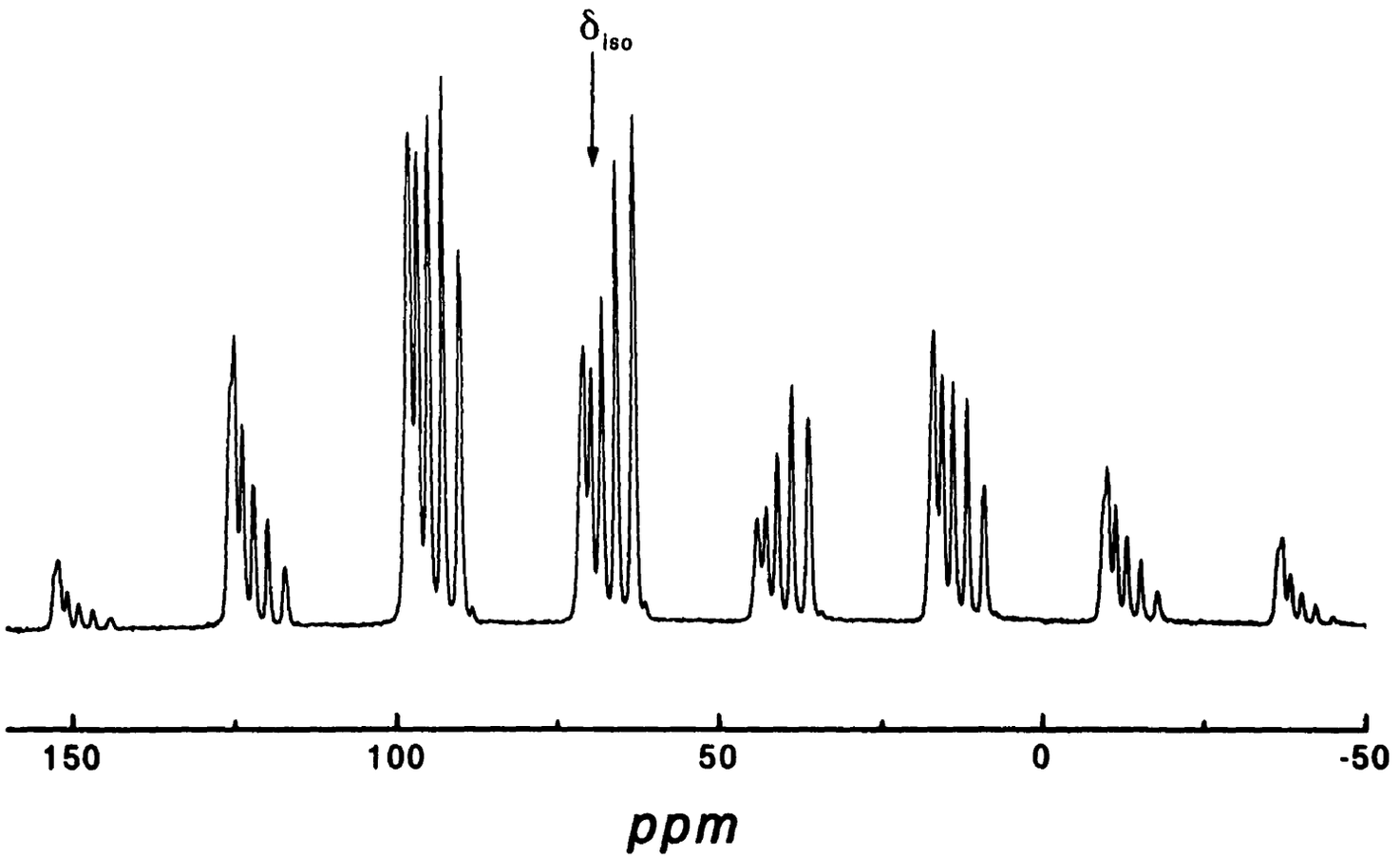

Figure 4.2. Solid-state ^{31}P CP-MAS NMR spectra of *cis*-$PhCH_2Mn(CO)_4PPh_3$, including spinning sidebands (rotor frequency = 2,800 Hz, 508 scans), obtained at 121.279 MHz with proton decoupling.

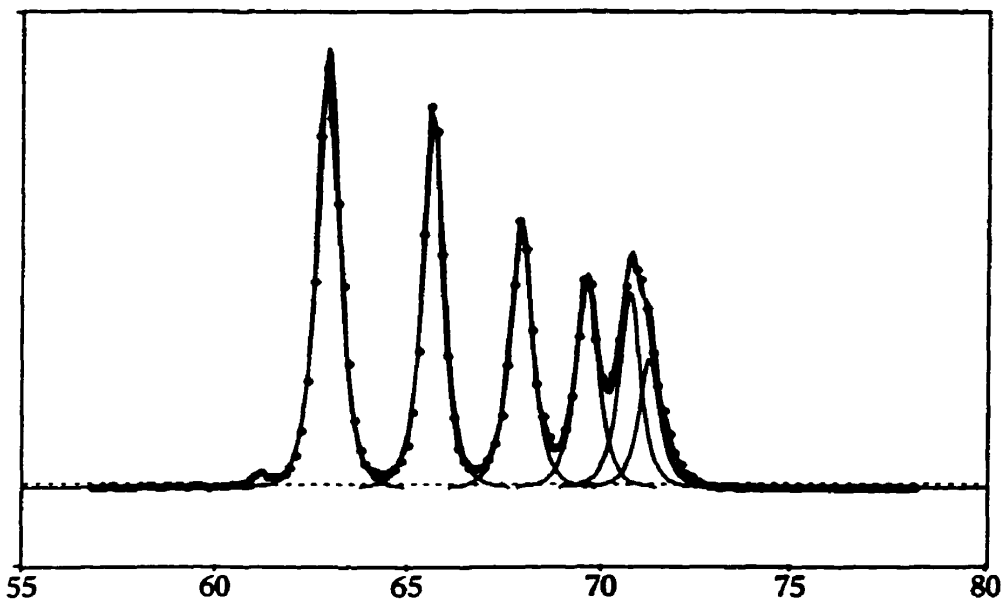

Figure 4.3. Experimental solid-state ^{31}P CP-MAS NMR centreband of *cis*-$PhCH_2$-$Mn(CO)_4PPh_3$ (upper trace) and simulated peakfit (bottom).

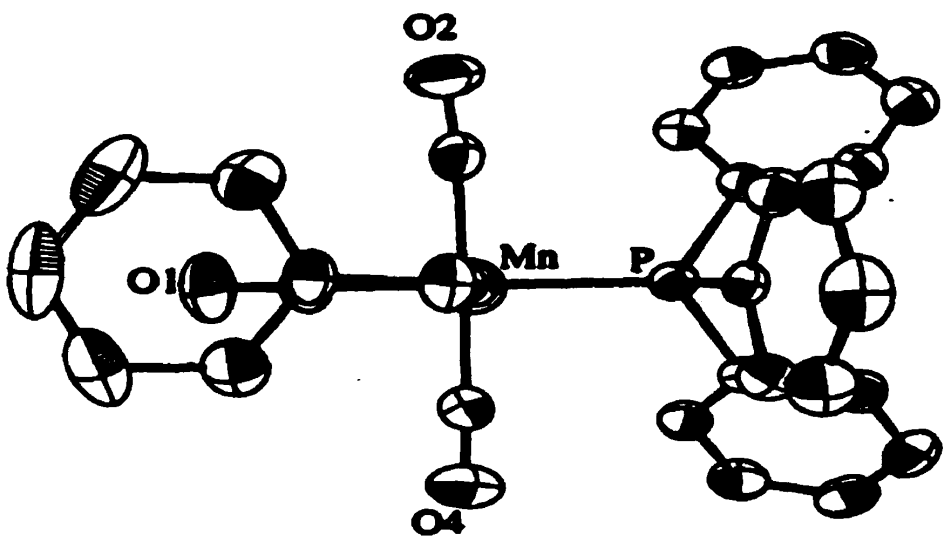

Figure 4.4. X-ray structure of *cis*-$BzMn(CO)_4PPh_3$ showing the mirror plane.

The solid-state ^{31}P NMR spectra are complicated (Fig. 4.2) and second-order effects are evident due to the presence of the quadrupolar ^{55}Mn nucleus (S = 5/2). Peak fitting (Fig. 4.3) and centreband analyses were feasible for all the compounds, by using Eq. [3.5.1], which resulted in the determination of J_{Mn-P}, the quadrupolar-dipolar constants, d, and the isotropic chemical shifts. The $^1J_{Mn-P}$ couplings for the acyl compounds lie in the 216-233 Hz range, about 10 Hz larger than for the alkyl complexes. The values for the substituted phenylacyl complexes, IV and VI, are about 12 Hz greater than are those for the unsubstituted phenylacyl compounds, III and V. The $^1J_{Mn-P}$ values obtained by Lindner *et al.*[18] for a series of bromo complexes lie in the range 197-210 Hz and are of similar magnitude to those obtained for the alkyl complexes. The values reported by Gobetto *et al.*[19] for $Mn_2(CO)_9PPh_3$ and $Mn_2(CO)_8(PPh_3)_2$ are 70 and 105 Hz larger, respectively, chiefly because of increasing π-donation to the phosphorus centre when compared to our *cis* complexes. The ^{31}P chemical shifts of the alkyl complexes, both in solution and the solid state, are about 10 ppm less shielded than are those for the acyl complexes (Table 4.2). These differences may be due to the steric and shielding effects of the oxygen atoms of the acyl groups on the tertiary phosphine ligand. The effective dipolar-quadrupolar term, d, shows little or no variation throughout the series of compounds investigated and falls in the 97-114 Hz range .

X-ray diffraction studies have shown that these types of alkyl complexes possess a plane of symmetry (Appendix I) which results in the angle α in Eq. [3.5.4] being equal to 0 or 90° (Fig. 4.4). In turn, this leads to a simplified expression for D', with only three unknowns (Eq. [4.2.1]):

$$D' = (D - \Delta J/3)\,(3\cos^2\beta - 1 - \eta\sin^2\beta) \qquad [4.2.1]$$

It is notoriously difficult to determine the angular term, β, and the asymmetry parameter, η. Using model calculations for bromo(pentacarbonyl)manganese(I), Lindner *et al.*[18] have estimated that η is in the range of 0-0.12. Later, based on symmetry arguments, Gobetto *et al.*[19] assumed η values of 0 for $[Mn(CO)_4(PPh_3)]_2$ and $Mn_2(CO)_9(PPh_3)$.

Crystal structures of the alkyl complexes have been determined and the *cis*-C-Mn-C angles were found to be within 5° of 90° (Appendix I) suggesting that η should be close to or equal to zero. It is known that trialkyl- and triarylphosphines are strong σ-donor and good π-acceptor ligands compared to alkyl groups. Therefore, the principal component of the electric field gradient, q_{zz}, is assumed to lie along the Mn-P bond direction. From the centreband analysis, it was shown that the effective dipolar-quadrupolar term, $(3/20)\chi D'/\nu_S$, is positive, i.e., bunching of the peaks occurs to lower field (Fig. 4.3). Brown *et al.*,[14] Lindner *et al.*[18] and Gobetto *et al.*[19] have demonstrated that the χ values for similar types of compound are always positive. Therefore, D' is also positive, which indicates further that the angle β is close to 0°. In principle, confirmation can be obtained from the spectrum of a second nucleus bonded to the manganese atom since the quadrupole coupling constant is unchanged but the angles α and β are different. The anisotropy of the spin-spin coupling, the quadrupole coupling, and the asymmetry in the field gradient remain unknown. We have examined the solid-state ^{13}C NMR signals of the benzyl methylene group in compound **V** at 2.5 and 7.5 T. The angle β was determined to be close to 90° in this case. Second-order effects were observed, with a bunching of the peaks to low frequency, but the spectra were difficult to analyze due to overlapping peaks, even at

low field. We attempted to fit the envelope of the methylene resonance with values for the spin-spin coupling, $^2J_{P\text{-}C}$, of 8.4 Hz from the ^{13}C solution spectrum and $^1J_{Mn\text{-}C}$ of 23.1 Hz estimated by Torochesnikov *et al.*[21] from the line broadening of the resonance line. Using the χ value from the ^{31}P spectrum, the difference between the inner and outer line positions was calculated to be 143 Hz, compared with the experimental value of 203 Hz. This result led us to believe that the value of $^1J_{Mn\text{-}C}$ reported by Torochesnikov *et al.*[21] is incorrect and in fact belong to the *trans* isomer, as was assumed from the ^{55}Mn solution NMR peak width at half-height. The value of $^1J_{Mn\text{-}C}$ obtained for the methylene carbon of compound VII is 38 Hz with the assumption that $\Delta J_{Mn\text{-}C}$ and η are zero, and $\beta^D = 90°$ for the ^{13}C NMR spectra. Based on the solid-state ^{13}C and ^{31}P NMR data and the crystal structures, we feel confident in assuming that the angular term $\beta = 0$ for the ^{31}P analysis. This leads to an even greater simplification of the expression for D' (Eq. [4.2.2]):

$$D' = 2\,(D - \Delta J/3) \qquad [4.2.2]$$

In principle, the chemical shift tensors for each of the m-I transitions can be obtained from the non-spinning spectra, but these were very difficult to analyze for the compounds studied, because of the overlapping of six powder patterns (Fig. 4.5). However, bandfitting of the spinning sidebands and using a modified Herzfeld and Berger program[20] afforded the chemical shift tensors (Table 4.3). The differences between successive values of δ_{Im} (Eq. [3.5.5]) are constant and equal to D'. Values of D' were obtained from a regression plot of m *vs.* δ_{Im}, where the slope of the graph is equal to $-2D'/\nu_I$ and the intercept equals δ_I (Eq. [3.5.5]), Fig 4.6. The average values of $(D\text{-}\Delta J/3)$ were found to lie in the 1030-1135 Hz range and χ, using Eq. 3.5.1, is about 23-26 MHz

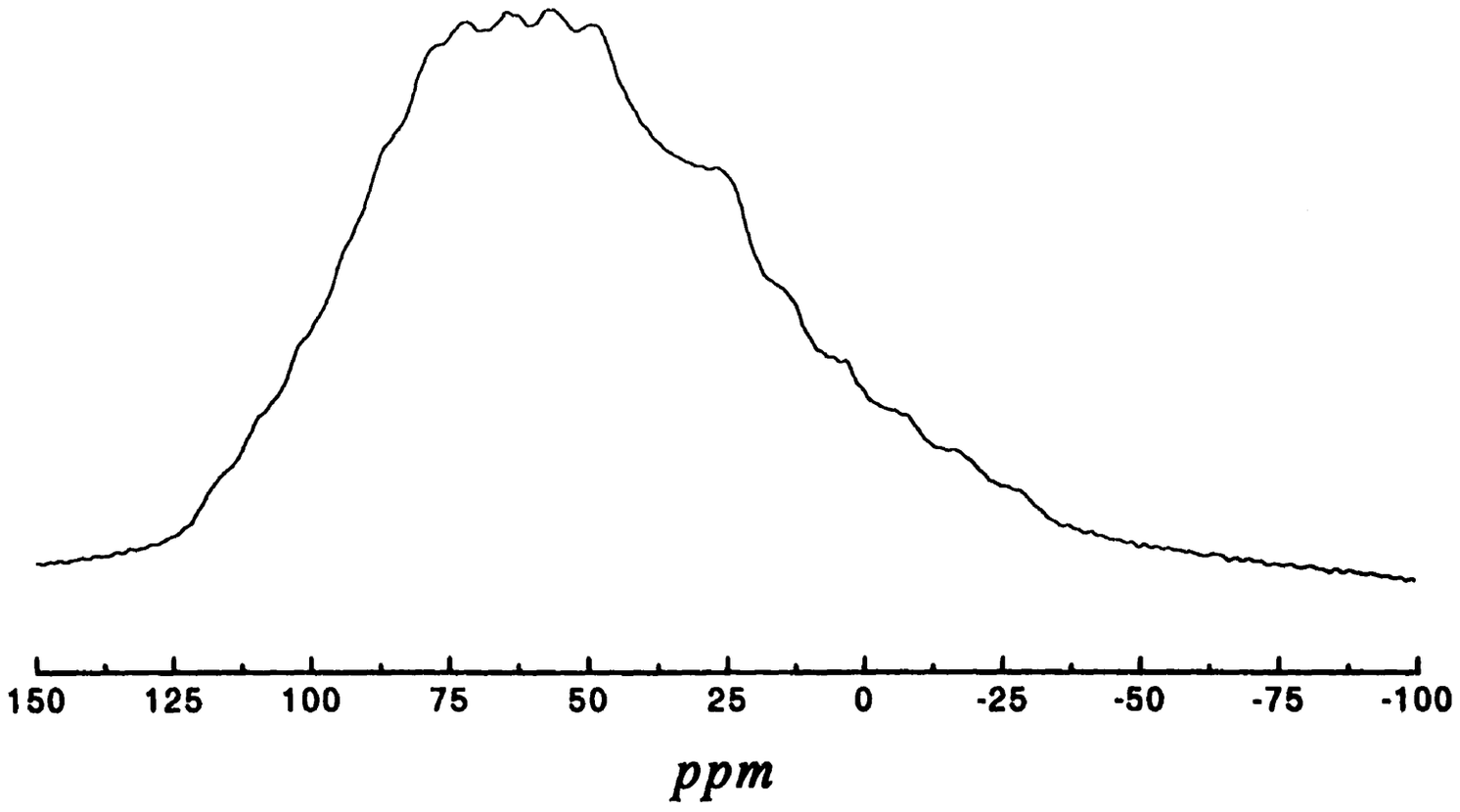

Figure 4.5. Solid-state ^{31}P CP-NMR power pattern for *cis*-$MesCH_2C(O)Mn(CO)_4PCy_3$.

Table 4.3. Effective dipolar and chemical shift tensor data for *cis*-$BzMn(CO)_4(PPh_3)$ from spinning sidebands analysis[a]

m	Centreband δ (± 0.2 ppm)	δ_{11} (ppm)	δ_{22} (ppm)	δ_{33} (ppm)	$\Delta\delta_{lm}$ (ppm)	D' (Hz)
5/2	62.9	111.4	82.2	-4.8	-101.6	1097
3/2	65.7	120.4	90.6	-14.0	-119.5	1105
1/2	67.9	127.0	100.3	-23.6	-137.3	1163
-1/2	69.6	134.8	108.9	-34.8	-156.6	1190
-3/2	70.7	141.3	122.1	-51.3	-183.0	1460[b]
-5/2	71.7	157.0	107.3	-50.9	-183.1	880[b]

[a]Uncertainty is ± 2 ppm for tensor quantities obtained from the MAS spectra at three different spinning speeds.
[b]Reduced accuracy because of overlapping peaks.

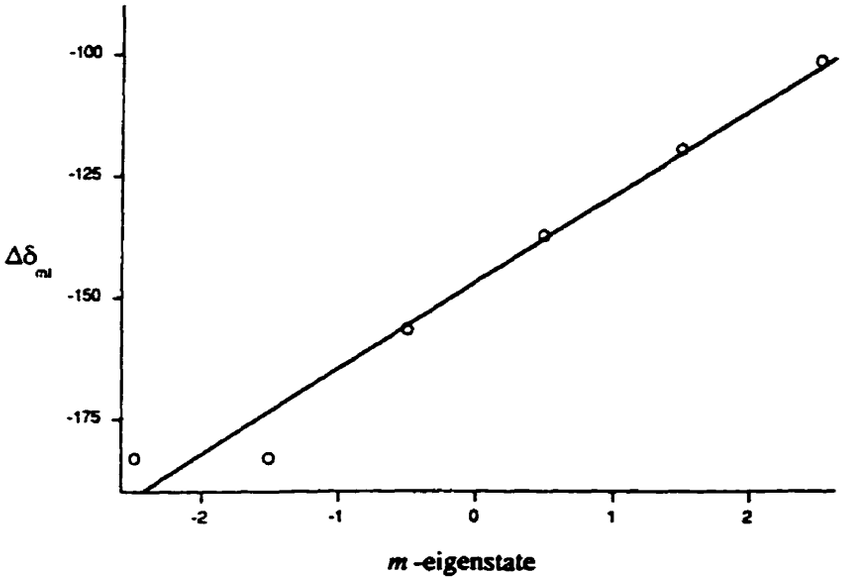

Figure 4.6. Regression plot of m eigenstate of the quadrupolar (^{55}Mn) nucleus *versus* the shielding anisotropy, $\Delta\delta_{ml}$ for *cis*-$BzMn(CO)_4(PPh_3)$.

for the compounds studied, with the exception of compound III (Table 4.4).

Brown and co-workers[14] have shown that the line widths in the solution spectra of the quadrupolar nucleus are proportional to the square of the nuclear quadrupole coupling constant, provided that the molecules have the same correlation time for molecular rotation, which in turn depends upon the molecular volume and solvent viscosity. Quadrupolar relaxation must be dominant and, since $^{1}J_{Mn-P}$ was observed in the ^{55}Mn spectra of the alkyl compounds, this mechanism does not apply in these cases. The molecular volumes of the alkyl and acyl complexes are much larger than are the volumes of the compounds examined by Brown *et al.*[14] and thus the line-width dependence on the quadrupole moment should reflect this. Only a poor correlation was obtained for the acyl complexes due to the narrow range covered by the data.

Table 4.4. Calculated effective dipolar coupling constants, quadrupolar coupling constants, and spin-spin anisotropy for compounds III-IX

compound	D (Hz)	χ (MHz)	χ[a] (MHz)	ΔJ (Hz)
$BzC(O)Mn(CO)_4(PPh_3)$ (III)	1342(131)	20.2(0.7)	29.3	1219(43)
$MesCH_2C(O)Mn(CO)_4(PPh_3)$ (IV)	1132(46)	24.5(1.0)	34.5	589(24)
$BzC(O)Mn(CO)_4[P(C_6H_{11})_3]$ (V)	1079(73)	24.8(1.6)	37.6	639(41)
$MesCH_2C(O)Mn(CO)_4[P(C_6H_{11})_3]$ (VI)	1031(19)	23.3(0.4)	38.7	495(10)
$BzMn(CO)_4(PPh_3)$ (VII)	1073(35)	25.4(0.8)	8.44	412(13)
$BzMn(CO)_4[P(Tolyl)_3]$ (VIII)	1105(50)	23.1(1.0)	7.71	508(22)
$BzMn(CO)_4[P(PhF)_3]$ (IX)	1115(54)	25.4(1.2)	9.43	538(30)

[a]Calculated from linewidth dependence according to ref (14).

The χ values obtained from our solid-state ^{31}P NMR experiments can be compared with the value of 16.9 MHz obtained by Lindner *et al.*[18] for the bromo-substituted manganese-triphenylphosphine complex, but where the anisotropy in the spin-spin coupling was neglected, and the 17.5 MHz value obtained by Brown *et al.*[14] for $BrMn(CO)_5$. The value calculated by Gobetto *et al.*[19] for $Mn_2(CO)_9PPh_3$ was 41.6 MHz, which is nearly twice the value observed for the compounds studied in the present work. This discrepancy is due to an error in the calculation of D' by Gobetto *et al.*[19] and recalculation of D' using the values given in Table IV of reference 19, affords D' = 1033 $\pm$ 21 Hz and χ = 29.5 $\pm$ 0.6 MHz, which are closer to the values obtained for compounds III-IX. From the crystal structural data and spinning sidebands analysis, the dipolar coupling constants and the spin-spin anisotropies were determined to be in the range of 869-945 Hz and 400-640 Hz, respectively, with the exception of compound IV, where ΔJ was much larger (1220 Hz). The values of D and ΔJ for the acyl complexes were calculated with the assumption that r_{Mn-P} is the same as those of the respective alkyl-phosphine complexes. This assumption was based on the fact that the r_{Mn-P} values for $CH_3C(O)Mn(CO)_4(PPh_3)$ and $CH_3Mn(CO)_4(PPh_3)$, of 2.315 and 2.311 $\pm$ 0.018 Å, respectively, show little change on going from the acetyl to the methyl complex.

The magnitude and principal components of the phosphorus chemical shifts tensors are given in Table 4.5. There is very little change in the ^{31}P isotropic chemical shifts for the alkyl complexes containing *para*-substituted triarylphosphines. This was also observed for the phenylacyl and substituted phenylacyl complexes with triphenylphosphine and tricyclohexylphosphine (Table 4.2). However, there are major

differences in the anisotropy parameter, $\Delta\delta$, and the span of the chemical shifts tensors, δ_{33}-δ_{11}, both of which are larger for the benzyl complexes than for the phenylacyl derivatives. The δ_{33} value shows little variation for the triarylphosphine complexes, ranging from -18.4 to -32.2 ppm. These values are in the same range as those obtained by Lindner *et al.*[18], -16 to -32 ppm, for a series of alkyl(diaryl)phosphine complexes. From these results, the orientation of δ_{33} at the phosphorus atom was assigned as lying close to, or along, the Mn-P bond, and the remaining two components, δ_{11} and δ_{22}, must therefore lie perpendicular to this axis. It was observed that δ_{22} is more shielded, >28 ppm, for the acyl complexes than for the alkyl compounds investigated. From these observations, we assign δ_{22} to be perpendicular to the Mn-C bond of the acyl and the alkyl groups.

Table 4.5. ^{31}P-NMR chemical shift tensors for alkyl- and acylmanganese(I) complexes **III-IX** calculated from CP-MAS and spinning sideband Analysis[a]

compound	δ_{11} (ppm)	δ_{22} (ppm)	δ_{33} (ppm)	$\Delta\delta_t$ (ppm)	no. of spinning rates
$PhCH_2C(O)Mn(CO)_4(PPh_3)$ **(III)**	120.5	71.4	-25.5	-121.5	3
$MesCH_2C(O)Mn(CO)_4(PPh_3)$ **(IV)**	120.3	58.6	-18.4	-107.9	3
$PhCH_2C(O)Mn(CO)_4[P(C_6H_{11})_3]$ **(V)**	110.6	71.0	-1.0	-91.6	2
$MesCH_2C(O)Mn(CO)_4[P(C_6H_{11})_3]$ **(VI)**	98.6	67.2	-2.6	-86.2	3
$PhCH_2Mn(CO)_4(PPh_3)$ **(VII)**	132.1	101.5	-27.7	-144.5	3
$PhCH_2Mn(CO)_4[P(Tolyl)_3]$ **(VIII)**	125.1	99.0	-25.5	-137.5	3
$PhCH_2Mn(CO)_4[P(PhF)_3]$ **(IX)**	130.2	100.7	-32.2	-147.6	2

[a]Uncertainties are ± 1.5 and ± 2.5 ppm for chemical shifts tensors and $\Delta\delta$, respectively.

References

(1) S. O. Grim, D. W. Wheatland and W. McFarlane *J. Am. Chem. Soc.*, **89**, 5573 (1967).

(2) P. S. Pregosin and R. W. Kunz, *NMR Basic Princ. Prog., Vol. 16: ^{31}P and ^{13}C NMR of Transition Metal Phosphine Complexes*, Springer-Verglag, Berlin, 1979.

(3) R. Mathieu, M. Lenzi and R. Poilblanc, *Inorg. Chem.*, **9**, 2030 (1970).

(4) K. Ziegler, E. Holzkamp, H. Breil and H. Martin, *Angew. Chem.*, **69**, 541 (1955).

(5) J. A. Osborn, F. H. Jardine, J. F. Young and G. Wilkinson *J. Chem. Soc. A*, 1711 (1966).

(6) O. Roelen, *Angew. Chem.*, **60**, 62 (1948).

(7) C. S. Kraihanzel and P. K. Maple, *J. Am. Chem. Soc.*, **87**, 5267 (1965).

(8) A. Mawby and G. E. Pringle, *J. Inorg. Nucl. Chem.*, **34**, 877 (1972).

(9) R. J. Ferdericks, *Acta. Crystallogr.*, **25A**, S157 (1969).

(10) T. C. Flood, J. E. Jensen and J. A. Statler, *J. Am. Chem. Soc.*, **103**, 4410 (1981).

(11) J. D. Cotton, M. M. Kroes, R. D. Markwell and E. A. Miles, *J. Organomet. Chem.*, **388**, 133 (1990).

(12) J. D. Cotton and R. D. Markwell, *J. Organomet. Chem.*, **388**, 123 (1990).

(13) J. D. Cotton and R. D. Markwell, *Inorg. Chim. Acta.*, **175**, 187 (1990).

(14) P. S. Ireland, C. A. Derkert and T. L. Brown, *J. Magn. Reson.*, **23**, 485 (1976), and references therein.

(15) D. Rehder, *Magn. Reson. Rev.*, **9**, 164 (1984).

(16) P. DeShong, G. A. Slough, D. R. Slider, P. J. Rybczynski, W. Philipsborn, R. W. Kunz, B. E. Bursten and Jr T. W. Clayton, *Organometallics* **8**, 1831 (1989).

(17) V. Torocheshnikov, D. Rentsch and W. Philipsborn, *Magn. Reson. Chem.*, **32**, 348 (1994).

(18) E. Lindner, R. Fawzi, H. A. Mayer, K. Eichele and K. Pohmer, *Inorg. Chem.*, **30**, 1102 (1991).

(19) R. Gobetto, R. K. Harris and D. C. Apperley, *J. Magn. Chem.*, **96**, 119 (1992).

(20) A. P. Kentgens, W. Power and R. E. Wasylishen, *HBLQFIT Sideband Analysis, version 2.2.*, Dalhousie University, Halifax, Nova Scotia, Canada B3H 4J3, 1991.

Chapter 5

Solid-state Multinuclear NMR Spectroscopy of Group 14 (IVA) Pentacarbonylmanganese(I) complexes

5.1 Introduction

The coordination chemistry of strong covalent organometallic complexes containing a group 14 (IVA) metal directly bonded to transition metal carbonyl was first explored by Hein *et al.* in the early 1940s.[1,2] Subsequently, other stable mixed metal carbonyl compounds containing a group 14 metal and a first-row transition metal were prepared.[3-8] The most widely studied complexes of this type are those containing tetracarbonylcobalt(I), pentacarbonylmanganese(I) and pentacarbonylrhenium(I) derivatives of silicon, germanium, tin and lead. In general, the pentacarbonyl-manganese(I) and pentacarbonylrhenium(I) derivatives are more thermally stable and are more easily prepared than are the analogous tetracarbonylcobalt(I) species. There are two naturally occurring NMR-active spin-5/2 isotopes of rhenium, ^{185}Re (37.1%) and ^{187}Re (62.9%), while there is only one NMR-active isotope of manganese, ^{55}Mn (spin-5/2). Consequently, we decided to focus our attention on the simpler pentacarbonyl-manganese(I) system.

Gorsich[5] showed in the early 1960s that the *trans* carbonyl in $(C_6H_5)_3SnMn(CO)_5$ (XII) is more weakly bonded than are the *cis* carbonyl groups and can be replaced quantitatively (> 94 % yield) by PPh_3 at 195 °C to form *trans*-$(C_6H_5)_3Sn$-$Mn(CO)_4(PPh_3)$ (XVII). This led to the examination of σ- and π-bonding interactions for the group 14 derivatives using infrared spectroscopy.[6] On the basis of these studies, the R_3Sn ligands

were characterized as weak σ-donors and good π-acceptors. These results were confirmed by single crystal X-ray diffraction analyses of compounds **XII** and **XVII**,[9,10] where the Mn-Sn bond distance in **XVII** is 0.04-0.05 Å shorter than is that in **XII**. Also, the Mn-P bond distance in **XVII** is ~0.07 Å shorter than is usually found for a typical Mn-P bond in tertiary phosphine-substituted alkyl(tetracarbonyl)manganese(I) complexes (Appendix I). These findings indicate that R_3Sn ligands are better σ-donor and π-acceptors than is the *trans* carbonyl group.

The purpose of the present work was to examine the various parameters obtained from the solid-state CP-MAS (^{29}Si, ^{119}Sn and ^{207}Pb) spectra of strong bimetallic complexes and to compare these parameters with single-crystal X-ray diffraction data of triphenylsilyl-, triphenyltin- and triphenyllead(pentacarbonyl)manganese(I) complexes, $Ph_3EMn(CO)_5$ (E = Si, Sn, Pb). These covalent bimetallic compounds offer a unique opportunity to examine the spin-spin coupling between a main group element and a transition-metal and the nuclear quadrupole coupling constant of the metal for the first time. The crystal structure of $Ph_3SnMn(CO)_5$ has been determined previously,[9] whereas the structure of $Ph_3SiMn(CO)_5$ (Appendix II), and some preliminary results for the lead complex, are discussed in this section. In the case of the silicon complex, there are two non-equivalent molecules per unit cell, but there are four non-equivalent molecules for the tin and lead complexes. The nuclear quadrupole coupling constants have been measured previously by solid-state, broad-line ^{55}Mn NMR spectroscopy of single crystals of the triphenyl-germanium, triphenyltin, and triphenyllead complexes.[11] However, there are no NQR or NMR results reported in the literature for the triphenylsilyl complex. It

should be noted that the triphenylgermanium compound was not studied, due to the fact that the principal isotope, germanium-73, is a quadrupolar nucleus and is very difficult to study by solid-state ^{73}Ge NMR spectroscopy.

5.2 Results and Discussion

The centreband resonances of the ^{29}Si, ^{119}Sn and ^{207}Pb solid-state NMR, CP-MAS, spectra are shown in Figs. 5.1-5.3 for the three pentacarbonylmanganese(I) complexes under investigation. These isotropic centrebands are very complex and may result from the presence of more than one group 14 metal site in the crystalline materials. The ^{207}Pb chemical shifts for $Ph_3PbMn(CO)_5$ are well resolved when compared to those of ^{29}Si and ^{119}Sn NMR spectra, and were very different when the complex was recrystallised from octane than from a 50/50 mixture of benzene and octane. Single-crystal X-ray diffraction determinations of these two different polymorphs were attempted, but, due to strong absorption of the lead atoms, the structures were nearly impossible to solve. However, preliminary results indicated that this complex crystallizes in the space group C_2/m with 4 different molecules in the asymmetric unit when octane was used as the only solvent. Crystal structure determination of both this polymorph and that obtained from benzene/octane mixture are currently being studied using a CCD detector at McMaster University. It was suggested, from the results of the single-crystal, broad-line, ^{55}Mn NMR experiment,[11] that this triphenyllead(pentacarbonyl)manganese(I) complex should crystallize in the monoclinic space group and have 2/m symmetry with 2 crystallographically independent sites across a mirror plane. This is in agreement

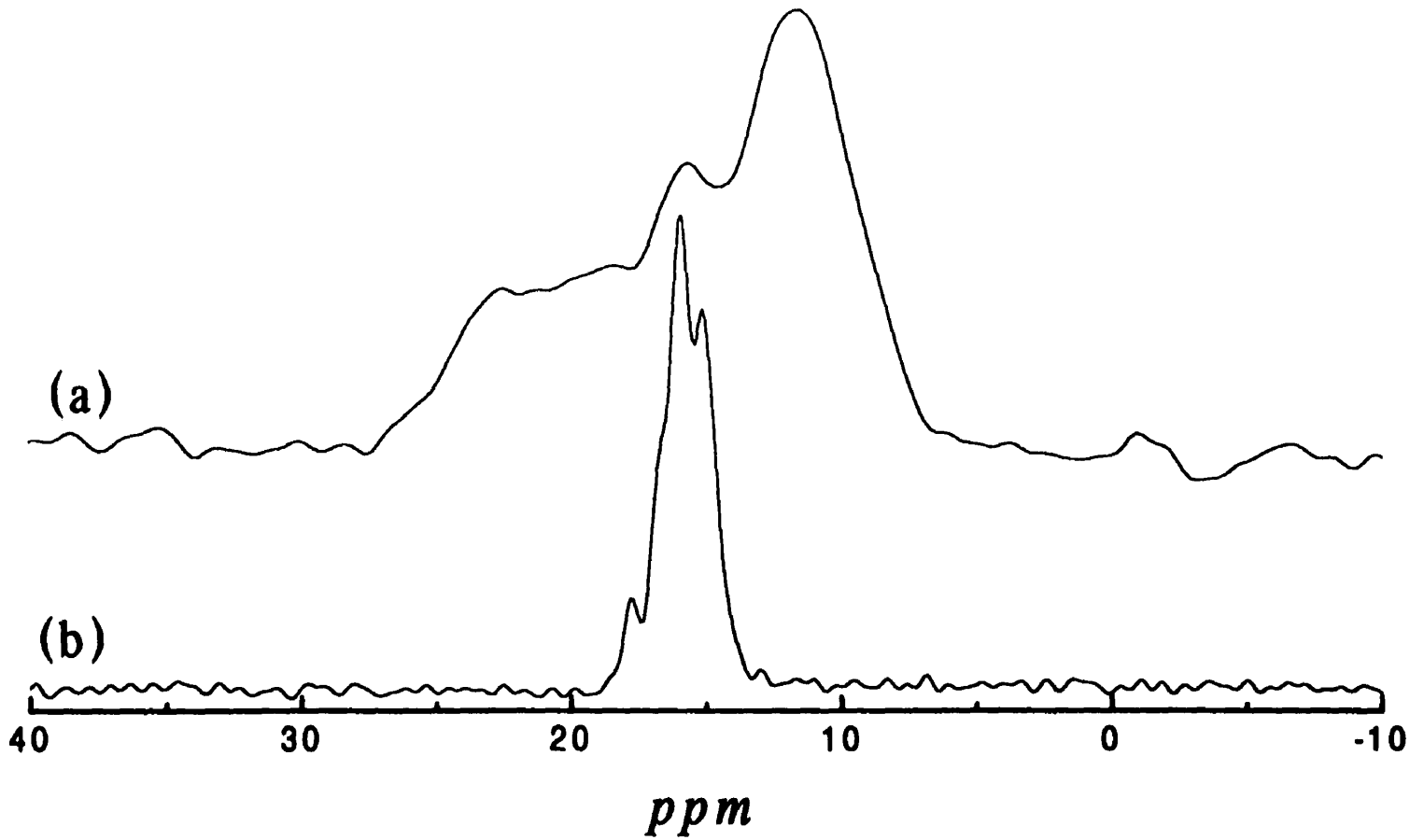

Figure 5.1. ^{29}Si CP-MAS spectra of $Ph_3SiMn(CO)_5$, (a) at 19.85 MHz: contact time 2 ms; pulse delay 30 s; spinning speed 0.30 kHz; 2000 transients, and (b) at 59.4 MHz: contact time 3 ms; pulse delay 60 s; spinning speed 2.0 kHz; 1150 transients.

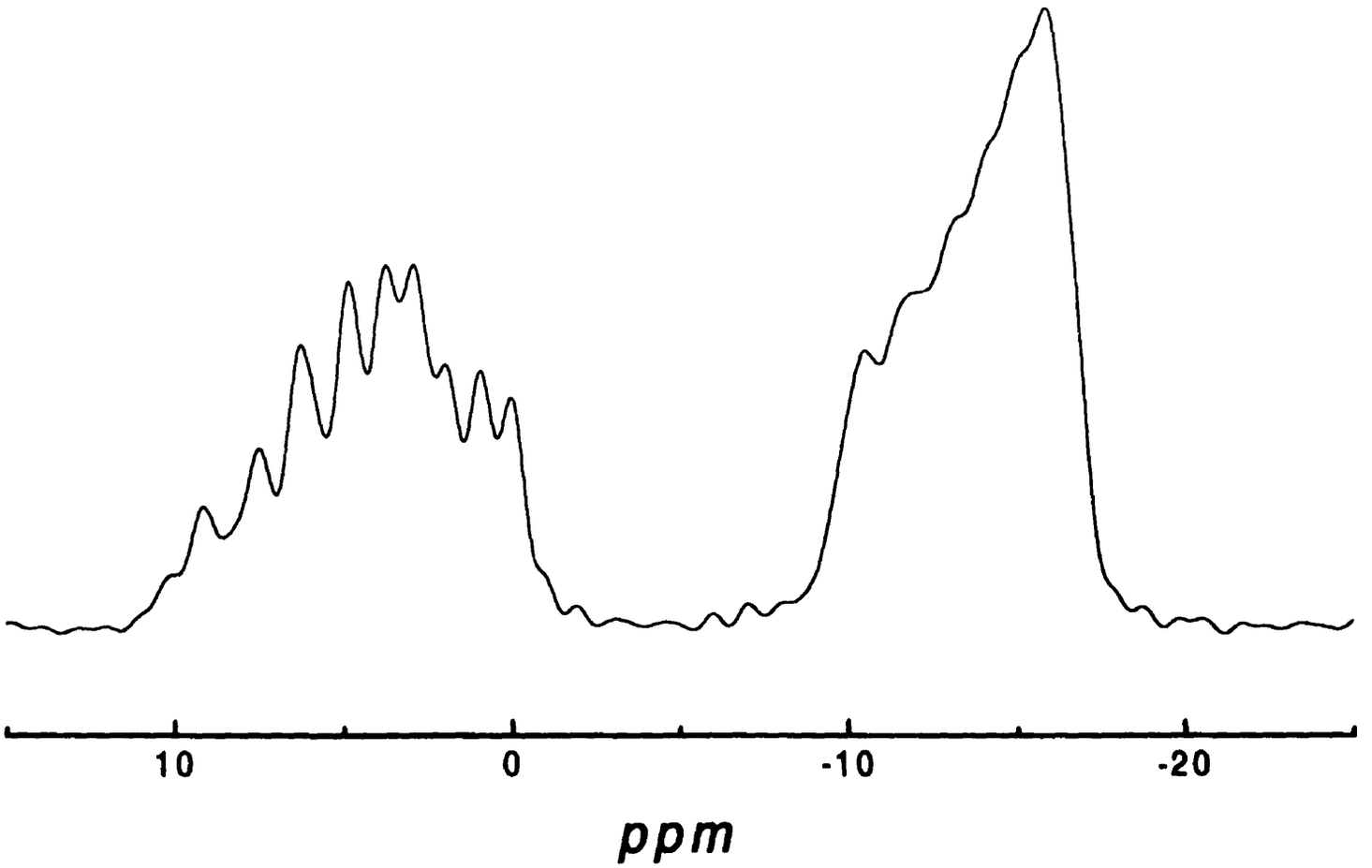

Figure 5.2. Part of the CP-MAS ^{119}Sn NMR spectrum of $Ph_3SnMn(CO)_5$ at 111.7 MHz, showing three sets of centre bands. Spinning speed 4.5 kHz; pulse delay 10 s; contact time 1 ms; 6000 transients.

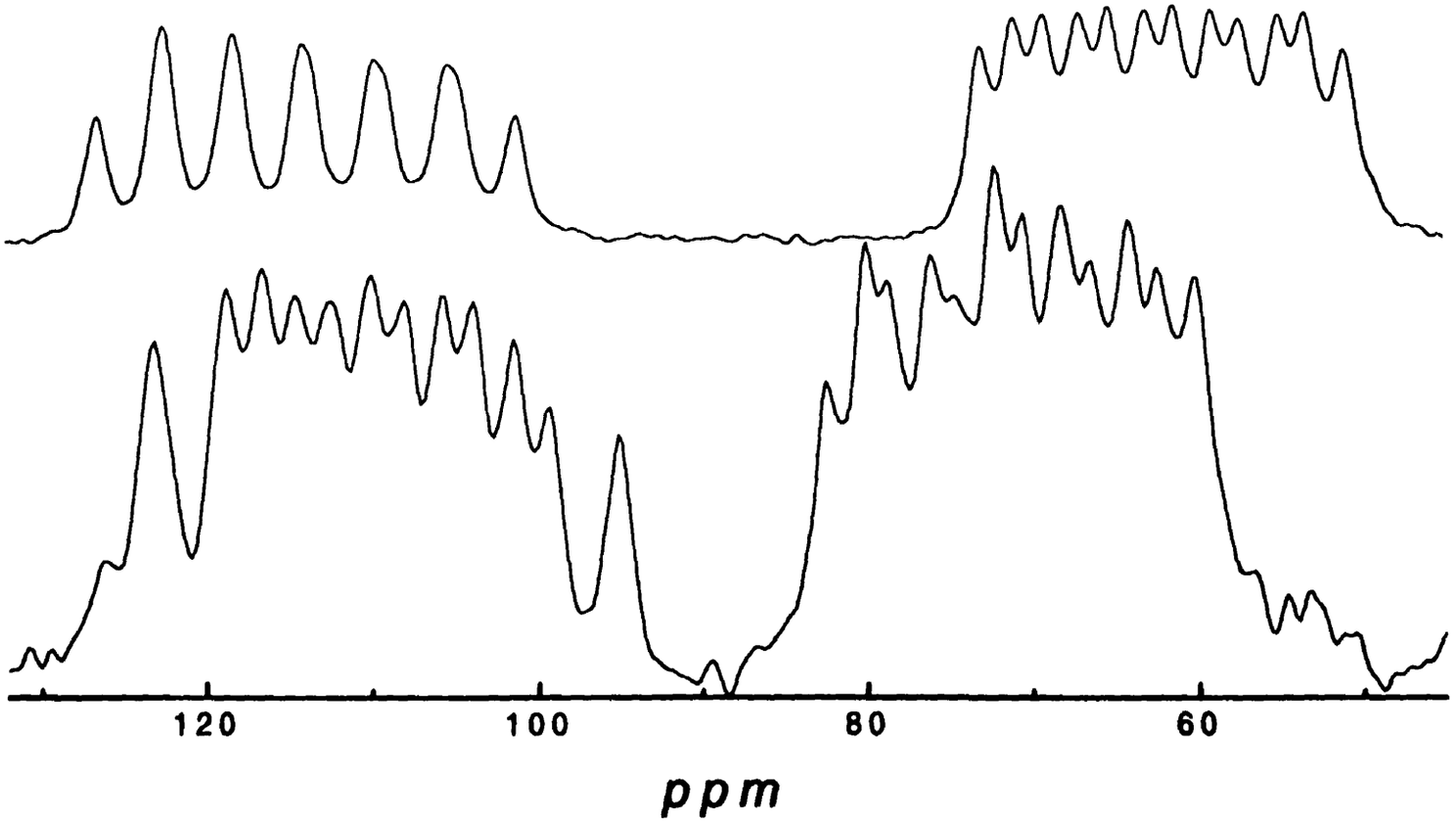

Figure 5.3. Part of the CP-MAS ^{207}Pb NMR spectra of $Ph_3PbMn(CO)_5$ at 62.7 MHz, showing four sets of overlapping centrebands for the two polymorphs. Sample recrystallized (a) from octane; spinning speed 5.0 kHz; pulse delay 25 s; contact time 2 ms; 4000 transients. (b) from benzene/octane; spinning speed 5.0 kHz; pulse delay 25 s; contact time 2 ms; 4000 transients.

with the present work because the lead chemical shifts occur in two pairs of twelve peaks. Only small differences occur in the ^{55}Mn quadrupole coupling constants, which could not be detected in the broad-line ^{55}Mn NMR experiment, but were observed in the higher resolution ^{207}Pb, CP-MAS, NMR experiment.

Table 5.1. CP/MAS ^{21}Si NMR results of $Ph_3SiMn(CO)_5$ at 59.5 and 19.85 MHz[a]

	At 59.4 MHz		At 19.85 MHz	
	Site A	Site B	Site A	Site B
δ_{iso} (solution)	17.85			
δ_{iso} (ppm)	15.8	17.0	15.5	16.9
$^1J_{Si-Mn}$ (Hz)[b]	15.9	15.3	16.7	12.9
d[c]	-39.1	-35.2	-118.0	-104.9
χ (MHz)[d]	25.9	23.0	25.9	22.7
D (Hz)	-375 (± 2)	-380 (± 2)	-375 (± 2)	-380 (± 2)

[a]Uncertainties are ± 0.05 and ± 1.0 ppm for the solution and solid-state ^{29}Si NMR spectra, respectively.
[b]J values were determined from simulated spectra and are considered to be accurate to ± 2.0 Hz.
[c]$d = 3\chi D''/ 10\nu_S$
[d]Values were obtained with the assumption of $\Delta J = 0$.

Table 5.2. ^{119}Sn NMR data for $Ph_3SnMn(CO)_5$ at 7.05T[a]

	Site A	Site B	Site C
δ_{iso} (solution) (ppm)		-11.93 (± 0.05)	
δ_{iso} (ppm)	-13.6	2.8	5.6
$^1J_{Sn-Mn}$ (Hz)	135 (± 1)	142 (± 2)	141 (± 1)
d[a] (Hz)	34.4 (± 0.5)	34.3 (± 0.3)	30.3 (± 3.3)
δ_{11} (ppm)	71.6	81.1	89.4
δ_{22} (ppm)	2.8	50.1	47.3
δ_{33} (ppm)	-115.2	-122.8	-119.9
$\Delta\delta$ (ppm)	-152.4	-188.4	-188.3
η	0.677	0.247	0.335
χ (MHz)[b]		18.33 (± 0.03)	
D″ (Hz)	466 (± 7)	465 (± 7)	411(± 45)
D (Hz)	584 (± 4)	584 (± 4)	580 (± 4)
ΔJ (Hz)	353 (± 8)	345 (± 8)	507 (± 55)

[a]Uncertainties are ± 0.3 and ± 3.0 ppm for the isotropic chemical shifts and chemical shift tensors, respectively.

[b]Value taken from ref. 11.

Table 5.3. ^{207}Pb NMR data for $Ph_3PbMn(CO)_5$, recrystallized from octane, at 7.05 T[a]

	Site A[b]	Site B[b]	Site C[c]	Site D[c]
δ_{iso} (solution) (ppm)		48.4 (± 0.1)		
δ_{iso} (ppm)	70.1	72.4	105.8	112.2
$^1J_{Pb-Mn}$ (Hz)	250 (± 4)	253 (± 4)	275 (± 8)	274 (± 7)
d (Hz)	2.30 (± 0.6)	9.19 (± 0.74)	11.4 (± 0.5)	2.26 (± 0.1)
δ_{11} (ppm)	-65.2	-54.4	-96.3	-74.7
δ_{22} (ppm)	59.2	57.3	180.4	186.9
δ_{33} (ppm)	216.3	214.4	233.3	224.4
$\Delta\delta$ (ppm)	222.3	211.5	-197.4	-168.2
η	0.434	0.389	0.262	0.201
χ (MHz)[d]	12.04 (± 0.01)		10.6 (± 0.4)	
D″ (Hz)	47.4 (± 12.4)	190 (± 15)	267 (± 22)	52.9 (± 4.3)

[a]Uncertainties are ± 0.3 and ± 5.0 ppm for the isotropic chemical shifts and chemical shift tensors, respectively.
[b]For $|\delta_{33} - \delta_{iso}| > |\delta_{11} - \delta_{iso}|$, Anisotropy parameter $\Delta\delta = \delta_{33} - 1/2\ (\delta_{11} + \delta_{22})$ and Asymmetry parameter $\eta = |(\delta_{11} - \delta_{22}) / (\delta_{22} - \delta_{iso})|$.
[c]For $|\delta_{11} - \delta_{iso}| > |\delta_{33} - \delta_{iso}|$, Anisotropy parameter $\Delta\delta = \delta_{11} - 1/2\ (\delta_{33} + \delta_{22})$ and Asymmetry parameter $\eta = |(\delta_{33} - \delta_{22}) / (\delta_{11} - \delta_{iso})|$.
[d]Value taken from ref. 11.

Table 5.4. ^{207}Pb NMR data for $Ph_3PbMn(CO)_5$, recrystallized from benzene/octane mixture, at 7.05 T[a]

	Site A	Site B	Site C	Site D
δ_{iso} (solution) (ppm)		48.4 (± 0.1)		
δ_{iso} (ppm)	61.0	63.2	112.0	115.5
$^1J_{Pb-Mn}$ (Hz)	251 (± 1)	247 (± 1)	273 (± 3)	274 (± 1)
d (Hz)	2.41 (± 0.02)	3.19 (± 0.11)	4.14 (± 0.15)	2.25 (± 0.06)
δ_{11} (ppm)	-57.9	-69.5	-91.4	-86.9
δ_{22} (ppm)	32.5	62.3	166.5	195.9
δ_{33} (ppm)	208.4	196.7	260.9	237.5
$\Delta\delta$ (ppm)	222.3	211.5	-193.1	-188.1
η	0.434	0.389	0.464	0.206
χ (MHz)	12.04 (± 0.01)		10.6 (± 0.4)	
D″ (Hz)	49.7 (± 0.4)	65.8 (± 2.3)	97.0 (± 6.5)	52.7 (± 2.2)

[a] See Table 5.3.

The NMR parameters for the three pentacarbonylmanganese(I) compounds are given in Tables 5.1-5.4, together with the solution-state chemical shifts. Because of the small chemical shift anisotropy of the silicon complex, spinning sidebands were not obtained and the shift anisotropy could not be determined. The crystal structure of the silicon complex showed two molecules in the asymmetric unit cell and so two chemical shifts and a total of twelve lines are expected in the spectrum. Clearly, the solid-state NMR spectrum cannot be fitted easily at 59.5 MHz; therefore, the spectrum was also

measured at 19.8 MHz where the second-order splitting is increased by a factor of three while the spin-spin coupling constant, $^1J_{Si-Mn}$ in Hz, remains the same. The extra information this provided made it possible to fit both spectra and obtain consistent values for the second-order splitting, the spin-spin coupling and the chemical shifts (Table 5.1).

The spectrum of the tin complex shows that there are three chemical shifts, but the highest field centreband arises from the overlap of two resonances, Fig. 5.2. This is consistent with the crystal structure,[9] where there are four molecules in the asymmetric unit. The differences in the molecular structure are slight, but the probable cause of the different chemical shifts arises from the differences in the twist angles of the phenyl rings. The dihedral angles lie in quite narrow ranges, but are associated with two pairs of molecules. The data in Table 5.5 indicate that the tin atoms in molecules I and IV are almost equivalent, with the exception of the angle of tilt of phenyl ring 2 by one degree. The Mn-Sn-C bond angles, for these molecules, are almost identical and the two tin environments were considered to be equivalent. For molecules II and III, only the angle of tilt of phenyl ring 2 remains the same, while the bond angles, Mn-Sn-C, differ by as much as 1.8°. These results indicate that molecules II and III have different structures and, therefore, two different tin environments. In order to separate the chemical shifts, a higher field spectrometer (7.05 T) was used and the spinning rates were fast enough to prevent the overlap of the spinning side-bands with the centrebands. As a result, only a few spinning side-bands occurred, Fig. 5.4, and in the case of the lower field resonance it was not possible to obtain, with any accuracy, the chemical shift anisotropy of the m eigenstates.

Table 5.5. Dihedral angles, Mn-Sn-C-C, and bond angles, Mn-Sn-C, of triphenyltin(pentacarbonyl)manganese(I)[a]

	Molecule I	Molecule II	Molecule III	Molecule IV
Dihedral angle (°)				
ring 1	40.8	42.2	41.2	40.8
ring 2	59.6	59.8	59.8	60.6
ring 3	65.4	59.3	58.8	65.6
Bond angle (°)				
ring 1	111.2	113.2	111.9	110.9
ring 2	113.0	114.9	113.1	112.6
ring 3	114.0	112.0	113.1	113.0

[a]Values taken from ref. 9.

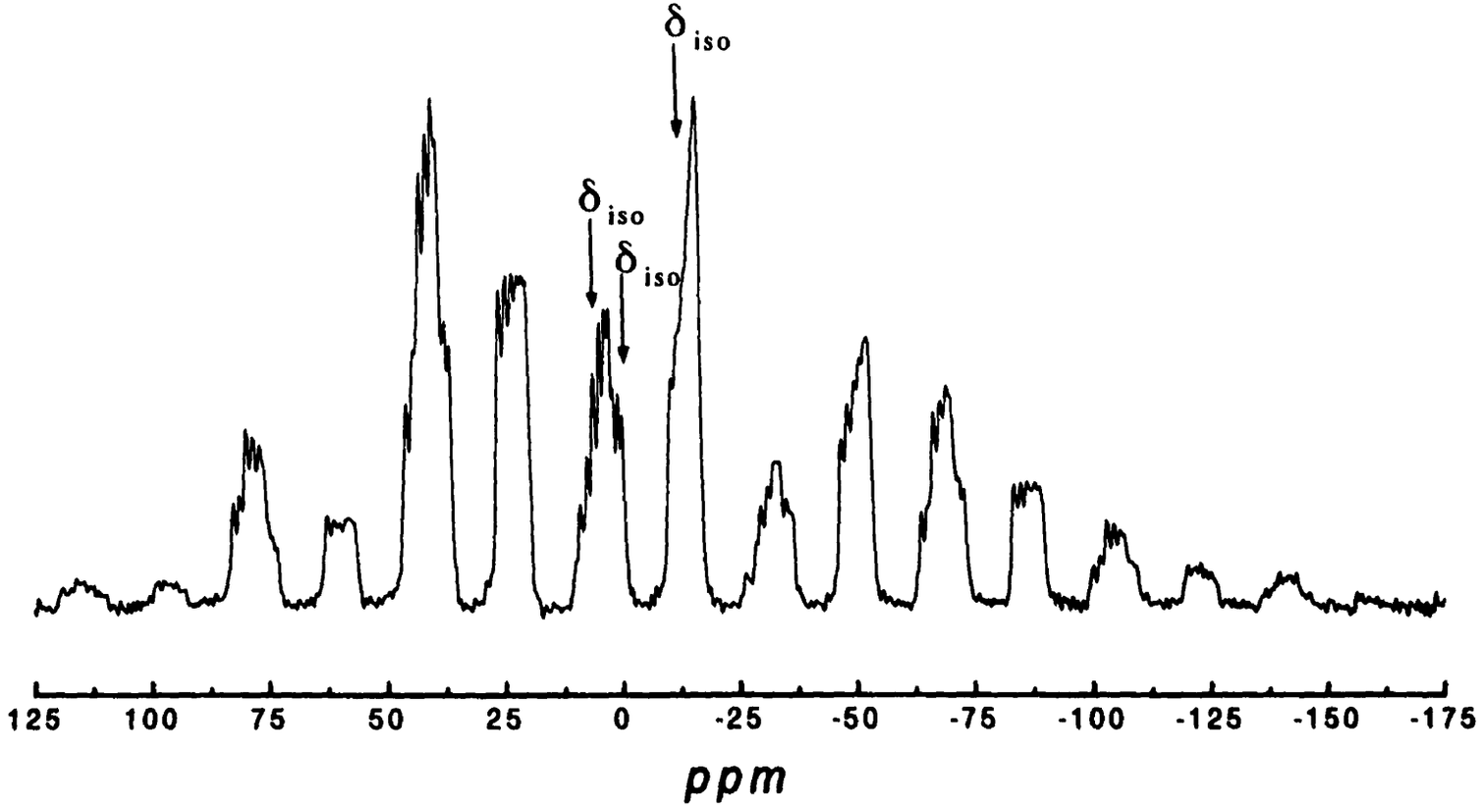

Figure 5.4. Solid-state CP-MAS ^{119}Sn spectrum of $Ph_3SnMn(CO)_5$ at 111.7 MHz. Low field centrebands are due to overlap of two slightly different tin chemical shifts. The intensity variations are produced by the interaction of the dipolar, indirect coupling and shielding tensors.

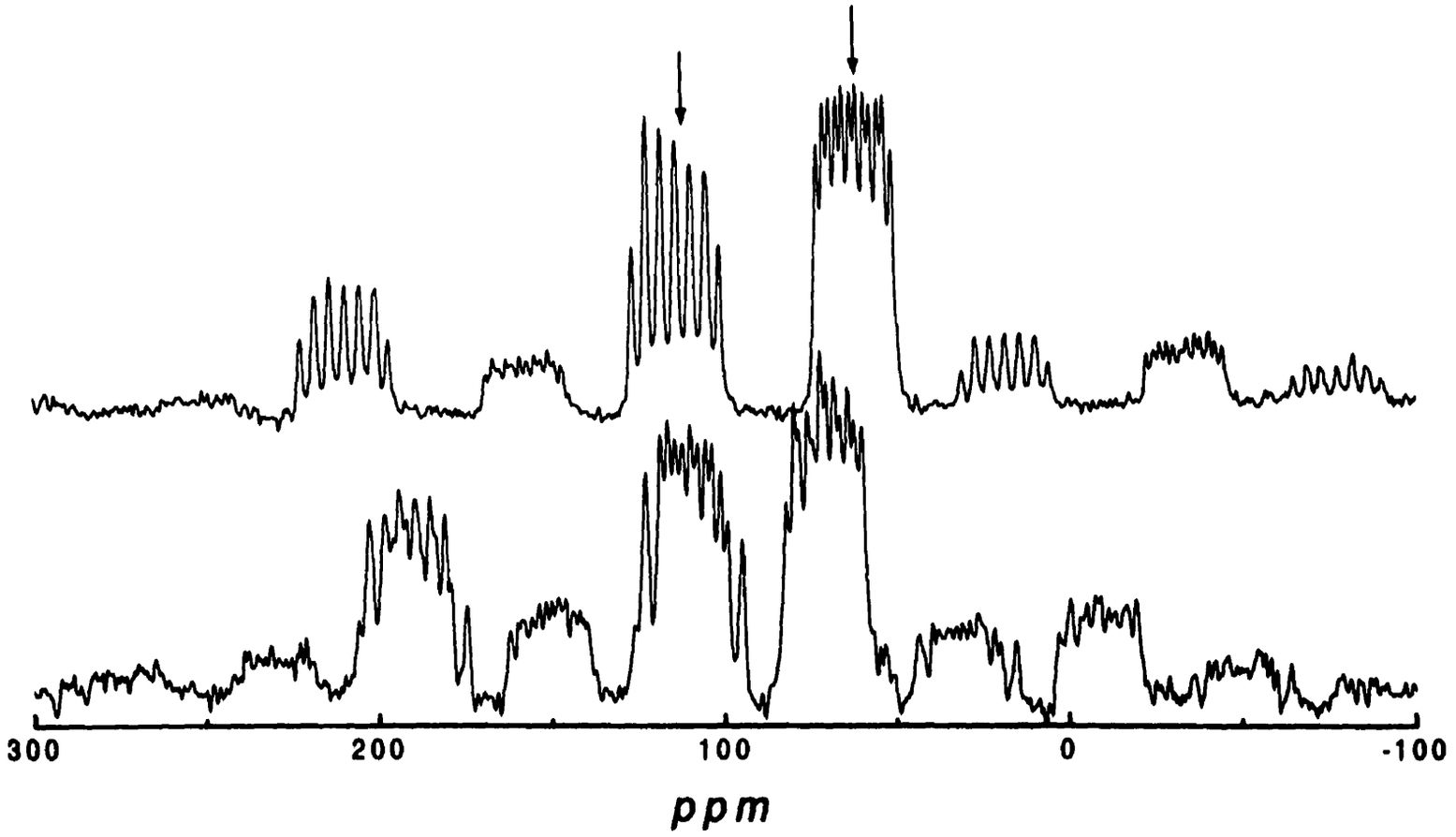

Figure 5.5. Solid-state CP-MAS ^{207}Pb spectrum of $Ph_3PbMn(CO)_5$ at 62.7 MHz. Low-field and high-field centrebands are due to two slightly different lead chemical shifts, resulting in sets of twelve peaks in each centreband. Recrystallized from (a) octane and (b) a 50/50 benzene/octane mixture.

The spectra of the lead complex are much more complicated than are those of the silicon or the tin compounds, Fig. 5.3, with four sets of chemical shifts, which occur in pairs and result in two sets of twelve peaks for both polymorphs. The chemical shifts were identified by the use of the high-field spectrometer (7.05 T) with faster spinning rates and, again, it was not possible to obtain the chemical shift anisotropies of the m eigenstates, due to lack of spinning side-bands, Fig. 5.5. The spin-spin couplings of the high-field centrebands were 22 Hz smaller than were those of the low-field centreband, Tables 5.3 and 5.4, and were assigned the larger value of the nuclear quadrupole coupling constant (12.04 ± 0.01 MHz) rather than the value of 10.6 ± 0.4 MHz (6). This distinction was based on the fact that the ^1J coupling is inversely proportional to the NQR coupling constant[12] if the Fermi contact term is the dominant mechanism of spin-spin coupling,[13] and the Townes and Dailey theory is used in the estimation of the field gradient at the nucleus.[14] It was predicted by Gonzalez *et al.*[15] that the Fermi contact mechanism is indeed the domant factor in determining J values for group-14 metal complex, MH_4 and $M(CH_3)_4$ (M = C, Si, Sn, Pb)

To compare the spin-spin coupling constants, it is more informative to use the reduced coupling constants, $K_{Mn\text{-}E} = 4\pi^2 J_{Mn\text{-}E}/(h\, \gamma_{Mn}\, \gamma_E)$, and average values of $|^1K_{Mn\text{-}Si}| = 2.64 \times 10^{20}\ T^2\ J^{-1}$, $|^1K_{Mn\text{-}Sn}| = 1.25 \times 10^{21}\ T^2\ J^{-1}$ and $|^1K_{Mn\text{-}Pb}| = 4.18 \times 10^{21}\ T^2\ J^{-1}$ were obtained. These can be compared with the respective s-electron densities at the nuclei.[17] A plot of the reduced couplings, $|K_{Mn\text{-}E}|$, against the s-electron densities, $|\Psi(0)|^2$, for the silicon, tin and lead nuclei,[16] Fig. 5.6, gave a linear relationship, indicating that the Fermi contact term is the dominant factor in determining the spin-spin coupling, and the s bond

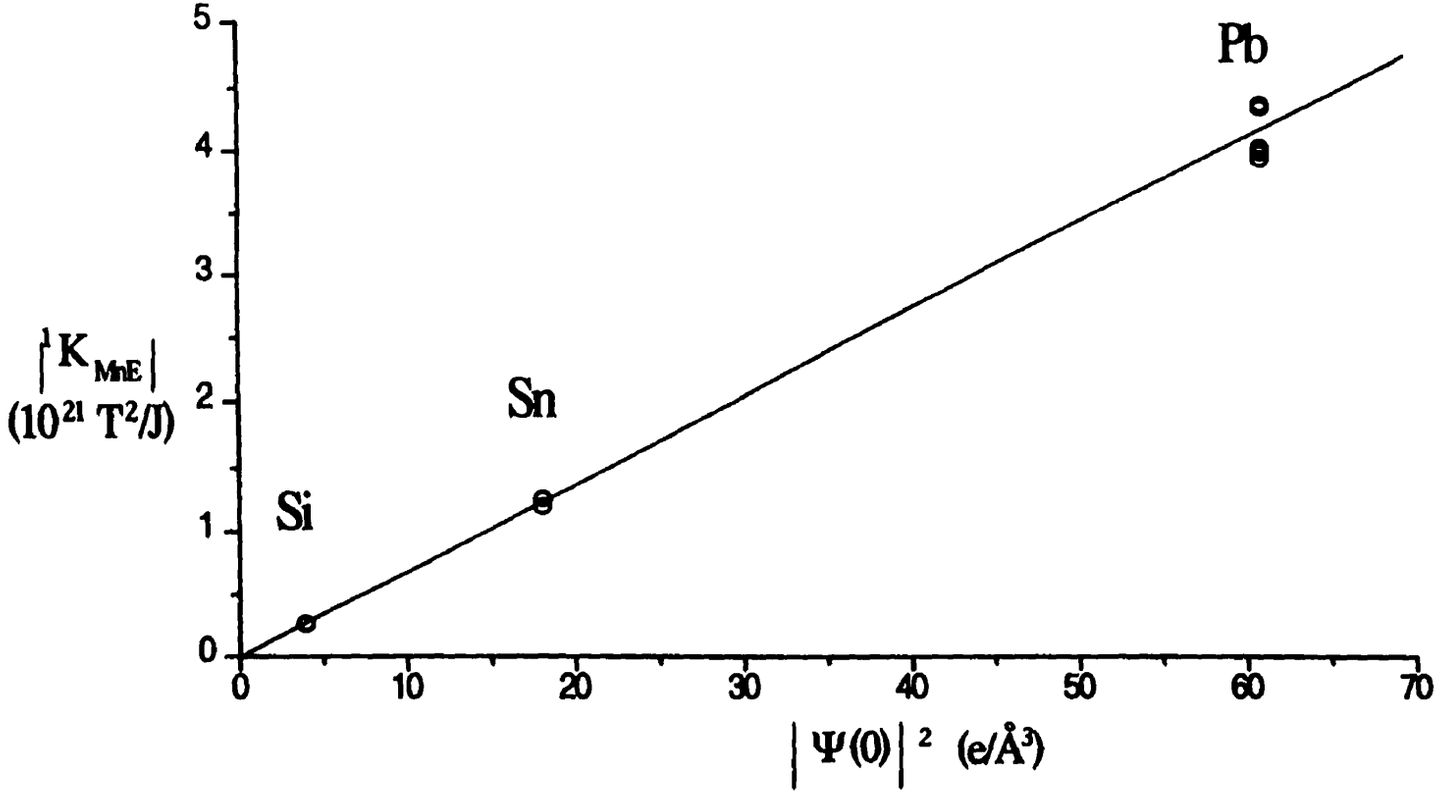

Figure 5.6. Plot of one-bond reduced spin-spin coupling constant $|^1K_{Mn\text{-}E}|$ for Mn-Group 14 (IVA) complexes *vs.* electron density, $|\Psi(0)|^2$, at the Group 14 (IVA) nucleus.

order and the average excitation energy, ΔE, are nearly the same in all cases. Correlations between different coupling constants have been reported by Wrackmeyer and co-workers for tin and lead coupling constants in various series of related compounds.[17-24]

It is clear from Eqs. [3.5.1] and [3.5.4] that a knowledge of the interatomic distances and the angular terms, α^D and β^D, are not sufficient to determine the quadrupolar coupling constant if the anisotropy of the spin-spin coupling is large. The local symmetry about the Mn-E bonds in the $(Ph_3E)Mn(CO)_5$ complexes is sufficiently high that the angle β^D is equal to 0°. Thus Eq. [3.5.4] is reduced to a much simpler form

$$D'' = (D - \Delta J/3) \qquad [5.2.1]$$

Gobetto and co-workers[25] have shown that the effective dipolar coupling constant D'' can be obtained from an analysis of chemical shift anisotropy for each of the spinning sideband manifolds, Eq [3.5.5]. Due to the presence of only few spinning sidebands, it was difficult to obtain the m eigenstate chemical shift anisotropies. However, the chemical shift tensors were obtained for the tin and lead compounds, and the spans, $\delta_{33} - \delta_{11}$, were found to increase as the size of the valence *s*- and *p*-electron radius, $\langle r^{-3} \rangle_{ns}$ and $\langle r^{-3} \rangle_{np}$, of the probe nucleus increases. However, this is only true for a periodic row with analogous groups bonded the probe nucleus. The span for the silyl complex is very small and could not be determined from the ^{29}Si CP/MAS experiment. This type of difficulty was encountered previously for other organosilyl complexes in an asymmetric environment, such as the bis(pentamethlcyclopentadienyl)silicon ($Cp^*_2Si(II)$),[24] Hexamethylcyclotrisilazane and Octamethylcyclotrisilazane, $[(CH_3)_2SiNH]_n$ (n = 3, 4).[26] However, the bis(pentamethylcyclopentadienyl)lead(II) compound, Cp^*_2Pb,[24] was found

to have a span of 1940 ppm which is considerably larger than the approximate value of 350 ppm we obtained for the triphenyllead complex. This difference is due to the coordination number and/or the oxidation state of the lead nucleus, which changes the electronic environment around the lead nucleus. Recently, Harris *et al.*[27-29] have examined triorganolead(IV) compounds, using solid-state ^{207}Pb NMR, and found that the span of the chemical shift tensors was larger than 600 ppm. The values obtained in the present studies are the smallest ever observed for Ph_3PbX (when $X \neq Ph$). The ^{119}Sn chemical shift tensor values, Table 5.2., are similar to those obtained for other triphenyltin complexes,[30,31] but, as the coordination number of the tin nucleus increases, the span of the tensor increases. This observation may also explain the result for the $Cp^*_2Pb(II)$ compound when compared to lead(IV) complexes. The chemical shifts tensors obtained from solid-state, CP/MAS, NMR experiment might actually help in determining the coordination number and/or the oxidation state of the nucleus under investigation.

References

(1) F. Hein, H. Pobloth and E. Z. Heuser, *Anorg. Allgem. Chem.*, **248**, 84 (1941).

(2) F. Hein, H. Pobloth and E. Z. Heuser, *Anorg. Allgem. Chem.*, **249**, 293 (1942); **254**, 138 (1947); **255**, 125 (1948).

(3) T. S. Piper, O. Lemal and G. Wilkinson, *J. Am. Chem. Soc.*, **43**, 129 (1956).

(4) W. Hieber and R. Breu, *Chem. Ber.*, **90**, 1270 (1957).

(5) R. D. Gorsich, *J. Am. Chem. Soc.*, **84**, 2486 (1962).

(6) H. R. H. Patil and W. A. G. Graham, *Inorg. Chem.*, **5**, 1401 (1966).

(7) W. Jetz, P. B. Simons, J. A. J. Thompson and W. A. G. Graham, *Inorg. Chem.*, **5**, 2217 (1966).

(8) D. J. Patmore and W. A. G. Graham, *Organomet. Chem.* **6**, 981 (1967).

(9) H. P. Weber and R. F. Bryan, *Acta Cryst.*, **22**, 822 (1967).

(10) R. F. Bryan, *J. Chem. Soc. A*, 172 (1967).

(11) J. L. Slater, M. Pupp and R. K. Sheline, *J. Chem. Phys.*, **57**, 2105 (1972).

(12) D. F. R. Gilson, *J. Chem. Phys.*, **43**, 312 (1965).

(13) B. P. Dailey and C. H. Townes, *J. Chem. Phys.*, **23**, 118 (1955).

(14) C. Juan, and H. S. Gutowsky, *J. Chem. Phys.*, **37**, 2198 (1962).

(15) J. A. Gonzalez, G. A. Aucar, M. C. Ruiz and R. H. Contreras, *Int. J. Quantum Chem.*, **66**, 823 (1997).

(16) P. Pyykko and L. Weisenfeld, *Mol. Phys.*, **43**, 557 (1981).

(17) C. J. Jameson, in *Multinuclear NMR Spectroscopy, Chapter 4.*, J. Mason, Ed, Plenum: New York, 1987.

(18) B. Wrackmeyer and W. Biffar, *Z. Naturforsch.*, B **34**, 1270 (1979).

(19) J. D. Kennedy, W. McFarlane and B. Wrackmeyer, *Inorg. Chem.*, **15**, 1299 (1976).

(20) J. D. Kennedy, W. McFarlane, G. S. Pyne and B.Wrackmeyer, *J. Chem. Soc. Dalton*, 386 (1975).

(21) B. Wrackmeyer and K. Horchler, *Magn. Reson. Chem.*, **28**, 56 (1990).

(22) B. Wrackmeyer and K. Horchler, in *Ann. Rep. NMR spectrosc.*, G. A. Webb, Ed, Academic Press, New York, **22**, 249 (1990).

(23) B. Wrackmeyer, A. Sebald and L. H. Merwin, *Magn. Reson. Chem.*, **29**, 260 (1991).

(24) B. Wrackmeyer, K. Horchler, A. Sebald and L. H. Merwin, *Magn. Reson. Chem.*, **28**, 465 (1990).(12)

(25) R. Gobetto, R. K. Harris and D. C. Apperley, *J. Magn. Res.*, **96**, 119 (1992).

(26) H. Li, I. S. Butler, D. F. R. Gilson, J. F. Harrod and F. G. Morin, *J. Phys. Chem.*, **99**, 8490 (1995).

(27) J. R. Ascenso and R. K. Harris, *J. Organomet. Chem.*, **301**, C23 (1986).

(28) U. Behrens, A. K. Brimah, T. M. Sollman, R. D. Fischer, D. C. Apperley, N. A. Davis and R. K. Harris, *Organomet.*, **11**, 1718 (1992).

(29) R. K. Harris, A. Sebald, *Magn. Reson. Chem.*, **28**, 81 (1989).

(30) R. K. Harris, S. E. Lawrence, Se-Woung Oh and V. G. Kumar Das, *J. Mol. Struct.*, **347**, 309 (1995).

(31) R. K. Harris and A. Sebald, *Magn. Reson. Chem.*,**25**, 1058 (1987).

Chapter 6

Spectroscopic and Structural Studies of *para*-Substituted Triaryltin(pentacarbonyl)manganese(I) Complexes

6.1 Introduction

Studies of substituent electronic effects on NMR chemical shifts and spin-spin coupling constants date back to the early days of NMR spectroscopy and have been reported for a wide range of nuclei,[1] including those of tin in tetra- and triaryltin complexes.[2,3] It was found by Kroth *et al.*[2] and by Wharf[3] that the ^{119}Sn chemical shifts for the tetraaryltin compounds show good correlations ($r > 0.95$) with substituent constants (σ_R or σ_R°), whereas those of the triaryltin halides only correlate well with a combination of substituent constants (σ_R, σ_I) or (σ_R°, σ_I). However, attempts to correlate the results with Hammett or Taft substituent constants (σ_P or σ_P°) afforded very poor correlations ($r < 0.90$). This implies that the electronic *para*-substituent effects are transmitted through the benzene rings by a combination of inductive and resonance effects for the triaryltin halides. It was also found that $^1J(^{119}Sn\text{-}^{13}C)$ values show good correlations with Hammett resonance substituent constants (σ_R) for five series of aryltin complexes.[3] The tin chemical shifts were described as unusual in that electron-withdrawing substituents were more shielded than was the parent phenyltin compound. However, no analysis was done for the *ipso*-carbon chemical shifts for the five series of compounds studied by Wharf.[3]

The three pentacarbonylmanganese(I) derivatives of the type $Ph_3EMn(CO)_5$ (E = Si, Sn, Pb), studied in Chapter 5, resulted in complex solid-state NMR spectra; however, the $Ph_3SnMn(CO)_5$ complex is more thermally stable and is more easily prepared than are

the analogous silicon and lead complexes. Therefore, a new series of *para*-substituted triaryltinmanganese(I) complexes, (*para*-XC_6H_4)$Sn(CO)_5Mn$ [X = F, Cl, CH_3, OCH_3, SCH_3, and $S(O)_2CH_3$], was prepared in order to study the substituent electronic effects on the ^{55}Mn, ^{119}Sn and ^{13}C chemical shifts and the spin-spin coupling constants and the Mn-Sn bond lengths. These compounds have been fully characterized by various techniques, including vibrational and multinuclear NMR spectroscopy, and single-crystal X-ray diffraction. The results of this study provide an opportunity to determine and correlate the spectroscopic data obtained with substituent constants and will be the major focus of this chapter.

6.2 Result and Discussion

A series of *para*-substituted triaryltin(pentacarbonyl)manganese(I) compounds, (*para*-$XC_6H_4)_3Sn(CO)_5Mn$ [X = F, Cl, CH_3, CH_3S, and $CH_3S(O)_2$], were prepared in high yield as white or pale yellow solids (Table 6.1) by conventional halide displacement reactions, Eq. [6.1.1],[4] with the exception of X = $CH_3S(O)_2$.

$$Ar_3SnCl + Na[Mn(CO)_5] \rightarrow Ar_3SnMn(CO)_5 + NaCl \qquad [6.1.1]$$

The products are stable, crystalline materials, which eventually oxidize to the metal oxide, MnO_2, on exposure to air over a period of two to three months. The reactions of $Na[Mn(CO)_5]$ with (*para*-$XC_6H_4)_3SnCl$ (X = CF_3 and $CH_3S(O)_2$) were unsuccessful, possibly due to the strong electron-withdrawing abilities of these *para* substituents. This withdrawing effect strengthens the Sn-Cl bond and hinders the displacement of chloride by the nucleophile $[Mn(CO)_5]^-$. However, the sulphone complex was prepared by double

oxidation of the sulfur atoms of (*para*-$H_3CSC_6H_4)_3SnMn(CO)_5$ using MCPBA as a mild oxidizing agent. This method does not result in the metal oxide, MnO_2, provided that the reaction temperature is held below -10 °C for a period of 2 h after the addition of MCPBA.

Table 6.1. Some physical properties of $Ar_3SnMn(CO)_5$ (Ar = *para*-XC_6H_5)

X	Solvent[a]	Yield (%)	M.P. (°C)	Color
H	*n*-C_6H_{14}	85	150-152	white
CH_3	CH_2Cl_2 / *n*-C_6H_{14}	67	137-138	white
OCH_3	*n*-C_6H_{14}	75	146-148	white
SCH_3	CH_2Cl_2 / *n*-C_6H_{14}	74	126-128	pale yellow
F	C_6H_6 / *n*-C_7H_{16}	70	128-130	white
Cl	CH_2Cl_2 / n-C_4H_9OH	73	143-145	white
$S(O)_2CH_3$	$CH_3C(O)CH_3$ / C_6H_6	65	260-264[b]	off-white

[a]Solvent used for obtaining single crystals.
[b]Melts with decomposition.

6.2.1 Vibrational Spectra

The FT-IR and FT-Raman spectra of the (*para*-$XC_6H_4)_3SnMn(CO)_5$ complexes exhibit four to six vibrational modes in the carbonyl region, 2250-1850 cm^{-1} (Table 6.2 and Fig. 6.1). Group theory predicts three IR-active ($2a_1 + e$) and four Raman-active ($2a_1 + b_1 + e$) carbonyl stretching modes for an octahedral $R_3EMn(CO)_5$ species with C_{4v} symmetry about Mn. There is little question that the medium intensity band at highest

Table 6.2. FT-IR[a] and Raman[b] carbonyl stretching frequencies of $Ar_3SnMn(CO)_5$ (Ar = *para*-XC_6H_5)

X	a_1^2	b	e	a_1^1	
H	2091.8	2029.2	2012.5 1997.9	1982.8 1974.9	IR
	2093.3	2023.8	2013.4	1991.2 1975.2	R
CH_3	2090.5	2029.5	2008.8	1992.3 1981.0	IR
	2090.9	2025.8	2006.0	1991.2 1986.3	R
OCH_3	2094.7	2032.8	2013.8	1997.6 1982.9	IR
	2093.2	2022.7	2013.8	2001.0 1988.4	R
SCH_3	2095.2	2033.7	2001.4	1979.1	IR
	2095.2	2031.5	2007.6	1990.6	R
F	2095.5	2030.7	2008.9	1998.8 1990.7	IR
	2094.7	2031.2	2011.6	2001.9 1990.6	R
Cl	2095.9	2035.4	2012.4	1997.6 1983.2	IR
	2095.7	2033.1	2022.4	2001.2 1994.5	R
$S(O)_2CH_3$	2106.2	2050.6	2027.3 2009.4	1988.6 1979.9	IR
	2107.0	2050.8	2029.2 2015.0	1991.3 1981.3	R

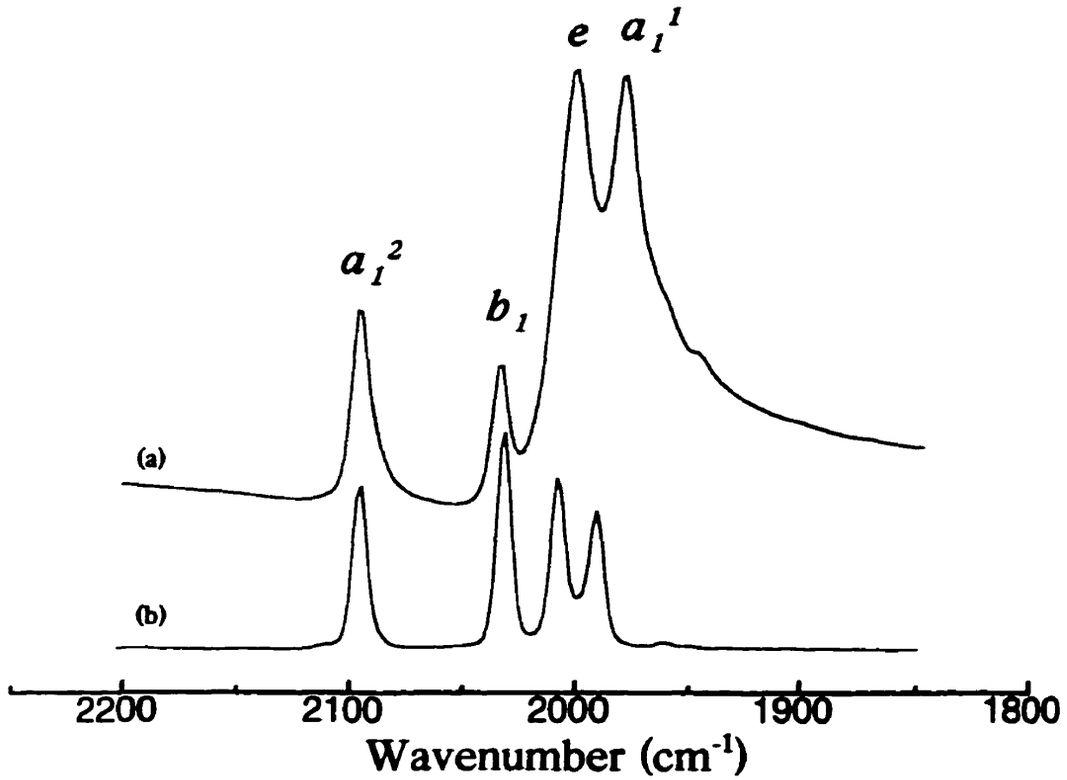

Figure 6.1. (a) FT-IR and (b) FT-Raman spectra of (*para*-$CH_3SC_6H_4)_3SnMn(CO)_5$ in the carbonyl region showing the four typical vibrational modes, a_1^2, b_1, e and a_1^1.

frequency (> 2090 cm^{-1}), in both the IR and Raman spectra, is an a_1^2 mode.[5-8] The true symmetry of the molecule is lower than C_{4V} and the lifting of the selection rules by the asymmetry induced by the R_3Sn (C_{3V} symmetry) fragment results in a weak IR b_1 mode appearing close in energy to the a_1^2 mode.[8] The Raman spectra are in excellent agreement with this prediction, showing a strong band coincident with the weak b_1 mode observed in the IR spectrum (> 2020 cm^{-1}). The strongest IR absorption is expected to be the e mode, and the a_1^1 mode may lie at higher or lower frequency than the e mode or may be

accidentally degenerate with the *e* mode, as has been found in solution studies of triaryltin(pentacarbonyl)manganese(I) complexes.[9-10] It was observed in these studies that the intense *e* modes are at higher frequencies than are the a_1^1 modes (Table 6.2 and Fig. 6.1). There is also splitting of the a_1^1 mode (Fig. 6.2) with the exception of the thioanisyl complex. This type of factor group splitting is not unusual for the a_1^1 mode as it has been previously observed for a series of halo(pentacarbonyl)manganese(I) derivatives.[5]

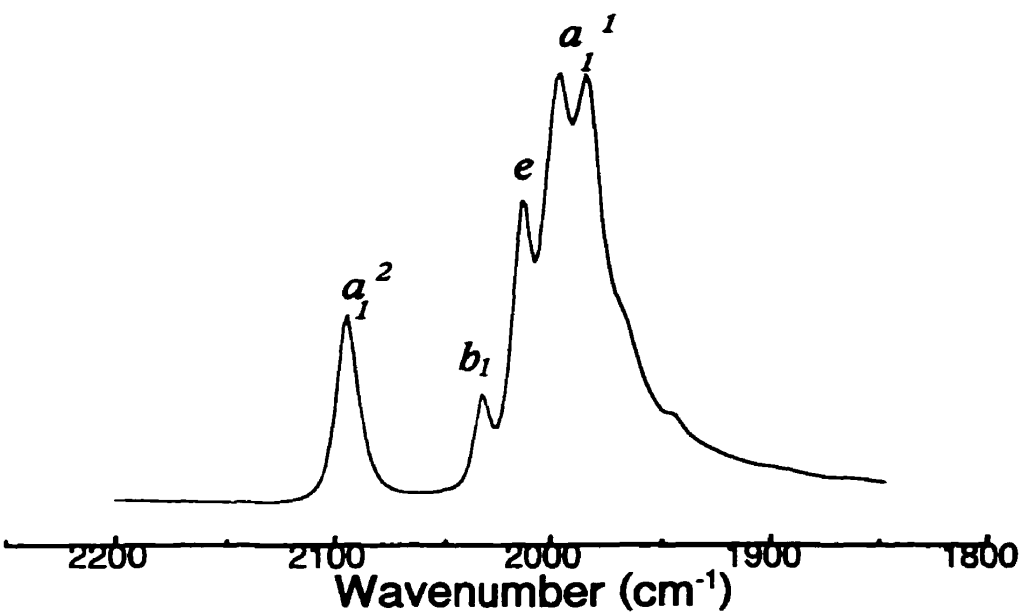

Figure 6.2. FT-IR spectrum of (*para*-$CH_3OC_6H_4)_3SnMn(CO)_5$ in the carbonyl region showing the a_1^2, b_1 and *e* modes, and the splitting of the a_1^1 vibrational mode.

The presence of the sulphone functional group in (*para*-$CH_3S(O)_2C_6H_5)_3Sn$-$Mn(CO)_5$ was easily ascertained. In addition to the strong carbonyl vibrational modes, the FT-IR and FT-Raman spectra show strong bands in the 1300-1320 and 1140-1160 cm^{-1} regions due to the antisymmetric and symmetric stretching modes of the SO_2 group.[11]

6.2.2 Single-Crystal X-ray Diffraction Studies

In view of the lack of well-studied examples of triaryltin(pentacarbonyl)-manganese(I) complexes and in an attempt to identify trends in the geometric parameters and correlate these with their behavior in solution (multinuclear magnetic resonance spectroscopy), X-ray structure analyses of a series of *para*-substituted triaryltin-manganese complex were undertaken. The compounds studied crystallize either in monoclinic ($P2_1/n$ and $P2_1/c$) or triclinic ($P\ \bar{1}$) space groups with a single molecule in the asymmetric unit, except for the $(para\text{-}FC_6H_4)_3Sn$ derivative which was found to have two molecules in the asymmetric unit, (Table 6.3, Appendix II). The structures were solved by the Patterson method[12] and were refined on F^2 by full-matrix least squares calculations to $R < 0.055$ for independent reflections, and all atoms, except for hydrogens, were accounted for satisfactorily. The space groups obtained are not unusual as it was found that the triphenyltin complex can crystallize either in the monoclinic C2/c or $P2_1$ space groups,[13-14] with two and four molecules in the asymmetric units, respectively, depending on the crystallization conditions. The trimethyltin compound was also found to crystallize in the monoclinic $P2_1/n$ space group with one molecule in the asymmetric unit.[15]

Crystallographic data for $(para\text{-}FC_6H_4)_3SnMn(CO)_5$ showed that the two tin sites differ with respect to the orientation of the phenyl rings, whose torsion angles, Mn-Sn-C-C, are 39.6(7)°, 59.6(6)°, 66.0(6)° and -54.0(6)°, -53.0(8)°, -67.8(6)° for molecules I and II, respectively (Table 6.4). The existence of two non-equivalent tin environments was first observed by solid-state ^{119}Sn, CP-MAS, NMR spectroscopy (Chapter 7), and the high symmetry of the $(para\text{-}FC_6H_4)_3Sn$ fragment in molecule II was

Table 6.3. Crystallographic data for (*para*-$XC_6H_4)_3SnMn(CO)_5$ complexes

X	CH_3	OCH_3	SCH_3	F	Cl
Formula	$C_{26}H_{21}O_5MnSn$	$C_{26}H_{21}O_8MnSn$	$C_{26}H_{21}O_5S_3MnSn$	$C_{23}H_{12}O_5F_3MnSn$	$C_{23}H_{12}O_5Cl_3MnSn$
FW	587.06	635.06	683.24	598.96	648.31
Crystal system	Triclinic	Monoclinic	Monoclinic	Triclinic	Monoclinic
Space group	P $\bar{1}$	$P2_1/c$	$P2_1/n$	P $\bar{1}$	$P2_1/c$
Crystal shape	Block	Block	Block	Plate	Plate
Crystal color	Colorless	Colorless	Pale yellow	Colorless	Colorless
Crystal size (mm)	0.36×0.18×0.13	0.35×0.22×0.12	0.45×0.25×0.22	0.52×0.35×0.12	0.51×0.49×0.09
Z[a]	2	4	4	4	4
Z'[b]	1	1	1	2	1
a (Å)	8.815(2)	14.096(2)	10.966(1)	10.636(5)	9.918(2)
b (Å)	11.160(3)	11.161(2)	21.229(2)	11.450(3)	22.940(4)
c (Å)	13.689(2)	17.000(10)	12.297(3)	21.992(7)	11.718(2)
α (°)	98.28(2)	90	90	83.20(3)	90
β (°)	91.11(2)	91.71(2)	101.22(1)	78.30(4)	109.78(1)
γ (°)	106.31(2)	90	90	63.03(2)	90
V (Å^3)	1276.4(4)	2673(2)	2808.0(8)	2336(2)	2580.8(8)
F(000)	584	1264	1360	1168	1264

Table 6.3. (*continued*)

μ (cm^{-1})	15.05	14.52	15.96	16.64	18.49
ρ (g / cm^{-3})	1.527	1.578	1.616	1.703	1.716
Transmission range	0.67 - 0.71	0.64 - 0.76	0.57 - 0.66	0.45 - 0.66	0.33 - 0.62
Reflections measured	9016	9414	9864	16582	8805
Independent reflections (R_{int})	4508 (0.025)	4716 (0.083)	4961 (0.077)	8291 (0.079)	4412 (0.062)
Observed reflections[c] [I>2σI]	3314	2891	3188	5383	3381
# variables in l.s.	302	323	329	596	299
R_1[d], wR_2[e] (obs)	0.0400, 0.0723	0.0546, 0.0918	0.0544, 0.1079	0.0518, 0.0997	0.0474, 0.1192
R_1, wR_2 (all data)	0.0678, 0.0788	0.1121, 0.1033	0.1073, 0.1240	0.0988, 0.1108	0.0748, 0.1264
S[f]	1.044	1.023	1.037	1.101	1.068
Least ΔF map ($e / Å^3$)	0.396 to -0.399	0.570 to -0.595	0.522 to -0.673	0.524 to -0.550	0.958 to -0.626

[a]Number of molecules in the cell.

[b]Number of molecules in the asymmetric unit.

[c]$[I > 2\sigma (I)]$

[d]$R_1 = \Sigma(Fo - Fc) / \Sigma Fo$

[e]$wR_2 = [\Sigma[w(Fo^2 - Fc^2)^2] / \Sigma[w(Fo^2)^2]]^{1/2}$

[f]Goodness-of-fit on F^2; $GoF = [\Sigma[(wFo^2 - Fc^2)^2 / (\text{No. of reflns} - \text{No. of params})]^{1/2}$

apparent in the value of the chemical shift anisotropy. Thus solid-state NMR can be complementary to single-crystal X-ray diffraction studies and can shed light on the nature of the asymmetric unit where there may be some doubt.

The structures of (*para*-$CH_3OC_6H_4)_3SnMn(CO)_5$ and (*para*-$CH_3SC_6H_4)_3SnMn(CO)_5$ are not exactly isomorphous in the crystalline state, although these two compounds crystallize in closely related monoclinic space groups, $P2_1/c$ and $P2_1/n$, respectively. The major differences lie in the torsion angles of the phenyl rings, Table 6.4, and the orientation of the three methyl groups in the crystal lattice, Fig. 6.3. The methyl groups of (*para*-$CH_3OC_6H_4)_3SnMn(CO)_5$ adopt an all-*exo* conformation, whereas in the thiomethyl complex one CH_3 has the *endo*-conformation. The torsion angle for Mn-Sn-phenyl(3) in (*para*-$CH_3SC_6H_4)_3SnMn(CO)_5$ was very different from those obtained for Ph_3Sn-$Mn(CO)_5$[13] and the rest of the complexes studied, Table 6.4. These differences in conformation for the methyl and phenyl groups may be due to the packing effects in the crystal of the *para*-thiomethyl compound.

The most important results of the X-ray diffraction analyses are the Mn-Sn distances, which range from 2.656(2) to 2.693(2) Å (Table 6.4), and all are shorter than the expected value of 2.87 Å derived from Sn-Sn and Mn-Mn distances in the polymer ring of $[(C_6H_5)_2Sn]_6$[16] and in $Mn_2(CO)_{10}$,[17-18] respectively. This observation indicates that appreciable π-backbonding does occur between the manganese 3d orbitals and the tin 5d orbitals and that both the Ar_3Sn and *trans*-CO ligands in the molecule can undergo π-bonding with the same two Mn 3d orbitals. It is, however, difficult to assess the fraction of the π-contribution shared between the R_3Sn moiety and the *trans*-CO ligand,

Table 6.4. Selected bond lengths and angles for (*para*-$XC_6H_5)_3SnMn(CO)_5$

X	CH_3	OCH_3	SCH_3	F		Cl
				Mol I	Mol II	
Distances (Å)						
Mn-Sn	2.6932(11)	2.669(2)	2.6596(12)	2.656(2)	2.664(2)	2.6814(12)
Mn-CO (cis)	1.829(5)	1.854(9)	1.827(8)	1.848(9)	1.847(9)	1.821(10)
	1.847(5)	1.849(8)	1.849(9)	1.823(9)	1.826(8)	1.841(8)
	1.839(6)	1.837(8)	1.867(8)	1.842(9)	1.834(9)	1.836(9)
	1.845(5)	1.824(8)	1.856(9)	1.838(9)	1.852(10)	1.824(9)
Mn-CO (trans)	1.812(7)	1.808(9)	1.832(9)	1.820(8)	1.841(9)	1.821(10)
Sn-C11	2.150(4)	2.144(6)	2.156(7)	2.147(6)	2.145(7)	2.142(6)
Sn-C21	2.159(4)	2.153(4)	2.145(7)	2.143(7)	2.153(7)	2.143(6)
Sn-C31	2.145(4)	2.163(6)	2.171(7)	2.151(7)	2.155(7)	2.151(7)
Angles (°)						
Sn-Mn-C (cis)	84.2(2)	86.7(3)	83.5(2)	83.6(3)	85.6(2)	85.6(3)
	84.3(2)	85.3(2)	84.9(2)	84.5(3)	86.5(3)	82.5(3)
	86.2(2)	83.8(2)	88.3(2)	87.6(2)	83.5(3)	89.3(3)
	87.7(2)	85.9(2)	88.9(2)	86.0(2)	87.9(3)	86.6(3)
Sn-Mn-C (trans)	179.0(2)	177.4(3)	174.4(3)	178.4(2)	178.9(3)	177.5(3)
Mn-Sn-C	112.6(1)	113.0(2)	114.8(2)	114.8(2)	113.8(2)	105.2(2)
	110.3(1)	112.2(1)	112.8(2)	114.1(2)	110.5(2)	114.5(2)
	111.7(1)	115.0(2)	115.1(2)	110.5(2)	115.3(2)	113.2(2)
Torsion angles (°)						
Mn-Sn-phenyl1	56.4(4)	78.7(5)	48.3(7)	39.6(7)	-54.0(6)	76.1(6)
Mn-Sn-phenyl2	59.0(3)	54.9(4)	63.7(6)	59.6(6)	-53.0(8)	54.0(5)
Mn-Sn-phenyl3	69.4(4)	31.3(6)	-22.0(7)	66.0(6)	-67.8(6)	62.6(6)
phenyl1-E-CH_3[a]	---	-172.8(8)	176.4(7)	---	---	---
phenyl2-E-CH_3[a]	---	176.6(7)	168.5(6)	---	---	---
phenyl3-E-CH_3[a]	---	-176.9(7)	-150.5(6)	---	---	---

[a] E = O or S

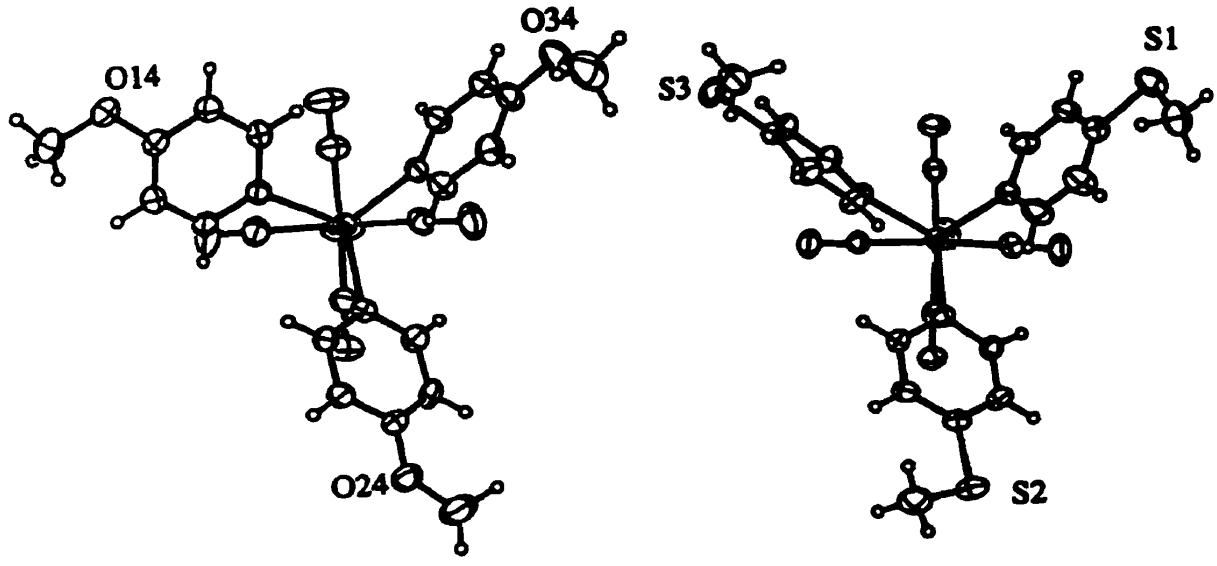

Figure 6.3. View of two different methyl groups conformations in (*para*-$CH_3OC_6H_4)_3Sn$-$Mn(CO)_5$ and (*para*-$CH_3SC_6H_4)_3SnMn(CO)_5$ molecules. Ellipsoids are shown at 30% probability.

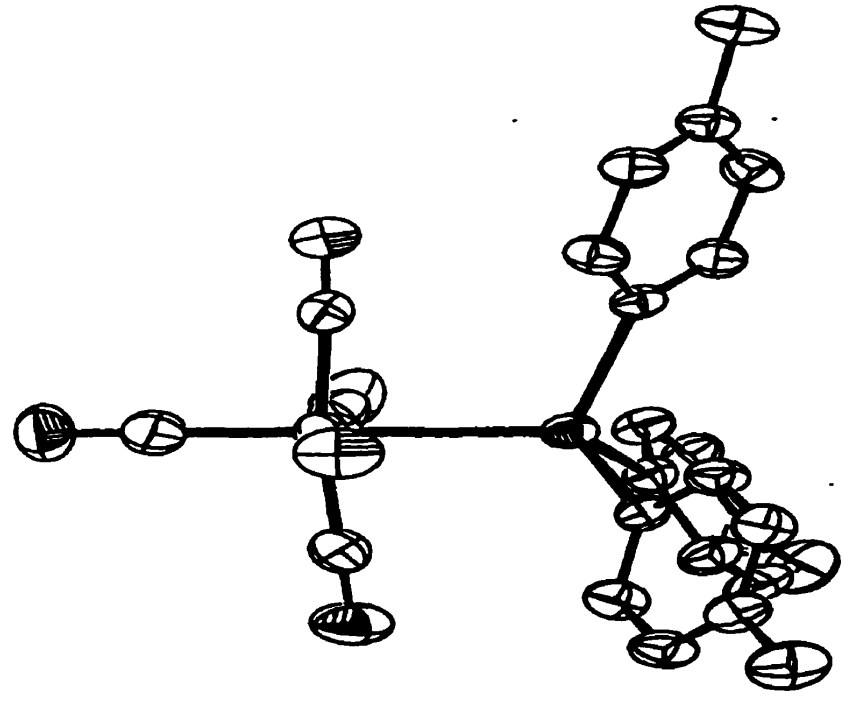

Figure 6.4. ORTEP plot of a (*para*-$CH_3C_6H_4)_3SnMn(CO)_5$ molecule showing the four equatorial carbonyl groups bending towards the Ar_3Sn moiety. Ellipsoids are shown at 30% probability.

as the *trans*-CO Mn-C distances, ranging from 1.805(8) to 1.850(10) Å, lie within the range [1.820(10) to 1.866(9) Å] of the *cis*-CO Mn-C distances (Table 6.4). Nevertheless, it can be concluded that the R_3Sn fragment is at least as good, but not a better π-acceptor ligand than is the carbonyl group. The four *cis*-CO groups around the manganese atoms (Fig. 6.4) show the typical arrangement seen in complexes of this type in that they are bent towards the tin atom,[13-15] with Sn-Mn-C bond angles in the range of 83.6(3) to 89.6(2)°.

6.2.3 Multinuclear Magnetic Resonance Studies.

The ^{119}Sn solution NMR spectra exhibit sharp singlets in the -12.0 to 5.0 ppm range (Table 6.5), indicating the presence of a single tin environment with no spin-spin coupling to the spin-5/2 ^{55}Mn nucleus. The $^1J_{Mn-Sn}$ values cannot be obtained from solution spectra of either the spin-1/2 or the quadrupolar nucleus, due to rapid relaxation of the quadrupolar nucleus. The small ^{119}Sn chemical shift range observed (17 ppm) for all the complexes suggests that the tin centres are in very similar chemical environments and no changes in coordination occur. The $\delta(^{119}Sn)$ values show no correlation with the Hammett (σ_p), Taft (σ_p°), or resonance (σ_R or σ_R°) parameters.[19] However, the ^{119}Sn chemical shifts do show a tendency to move upfield with electron donating groups in the *para* position. This effect is not unusual, since electron-donating substituents will increase the electron density at the *ipso*-carbon atom, which is then transferred onto the tin nucleus and results in shifts of the ^{119}Sn resonances to high field (low frequency). Previous studies of tetraaryltins and triaryltin halides[1-3] showed that the ^{119}Sn chemical shifts failed to change with electron-donor substituents in the anticipated manner, and no satisfactory

interpretation or discussion of these chemical shifts in terms of current theories of shielding was provided.

Table 6.5. ^{119}Sn and ^{55}Mn NMR Parameters of $Ar_3SnMn(CO)_5$ (Ar = *para*-XC_6H_5)

X	$\delta(^{119}Sn)$ (± 0.05 ppm)	$\delta(^{55}Mn)$ (± 5.0 ppm)	$\Delta\nu_{1/2}$[a] (Hz)
H	-11.93	2502	4470
CH_3	-10.37	2526	5662
OCH_3	-6.33	2524	5736
SCH_3	-4.84	2498	9089
F	-0.19	2493	5588
Cl	1.13	2479	6407
$S(O)_2CH3$	5.14	2435	8642

[a]Manganese-55 NMR line width at half-height.

The ^{55}Mn NMR spectra exhibit broad peaks (Table 6.5) with no spin-spin coupling to the tin nucleus. It was expected that the manganese nucleus would become more shielded as the electron-donating power of the *para*-substituent groups increases and the ^{55}Mn chemical shift should move progressively to higher field. However, the chemical shifts show the opposite trend and do not correlate with single substituent parameters. It was believed that, as the electron releasing power of the *para* group increases, the electron density at the tin nucleus will increase, as was illustrated by the $\delta(^{119}Sn)$ data.

This will result in an increase of the σ-bonding interaction between the two metal nuclei, and may even strengthen the π-donor ability of the Mn nucleus. This interpretation would account for the contradictory results observed for the ^{55}Mn chemical shift data. These effects are not reflected in the Mn-Sn bond lengths, Table 6.4. Bancroft *et al.*[20] have obtained a linear correlation between the chemical shifts and line widths for a series of $Ph_n(F_5C_6)_{3-n}SnMn(CO)_5$ complexes. For the complexes studied in this work, no such correlation was observed.

The ^{13}C chemical shift data and $^{n}J(^{119}Sn\text{-}^{13}C)$ values are given in Table 6.6. The spin-spin coupling constants follow the typical trend for substituted benzene compounds in that $^{1}J(^{119}Sn\text{-}^{13}C) > {}^{3}J(^{119}Sn\text{-}^{13}C) > {}^{2}J(^{119}Sn\text{-}^{13}C) > {}^{4}J(^{119}Sn\text{-}^{13}C) \approx 0$ Hz. The $^{1}J(^{119}Sn\text{-}^{13}C)$ values lie in the 405-336 Hz range, and are about 20% smaller than are the values obtained by Wharf[3] for series of *para*-substituted tetra- and triaryltin complexes. This result also confirms, according to the Fermi contact mechanism, that there is considerable π-backbonding between the two metal nuclei, an effect that predicts that the $^{1}J(Sn\text{-}^{13}C)$ values should be smaller than those obtained for the tin complexes studied by Wharf.[3] The chemical shifts and spin-spin coupling constants show no correlations with Hammett σ_p or Taft σ_p° substituent parameters. However, the *ipso*-carbon δ_{iso} values do show a moderately good-fit ($r > 0.92$) with the resonance parameters σ_R and σ_R° (Fig. 6.4.).

The chemical shifts and one-bond coupling constants do correlate, however, with dual substituent parameters (DSP) (σ_I, σ_R) and (σ_I, σ_R°), as shown in Table 6.7. The relationship between the chemical shifts and spin-spin coupling constant, and the DSP meet the requirements stated by Brownlee *et al.*[21-22] that data for NMR correlations should

Table 6.6. ^{13}C NMR Parameters, δ (± 0.1 ppm), $^{n}J_{Sn\text{-}C}$ (± 0.3 Hz), of $Ar_3SnMn(CO)_5$ (Ar = *para*-XC_6H_5) in $CDCl_3$

X	$\delta(C_{ipso})$ $^{1}J(^{119}Sn\text{-}^{13}C)$	$\delta(C_{ortho})$ $^{2}J(^{119}Sn\text{-}^{13}C)$	$\delta(C_{meta})$ $^{3}J(^{119}Sn\text{-}^{13}C)$	$\delta(C_{para})$	$\delta(CO_{eq})$	$\delta(CO_{ax})$	$\delta(CH_3)$
H	141.2 (382.3)	136.7 (37.6)	128.5 (46.6)	128.6	213.4	211.6	---
CH_3	137.4 (393.5)	136.6 (38.3)	129.3 (48.6)	138.3	213.4	211.7	21.4
OCH_3	131.7 (405.2)	137.7 (43.4)	114.4 (51.8)	160.1	213.6	211.7	54.9
SCH_3	137.0 (388.9)	136.7 (38.5)	126.1 (47.5)	139.4	212.9	211.2	15.1
F[a]	135.7 (383.5)	138.0 (43.8)	115.7 (51.1)	163.5	212.6	210.8	---
Cl	137.4 (372.8)	137.7 (41.3)	128.9 (47.1)	135.5	212.3	210.6	---
$S(O)_2CH_3$	148.5 (336.2)	137.6 (38.3)	127.1 (43.8)	141.7	211.8	210.2	44.5

[a] ($^{1}J_{C\text{-}F}$ = 247.9Hz, $^{2}J_{C\text{-}F}$ = 19.5, $^{3}J_{C\text{-}F}$ = 6.5, and $^{4}J_{C\text{-}F}$ = 3.9 Hz.)

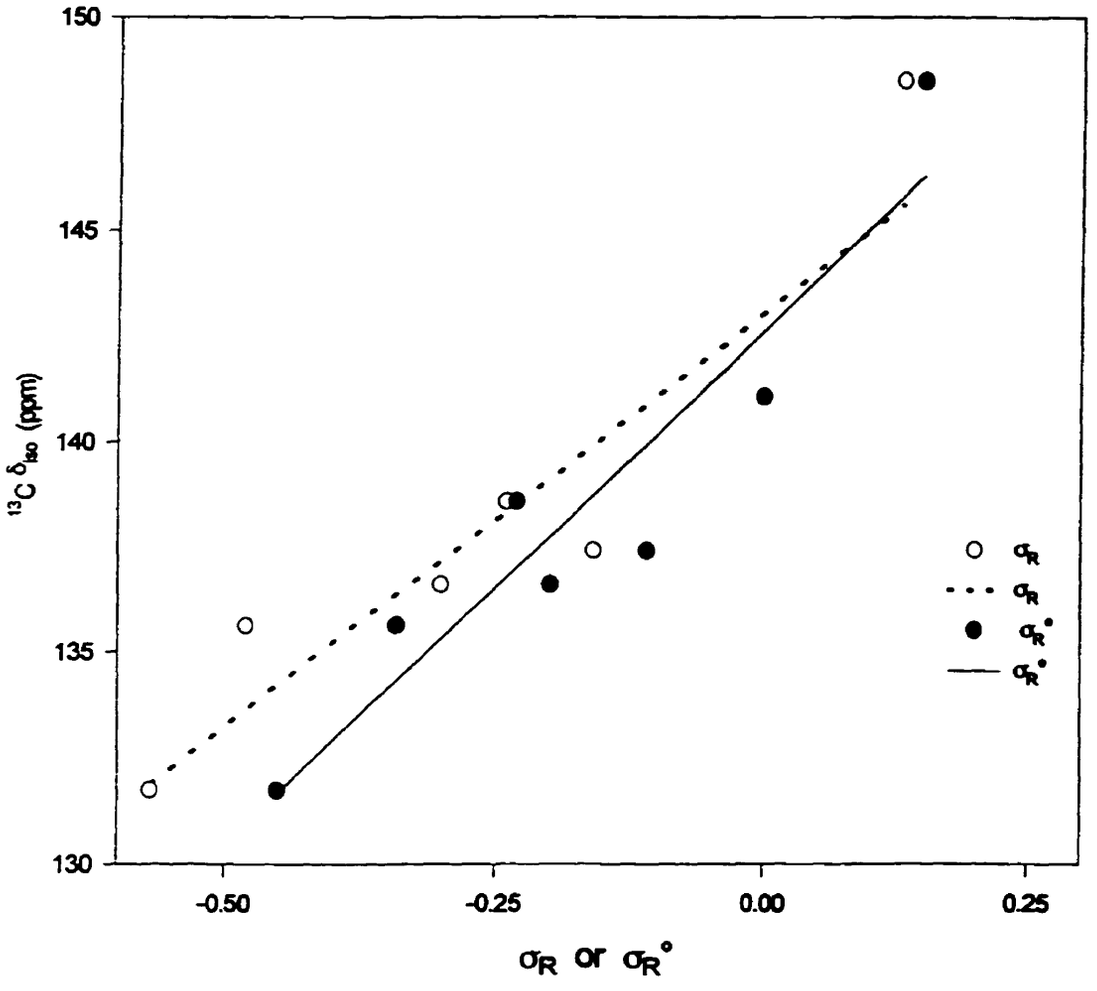

Figure 6.5. Plot of *ipso*-^{13}C chemical shift values for (*para*-$XC_6H_4)_3SnMn(CO)_5$ in $CDCl_3$ against single substituent parameters, σ_R (o) and σ_R° (•); solid lines (–) r = 0.956 or broken lines (---) r = 0.952.

be derived from measurements on a large number of representative compounds, giving correlation coefficients r > 0.95. The regression analyses show excellent correlations with both (σ_I, σ_R) and (σ_I, σ_R°). However, the results obtained from (σ_I, σ_R°) give slightly less

satisfactory fits than do those obtained from (σ_I, σ_R). The correlation coefficients were also tested by means of the "goodness-of-fit" parameter, f = SD/ RMS, where SD is the standard deviation of residuals and RMS is the root-mean-square size of the experimental data. The goodness-of-fit data were in excellent agreement with the required criterion, $f <$ 0.15. The DSP fits indicate that both the inductive and resonance effects are important in determining the chemical shift and spin-spin coupling constants for *para*-subsituted aryltin complexes, (Table 6.7).

The *ipso*-^{13}C chemical shift values show a strong dependence on the resonance parameter σ_R, but the influence of the inductive effect is still significant, showing why single substituent parameter treatments are inadequate in this case. The extent of these interactions can be gauged from the sign and magnitude of the demand parameters ϱ_I and ϱ_R. The positive values obtained for both ϱ_I and ϱ_R (Table 6.7) for the *ipso*-^{13}C shifts indicate that electron density is transmitted by polar and resonance effects away from *para* electron donating groups towards the *ipso*-carbon atoms and can be best described by Fig. 6.6. However, the correlation of the ^{119}Sn chemical shifts with DSP show that inductive effects are the major contributor, and resonance effects account for less than 10% of the overall transmission. These effects were not unexpected, since previous studies, both experimental[3] and theoretical,[23,24] have shown that little or no p_x-d_x interaction occurs between the carbon-2p and tin-5d orbitals.

Table 6.7. Chemical Shifts Regression Analysis Parameters[a] for the seven *para*-Subsituted $Ar_3SnMn(CO)_5$ complexes studied

	ϱ_I	ϱ_R	C	r[b]	SD[c]	f[d]
$\delta = \varrho_I\sigma_I + \varrho_R\sigma_R + C$						
$\delta(^{119}Sn)$	25.78	5.61	-10.73	0.991	0.800	0.138
$\delta(^{55}Mn)$	-104.1	-85.53	2507.0	0.996	2.59	0.084
$\delta(^{13}C_{ipso})$	7.81	20.62	140.8	0.995	0.481	0.098
$^1J(^{119}Sn\text{-}^{13}C)$	-60.54	-72.96	382.1	0.999	0.909	0.045
$\delta = \varrho_I\sigma_I + \varrho_R\sigma^\circ_R + C$						
$\delta(^{119}Sn)$	25.54	6.52	-10.86	0.988	0.900	0.154
$\delta(^{55}Mn)$	-100.71	-103.13	2508.0	0.990	3.96	0.129
$\delta(^{13}C_{ipso})$	7.01	25.14	140.6	0.994	0.518	0.106
$^1J(^{119}Sn\text{-}^{13}C)$	-57.67	-88.54	383.2	0.995	1.97	0.098

[a]Values for σ_I, σ_R and σ°_R are from ref. 19.
[b]Multiple correlation coefficient.
[c]Standard deviation of residuals.
[d]Goodness-of-fit parameter, SD/RMS.

The DSP analyses of the ^{55}Mn chemical shift and spin-spin coupling values show that resonance effects and polar effects contribute approximately equally (Table 6.7). The ^{55}Mn chemical shifts reveal the expected trend that as the inductive interaction increases between the tin and carbon atoms, the σ-donor ability of the tin towards the manganese nucleus decreases. This decrease in σ-donor ability is compensated by an increase in d_z-d_z backbonding between the two metal nuclei and, as a result, a decrease in electron density at the transition metal nucleus is observed, with negative ϱ_I, ϱ_R and ϱ_R° values (Table 6.7). The results of the fits of chemical shift and spin-spin coupling analyses with DSP indicate that single substituent parameters, such as the Hammett σ_P or Taft σ_P° parameters, are inadequate for any given system.

(a)

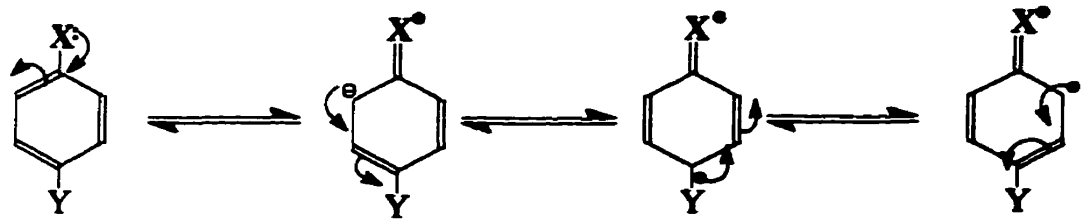

(b)

Figure 6.6. Representation of (a) resonance and (b) induction effects in 1,4-disubstituted benzene complexes, where $|-\delta\pm| = |-(\delta\pm + \delta\delta\pm + \delta\delta\delta\pm)|$.

References

(1) D. J. Craik, in *Annual Reports on N.M.R. Spectroscopy*, (G. A. Webb ed.), Academic Press, New York, **15**, 1 (1983).

(2) H. J. Kroth, H. Schumann, H. G. Kuivala, C. D. Jr Schaeffer and J. J. Zuckerman, *J. Am. Chem. Soc.* **97**, 1754 (1975).

(3) I. Wharf, *Inorg. Chim. Acta* **159**, 41 (1989).

(4) R. D. Gorsich, *J. Am. Chem. Soc.*, **84**, 2486 (1962).

(5) I. S. Butler and H. K. Spendjian, *Can. J. Chem.* **47**, 4117 (1969).

(6) A. M. English, K. P. Plowman and I. S. Butler, *Inorg. Chem.* **20**, 2553 (1981).

(7) D. M. Adams and I. O. C. Ekejiuba, *J. Chem. Phys.* **77**, 4793 (1982).

(8) D. M. Adams, in *Metal-Ligand and Related Vibrations:A Critical Survey of the Infrared and Raman Spectra of Metallic and Organometallic Compounds*, Edward Arnold Ltd., London, 84 (1967).

(9) W. Jetz, P. B. Simons, J. A. J. Thompson and W. A. G. Graham, *Inorg. Chem.*, **5**, 2217 (1966).

(10) D. J. Patmore and W. A. G. Graham, J. *Organomet. Chem.* **6**, 981 (1967).

(11) M. Bouquet, G. Chassaing, J. Corset, J. Favrot and J. Limouzi, *Spectrochimica Acta* **37**, *37*, 727 (1981).

(12) J. C. Calbrese, *Phase-Patterson Heavy Atom Solution Extractor*, University of Wisconsin, Madison, Ph. D. Thesis (1972).

(13) H. P. Weber and R. F. Bryan, *Acta Cryst.*. **22**, 822 (1967).

(14) R. F. Bryan, *J. Chem. Soc. A*, 696 (1968).

(15) Kh. A. I. F. M. Mannan, *Acta Cryst.* **B24**, 603 (1968).

(16) D. H. Olson and R. E. Rundle *Inorg.Chem.* **2**, 1310 (1963).

(17) L. F. Dahl and R. E. Rundle, *J. Chem. Phys.* **26**, 1750 (1957).

(18) L. F. Dahl and R. E. Rundle, *Acta Cryst.* **16**, 419 (1963).

(19) C. Hansch and A. Leo, in *Substituent Constants for Correlation Analysis in Chemistry and Biology*, Wiley, New York (1979).

(20) G. M. Bancroft, H. C. Clark, R. G. Kidd, A. T. Rake and H. G. Spinney, *Inorg.Chem.* **14**, 2643 (1973).

(21) S. Ehrenson, R. T. C. Brownlee and R. W. Taft, *Prog. Phys. Org. Chem.* **6**, 147 (1968).

(22) J. Bromilow and R. T. C. Brownlee, *J. Org. Chem.*, **44**, 1261 (1979).

(23) P. G. Perkins and D. H. Wall, *J. Chem. Soc. A*, 3670 (1971).

(24) E. M. Berksoy and M. A. Whitehead, *Tetrahedron*, (1988) .

Chapter 7

Second-order Effects in Solid-State, CP-MAS, Tin-119 NMR Spectra of *para*-Substituted Triaryltin(pentacarbonyl)manganese(I) Complexes

7.1 Introduction

Solid-state, CP-MAS, ^{119}Sn NMR spectra of organometallic complexes containing a main-group quadrupolar nucleus have proved particularly useful in recent years in understanding the structures, bonding interactions, and molecular dynamics of organotin complexes.[1-6] However, no solid-state NMR study has been reported in the literature concerning covalent bimetallic complexes involving tin [or any other group 14 (IVA) element] and a transition metal. Examples of such bimetallic compounds containing manganese carbonyl and triorganotin fragments were first prepared many years ago by Gorsich[7] and Jetz *et al.*,[8] and the triorganotin radicals in the $R_3SnMn(CO)_5$ compounds were characterized as good σ-donors and π-acceptors on the basis of IR, Raman and X-ray crystallographic data.[9-12] Most of the theoretical and experimental work on *para*-substituted tri- and tetra-aryltin complexes has involved solution studies of the isotropic tin-119 chemical shifts and spin-spin coupling ($^nJ_{C\text{-}Sn}$) between ^{13}C and ^{119}Sn, and it has been found that small changes in molecular structure can lead to significant changes in both of these parameters.[13,14] These changes have been related to the electronegativities of the substituents, their σ- and π-bonding character, and the coordination state of the tin atom.[13]

The objective of the present study was to investigate the effects of *para*-substituents on the aryl rings in the solid-state, CP-MAS, ^{119}Sn NMR spectra of the

compounds described in chapter 6. The specific parameters under investigation were the manganese-tin spin-spin coupling constants ($^1J_{Mn-Sn}$), the effective dipolar coupling constants, and the ^{55}Mn quadrupole coupling constants. This study provides an opportunity to examine the relationship between the $^1J_{Mn-Sn}$ coupling and the nuclear quadrupole coupling constant, χ, in these triarytin(pentacarbonyl)manganese(I) derivatives.

7.2 Results and Discussion

When a spin-1/2 nucleus, such as ^{119}Sn, is bonded to a quadrupolar nucleus, the solid-state NMR spectrum is more complex than is the solution spectrum (Fig. 7.1). The latter often shows only a single line without spin-spin coupling, whereas in the solid-state CP-MAS spectrum, multiplets with uneven spacings are observed. Examples of spin pairs involving either a $^{117/119}Sn$ or ^{55}Mn nucleus for which such effects have been reported are (^{119}Sn, $^{35/37}Cl$),[2-3] (^{13}C, ^{55}Mn)[15] and(^{31}P, ^{55}Mn).[15-17] However, the solid-state ^{119}Sn NMR spectrum of the $Ph_3Sn(CO)_5Mn$ system, discussed in Chapter 5, was complicated by the presence of four molecules in the asymmetric unit cell[10] with three isotropic chemical shifts. The spectra of the complexes studied in this part of the thesis are much simpler, with one or two sets of isotropic chemical shifts and without any overlapping peaks. The solid-state ^{119}Sn NMR spectrum of $(p\text{-}FC_6H_4)_3Sn\text{-}(CO)_5Mn$ consists of two sets of centreband multiplets, while the other complexes in the series exhibit a single set of

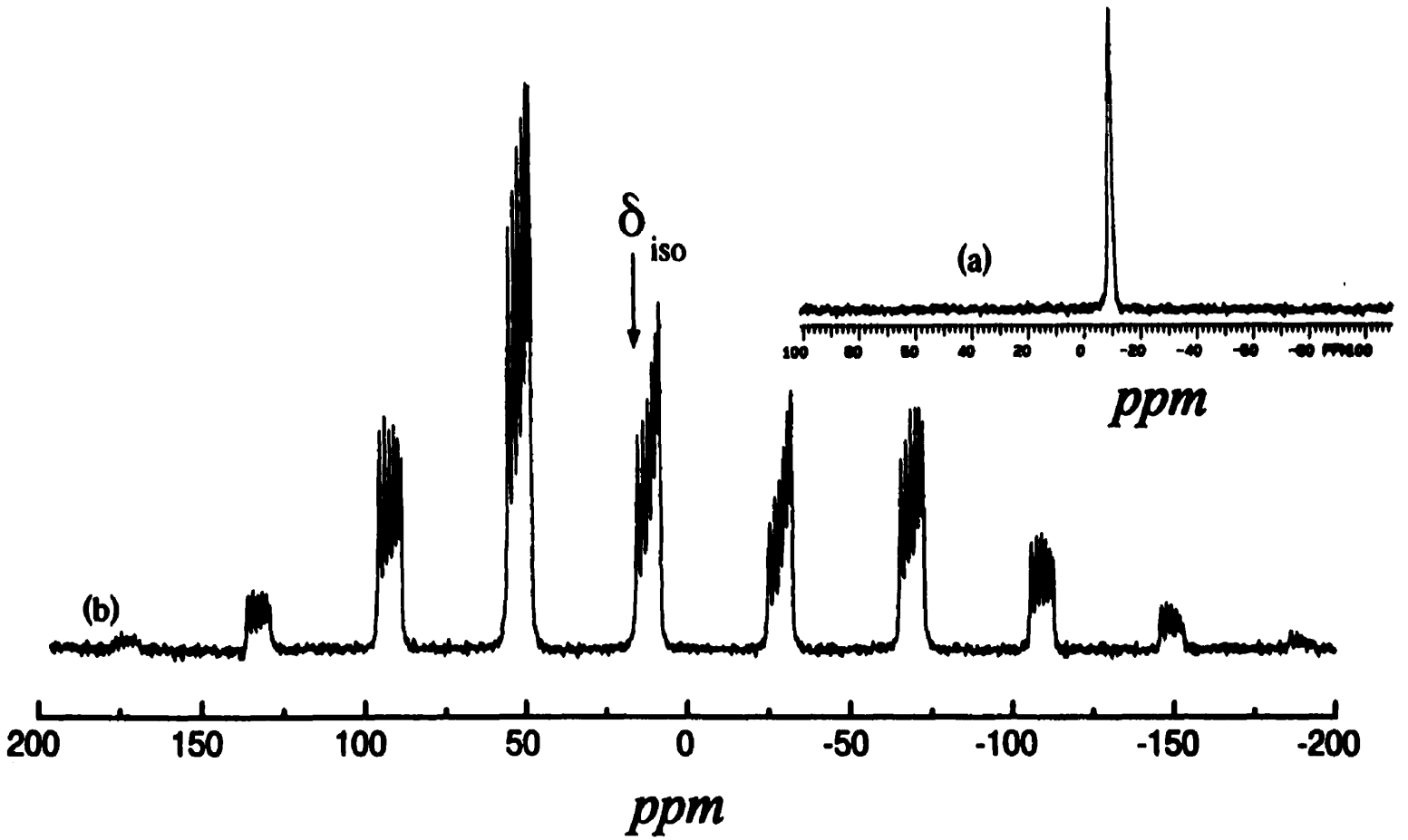

Figure 7.1. (a) Solution and (b) solid-state ^{119}Sn NMR spectra of (*para*-$CH_3OC_6H_4)_3$Sn-$(CO)_5$Mn obtained at 111.725 MHz with proton decoupling. Solid-state experimental conditions: contact time 3 ms, recycle delay 3 s, number of transients 20,000.

122

centreband multiplets (Fig. 7.2). This difference indicates that there are at least two distinct tin environments in solid $(p\text{-}FC_6H_4)_3Sn(CO)_5Mn$. X-ray crystallographic data for this compound show that it crystallizes in the space group $P\ \bar{1}$, with four molecules in the unit cell (Chapter 6, Appendix II). Thus, the asymmetric unit contains two different molecules and two non-equivalent tin atoms, in excellent agreement with the solid-state NMR result. The crystal structures of the remaining complexes were also determined, and all were found to contain one molecule in the asymmetric unit. These results are also consistent with those obtained from the solid-state ^{119}Sn NMR spectra.

From single crystal, broad-line, ^{55}Mn NMR studies and molecular symmetry arguments,[17] it was shown that the electric field gradient tensors are close to axial symmetry for $X_3Sn(CO)_5Mn(I)$ (X = Cl, Ph). This implies that the principal component of the electric field gradient, q_{ZZ}, lies near or along the internuclear vector $r_{Mn\text{-}Sn}$ and the angular factors in Eq [3.5.4] are small or equal to zero. In such circumstances, which are assumed for for the *para*-triaryltin(pentacarbonyl)manganese(I) cases, there is a much simpler expression for D″ (Eq. [5.2.1]):

Analysis of the splitting patterns (Fig. 3.7) was possible for all the complexes studied, by using Eq. [5.2.1], which resulted in the determination of the isotropic chemical shifts, δ_{iso}, the spin-spin coupling constants, $^1J_{Mn\text{-}Sn}$, and the effective dipolar-quadrupolar constants, $3\chi(D\text{-}\Delta J/3)/10\nu_S$ (Table 7.1). The isotropic shifts of the complexes in the solid state vary from those obtained from the solution NMR spectra, differing by as much as 33 ppm in the case of the *para*-chloro complex. This is mainly due to the sensitivity of ^{119}Sn chemical shifts to the electronic environment and not to changes in

Table 7.1. Solid-state and solution ^{119}Sn NMR isotropic chemical shifts and coupling constants of (*para*-XC_6H_4)$SnMn(CO)_5$

X	δ_{iso} (soln)	δ_{iso} (solid)	J_{Mn-Sn} (solid) (Hz)	d (Hz)
CH_3	-10.37	-16.6	132(2)	33.3(1.0)
H (a,b)[a]	-11.93	-13.6	135(2)	34.4(0.4)
H (c)	-11.93	2.82	141(3)	30.3(2.8)
H (d)	-11.93	5.66	141(2)	34.3(0.3)
OCH_3	-6.33	11.4	149(1)	28.9(0.8)
F (a)	-0.19	6.6	165(2)	22.7(0.5)
F (b)	-0.19	16.0	151(2)	26.2(0.8)
Cl	1.13	-32.1	160(2)	25.7(1.5)
SCH_3	-4.84	12.6	170(1)	25.1(0.2)
$S(O)_2CH_3$[b]	6.63	-10.1	250(3)	36.1(1.0)

[a]Two equivalent tin atoms.
[b]Spectrum was recorded on a Chemagnetics M-100 spectrometer operating at a field strength of 2.35 T.

coordination number of the tin or manganese nucleus in solution. This type of effect has also been observed for Ph_4Sn, Ph_3SnCl and other tin complexes.[1] The spin-spin coupling between ^{117}Sn or ^{119}Sn and ^{55}Mn, $^1J_{Mn-Sn}$, was not observed in the solution ^{117}Sn or ^{119}Sn NMR spectra due to fast quadrupolar relaxation of ^{55}Mn nuclei. However, this coupling is observed in the solid-state ^{117}Sn and ^{119}Sn NMR spectra. The $^1J_{Mn-Sn}$ couplings were determined and found to lie in the range of 132 to 250 Hz for the triaryltin complexes. It was difficult to resolve the peak positions of the centreband and sidebands of the

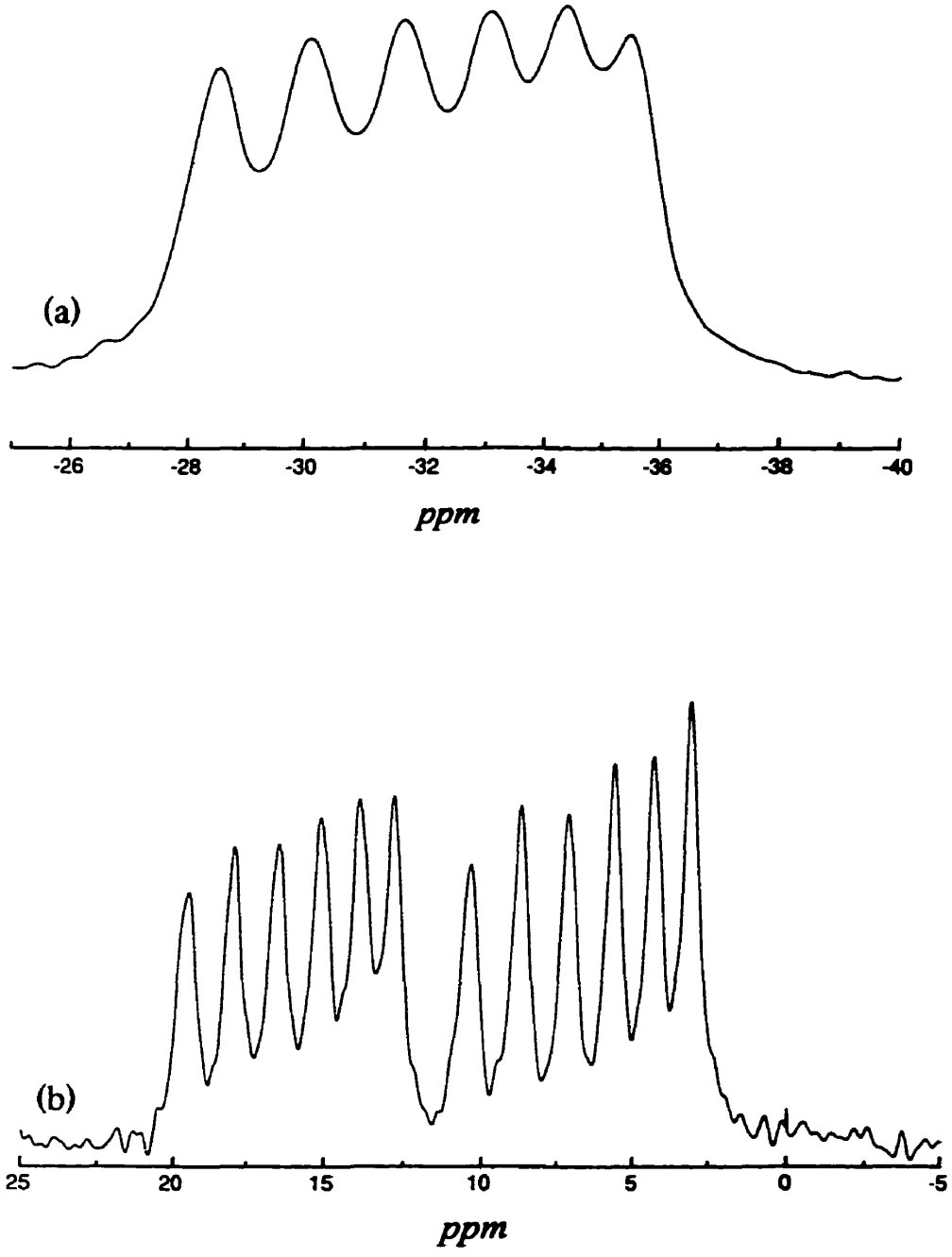

Figure 7.2. Centreband regions of the ^{119}Sn NMR spectra of (a) (*para*-$ClC_6H_4)_3Sn$-$(CO)_5Mn$ and (b) (*para*-$FC_6H_4)_3Sn(CO)_5Mn$ obtained at 111.725 MHz with proton decoupling showing one and two distinct tin environments in the solid-state. Experimental conditions: (a) contact time 3 ms, pulse delay 5 s, number of transients 12,000; (b) contact time 3 ms, pulse delay 4 s, number of transients 19,500.

spectrum obtained at 111.7 MHz for the sulfone derivative (Fig 7.3). However at 37.2 MHz, the centreband and the spinning sidebands of the spectrum, for this complex are well resolved and the values of the spin-spin and effective dipolar-quadrupolar constants were easily determined. Both the ^{117}Sn and ^{119}Sn NMR spectra were recorded for the *para*-SCH_3 complex (Fig. 7.4) but only ^{119}Sn spectra were recorded for the other complexes, because of the lower receptivity of the ^{117}Sn nucleus. However, the reduced coupling constants (Eq. [7.2.1]) for the *para*-SCH_3 complex, $^1K(^{117}Sn,^{55}Mn)$ and $^1K(^{119}Sn,^{55}Mn)$, were found to be the same, $-1.51\times10^{21}\ T^2J^{-1}$, from both solid-state spectra.

$$^nK(Sn,Mn) = 4\pi^2\ ^nJ(Sn,Mn) / (\gamma_{Sn}\ \gamma_{Mn})h \qquad [7.2.1]$$

The δ_{iso} and $^1J_{Mn\text{-}Sn}$ values in the solid-state are extremely sensitive to the electronic environment and to the nature of the *para*-substituents of the phenyl rings leading to changes in $^1J_{Mn\text{-}Sn}$ (by as much as 120 Hz) and in δ_{iso} (up to 44 ppm). For the two crystallographically non-equivalent molecules in $(p\text{-}FC_6H_4)_3Sn(CO)_5Mn(I)$, a slight change in the torsion angles of the phenyl rings modifies the environment around the tin atom, and also causes differences in δ_{iso} and $^1J_{Mn\text{-}Sn}$ (Table 7.1).

The effective dipolar coupling constants and the quadrupole coupling constants cannot be determined separately from the effective dipolar-quadrupolar couplings, unless one of these quantities is known. The quadrupole coupling constants can be obtained experimentally from either NQR measurements or single-crystal NMR studies, but are notoriously difficult to determine for manganese complexes. The values of D″, Eq.[3.5.5], were obtained from a regression plot of m *vs.* $\Delta\delta_{mI}$. The average values of D″ were determined from two or more spinning speeds and were found to lie in the range from

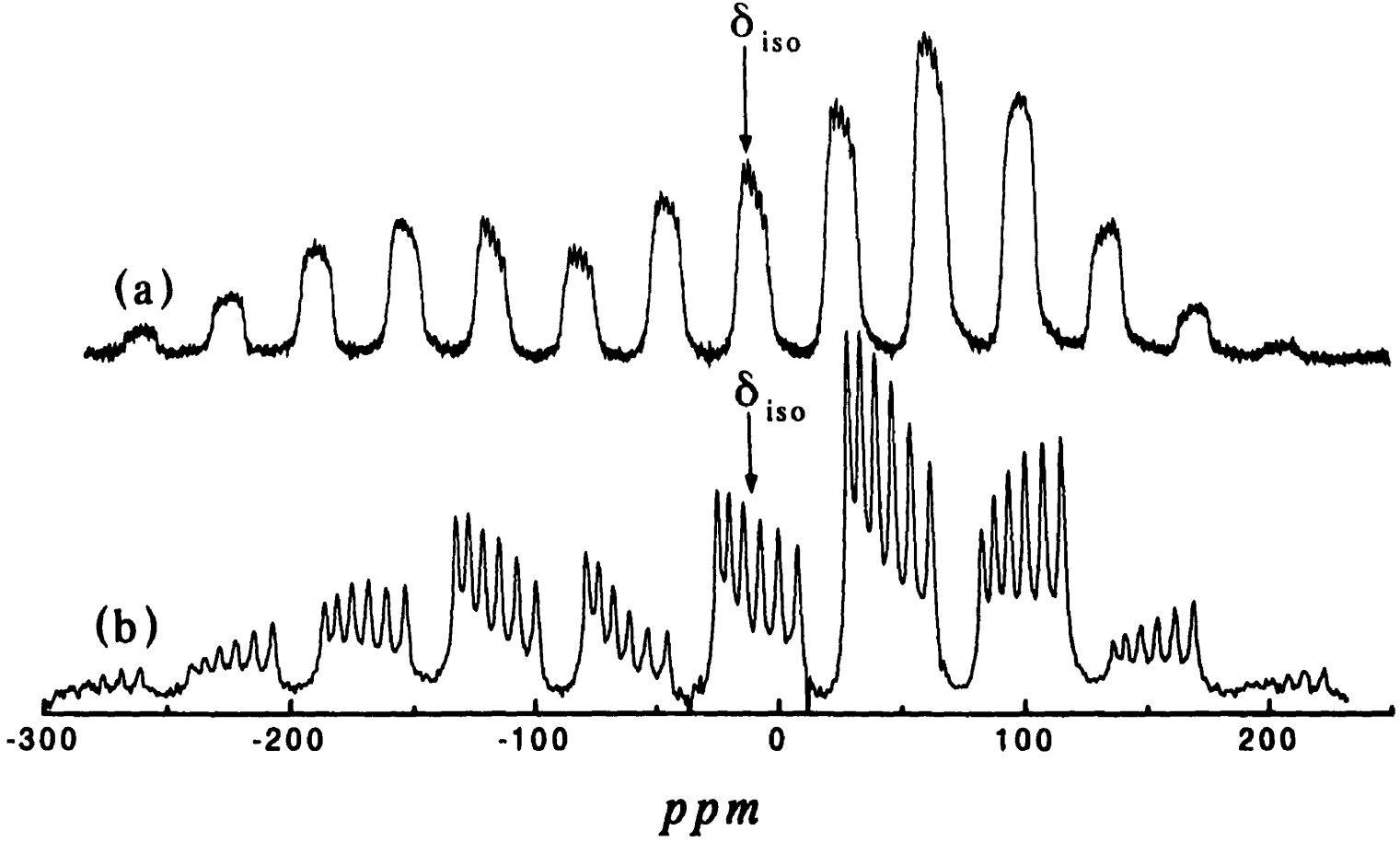

Figure 7.3. Solid-state ^{119}Sn NMR spectra of (*para*-$CH_3S(O)_2C_6H_4)_3Sn(CO)_5Mn$ obtained at (a) 111.725 MHz and (b) 37.252 MHz with proton decoupling. Spectrometers operating conditions: (a) contact time 2 ms, pulse delay 1 s, number of transients 20,000; (b) contact time 2 ms, pulse delay 1 s, number of transients 2,500.

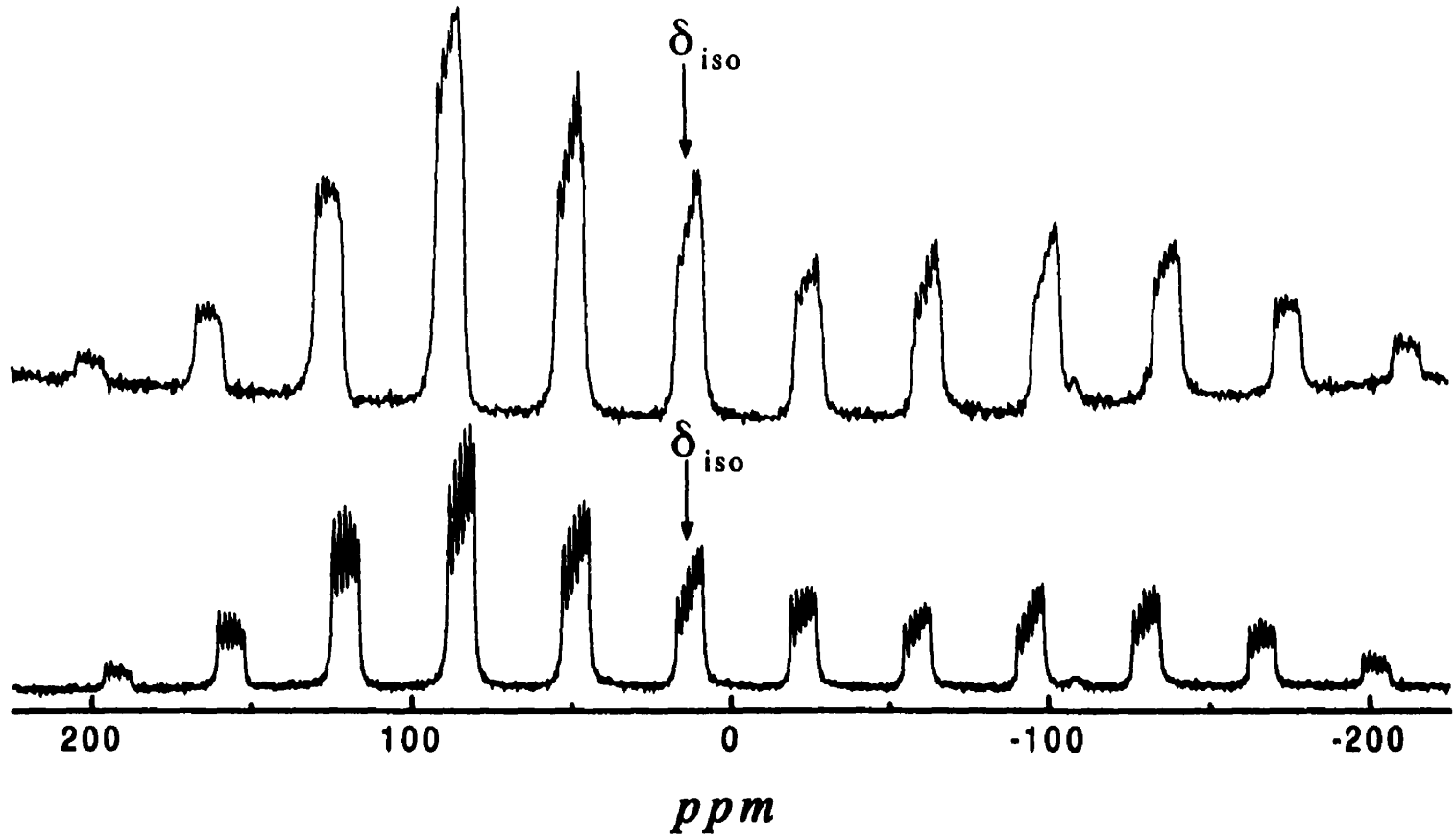

Figure 7.4. Solid-state (a) ^{117}Sn and (b) ^{119}Sn, CP-MAS, NMR spectra of (*para*-$CH_3SC_6H_4)_3Sn(CO)_5Mn$ obtained at (a) 111.725 MHz and (b) 106.757 MHz, respectively. Experimental conditions: (a) contact time 3 ms, pulse delay 2 s, number of transients 35,000; (b) contact time 3 ms, pulse delay 2 s, number of transients 20,000.

-363 to -493 Hz. The values of χ, using Eq. [3.5.1], were then determined to be in the -7.5 to 20 MHz range (Table 7.2). The quadrupole coupling constant for the sulfone complex was negative, which implies that the principal axis of the electric field gradient has reversed direction. This may due to the strong electron withdrawing ability of the sulfone group, which results in a decrease of electron density at the tin atom.

From the crystal structure data and spinning sideband analyses, the dipolar coupling constants, Eq [3.5.3], and the anisotropies in the spin-spin coupling, Eq [5.2.1], were shown to be in the range of -570 to -595 Hz and 268 to 622 Hz, respectively. The anisotropies of J are large and are similar in magnitude to the dipolar coupling constant and, therefore, should not be neglected in the calculation of the quadrupole coupling constant. The existence of large ΔJ values suggests that the Fermi contact term is not the sole mechanism contributing to spin-spin coupling.

The quadrupole coupling constants of the complexes studied (Tables 7.1 and 7.2) decrease linearly with the increase in the one-bond spin-spin coupling between tin-119 and manganese-55 nuclei, with the exception of the tris(*p*-methylthiophenyl)tin derivative (Fig. 7.5). The relationship between χ and $^1J_{Mn\text{-}Sn}$ is due to the dominance of the Fermi contact term for $^1J_{Sn\text{-}Mn}$, which increases as the *s*-bonding character increases (Eq. [3.4.2]), and the nuclear quadrupole coupling constant which, according to the Townes and Dailey theory, decreases as the *s*-bonding character increases (Eq. [3.4.3]). The complexes studied are known to be strong covalent bimetallics so that the contribution of the *para*-substituents towards ionic character is minimal. Also, it is expected that the π-donation of electrons from the manganese 3d orbitals towards the empty 5d orbitals of the tin atom

should remain constant through the series, since the $Mn(CO)_5$ fragment remains unchanged. The *para*-substitutents on the phenyl rings either increase or decrease the donor-acceptor ability of the tin, due to inductive and/or resonance effects, which are then transmitted onto the tin atom. This results in an increase or decrease in the *s*-character of the hybrid orbital used by the tin nucleus in bonding to the manganese atom. Therefore, the relationship obtained from $^1J_{Sn-Mn}$ and χ is mainly due to the change in the *s*-bonding character of the tin and manganese bond.

Table 7.2. Dipolar, effective dipolar and quadrupolar coupling constants, and spin-spin anisotropy for (*para*-XC_6H_4)$SnMn(CO)_5$[a]

X	D (Hz)	D″ (Hz)	ΔJ (Hz)	χ (MHz)
CH_3	-571 (2)	-363(14)	621(48)	20.4(0.8)
H (a,b)	-583 (9)	-465(6)	354(39)	18.3(0.1)[b]
H (c)	-582(9)	-410(8)	516(51)	18.3(0.1)[b]
H (d)	-582(9)	-465(4)	351(38)	18.3(0.1)[b]
OCH_3	-586 (4)	-455(15)	393(60)	16.4(0.3)
F (a)	-595 (4)	-461(14)	402(54)	12.2(0.4)
F (b)	-589 (4)	-401(11)	564(45)	16.2(0.4)
Cl	-578 (3)	-476(18)	324(63)	13.4(0.5)
SCH_3	-592 (3)	-425(18)	585(54)	14.6(0.6)
$S(O)_2CH_3$	-591.5 (2)	-397(10)	584(15)	-7.52(0.19)

[a]Uncertainties were determined from 3 or 4 different spectra at different spinning speeds.
[b]Values taken from ref. 17.

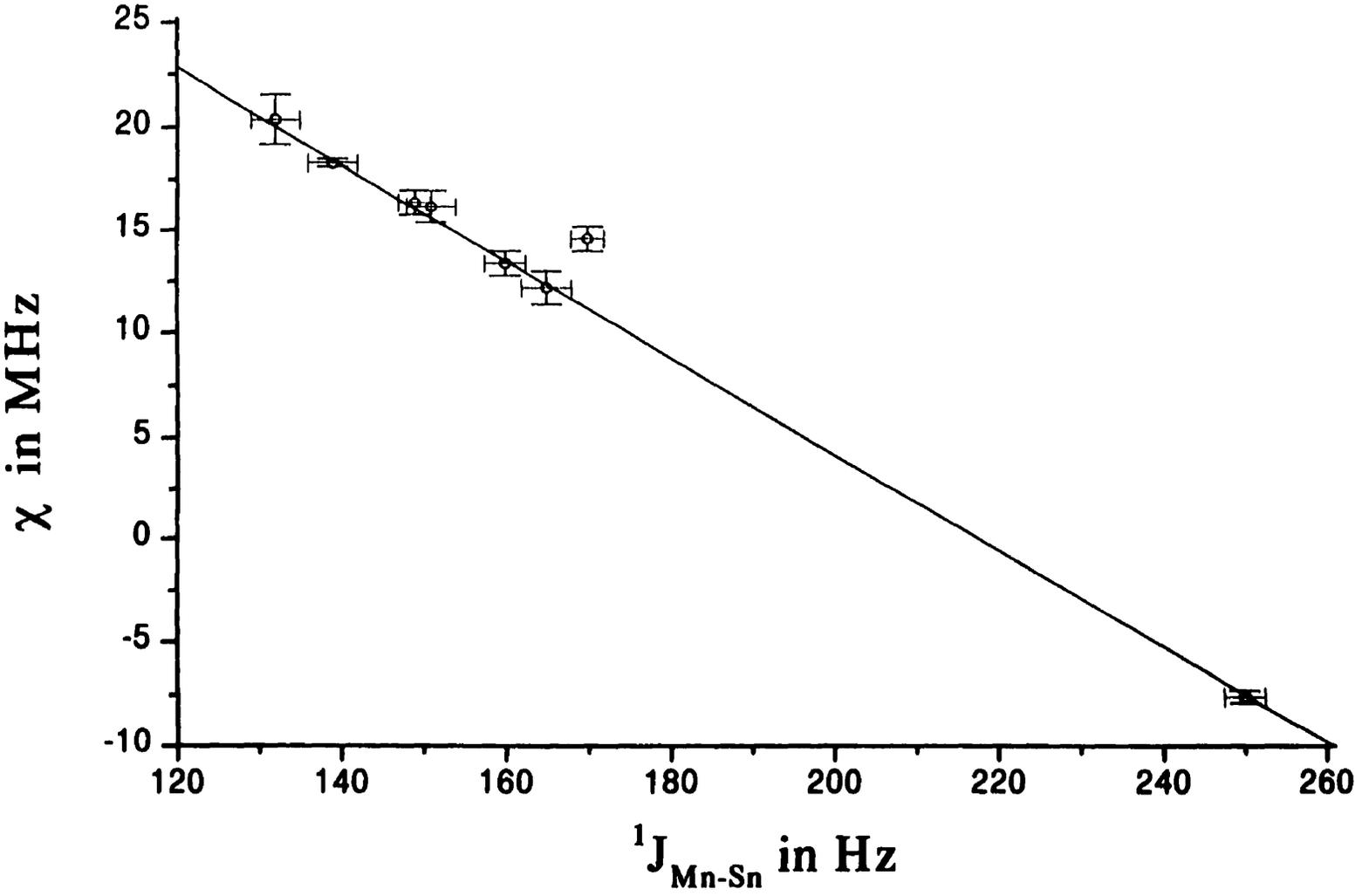

Figure 7.5. Plot of χ in MHz for the compounds in the series (*para*-$XC_6H_4)_3Sn(CO)_5Mn$ *vs.* the one-bond ^{119}Sn-^{55}Mn spin-spin coupling constant in Hz, $^{1}J_{Mn-Sn}$.

The (p-$CH_3SC_6H_4$)$_3$Sn(CO)$_5$Mn compound is yellow, whereas all other *para*-substituted tin complexes studied are colourless materials, which may suggest a smaller value for the average excitation energy term, ΔE, which is usually assumed to be constant for a similar series of complexes. The decrease in excitation energy may cause the spin-spin coupling constant for the thiomethyl derivative not to follow the χ versus $^1J_{Mn-Sn}$ behaviour. The crystal structure of tris(p-methylthiophenyl)tin compound (Appendix II) shows that its molecular structure differs from the other members of the (p-XC$_6$H$_4$)Sn(CO)$_5$Mn series. The dihedral angle of one of the phenyl rings of this compound is 167°, far from the general range of 40° to 80° for such angles. It appears that these torsional angles also have a profound influence on the components of the chemical shift tensor. For example, the phenyl ring torsion angles of (p-$CH_3C_6H_4$)$_3$Sn-(CO)$_5$Mn(I) are 56°, 69° and 55°, and the chemical shift tensor values are 38, 11 and -97 ppm. In comparison, the *para*-SCH_3 derivative has torsion angles of 63°, 49° and 167°, and tensor values of 172, 82 and 219 ppm. The large difference in torsion angle may influence the overlap of the π_{2pz} orbitals on the aromatic ring with the tin atom which can result in rehybridization for the 2p orbitals of the phenyl ring. This change in hybridization results in larger values for the tensor components, δ_{11} and δ_{22}.

The magnitudes and principal components of the tin chemical shifts tensors are given in Table 7.3. As $^1J_{Mn-Sn}$ increases, the tensor component δ_{33} increases, with the exception of the *para*-fluoro case. This result indicates that, as the *s*-bonding character increases, the δ_{33} value will increase if and only if the direction of δ_{33} is close to or along the tin-manganese bond. It was found from solid-state ^{119}Sn NMR measurements that

Table 7.3. ^{119}Sn Chemical Shift Tensors for (*para*-XC_6H_4)$SnMn(CO)_5$.[a]

X	δ_{11} (ppm)	δ_{22} (ppm)	δ_{33} (ppm)	$\Delta\delta$ (ppm)	η
CH_3	37.7	10.6	-97.3	-121.4	0.335
H (a,b)	71.6	2.8	-115.2	-152.4	0.677
H (c)	81.1	50.1	-122.8	-188.4	0.247
H (d)	89.4	47.3	-119.9	-188.3	0.335
OCH_3	125.1	54.3	-145.3	-235.0	0.452
F	77.2	77.2	-134.6	-211.8	0.000
	120.4	46.9	-119.2	-202.8	0.544
Cl	98.6	-39.4	-155.0	-184.6	0.885
SCH_3	171.7	82.3	-219.2	-346.2	0.417
$S(O)_2CH_3$	167.5	58.1	-256.0	-368.8	0.445

[a]Uncertainties are ± 1.5 and ± 2.5 ppm for chemical shifts tensors and $\Delta\delta$, respectively.

there are two non-equivalent tin sites in (p-FC_6H_4)$_3Sn(CO)_5Mn$ complex, which results in two sets of tensor quantities. One set of tensor values was determined, from spinning sideband analysis, to be symmetric while the other was asymmetric with an asymmetry factor, η_C, of 0.544. Crystal structure information showed that there are two distinct molecules in the asymmetric unit, with torsion angles of -53°, -53°, -67° and 59°, 65°, 39° about the Sn-C_{ipso} axis Fig. 7.6. These results indicate that the orientation of δ_{33} at the tin atom should be such that it lies along the Mn-Sn bond for the X-ray and NMR data to

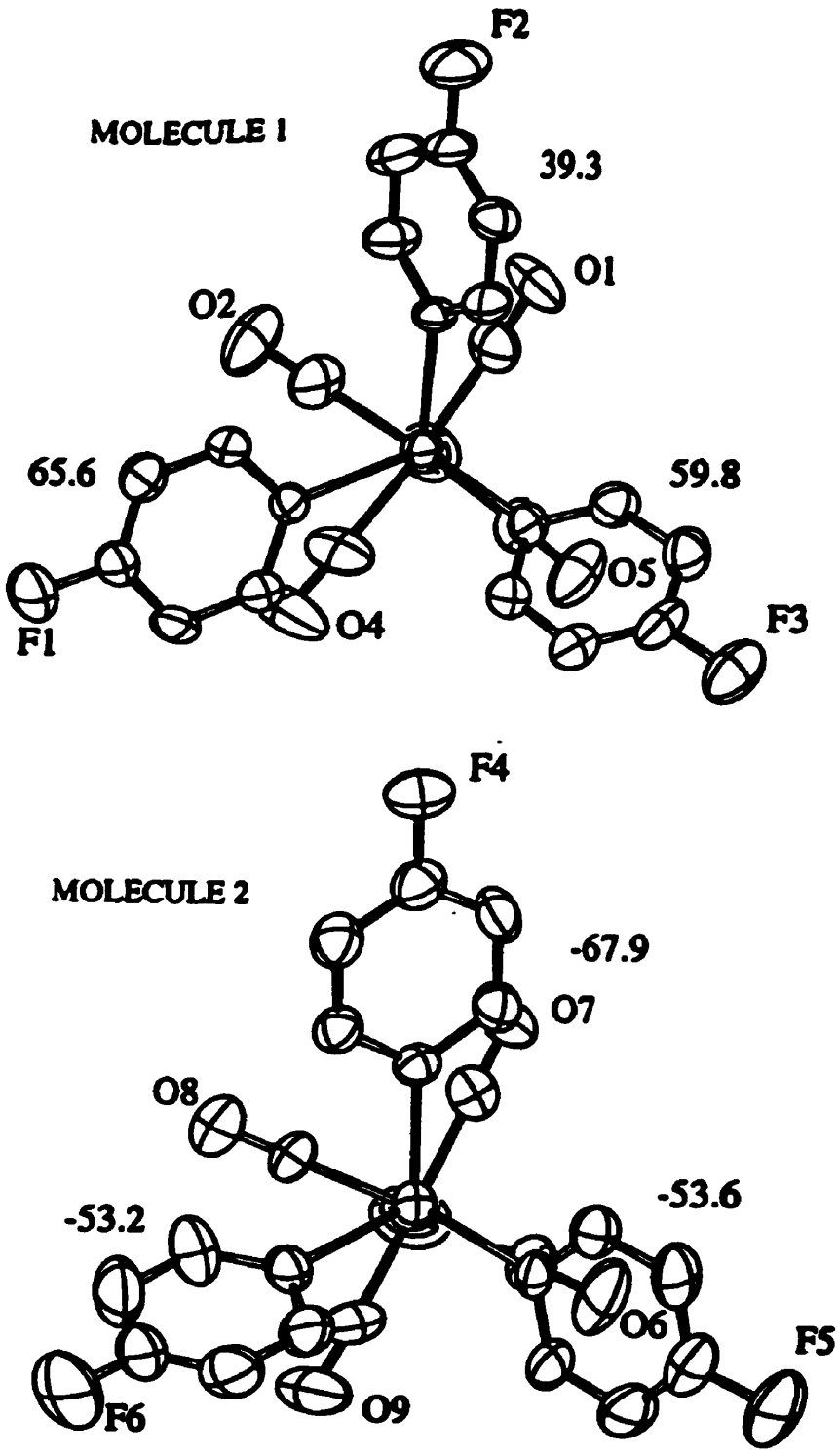

Figure 7.6. The view of the two $(p\text{-}FC_6H_4)_3Sn(CO)_5Mn$ molecules, shown perpendicular to the Mn-Sn axis.

agree. As a consequence, the remaining two components, δ_{11} and δ_{22}, must lie perpendicular to the δ_{33} axis. The tensor quantities δ_{11} and δ_{33} for the *para*-SCH_3 and *para*-$S(O)_2CH_3$ complexes are much larger in absolute value than are those for the other members of the series. The OCH_3 and $S(O)_2CH_3$ substituents are the strongest electron donating and strongest electron withdrawing substituents, respectively, but there is no correlation between any of the shift tensor components with either the Hammett or Taft constants, such as those found for the corresponding ^{119}Sn chemical shifts in solution. This observation is not surprising, since Hammett and Taft correlation constants are obtained from solution studies where the phenyl rings torsional angles are not constrained as they are in the solid-state. The asymmetry factor ranges from 0 to 0.885 through the series, showing that δ_{11} and δ_{22} are very sensitive to the torsion angles of the phenyl ring and to the *para*-substituent on the phenyl ring.

References

(1) R. A. Komoroski, R. G. Parker, A. M. Mazany and T. A. Early, *J. Magn. Reson.*, **73**, 389 (1987).

(2) R. K. Harris, *J. Magn. Reson.*, **78**, 389 (1988).

(3) D. A. Apperley, B. Haiping and R. K. Harris, *Mol. Phys.*, **68**, 1277 (1989).

(4) D. C. Apperley, N. A. Davies, R. K. Harris, A. K. Brimah, S. Eeller and R. Fischer, *Organometallics.*, **9**, 2672 (1990).

(5) H. Bai, R. K. Harris and H. Reuter, *J. Organomet. Chem.*, **408**, 167 (1991).

(6) R. K. Harris, S. E. Lawrence, S. Oh and V. G. Kumar Das, *J. Mol. Struct.*, **347**, 309 (1995).

(7) R. D. Gorsich, *J. Am. Chem. Soc.*, **84**, 2486 (1962).

(8) W. Jetz, P. B. Simons, J. A. J. Thompson and W. A. G. Graham, *Inorg. Chem.*, **5**, 2217 (1966).

(9) A. Terzis, T. C. Strekas and T. G. Spiro, *Inorg. Chem.*, **13**, 1346 (1974).

(10) H. P. Weber and F. R. Bryan, *Acta Cryst.*, **22**, 822 (1967).

(11) R. F. Bryan, *J. Chem. Soc. (A)*, 696 (1968).

(12) R. F. Bryan, *J. Chem. Soc. (A)*, 172 (1967).

(13) I. Wharf, *Inorg Chim Acta*, **159**, 41 (1989).

(14) D. J. Craik, in *Annual Reports on NMR Spectroscopy*, (G. A. Webb, ed.), Academic Press, New York, **15**, 1 (1983).

(15) D. Christendat, R. D. Markwell, D. F. Gilson, I. S. Butler and J. D. Cotton, *Inorg. Chem.*, **36**, 230 (1997).

(16) E. Lindner, R. Fawzi, H. A. Mayer, K. Eichele and K. Pohmer, *Inorg. Chem.*, **30**, 1102 (1991).

(17) J. L. Slater, M. Pupp and R. K. Sheline, *J. Chem. Phys.*, **57**, 2105 (1972).

Chapter 8

Crystal Structures and Solid-State (CP-MAS) Tin-119 and Lead-207 Nuclear Magnetic Resonance Studies of Bis[pentacarbonylmanganese(I)]diphenyltin(IV) and Bis[pentacarbonylmanganese(I)]diphenyllead(IV)

8.1 Introduction

In Chapters 4, 5 and 7, we have described and analyzed the solid-state NMR spectra of relatively complex, second-order, quadrupole-dipole effects in cases where a single quadrupolar nucleus is bonded to a spin-1/2 nucleus. This leads to the most logical question "What would the experimental spectrum look like and how difficult would it be to solve when more than one quadrupolar nucleus is bonded to the probe (spin-1/2) nucleus?" However, this question manifests itself in many different forms, i.e., the number of different quadrupolar nuclei bonded to the spin-1/2 probe nucleus and the symmetry around the quadrupolar moiety. In this section of the thesis, we will look at two cases where two $Mn(CO)_5$ fragments are directly bonded to diphenyltin[1] and diphenyllead moieties. These complexes were deliberately selected for three major reasons. The first is that they are simple to prepare and relatively stable under regular atmospheric conditions. The second reason is that the one-bond, spin-spin coupling constants (Chapters 5 and 7) are much larger (> 130 Hz) than are the second-order effects. Thirdly, by symmetry arguments, the $Mn(CO)_5$ fragments in the molecules are symmetric around the quadrupolar nucleus.

The crystal and molecular structures of $[(CO)_5Mn]_2SnPh_2$, the first to be investigated for complexes of this type[2], were determined to gain insight into the bonding interaction between the main group metal and the two transition metal fragments. It was found that the Mn-Sn distances were equivalent (2.70 ± 0.01 Å) but the two Mn atoms in a single molecule were not related by symmetry. The R value after least-squares refinement was determined to be 11.35 % and all atoms, except hydrogen, were accounted for satisfactorily. However, the low bond-length precision and high R value obtained by Kilbourn and Powell[2] have prompted us to re-investigate the structure of this complex, along with its lead analogue, $[(CO)_5Mn]_2PbPh_2$, using single-crystal X-ray diffraction, vibrational and solid-state NMR spectroscopy. To our knowledge, the $[(CO)_5Mn]_2PbPh_2$ complex has not been prepared previously and no crystal structures involving a lead atom directly bonded to one or more pentacarbonylmanganese(I) fragments have been reported in the literature. An attempt to prepare the analogous silicon complex by the regular displacement reaction of $[(CO)_5Mn]Na$ with Ph_2SiCl_2 and the facile reaction of Si-H bonds from Ph_2SiH_2 with excess dimanganese decacarbonyl, have been unsuccessful.

8.2 Results and Discussion

The solution ^{55}Mn, ^{119}Sn and ^{207}Pb NMR spectra of $[(CO)_5Mn]_2EPh_2$ (E = Sn, Pb) exhibited single broad peaks with no spin-spin coupling. This is not unusual for ^{55}Mn NMR measurements and is due to rapid relaxation of the quadrupolar nucleus in solution, but the broadening effect is unexpected for the spin-1/2, ^{119}Sn and ^{207}Pb, NMR spectra. The broadening of the ^{119}Sn and ^{207}Pb spectra, Fig. 8.1, was first assumed to be due to

quadrupolar relaxation effects which can lead to complete or partial collapse of the multiplets in the NMR spectra of spin-1/2 nuclei coupled to the quadrupolar nucleus, making the direct measurement of spin-spin coupling impossible. It was assumed from the NMR spectra, Fig. 8.1, that there was partial collapse of the multiplets and, hence, broad featureless peaks. The peculiar shaped peaks of the NMR spectra may also due to a combination of partial collapse of the multiplets and/or restrict free rotation of the individual $Mn(CO)_5$ fragments within the molecules. This type of steric restriction can be visualized by a ratchet mechanism where one of the CO group is interlocked with two other CO groups from the second $Mn(CO)_5$ moiety, Fig 8.2.

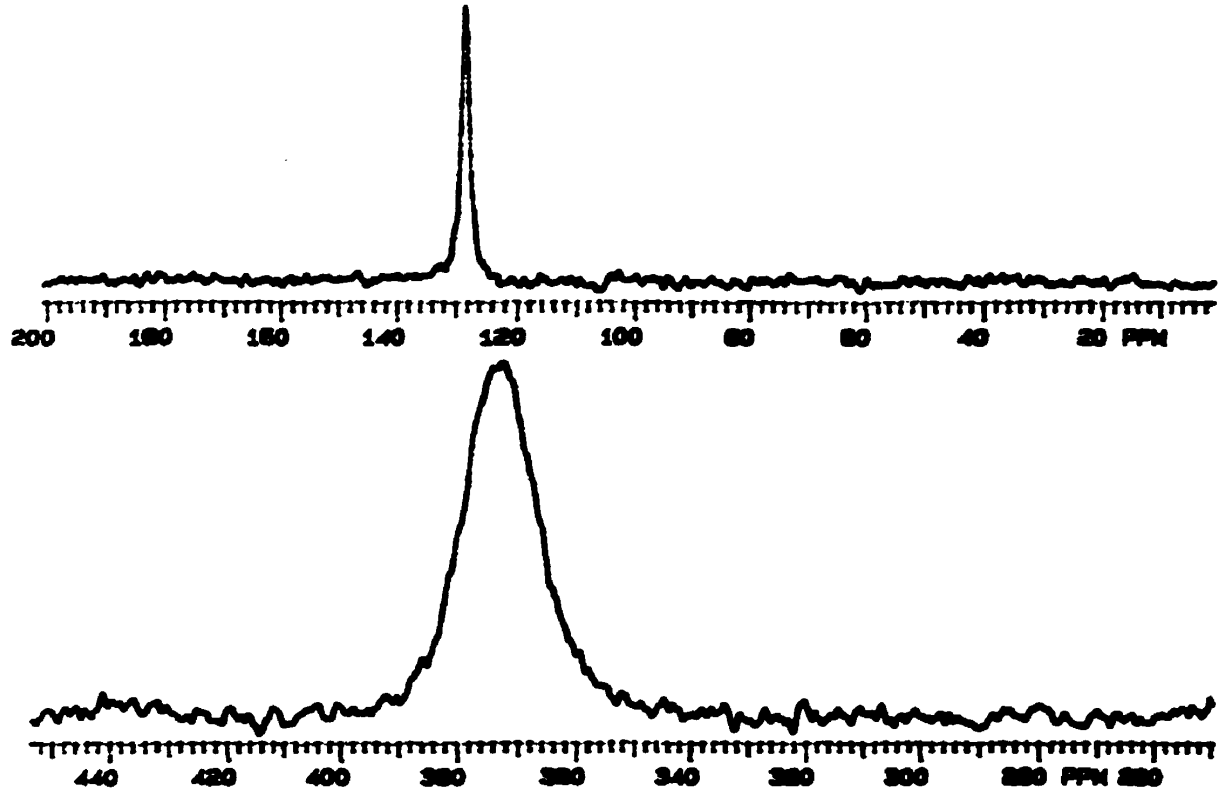

Figure 8.1. Solution ^{119}Sn and ^{207}Pb NMR spectra of (a) $[(CO)_5Mn]_2SnPh_2$ and (b) $[(CO)_5Mn]_2PbPh_2$ at 111.72 and 62.7 MHz, respectively.

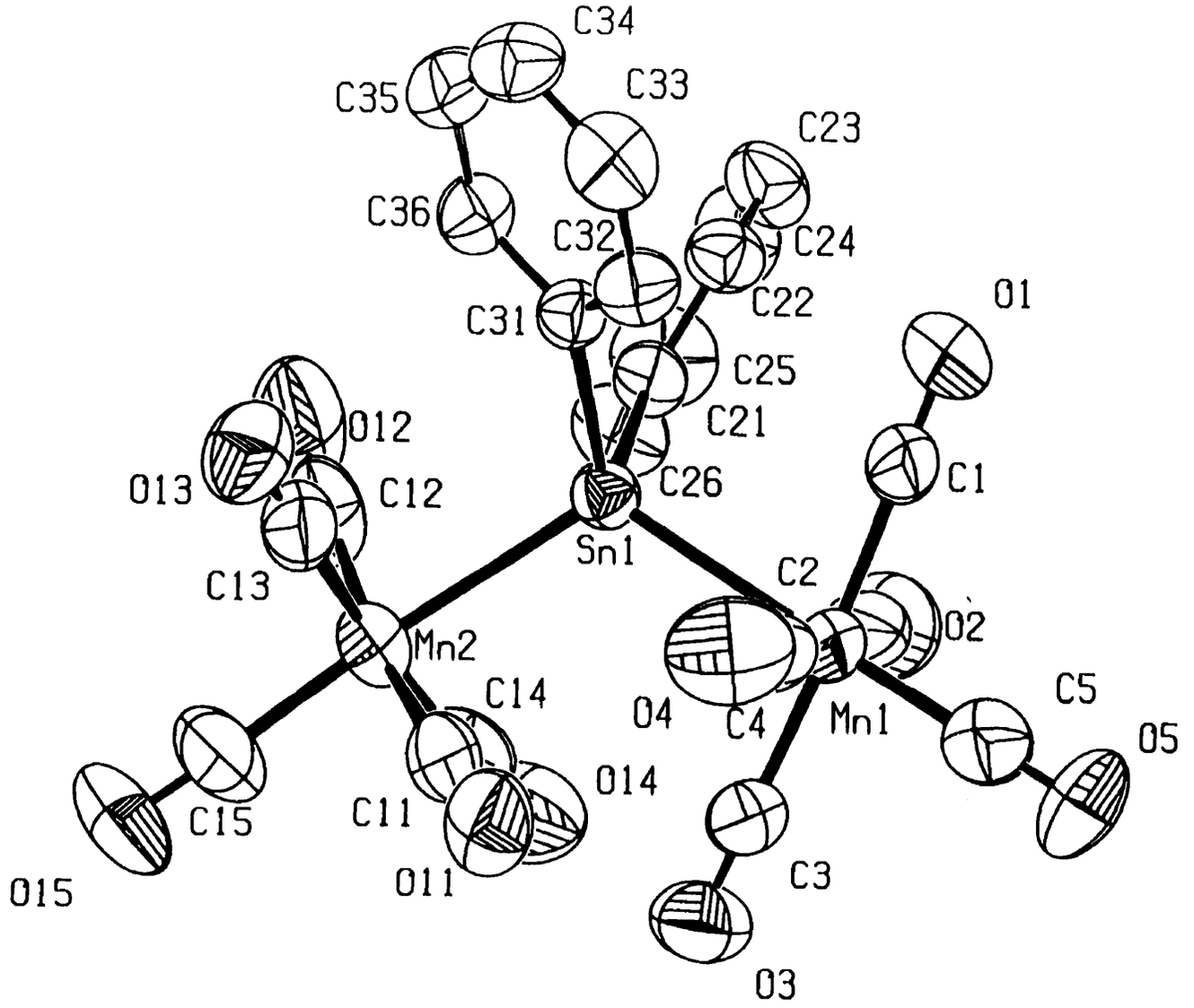

Figure 8.2. X-ray structure of $[(CO)_5Mn]_2SnPh_2$ showing the interlocking of one CO with two other CO groups from the second $Mn(CO)_5$ fragment.

The solution FT-IR spectra of the two complexes, $[(CO)_5Mn]_2EPh_2$ (E = Sn, Pb), are presented in Fig 8.3. It is at once apparent, by inspection of the FT-IR and Raman (Fig. 8.4) spectra, that there is appreciable coupling of the two $Mn(CO)_5$ moieties across the tin or lead atom and the assumption of C_{4V} symmetry is no longer valid with the tin or lead atom positioned at the fourfold axis (Section 6.2.1). For these type of complexes, the overall geometry of the molecules must be assigned and considered. The overall symmetry for these molecules is C_{2V}, for which group theory predicts eight infrared ($3a_1 + 3b_1 + 2b_2$) and ten Raman ($3a_1 + 2a_2 + 3b_1 + 2b_2$) active modes. In Figs. 8.3 and 8.4, six bands are clearly resolved. The conflicting results indicate that some of the vibrational modes may be accidentally degenerate.

Assignment of each mode in such complex spectra is extremely difficult, as was observed for the tetracarbonylcobalt analogue,[3] and we will discuss only the pair of high-frequency modes (2110-2050 cm^{-1}) present in the IR and Raman spectra for both compounds. These two modes arise from the symmetric and antisymmetric combination of the a_1^2 modes of the individual $Mn(CO)_5$ groups, as shown in Fig. 8.5. The higher frequency mode was assigned to be the a_1 mode due to the strong polarizability effects caused by the symmetric stretching of the ten carbonyl groups and hence a stronger Raman signal. The antisymmetric stretching of the carbonyl groups, Fig 8.5. (b), should be less polarized than is that of the symmetric stretching mode and a weaker Raman absorption is expected at lower energy. The results obtained from the Raman spectra are in excellent agreement with these expectations, showing a strong a_1 band at high frequency and a weak adjacent b_1 band at lower frequency. These assignments for the pairs of higher energy modes are consistent with the observed infrared intensities.

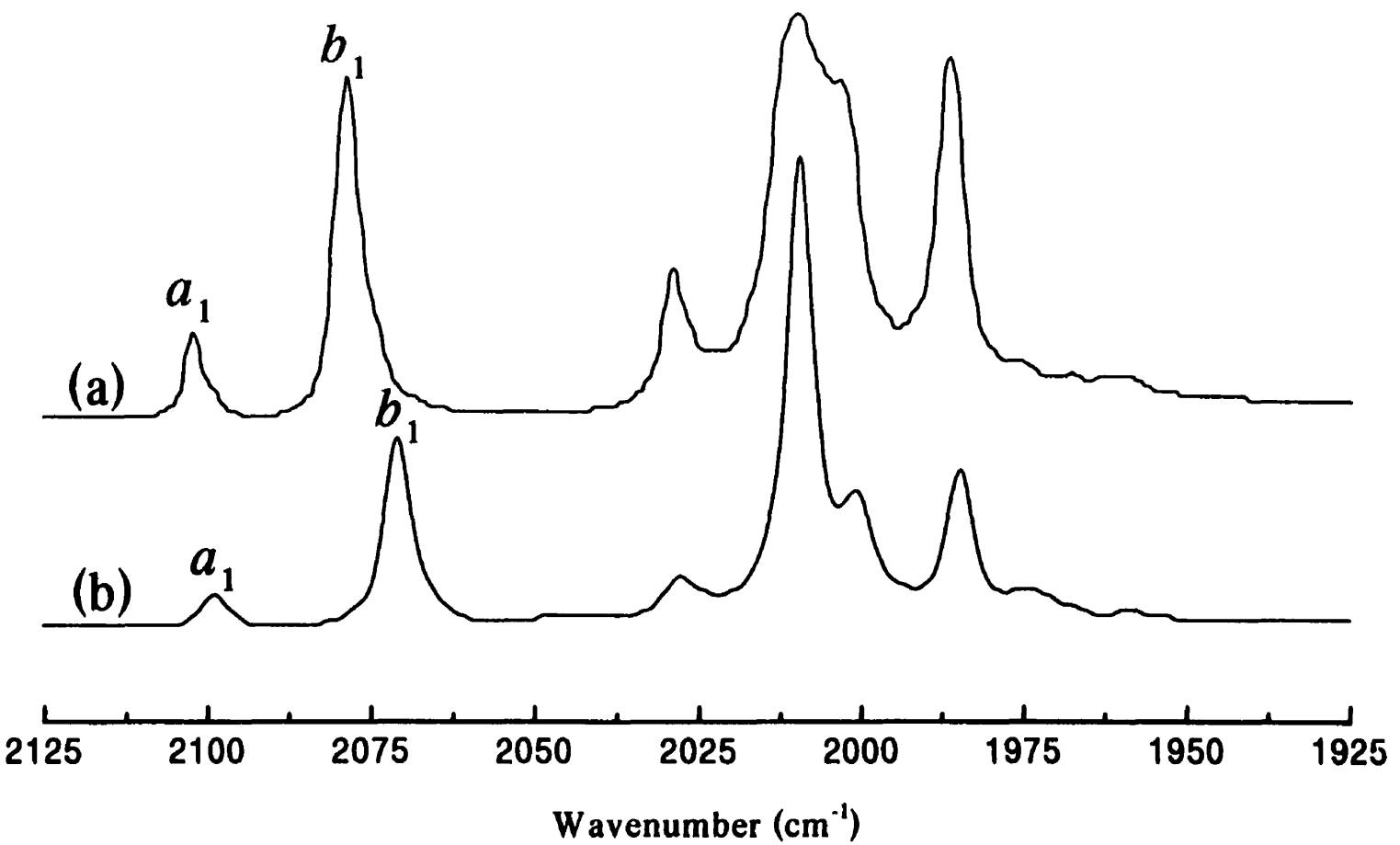

Figure 8.3. Solution infrared spectra of (a) $[(CO)_5Mn]_2SnPh_2$ and (b) $[(CO)_5Mn]_2PbPh_2$; ca. 1.5 mg/ml of hexane.

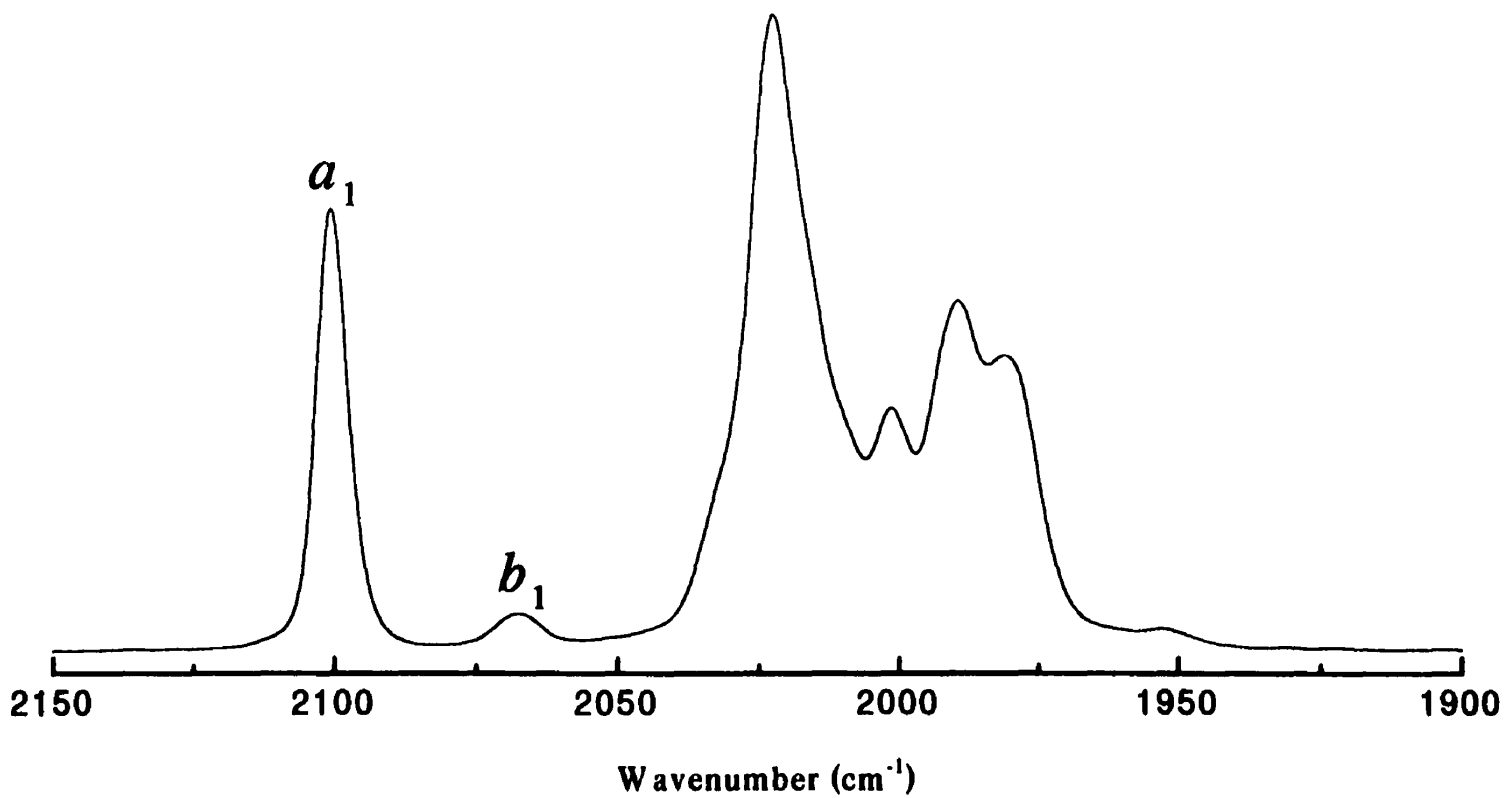

Figure 8.4. Raman spectrum of $[(CO)_5Mn]_2PbPh_2$ in the CO stretching region (powdered solid in sample cup).

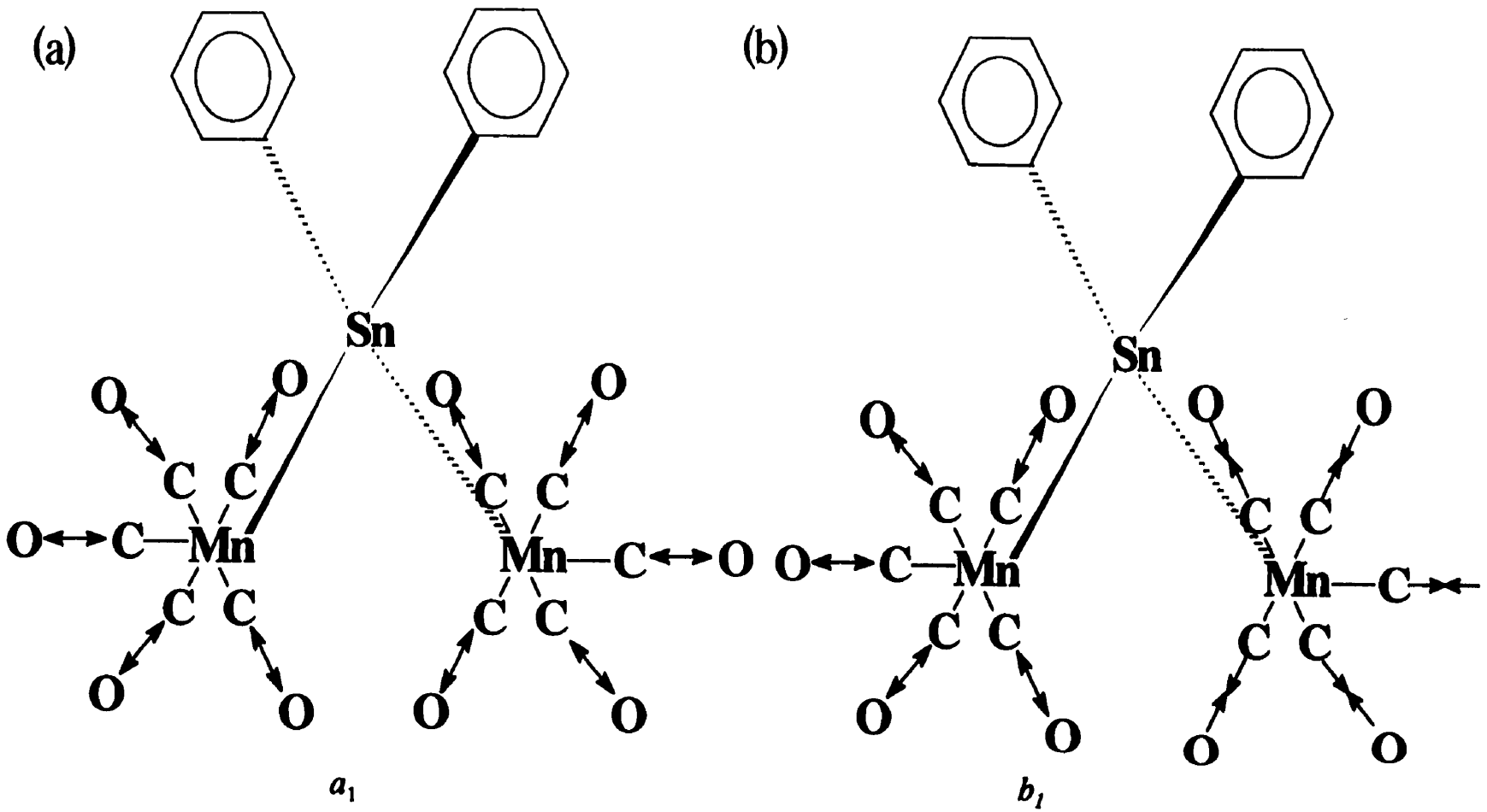

Figure 8.5. (a) symmetric, a_1, and (b) antisymmetric, b_1, stretching of the CO groups of the two $Mn(CO)_5$ fragments.

The resultant dipoles of the individual $Mn(CO)_5$ moieties tend to oppose one another for the symmetric a_1 vibration, whereas the resultant dipole for the antisymmetric b_1 vibration is always greater than is that of the symmetric mode. Therefore, the b_1 IR-vibrational intensity will always be greater than is that of the a_1 vibrational mode, as long as the Mn-E-Mn bond angle is greater than 90°. At this point, from Fig 8.5, it should be clear that the a_1 vibration mode will approach zero intensity as the Mn-E-Mn bond angle approaches 180° (zero resultant dipoles), whereas for a 90° bond angle the two modes should be of equal intensities. Therefore, it can be concluded from the FT-IR data that the Mn-Pb-Mn bond angle will be greater than that of the Mn-Sn-Mn bond angle, since the ratio of the a_1/b_1 intensities is greater for the lead complex.

The tin complex was found to crystallize in the monoclinic ($P2_1/a$) space group with one molecule in the asymmetric unit (Appendix II). The two $Mn(CO)_5$ groups of one molecule are not related by space group symmetry, in good agreement with the previously determined structure, and the two Mn-Sn distances are equivalent within experimental error, 2.707 and 2.713 ± 0.004 Å, and in agreement with the value of 2.70 ± 0.1 Å previously determined by Kilbourn *et al.*[2] The two $Mn(CO)_5$ groups crystallize in a ratchet conformation, Fig. 8.2, as was initially speculated from the solution NMR data. Single-crystal X-ray diffraction determination of the lead compound, $[(CO)_5Mn]_2PbPh_2$, was attempted but, due to strong absorption of the lead atom, the structure could not be refined satisfactorially. However, preliminary results indicated that this complex crystallized in the triclinic P $\bar{1}$ space group with two molecules in the asymmetric unit. The four Mn-Pb distances were determined to be 2.763(4) and 2.776(4) Å for molecule I,

and 2.769(4) and 2.782(4) Å for molecule II. The Mn-Pb-Mn bond angles, 119.27(12) and 119.70(12)°, are larger than that of the Mn-Sn-Mn bond angle, 117.16(4)°, in excellent agreement with the infrared prediction. In these two structures, the two $Mn(CO)_5$ groups were also found to crystallize in a ratchet conformation, in agreement with the broadening effects observed in the solution ^{207}Pb NMR spectrum.

The ^{119}Sn and ^{207}Pb solid-state, CP-MAS, NMR spectra are shown in Figs 8.6 and 8.7 for the diphenyltin(IV) and diphenyllead(IV) pentacarbonylmanganese(I) complexes, respectively. The isotropic centrebands are very complex due to the presence of two quadrupolar ^{55}Mn nuclei directly bonded to the spin-1/2 probe nucleus. However, the presence of a single isotropic centreband for the lead compound contradicts the result obtained by single-crystal X-ray diffraction studies. This conflicting result may be due to the absorption problem encountered for the lead atom and/or twinning of the crystal used for data collection, which could not be detected at the time of measurement and thus lead to an incorrect space group assignment.

Full theoretical treatments of second-order effects in solid-state, CP-MAS, NMR spectra are well known and well documented in the literature for spin-1/2 probe nuclei bonded to a single quadrupolar nuclei, Section 3.5. Recently, this theory has been expanded for systems involving a spin-1/2 nucleus bonded to more than one nitrogen (spin-1) nuclei.[4-7] The general expression for such a system can be written in the form of Eq.[8.2.1]:

$$\Delta\nu_m = -(\Sigma m_i)J_{iso} + (3\chi D''/20\nu_S)\ \{nS\ (S + 1) - 3\Sigma m_i^2\} / \{\ S\ (2S - 1)\} \quad [8.2.1]$$

where the symbols has their usual meaning as those in Section 3.5 and n is the number of

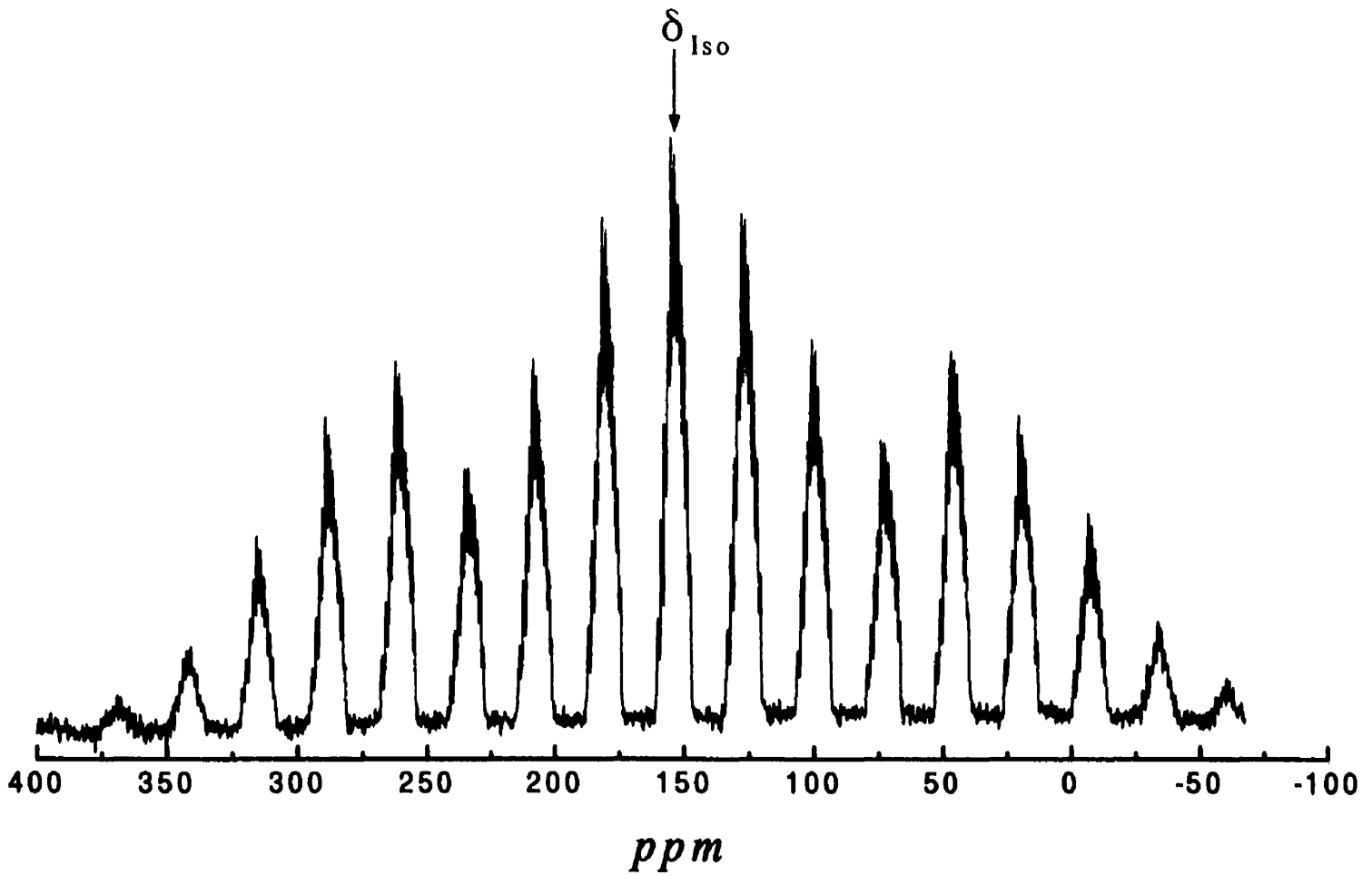

Figure 8.6. Solid-state, CP-MAS, ^{119}Sn NMR spectrum of $[(CO)_5Mn]_2SnPh_2$ at 111.74 MHz. Experimental conditions: contact time 3 ms, recycle delay 8 s, number of transients 7500.

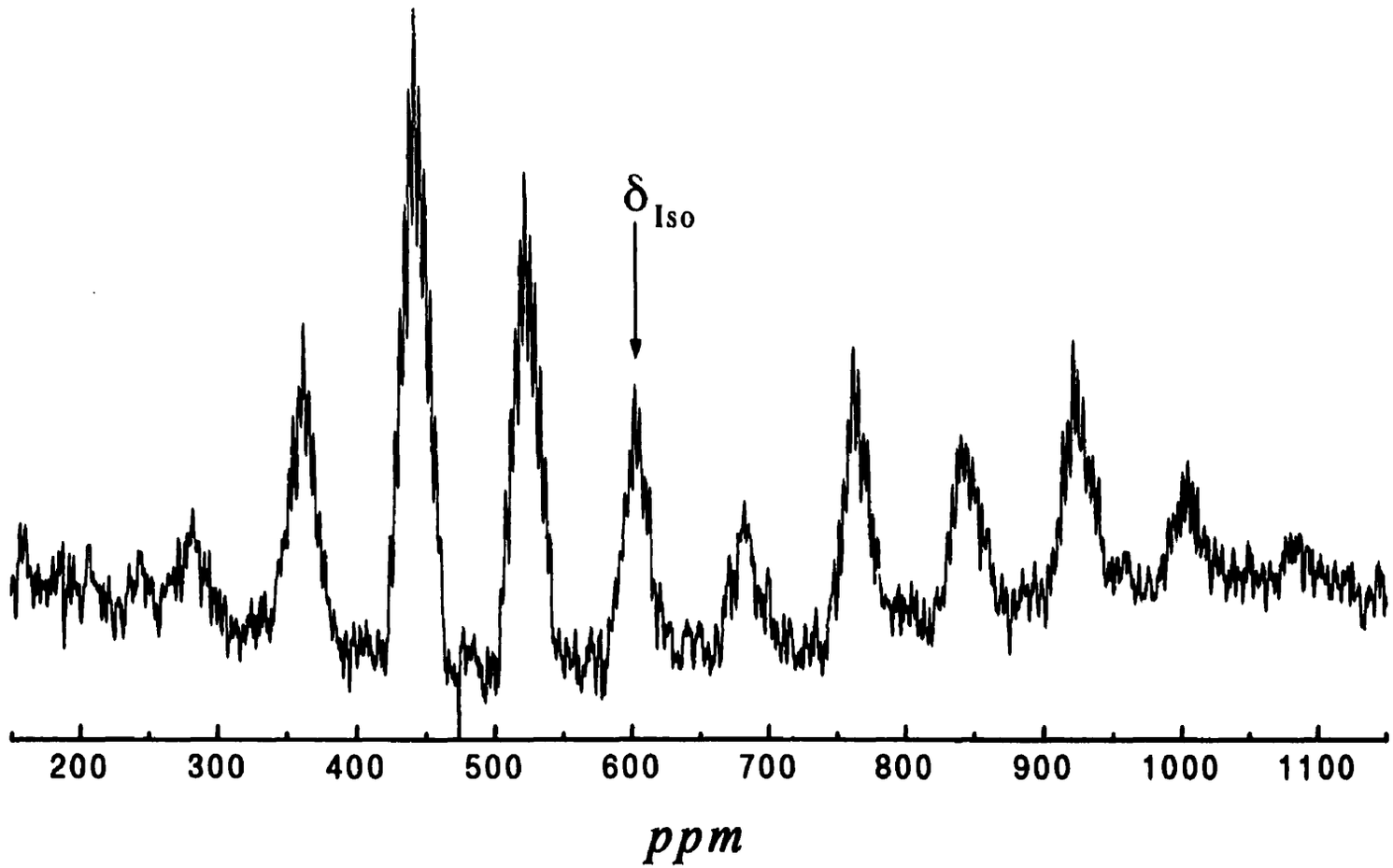

Figure 8.7. Solid-state, CP-MAS, ^{207}Pb NMR spectrum of $[(CO)_5Mn]_2PbPh_2$ at 62.7 MHz. Experimental conditions: contact time 3 ms, recycle delay 60 s, number of transients 1484.

quadrupolar nuclei bonded to the probe nucleus. However, the system becomes more complex when the quadrupolar sites are non-equivalent and Eq. [8.2.1] may be written in the general form of Eq. [8.2.2] to include different types of quadrupolar nuclei.

$$\Delta\nu_m = -[mJ_{I\text{-}S(1)} + mJ_{I\text{-}S(2)} + mJ_{I\text{-}S(3)} + \ldots] + [(3\chi D_1''/20\nu_{S(1)})\, 2\{S_1(S_1+1) - 3m^2\}/\{S_1(2S_1-1)\}$$
$$+ (3\chi D_2''/20\nu_{S(2)})\, 2\{S_2(S_2+1) - 3m^2\}/\{S_2(2S_2-1)\} + (3\chi D_3''/20\nu_{S(3)})$$
$$2\{S_3(S_3+1) - 3m^2\}/\{S_3(2S_3-1)\} + \ldots] \qquad [8.2.2]$$

where D_i'' is the effective-dipolar coupling constant, including the anisotropy in the spin-spin coupling (ΔJ), between the I-S_i spin pairs.

$$D_i'' = [D_i\,(3\cos^2\beta^D - 1 + \eta\sin^2\beta^D\cos 2\alpha^D) - (\Delta J/3)\,(3\cos^2\beta^J - 1 + \eta\sin^2\beta^J\cos 2\alpha^J)] \qquad [8.2.3]$$

where the angular terms α^D, β^D, α^J and β^J describe the orientation of the internuclear vector $r_{I\text{-}S(i)}$ and the indirect coupling tensor in the principal-axis system of the electric field gradient tensor q_i, η is the asymmetry parameter in q_i, and D_i is the direct dipolar coupling constant, $D_i = (\mu_o/4\pi)\,\gamma_I\,\gamma_S\,h/\,(4\pi^2\,(r_{I\text{-}S(i)})^3)$, between the spin-1/2 and quadrupolar nucleus.

For the complexes studied in this section, there are two possible methods of analysis. The first is to treat the $Mn(CO)_5$ fragments as equivalent, which will result in a single set of spin-spin coupling constants and a second-order value, $\chi D''/\nu_S$, as shown in Fig. 8.8, for negative $\chi D''/\nu_S$. The second case is much more complex and requires treating the two quadrupolar moieties as non-equivalent, which will result in two sets of spin-spin couplings and two different values of the second-order coupling, as depicted in Fig 8.9. However, the second set of second-order effects have not been added to the figure, due to the fact that the first set of second-order effects must be known or

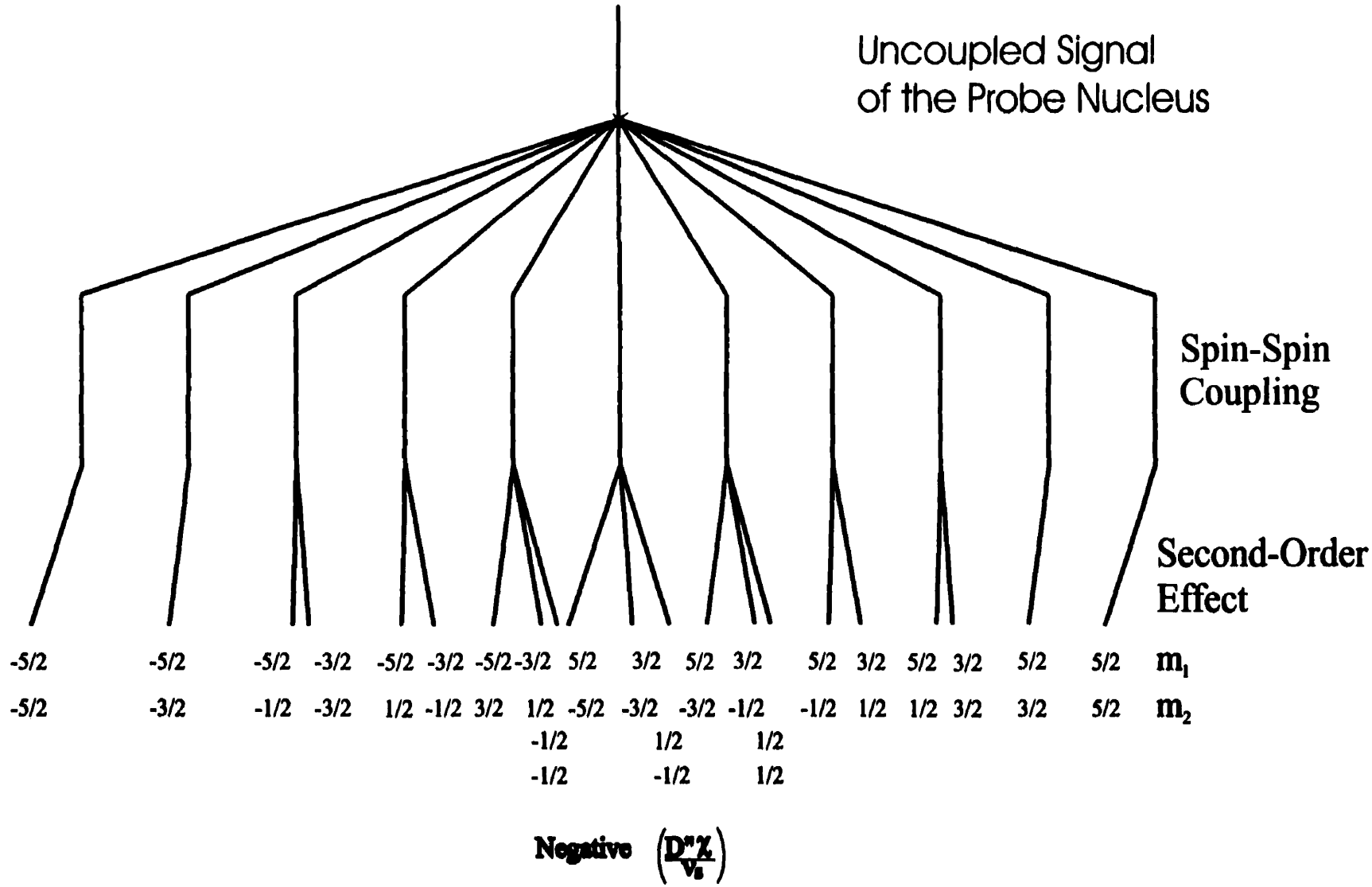

Figure 8.8. Influence of second-order parameter $\chi D''/\nu_S$ on the solid-state NMR spectrum of a spin-1/2 probe nucleus coupled to two equivalent spin-5/2 nuclei.

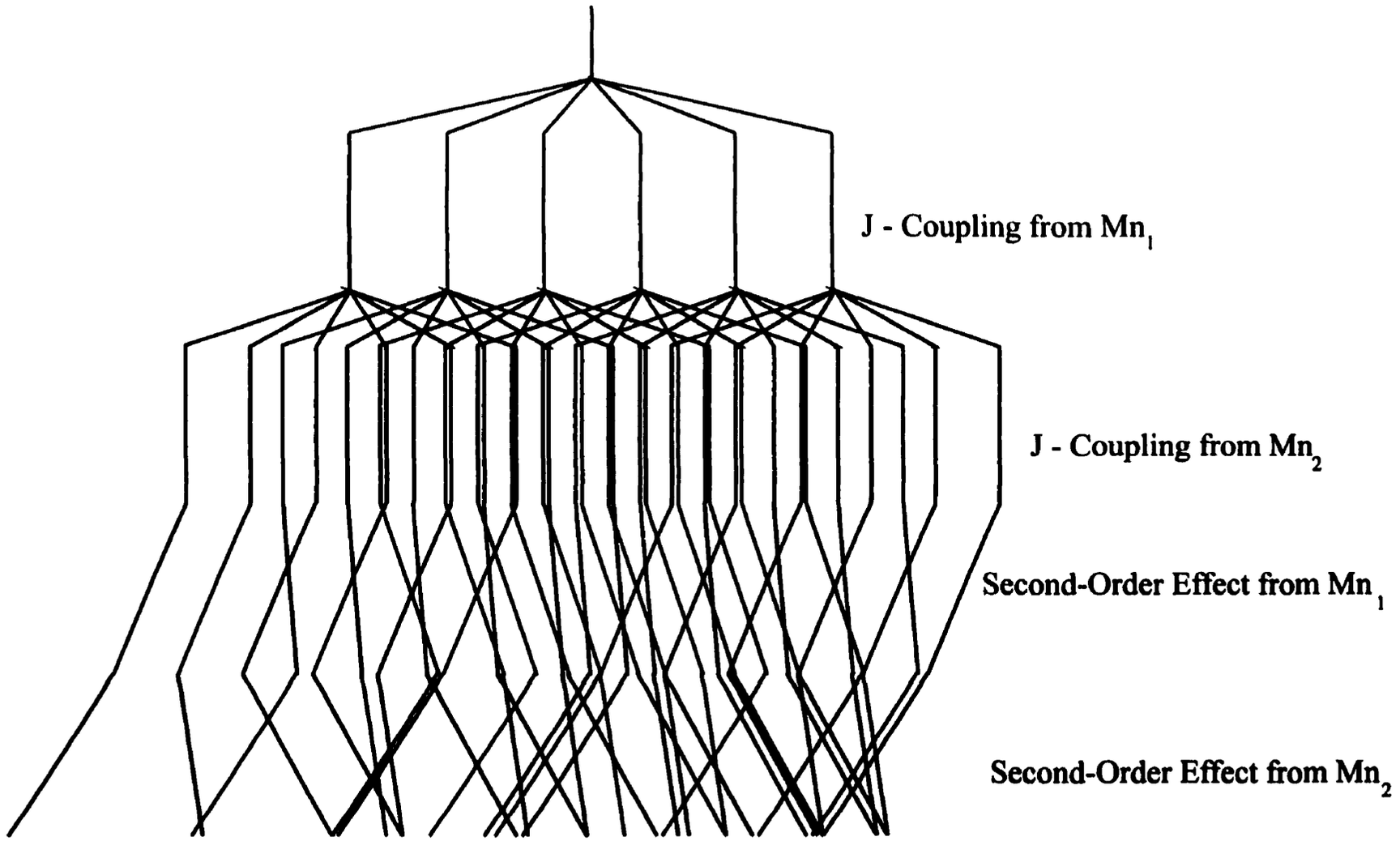

Figure 8.9. Influence of negative second-order parameter, $-\chi D''/\nu_S$, on the solid-state NMR spectrum of a spin-1/2 probe nucleus coupled to two non-equivalent spin-5/2 nuclei.

determined exactly, which is never the case, before the second set of splittings is added. Therefore, the experimental spectra for such cases must be solved by simulation methods.

From X-ray diffraction data and solid-state NMR studies, the two individual $Mn(CO)_5$ moieties of a single molecule may be considered to be equivalent. This resulted in the analysis of the experimental spectra using Eq. [8.2.1], Fig. 8.8. However, peak-fitting of the experimental centrebands, Fig. 8.10, reveals that there are only eleven peaks instead of twenty-one anticipated by Eq. [8.2.1], (Table 8.1, Fig. 8.8). This may due to a very small value for the second-order effects being smaller or comparable to the line-width function used in data analysis. The spin-spin coupling constants, $^1J_{Mn\text{-}Sn}$ and $^1J_{Mn\text{-}Pb}$, were determined from the four outermost peaks ($P_1 \rightarrow P_{11} = 10J_{Mn\text{-}E}$ and $P_2 \rightarrow P_{10} = 8J_{Mn\text{-}E}$), Fig. 8.8, Table 8.1, to be 139 ± 1 and 228 ± 1 Hz, respectively, for the diphenyltin and diphenyllead complexes. The $^1J_{Mn\text{-}Sn}$ value for the tin complex is comparable to the values, 135-142 Hz, obtained for the triphenyltin analogue, which indicates that the bonding interactions are about the same in both complexes. However, the value obtained for the diphenyllead compound are much smaller than are those obtained for the triphenyllead analogue, Tables 5.3-5.4. This result indicates that the π-bonding interactions between the Mn-Pb nuclei may be weaker in the diphenyllead complex.

From symmetry arguments, the largest component of the EFG and J tensors are expected to lie along the internuclear vector $r_{Mn\text{-}E}$, and this allows one to set the angles β^D and β^J equal 0° in Eq. [8.2.3]. This situation leads to a very simple expression for the effective dipolar coupling D″, Eq [8.2.4].

$$D'' = D - \Delta J/3 \qquad [8.2.4]$$

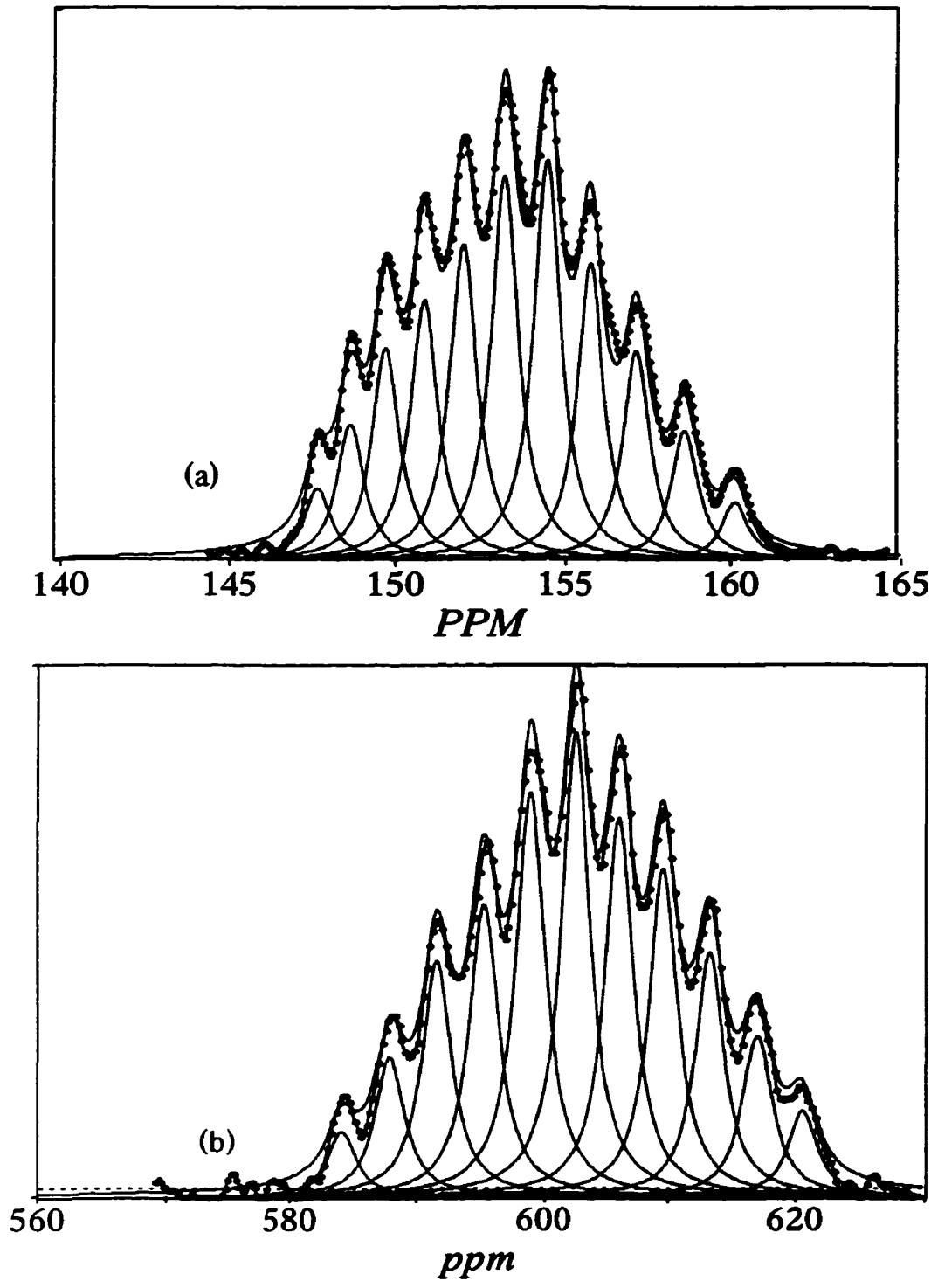

Figure 8.10. Centrebands ^{119}Sn and ^{207}Pb NMR results for (a) $[(CO)_5Mn]_2SnPh_2$ at 111.74 MHz and (b) $[(CO)_5Mn]_2PbPh_2$ at 62.7 MHz, respectively, showing the experimental spectra (dotted-line) and deconvolution into eleven peaks (solid-lines).

Table 8.1. Second-order shifts in the spectra of spin-1/2 nuclei coupled to two directly bonded spin-5/2 quadrupolar nuclei

Peak Number[a]	m_1	m_2	Peak position (ppm)
1	-5/2	-5/2	$\delta_{iso} + 5J - 2D''$
2	-5/2	-3/2	$\delta_{iso} + 4J - 4D''/5$
3	-5/2	-1/2	$\delta_{iso} + 3J - D''/5$
4	-3/2	-3/2	$\delta_{iso} + 3J + 2D''/5$
5	-5/2	+1/2	$\delta_{iso} + 2J - D''/5$
6	-3/2	-1/2	$\delta_{iso} + 2J - D''$
7	-5/2	+3/2	$\delta_{iso} + J - 4D''/5$
8	-3/2	+1/2	$\delta_{iso} + J + D''$
9	-1/2	-1/2	$\delta_{iso} + J + 8D''/5$
10	-5/2	+5/2	$\delta_{iso} - 2D''$
11	-3/2	+3/2	$\delta_{iso} + 2D''/5$
12	-1/2	+1/2	$\delta_{iso} + 8D''/5$
13	+5/2	-3/2	$\delta_{iso} - J - 4D''/5$
14	+3/2	-1/2	$\delta_{iso} - J + D''$
15	+1/2	+1/2	$\delta_{iso} - J + 8D''/5$
16	+5/2	-1/2	$\delta_{iso} - 2J - D''/5$
17	+3/2	+1/2	$\delta_{iso} - 2J - D''$
18	+5/2	+1/2	$\delta_{iso} - 3J + 2D''/5$
19	+3/2	+3/2	$\delta_{iso} - 3J - D''/5$
20	+5/2	+3/2	$\delta_{iso} - 4J - 4D''/5$
21	+5/2	+5/2	$\delta_{iso} - 5J - 2D''$

[a]Peak position starting at low-field.

Using peak positions (Fig. 8.10) 1, 2, 3 (as the average of $L_3 + L_4$), 9 (as the average of $L_{18} + L_{19}$), 10 and 11, the values of $3\chi(D - \Delta J/3)/10\nu_S$ were determined to be -23.6 ± 1.1 and 5.6 ± 0.4 Hz, respectively, for the tin and lead complexes. It should be noted that the $\chi D/\nu_S$ values for the two complexes are of opposite signs due to their magnetogyric ratios, γ, which are negative for the tin and positive for the lead nuclei. Therefore one would expect the bunching of peaks to occur in opposite directions and this was observed in the solid-state spectra for the two complexes under investigation, Fig 8.10. The quadrupole coupling constants are extremely difficult to determine by ^{55}Mn NQR measurements or single-crystal NMR studies for manganese compounds. However, the effective dipolar coupling constants can be obtained from spinning sidebands analysis, if the orientation of the chemical shift tensor with respect to the PAS of the EFG is known or can be assumed.

Wasylishen *et al.*[8-9] have shown that the orientation of the internuclear vector, $r_{I\text{-}S}$, with respect to the PAS of the chemical shift tensor can be obtained from the line shape of a static powder sample. The splitting patterns observed were represented by the following equations, Eqs. [8.2.5]-[8.2.7]

$$\Delta\nu_{11} = D'' (1 - 3\cos^2\alpha^\sigma \sin^2\beta^\sigma) \qquad [8.2.5]$$

$$\Delta\nu_{22} = D'' (1 - 3\sin^2\alpha^\sigma \sin^2\beta^\sigma) \qquad [8.2.5]$$

$$\Delta\nu_{33} = D'' (1 - 3\cos\beta^\sigma) \qquad [8.2.5]$$

where $\Delta\nu_{ii}$ represent the effective dipolar splitting of the δ_{ii} tensor and the angular terms α^σ and β^σ describe the orientation of the internuclear, $r_{I\text{-}S}$, in the PAS of the chemical shift tensor, σ. It should be noted that the method used for the determination D″ in Section 3.5,

Eq. [3.5.5], is a combination of Eqs. [8.2.5]-[8.2.7] provided that the spin-1/2 probe sites are axially symmetric.

The powder pattern for the diphenyltin compound is shown in Fig. 8.11 with very little or no splitting. This spectrum indicated that the effective dipolar coupling constant is very small or that the angular terms α^{σ} and β^{σ} are very close to 45.0 and 54.7°, respectively, which will result in the effective dipolar splitting, $\Delta\nu_{ii}$, equal to zero. X-ray structural data for $[(CO)_5Mn]_2SnPh_2$ shows that the Mn-Sn-Mn angle is a 117.1 ± 1°. If one assumes that the largest component of the shift tensor, δ_{33}, is bisecting the Mn-Sn-Mn angle (path of maximum electron current), then the angular term β^{σ} would be 58.55°. This will indeed result in very small undetectable splitting of the powder pattern, as was observed in the ^{119}Sn NMR spectrum, Fig. 8.11. Due to the similarity of the predicted angular term β^{σ} for the lead complex and large chemical shift span, δ_{11}- δ_{33} > 700 ppm, the static spectrum was not determined. However, the chemical shift tensors were extracted from spinning sidebands analyses, Table 8.2. The chemical shift tensors are much larger for the two diphenyl complexes than are the corresponding triphenyltin and triphenyllead complexes, Chapter 5.

The chemical shift spans were twice as large for the diphenyl complexes and the CSA are approximately three times larger than are those of the triphenyl analogues. The δ_{33} component show the largest shift from the isotropic chemical shifts and increase by about 70 and 325 ppm for the Ph_2Sn and Ph_2Pb complexes, respectively, when compared to the corresonding triphenyl compounds. The δ_{11} and δ_{22} values were also determined to show larger shifts from the isotropic values, with the exception of the δ_{22} for the

dipenhyltin, than are those of the $Ph_3EMn(CO)_5$ complexes. If our assumption of δ_{33} bisecting the Mn-E-Mn angles is valid, then either the δ_{11} or δ_{22} will be close or along the Mn-Sn-Phenyl plane, and will result in a larger values than the corresponding triphenyl compounds.

Table 8.2. ^{119}Sn and ^{207}Pb parameters of $[(CO)_5Mn]_2SnPh_2$ and $[(CO)_5Mn]_2PbPh_2$

NMR Parameters	$[(CO)_5Mn]_2SnPh_2$	$[(CO)_5Mn]_2PbPh_2$
δ_{iso} (solution) (ppm)	127.5 ± 0.1	378.3 ± 0.3
δ_{iso} (solid) (ppm)	153.3 ± 0.5	602.1 ± 0.5
$^1J_{Mn-E}$ (Hz)	139 ± 1	228 ± 1
δ_{11} (± 1.5 ppm)	342.1	319.1
δ_{22} (± 1.5 ppm)	153.4	408.7
δ_{33} (± 1.5 ppm)	-35.7	1078.4
$\Delta\delta$ (ppm)	283.8	714.5
η	0.998	0.188
$3\chi(D- 3\Delta J/3) / \nu_{Mn}$ (Hz)	-23.6 ± 0.6	5.64 ± 0.4
D (Hz)	-560 ± 4	293 ± 3

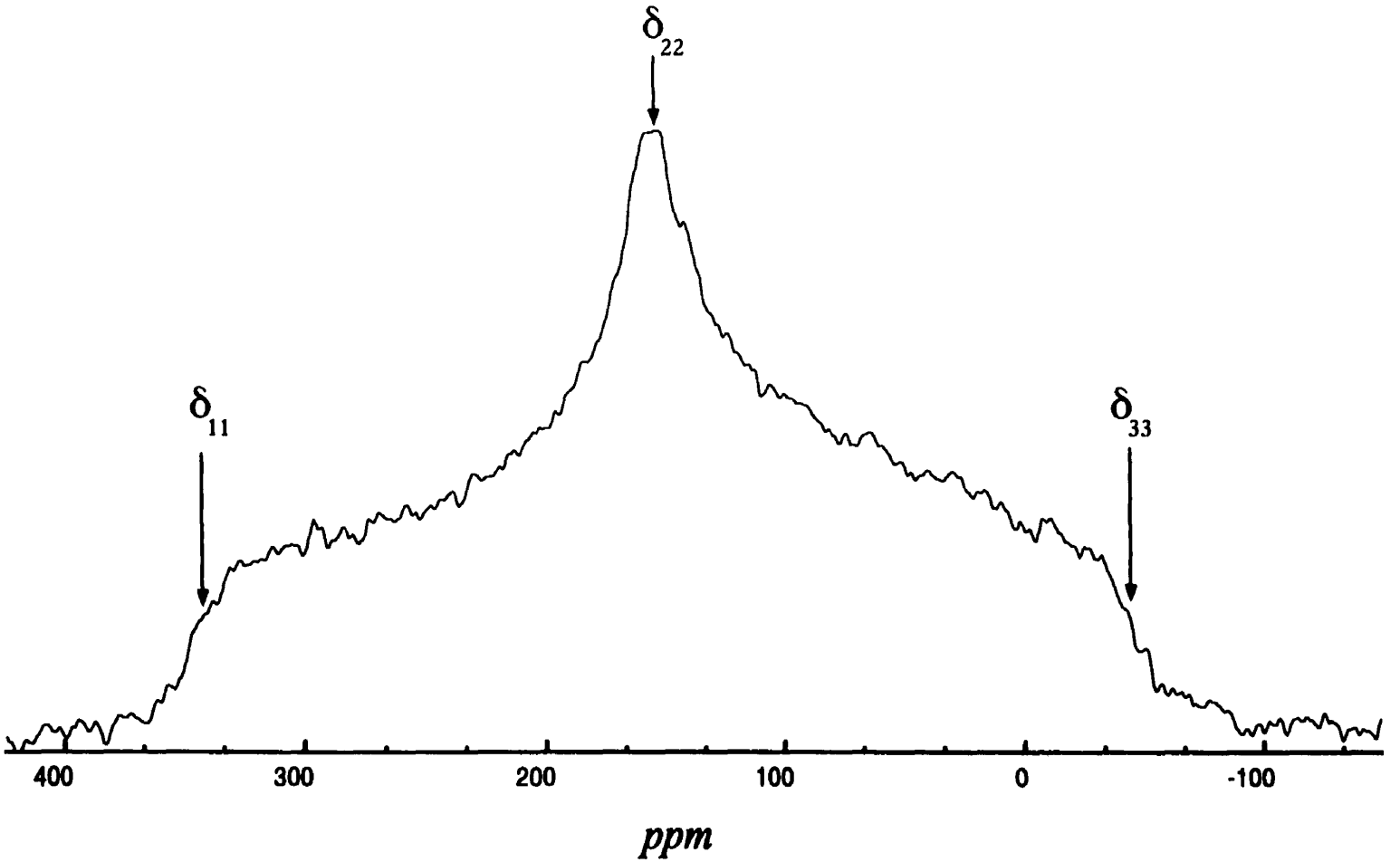

Figure 8.11 Experimental static powder ^{119}Sn NMR spectra of $[(CO)_5Mn]_2SnPh_2$ at 111.74 MHz. No apparent features of "effective" dipolar splitting were observed after 30,000 of transients.

References

(1) R. D. Gorsich, *J. Am. Chem. Soc.*, **84**, 2486 (1962).

(2) B. T. Kilbourn and H. M. Powell, *Chem. and Ind.*, 1587 (1964).

(3) D. J. Patmore, and W. A. G. Graham, *Inorg. Chem.*, **6**, 981 (1967).

(4) A. J. Olivieri, *J. Magn. Reson.*, **81**, 201 (1989).

(5) R. K. Harris and A. J. Olivieri, *Progr. NMR Spectrosc.* **24**, 435 (1992).

(6) H. Li, I. S. Butler, D. F. R. Gilson, J. F. Harrod and F. G. Morin, *J. Phys. Chem.*, **99**, 8490 (1995).

(7) A. J. Olivieri, *Magn. Reson. Chem.*, **34**, 365 (1996).

(8) K. Eichele, and R. E. Wasylishen, *J. Magn. Reson. Ser. A*, **106**, 46 (1994).

(9) C. W. Kirby, M. D. Lumsden and R. E. Wasylishen, *Can. J. Chem.*, **73**, 640 (1995).

Chapter 9

Crystal Structures and Phosphorus-31 Nuclear Magnetic Resonance Studies of Bis(trialkylphosphine)nickel(II) complexes

9.1 Introduction

The coordination chemistry of nickel(II), a group 10 (VIIIB) transition metal, with triorganophosphine ligands has been studied for more than five decades.[1-11] The type of phosphine as well as the other ligands play an important role in determining the coordination geometry. The stable geometries of nickel(II) complexes are square-planar, tetrahedral, trigonal-bipyramidal and square-pyramidal, and can be either a 16- or an 18-electron complex, depending on the coordination number of the metal atom. The reactions of nickel(II) halides with trialkylphosphines give the four-coordinate 16-electron species, $(R_3P)_2NiX_2$, with a *trans*-square planar structure, whereas those with triphenylphosphine have a tetrahedral geometry.[1] The observation of this change in structure led Browning *et al.*[1(c,d)] to investigate a new series of complexes of the type $(Ph_{3-n}R_nP)_2NiX_2$ for n = 0-3 (where R is Bu or Bz and X is Cl, Br, I, SCN or NO_3). These complexes shows some interesting changes in magnetic properties as the number of phenyl groups in the molecule decreases. The halide complexes of trialkyl- and dialkylphenylphosphines are diamagnetic, while those of the alkyldiphenyl-phosphines take an intermediate position, being paramagnetic in the solid-state and forming an equilibrium between diamagnetic and paramagnetic species in solution. The thiocyanate complexes were found be the *trans*-isomers but those of the nitrate were tetrahedral, regardless of the tertiary phosphine ligand used. It was later shown by Palmer *et al.*[5] that simply replacing one of the alkyl groups with a hydrogen atom on the trialkylphosphine

ligand for the $(Cy_3P)_2NiX_2$ resulted in the *cis*-square planar structures. However, the proton and phosphorus-31 NMR spectra analysis of $(Cy_2PH)_2NiX_2$ (X = Cl, Br, I) revealed that there is an equilibrium mixture of *cis* and *trans* isomers in dichloromethane solution.[6] It was also observed that the $(Cy_2PH)_2NiI_2$ complex exists only in the *trans* isomer in non-polar solvents such as toluene. Thus, solvent polarity has a drastic effect on the *cis-trans* equilibrium.[6]

In order to investigate the factors responsible for these changes in conformation, three series of complexes have been prepared; those of tribenzyl-, tricyclohexyl- and tris(α-cyclohexylmethyl)phosphine with nickel(II) chloride, bromide, iodide and thiocyanate. It was initially speculated by Browning *et al.*[1(c,d)] that the small electric dipole moments, Table 9.1, measured from benzene solutions of the bis(tribenzylphosphine)nickel(II) halides may be due to a small amount of *cis*-isomers present in the sample. Thus, there is opportunity to investigate these material in the solution and solid states by ^{31}P NMR spectroscopy for the presence of different isomers or coordination complexes other than the *trans* square-planar geometry.

9.2 Results and Discussion

9.2.1 Solid-State NMR

The solid-state ^{31}P NMR spectra of the three bis(tribenzylphosphine)nickel(II) dihalides, $(Bz_3P)_2NiX_2$, shown in Fig. 9.1, which exhibit sharp singlets with no sign of spin-spin couplings, $^1J_{Ni\text{-}P}$ or $^2J_{P\text{-}P}$. The absence of $^1J_{Ni\text{-}P}$ may be due to the low sensitivity natural abundance of the NMR active nickel-61 isotope (S = 3/2, 1.19%) and the expected

Table 9.1. Electric dipole moment and magnetic moment of tribenzylphosphine nickel(II) complexes[a]

Compound	Dipole moment, μ (D)	μ_{eff} (B.M)
$(Bz_3P)_2NiCl_2$	1.35	Diamagnetic
$(Bz_3P)_2NiBr_2$	1.77	Diamagnetic
$(Bz_3P)_2NiI_2$	3.69	Diamagnetic
$(Bz_3P)_2Ni(SCN)_2$	2.73	Diamagnetic
$(Bz_3P)_2Ni(NO)_2$	---[b]	Paramagnetic

[a]Values taken from ref. 1(d).
[b]Not measured.

triplets, spin-3/2 coupled to spin-1/2, may be so weak that they are lost in the base-line of the spectra. There appears to be no $^2J_{P\text{-}P}$ coupling for the three series of compounds studied, which indicates that the two phosphorus nuclei within the molecule are chemically and magnetically identical. The solid-state ^{31}P NMR spectra of $(Bz_3P)_2NiCl_2$ and $(Bz_3P)_2NiBr_2$ were found to contain two set of isotropic chemical shifts separated by more than 8 ppm, whereas the iodo- complex contained a single isotropic peak at 0.2 ± 0.1 ppm. These NMR results indicate that there are at least two distinct molecules or phosphorus sites for the chloro- and bromo- compounds, and a single phosphorus environment for the iodo- complexes. X-ray diffraction studies of $(Bz_3P)_2NiCl_2$ and $(Bz_3P)_2NiBr_2$, Fig. 9.2, revealed that there are two distinct molecules of the *trans*-isomer in the asymmetric unit and the two phosphorus ligands within a single molecule are

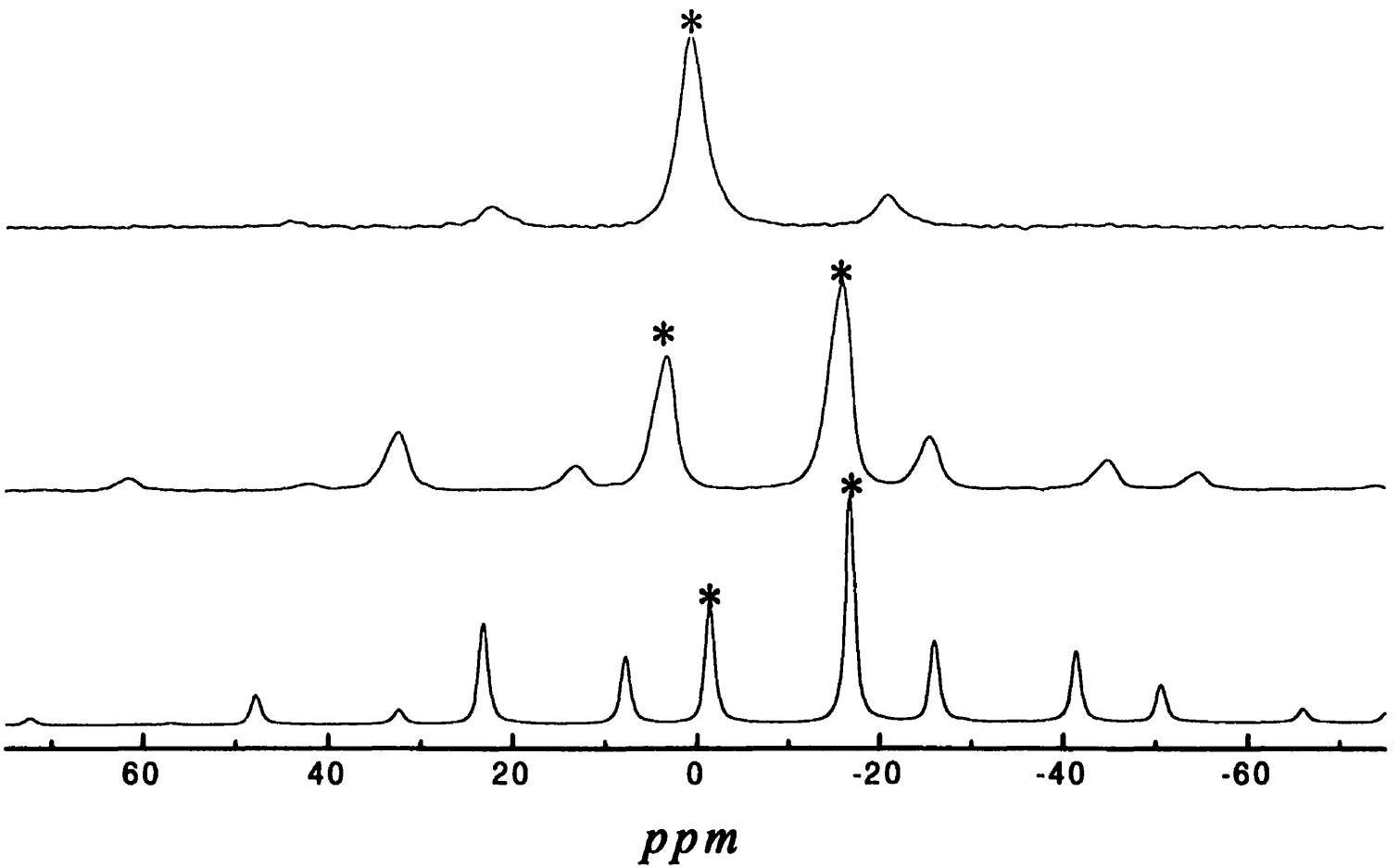

Figure 9.1. Solid-State ^{31}P NMR spectra of (a) $(Bz_3P)_2NiCl_2$, (b) $(Bz_3P)_2NiBr_2$ and (c) $(Bz_3P)_2NiI_2$ obtained at 121.28 MHz. The isotropic chemical shifts are label with asterisks and are referenced with respect to 85% H_3PO_4.

indeed equivalent. Attempts to grow single-crystals of suitable quality for the $(Bz_3P)_2NiI_2$ complex were unsuccessful, but preliminary results have shown that there is a single *trans*-square planar molecule in the asymmetric unit. Despite the problems encountered with the iodo- complex, it is safe to say that the NMR results are in good agreement with those obtained by single-crystal diffraction studies.

The spectra of the bis(tricyclohexylphosphine)- and bis[tris(α-cyclohexylmethyl)-phosphine]nickel(II) dihalides were found to contain a single set of centrebands, Table 9.2 (Fig. 9.3), and again with no spin-spin couplings. The structure of $(Cy_3P)_2NiCl_2$ was previously determined by Bellon *et al.*[13] and was found to contain a single molecule of the *trans*- isomer in excellent agreement with the solid-state ^{31}P NMR result. The data in Table 9.2 clearly indicate that as the size of the halogen increases the ^{31}P chemical shifts increase or as the electronegativity of the halogen decreases the ^{31}P chemical shifts increase.

The chemical shift tensor information for the nine nickel(II) halide complexes are presented in Table 9.2. In general, the δ_{11} tensor component tends to decrease as the electronegativity of the halides decrease, with the exception of $(Cy_3P)_2NiI_2$. However, this component shows little change for the two different crystallographic molecules in the asymmetric units of the $(Bz_3P)_2NiCl_2$ and $(Bz_3P)_2NiBr_2$ complexes, despite the major changes in orientation of the benzyl rings. This result may indicate that δ_{11} lies along the P-Ni bond and thus is expected to show very little change for the non-equivalent molecules. The two perpendicular tensor components, δ_{22} and δ_{33}, are then expected to

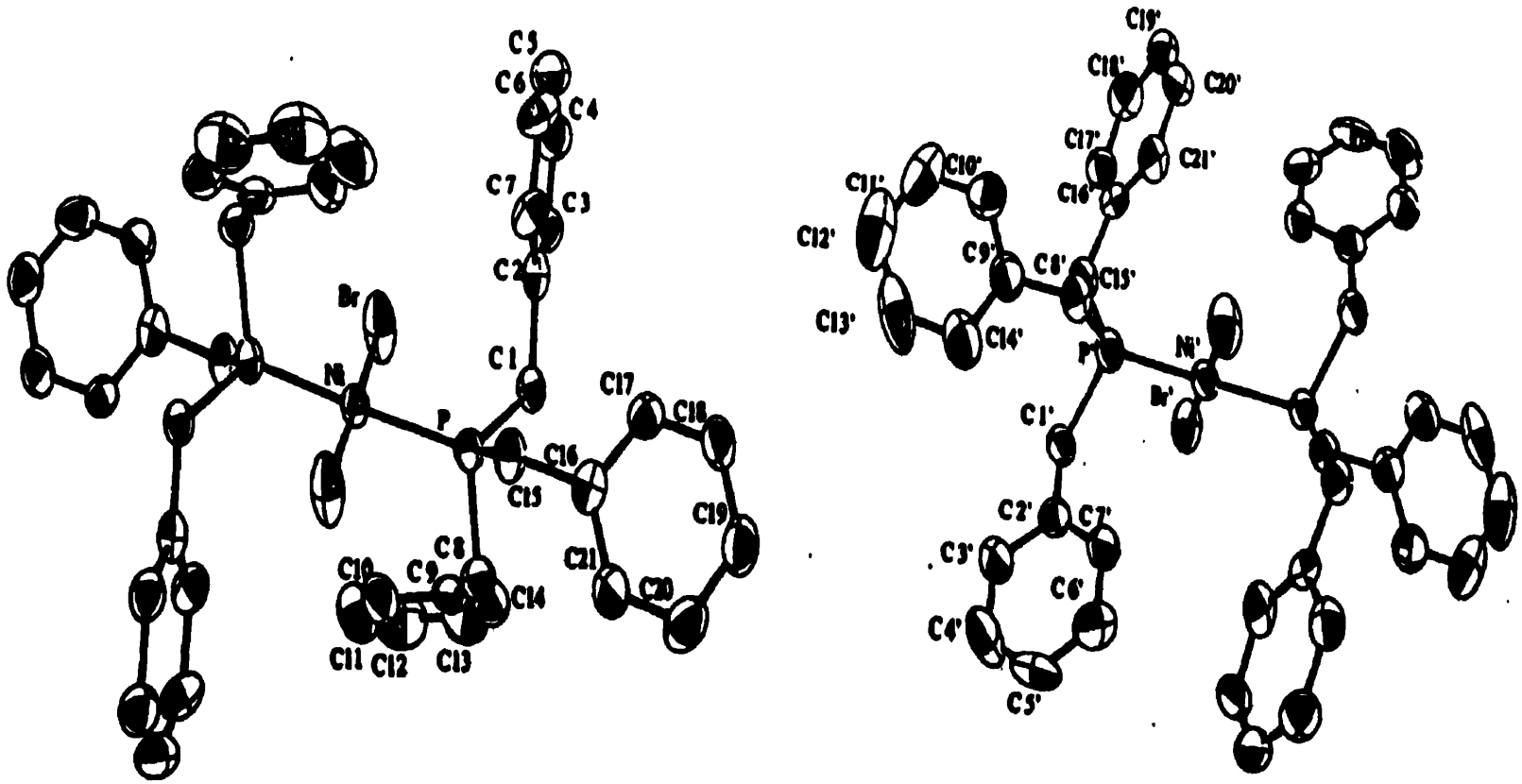

Figure 9.2 ORTEP representation of $(Bz_3P)_2NiBr_2$ showing the two different molecules in the asymmetric unit. Ellipsoids are shown at 30% probability. The major structural differences are the orientation of the benzyl groups around the phosphorus atoms.

Table 9.2. Phosphorus-31 NMR chemical shift tensor data for *trans*-(trialkylphosphine)nickel(II) halide and thiocyanate complexes.

Complex	δ_{iso} (ppm) (solution-state)	δ_{iso} (±0.1 ppm) (solid-state)	δ_{33} (±1 ppm)	δ_{22} (±1 ppm)	δ_{11} (±1 ppm)	$\Delta\delta$ [a,b] (ppm)	η [a,b]
$(Bz_3P)_2NiCl_2$	0.28 ± 0.02	-14.5	28	-16	-56	64	0.94
		1.4	61	7	-64	-98	0.83
$(Bz_3P)_2NiBr_2$	2.12 ± 0.02	-11.0	25	-18	-39	54	0.58
	5.40 ± 0.05	2.9	37	-4	-42	-62	0.87
$(Bz_3P)_2NiI_2$	36.5 ± 0.5	0.2	33	-7	-25	46	0.55
$(Cy_3P)_2NiCl_2$	-9.92 ± 0.02	2.8 (3.0)[c]	59	-4	-47	80	0.77
$(Cy_3P)_2NiBr_2$	15.4 ± 0.2	7.9	58	-3	-31	75	0.56
$(Cy_3P)_2NiI_2$	25.4 ± 0.5	8.3	46	13	-34	-66	0.78
$[(CyMe)_3P]_2NiCl_2$	-10.0 ± 0.2	-14.6	19	-16	-47	50	0.93
$[(CyMe)_3P]_2NiBr_2$	1.7 ± 0.2	-9.6	18	-14	-33	42	0.75
$[(CyMe)_3P]_2NiI_2$	20.9 ± 0.2	4.5	26	4	-17	36	0.98

[a]For $|\delta_{33} - \delta_{iso}| > |\delta_{11} - \delta_{iso}|$, Anisotropy parameter $\Delta\delta = \delta_{33} - 1/2\,(\delta_{11} + \delta_{22})$ and asymmetry parameter $\eta = |(\delta_{11} - \delta_{22}) / (\delta_{22} - \delta_{iso})|$.
[b]For $|\delta_{11} - \delta_{iso}| > |\delta_{33} - \delta_{iso}|$, Anisotropy parameter $\Delta\delta = \delta_{11} - 1/2\,(\delta_{33} + \delta_{22})$ and asymmetry parameter $\eta = |(\delta_{33} - \delta_{22}) / (\delta_{11} - \delta_{iso})|$.
[c]Datum taken from ref. 7.

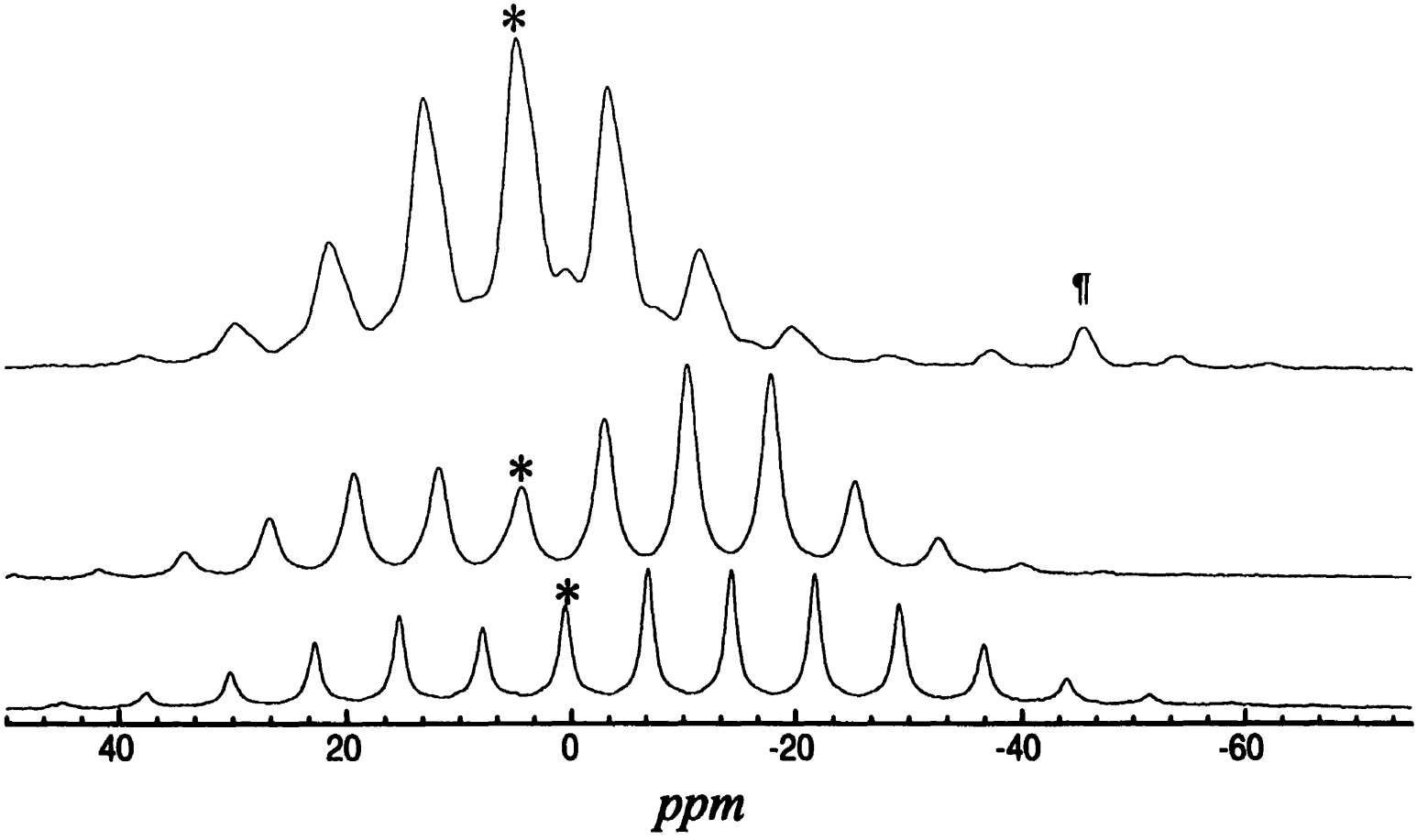

Figure 9.3. Solid-State ^{31}P NMR spectra of (a) $[(CyMe)_3P]_2NiCl_2$, (b) $(Bz_3P)_2NiBr_2$ and (c) $(Bz_3P)_2NiI_2$ obtained at 121.28 MHz. The isotropic chemical shifts are label with asterisks and impurities with ¶.

show major changes in magnitude for these two sites, and this was observed in both the $(Bz_3P)_2NiCl_2$ and $(Bz_3P)_2NiBr_2$ cases. The δ_{22} and δ_{33} tensor values show little change for the Cy_3P and $(CyMe)_3P$ ligands, with the exception of the iodo- complexes, and this may also indicate that these two components are perpendicular to the P-Ni bonds. It was observed that changing the phosphine ligand causes a large difference in the δ_{33} tensor value. A change of more than 20 ppm for δ_{33} was obtained by simply replacing the cyclohexyl group with mehylcyclohexane on the phosphine ligand.

Jarrett *et al.*[7] have obtained chemical shift tensor data for five different Ni(II) halide complexes containing dppe, $Ph_2PCH_2CH_2PPh_2$, and dppey, $Ph_2PCH{=}CHPPh_2$, ligands, Table 9.3. The isotropic chemical shift data also indicated that as the electronegativity of the halides increase the chemical shifts decrease. The orientation of the chemical shift tensors, however, could not be determined and may be due to the limited number of complexes studied. If our assignment of the most shielded component (δ_{11} in our case or δ_{33} for bidentate ligands) is along the Ni-P bond, then the values obtained by Jarrett *et al.*[7] should be about the same as those obtained in our studies. However, the values obtained by Jarrett *et al.*[7] are slightly less shielded than those of the monodentate phosphine ligands. The steric strain created by the ethyl or ethylene groups bridging the two phosphorus atoms may have decreased the bonding interactions between the nickel centre and the phosphorus nucleus, and may result in a deshielding effect of the chemical shift tensor component along the Ni-P bond. This steric strain may also result in the δ_{33} tensor component being slightly off the Ni-P bond. Therefore, the assumption of δ_{11} being along the Ni-P bond for the R_3PNiX_2 complexes is valid.

Table 9.3. Solid-state ^{31}P NMR chemical shift tensor data for bis(phosphine)nickel(II) halide complexes.[a]

Complex	δ_{iso} (±0.1 ppm) (solid-state)	δ_{11} (±1 ppm)	δ_{22} (±1 ppm)	δ_{33} (±1 ppm)	$\Delta\delta$[b] (ppm)	η[c]
(dppe)$NiCl_2$	53.1	156	54	-51	-156	0.98
	56.2	134	64	-29	128	0.82
	65.1	140	86	-31	144	0.56
	66.5	138	92	-31	146	0.47
(dppe)$NiBr_2$	66.6	---	---	---	---	---
	63.9	---	---	---	---	---
(dppe)NiI_2	75.5	165	93	-31	-160	0.68
	82.5	192	86	-30	-169	0.94
(dppey)$NiCl_2$	69.7	157	94	-42	168	0.56
	71.1	94	89	-39	131	0.05
(dppey)$NiBr_2$	72.2	178	82	-43	173	0.83

[a]Chemical shift tensor values from ref. 9.
[b]Recalculated using $|\delta_{33} - \delta_{iso}| > |\delta_{11} - \delta_{iso}|$, Anisotropy parameter $\Delta\delta = \delta_{33} - 1/2\ (\delta_{11} + \delta_{22})$.
[c]Asymmetry parameter $\eta = |(\delta_{11} - \delta_{22}) / (\delta_{33} - \delta_{iso})|$.

The solid-state ^{31}P NMR and X-ray diffraction studies clearly indicated that the bis(trialkylphosphine)nickel(II) halides are 100 % *trans*-isomers. Then the question is "Why is the dipole moment in solution not equal to zero, and why does it increase as the electronegativity of the halide decreases?" The solution to this problem is to study these complexes in solution using ^{31}P NMR spectroscopy, since the magnetic moment and dipole moment were measured in the solution.

9.2.2 Solution NMR Studies

The solution ^{31}P NMR spectra for $(Bz_3P)_2NiCl_2$, $(Bz_3P)_2NiBr_2$ and $(Bz_3P)_2NiI_2$ are shown in Fig. 9.4. The ^{31}P chemical shifts of the bromo- and iodo- complexes are very different from the solid-state measurements, whereas the $(Bz_3P)_2NiCl_2$ spectra are similar in both states (if the low-field peak is considered to be the same as that in the solid-state). Clearly the structures of the bromo- and iodo- complexes are different from the *trans*-square planar geometry obtained from solid-state studies. The bromo- complex exibited two very distinct peaks in CD_2Cl_2, at 2.12 and 5.40 ppm. The high-field peak is close to the value obtained in the solid-state for one of the crystallographically non-equivalent molecules, and can be assigned as having *trans*-square planar geometry. However, the species responsible for the low-field peak is unknown but may be the cause of the dipole moment obtained by Browning *et al.*[1(d)] The solution ^{31}P spectrum of the iodo- complex is broad with a chemical shift difference of over 30 ppm from the solid-state result, which definitely indicates a structural change. Chatt and Wilkins[14] have reported that there in an equilibrium between *cis-trans* isomers for bis(triethylphosphine)dihaloplatinum(II) and the ratios of *cis-trans* isomerization were found be solvent dependent. The change of solvent, from CD_2Cl_2 to C_6D_6 or $C_6D_5CD_3$, affected the shape and height of the peaks in the spectrum of the iodo- complex, Figs. 9.5 and 9.6, as well as the ratio of the two conformers for the bromo- complex. It was also found that the ^{31}P NMR chemical shift for the iodo- complex changed from 36.5 to about 43.7 ppm. These observations support the evidence of *cis-trans* isomerization in solution for the nickel(II) complexes. The mechanism, described by Chatt and Wilkins[13] for the platinum complexes, was assumed

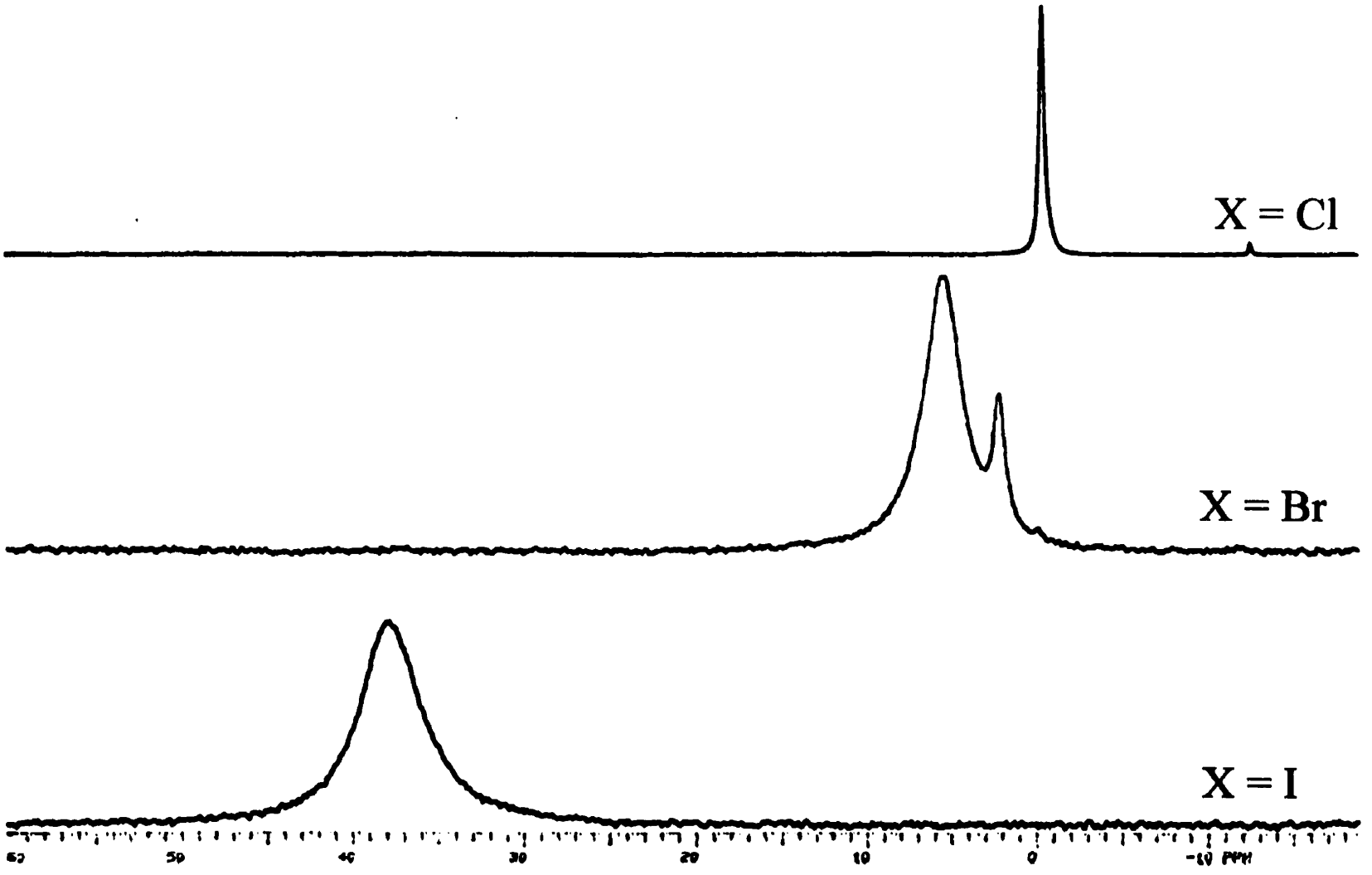

Figure 9.4. Proton decoupled ^{31}P NMR spectra of $(Bz_3P)_2NiX_2$ at 121.279 MHz; solvent CD_2Cl_2.

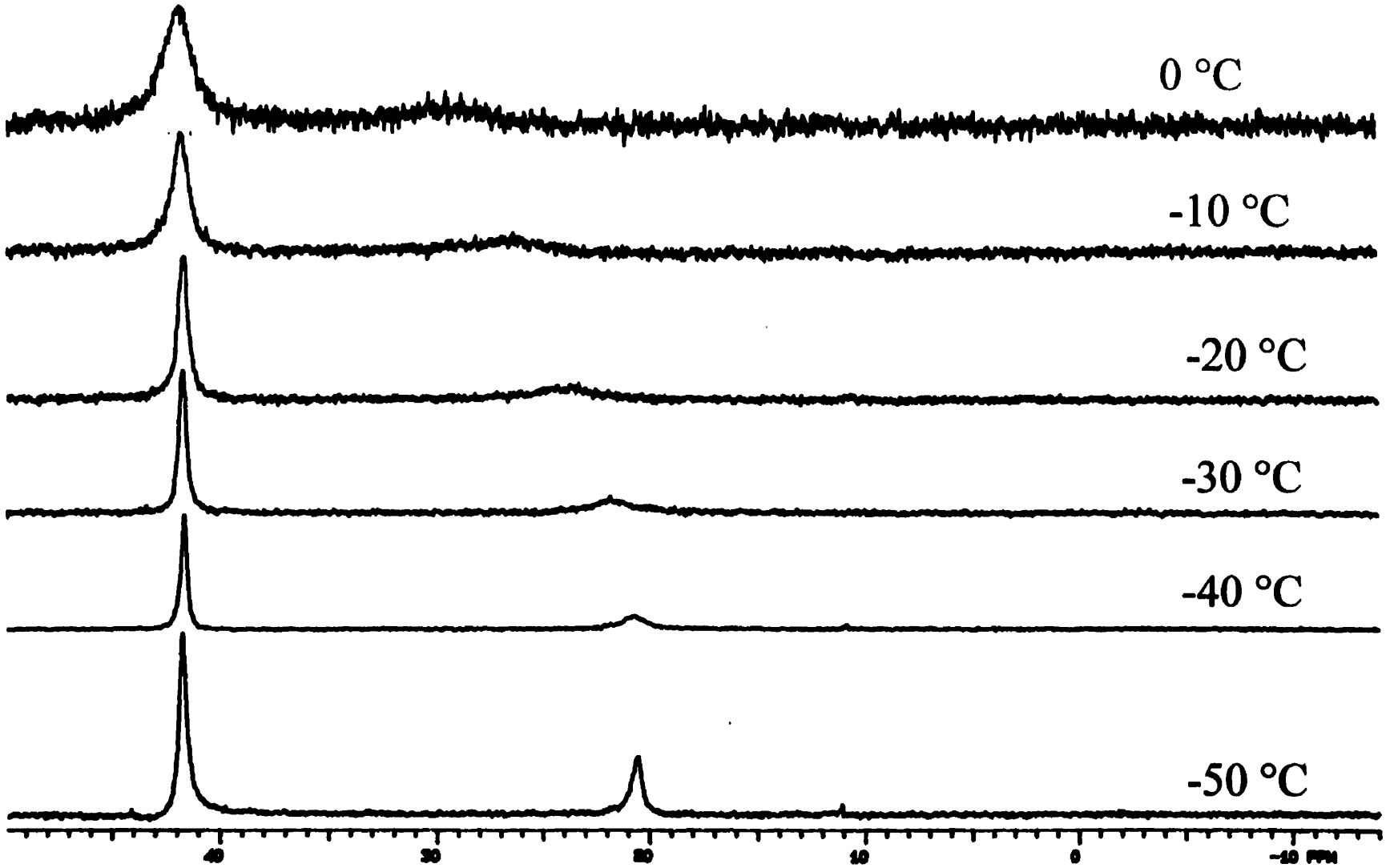

Figure 9.5. Variable temperature proton decoupled ^{31}P NMR spectra of $(Bz_3P)_2NiI_2$ in CD_2Cl_2.

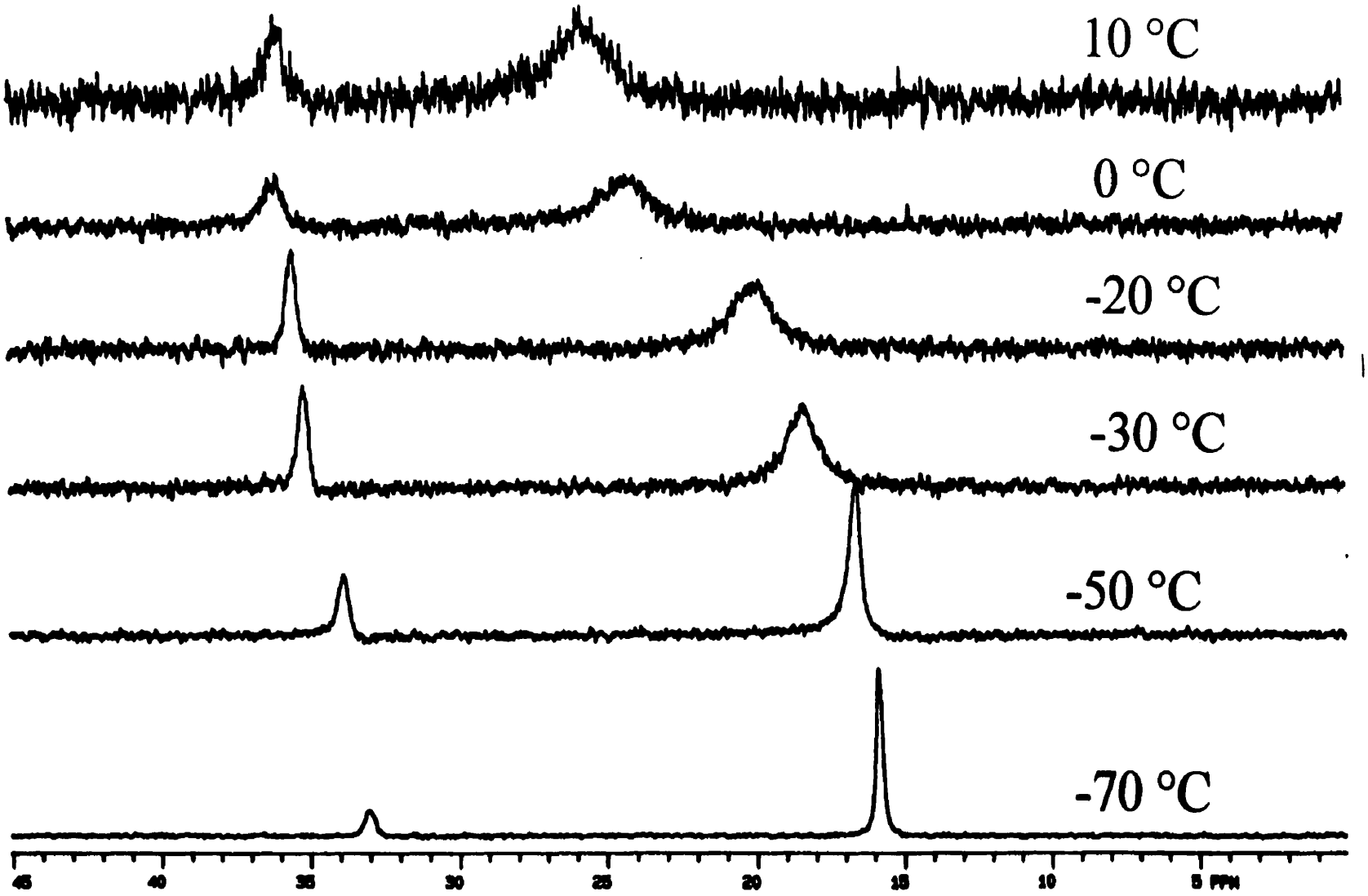

Figure 9.6. Variable temperature proton decoupled ^{31}P NMR spectra of $(Bz_3P)_2NiI_2$ in $C_6D_5CD_3$.

to involve the interactions of aromatic solvent molecules. We do not agree with this interpretation as there was no supporting experimental data for η^2-bonding interactions to the nickel(II) or platinum(II) centre. However, we do agree that the polarity of the solvent does have a pronounced effect on the *cis-trans* equilibrium, as was observed by Palmer *et al.*[6] for the nickel complexes.

Variable temperature, VT, ^{31}P NMR studied in CD_2Cl_2 and toluene-D_8 have revealed that there are indeed two different complexes present in solution, Figs. 9.5 and 9.6. The VT studies indicated that the low-field peak, believed to be the *cis*-isomer, is slowly converting to the *trans*-square planar complex.

There are a other possible mechanisms which could explain the *cis-trans* equilibrium, as shown in Fig. 9.7. The first proposed mechanism involves the combination of two molecules and the release of two free phosphines. However, no free tertiary phosphine or phosphine oxide was observed in the solution ^{31}P NMR spectra for the series of complexes studied. The second mechanism also involves the combination of two molecules with the dissociation of two halides, $2X^-$. Conductivity measurements in benzene and dichloromethane solutions gave negative results for the nine dihalogenated complexes investigated. The third and fourth mechanisms are most likely to occur, which involve paramagnetic tetrahedral species and would result in a broad-featureless ^{31}P NMR signal. The third mechanism could be tested by EPR spectroscopy but, due to the unavailability of an instrument at the time, no such measurements were possible. The fourth mechanism would eliminate the third, if it can be proven. This was achieved by mixing two different halide complexes with the same type of tertiary phosphine ligand,

such as $(Bz_3P)_2NiCl_2$ and $(Bz_3P)_2NiI_2$. The solution ^{31}P NMR spectra, Fig. 9.8, indicate the presence of a new peaks which increase in intensity as the concentration of $(Bz_3P)_2NiCl_2$ increase. Therefore, it is safe to say that the *cis-trans* isomerization occurs by dimerization of two nickel centres forming an 18-electron five-coordinate nickel centre that is responsible for the dipole moment obtained by Browning *et al.*[16d]

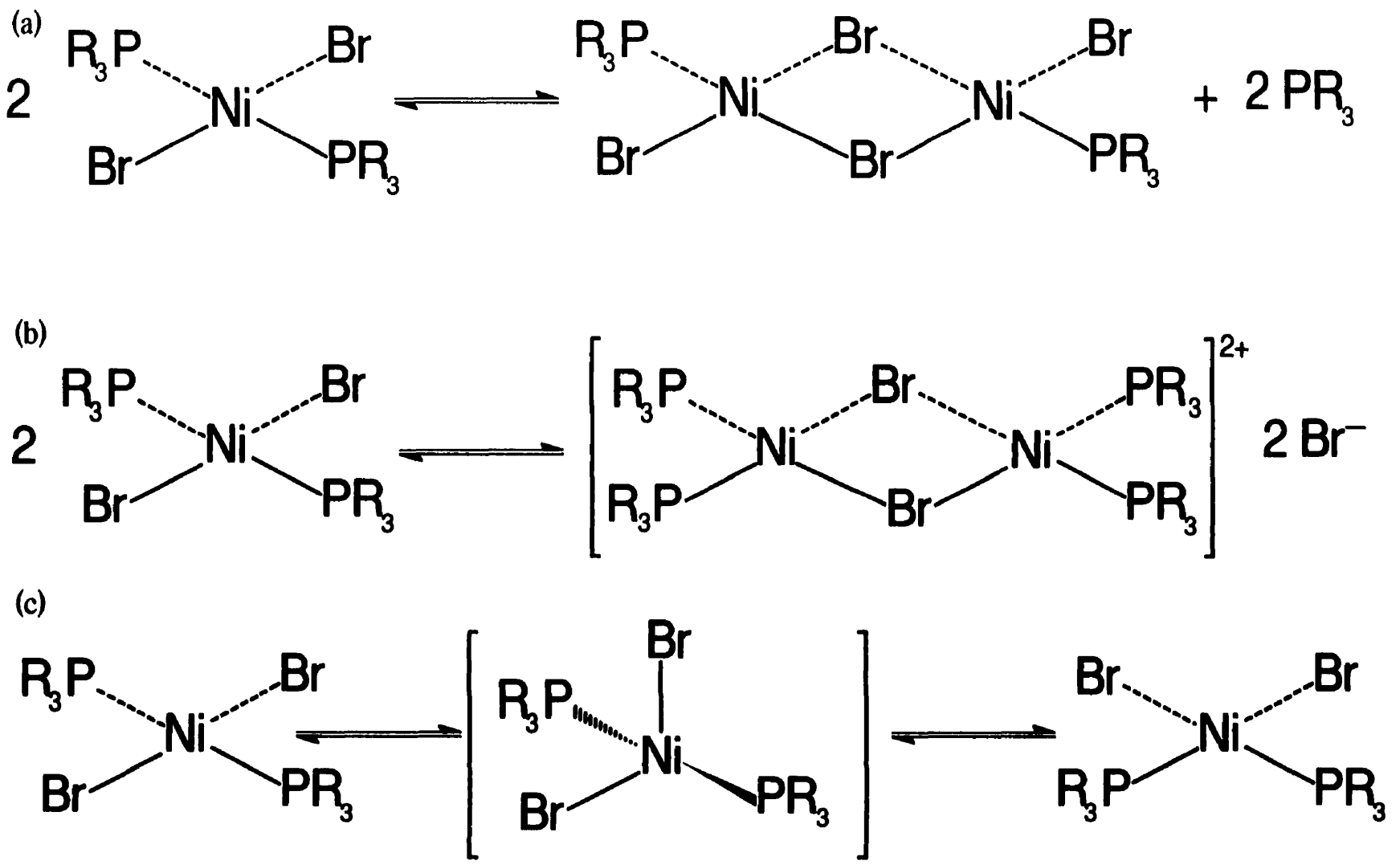

Figure 9.7. Possible mechanistic pathways for the *cis-trans* isomerization of bis(trialkylphosphine)nickel(II) halides.

(d)

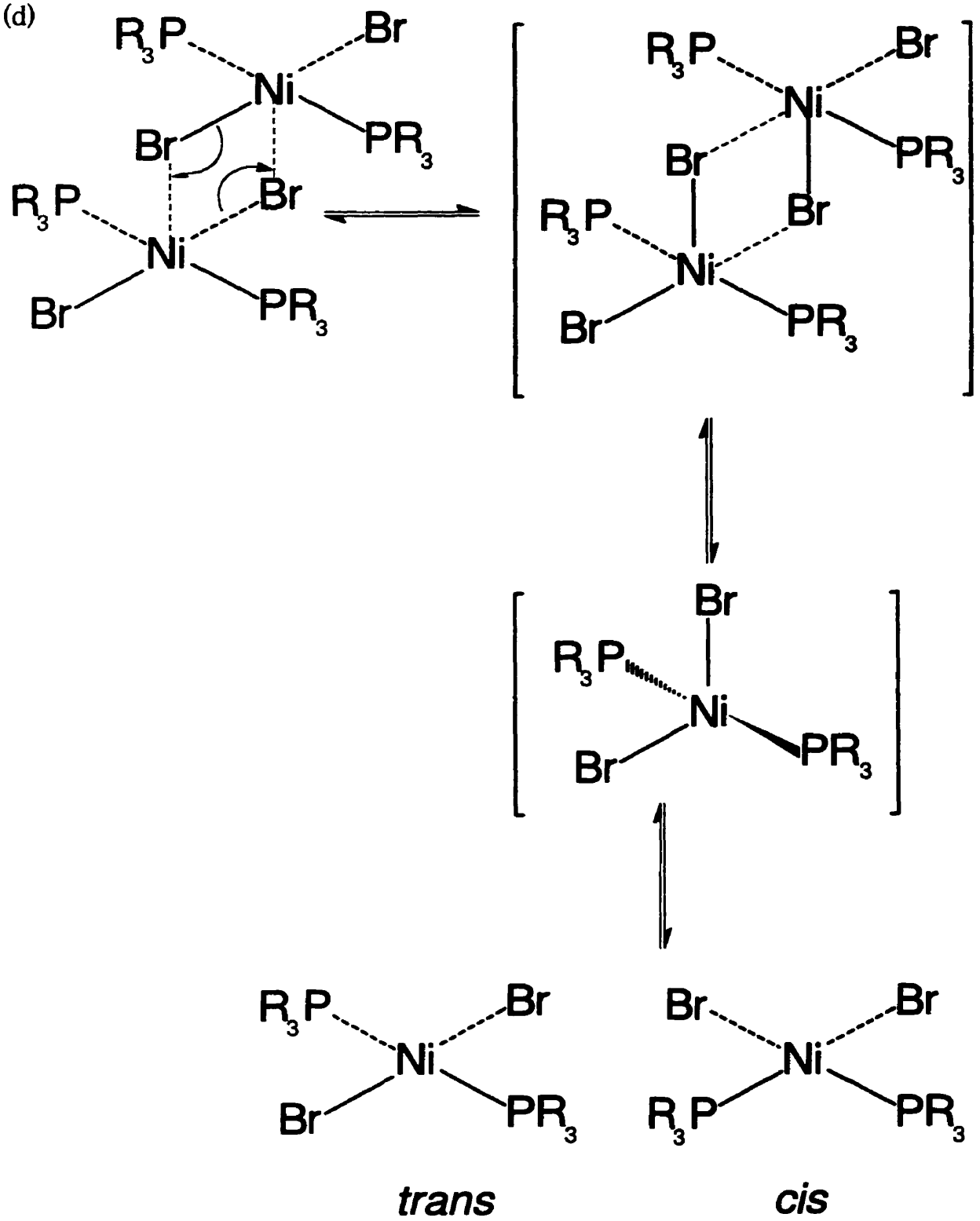

Figure 9.7. (*continued*)

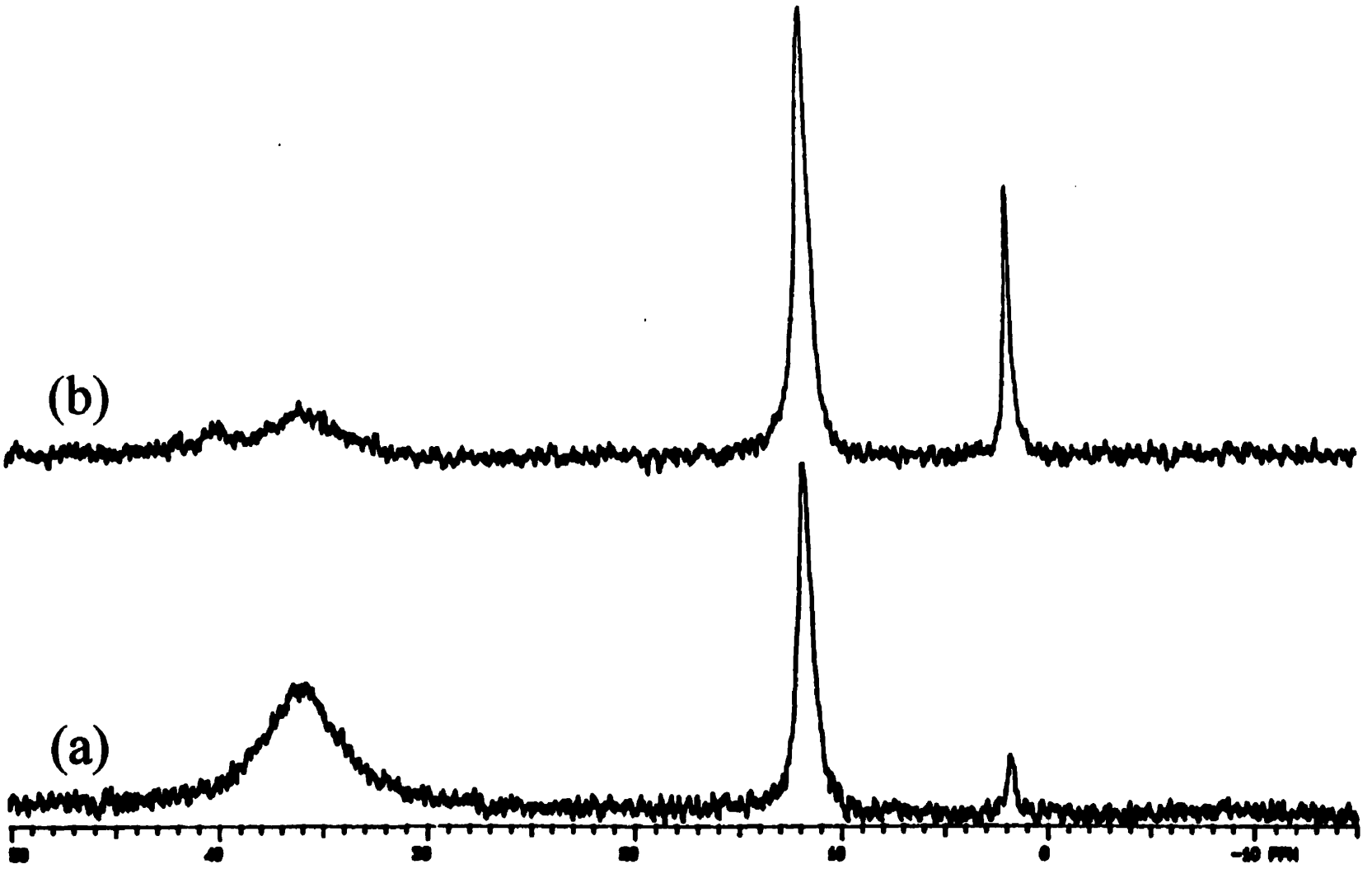

Figure 9.8. Proton decoupled ^{31}P NMR spectra of mixed $(Bz_3P)_2NiCl_2$ and $(Bz_3P)_2NiI_2$ in CD_2Cl_2.

References

(1) (a) C. R. C. Coussmaker, M. H. Hutchinson, J. R. Mellor, L. E. Sutton and L. M. Venanzi, *J. Chem. Soc.*, 719 (1958).

(b) C. R. C. Coussmaker, M. H. Hutchinson, J. R. Mellor, L. E. Sutton and L. M. Venanzi, *J. Chem. Soc.*, 2705 (1961).

(c) M. C. Browning, R. F. B. Davies, D. J Morgan, L. E. Sutton and L. M. Venanzi, *J. Chem. Soc.*, 4816 (1961).

(d) M. C. Browning, J. R. Mellor, D. J Morgan, S. A. J. Pratt, L. E. Sutton and L. M. Venanzi, *J. Chem. Soc.*, 693 (1962).

(2) L. H. Pignolet, W DeW. Horrocks, Jr., and R. H. Holm, *J. Am. Chem. Soc.*, **92**, 1855 (1970).

(3) L. Que, Jr. and L. H. Pignolet, *Inorg. Chem.*, **12**, 156 (1973).

(4) J. W Dawson, T. J. McLennan, W. Robinson, A Merie, M. Dartiguenave, Y. Dartiguenave and H. B. Gray, *J. Am. Chem. Soc.*, **96**, 4428 (1974).

(5) R. A. Palmer, H. F. Giles, Jr. and D. R. Whitcomb, *J. Chem. Soc. Dalton Trans.*, 1671 (1978).

(6) R. A. Palmer and D. R. Whitcomb, *J. Magn. Reson.*, **39**, 371 (1979).

(7) L. Bemi, H. C. Clark, J. A. Davies, C. A. Fyfe and R. E. Wasylishen, *J. Am. Chem. Soc.*, **104**, 438 (1982).

(8) M. Bochmann, I. Hawkins, M. B. Hursthouse and R. L. Short, *J. Chem. Soc. Dalton Trans.*, 1213 (1990).

(9) P. S. Jarrett and P. J. Sadler, *Inorg. Chem.*, **30**, 2098 (1991).

(10) M. Lautens, L. G. Edwards, W. Tam and A. J. Lough, *J. Am. Chem. Soc.*, **117**, 10276 (1995).

(11) S. J. Chadwell, S. J. Coles, P. G. Edwards, M. B. Hursthouse and A. Imran, *Polyhedron*, **14**, 1057 (1995).

(12) D. H Nguyen, Hua-Fen Hsu, M. Millar and S. A. Koch, *J. Am. Chem. Soc.*, **118**, 8963 (1996).

(13) P. L. Bellon, V. Albano, V. D. Bianco, F. Pompa and V. Scatturin, *Ric. Sci.*, **33**, 1213 (1963).

(14) J. Chatt and R. G. Wilkins, *J. Chem. Soc.*, 273 (1952).

Contributions to Knowledge

X-ray crystallography, vibrational and multinuclear magnetic resonance spectroscopy have been used to study the structures the bonding interactions of alkyl-, acyl-, silyl-, stannyl- and plumbly-carbonylmanganese(I) complexes. The vibrational spectra in the carbonyl region, 2250-1850 cm^{-1}, were discussed in terms of vibrational group theory. Complex solid-state splittings, induced by the interaction of manganese-55 with the spin-1/2 nuclei, have been detected in the ^{13}C, ^{29}Si, ^{31}P, ^{117}Sn, ^{119}Sn and ^{207}Pb CP-MAS NMR spectra. In all cases, the isotropic chemical shifts, the chemical shift tensors, the spin-spin coupling constants, the "effective" dipolar coupling constants and the quadrupole coupling constants, along with the anisotropies in the spin-spin coupling and the chemical shift, have been extracted from the solid-state spectra. These interactions could not be observed by manganese-55 NMR spectroscopy in solution due to fast quadrupolar relaxation of the manganese nucleus. The spin-spin coupling constants and the chemical shift anisotropies of the alkyl complexes have all been found to be larger than are those for the acyl complexes. The solid-state $^1J_{Mn-P}$ shows little variation within the series, and range from 196 to 204 Hz for the alkyl compounds and from 216 to 233 Hz for the acyl complexes. The $^1J_{Mn-P}$ values obtained from the ^{55}Mn NMR spectra for the alkyl complexes are ~50Hz larger than are those obtained from the ^{31}P solid-state studies. The nuclear quadrupole coupling constants show little or no variation for the series of phosphine ligands used and range from 23 to 25 MHz.

The crystal structures of tertiary phosphine benzyl(tetracarbonyl)manganese(I) complexes, **VII-X**, have been determined for the first time by three-dimensional X-ray diffraction and were found to crystallize with *cis* geometry.

The solid-state ^{29}Si, ^{117}Sn, ^{119}Sn and ^{207}Pb, CP-MAS, NMR spectra of strong covalent bimetallic complexes (featuring directly bonded metal atoms) involving a main group metal and a transition metal have been measured for the first time. The presence of different polymorphs, obtained for $Ph_3PbMn(CO)_5$ from octane and a benzene/octane mixture, was demonstrated from ^{207}Pb solid-state NMR spectroscopy and confirmed by preliminary single-crystal X-ray structural analysis. Three new spin-spin coupling constants have been determined and the average absolute values of the reduce coupling constants, $^1K_{Si-Mn}$, $^1K_{Sn-Mn}$, and $^1K_{Pb-Mn}$, for the triphenyl complexes, were compared with the *s*-electron densities at the respective metal nuclei. The results obtained clearly indicate that the Fermi contact term is the dominant factor in determining the isotropic spin-spin coupling. The dominance of the Fermi contact contribution to the spin-spin coupling was further demonstrated for a new series of *para*-substituted triaryltin(pentacarbonyl)manganese(I) complexes. The spin-spin coupling, $^1J_{Sn-Mn}$, and nuclear quadrupole coupling constants for these covalent bimetallic complexes show linear correlation, and this is attributed mainly to the *s*-character of the hybrid used in the bonding orbitals between the two metal nuclei.

The crystal structures of $Ph_3SiMn(CO)_5$ and (*para*-$XC_6H_4)_3SnMn(CO)_5$ complexes (X = CH_3, OCH_3, SCH_3, F, Cl) have been determined by single-crystal X-ray diffraction. The magnitudes of the principal elements of the chemical shift tensors for these complexes and $Ph_3PbMn(CO)_5$ have been determined and appear to be strongly

influenced by the ring torsion angles and the *para*-substituents on the phenyl rings. The electron-withdrawing ability of the *para*-substituents has also been shown to play an important role in determining the magnitude and direction of the electric field gradient. It has been shown that, in order to understand the nature of the metal-metal interactions, a comparison of the reduced coupling constants and the shift tensors is much more informative than is the use of the isotropic chemical shift and spin-spin coupling values

The solution phase ^{1}H, ^{13}C, ^{29}Si, ^{31}P, ^{55}Mn, ^{119}Sn and ^{207}Pb NMR spectra have been measured for the thirty-three complexes studied in this thesis. The ^{13}C, ^{55}Mn and ^{119}Sn chemical shifts, δ_{iso}, and the one-bond spin-spin coupling, $^{1}J(^{119}Sn\text{-}^{13}C)$, for the *para*-substituted triphenyltin complexes have been shown to show excellent correlation ($r>0.988$) with pairs of Hammett and Taft inductive and resonance substituent constants, (σ_I, σ_R) and (σ_I, σ_R°).

Solid-state and solution ^{31}P NMR spectroscopy have been used to study three series of bis(trialkylphosphine)dihalonickel(II) complexes, $(Bz_3P)_2NiX_2$, $(Cy_3P)_2NiX_2$ and $[(CyCH_2)_3P]_2NiX_2$ (X = Cl, Br, I). The solution ^{31}P isotropic chemical shifts for the bromo and iodo- compounds have been shown to be very different than are those obtained from solid-state measurements. The crystal structures of $(Bz_3P)_2NiX_2$ have been determined by single-crystal X-ray diffraction, and the geometry of the nickel(II) complexes studied has been estiblished as *trans* square-planar structure. Variable temperature ^{31}P NMR measurements for $(Bz_3P)_2NiBr_2$ and $(Bz_3P)_2NiI_2$ have demonstrated the presence of two different structural isomers in solution. The two structural isomers are produced from the

dimerization of two *trans* molecules, where the halides interact with the nickel(II) centre to form a bridged trigonal-bipyramidal intermediate.

Suggestions for Future Work

(1) Solid-state NMR spectroscopy of a spin-1/2 nucleus has been used to determine the manganese-55 quadrupole parameters from first-order perturbation theory. The accuracy of these parameters, χ and η_χ, are not known, but can be determined either by single-crystal, ^{55}Mn solid-state NMR measurements or by ^{55}Mn nuclear quadrupole resonance spectroscopy. The second method requires a large amount of sample, ~5.0g, in order to determine the magnitude of the NQR parameters, and the technique is difficult for manganese complexes. The first method was previously applied by Sheline *et al.*[1] for $Ph_3EMn(CO)_5$ (E = Sn, Ge, Pb) and should be used to study the alkyl- and acyl-manganese(I) and complexes, **III-IX**, where the molecular symmetry is lower than c_{4v} for the manganese moieties.

(2) Triaryltin compounds have numerous important industrial applications,[2] such as antifouling paint biocides, agricultural fungicides and anti-feedants. However, no such studies have been carried out on triorganotin-metal complexes. Therefore, it would be important to investigate the series of *para*-substituted triaryltin(pentacarbonyl)-manganese(I) compounds studied in this thesis to see if they have any such properties.

(3) The absorption of alkyl thiols onto gold and silver surfaces is known to have many electronic applications. One of the major problems encountered in coating the metal surfaces with thiols is forming a homogenous monolayer. It is also known that the absorbed thiols can be easily removed when a small amount of electrical current is

applied to the surface. We believe that these problems can be overcome by creating tripod thiols, where they can strongly anchor on to the gold and silver surfaces, compared to regular thiols, to form a homogenous monolayer. These types of tripod thiols can be prepared by reductive cleavage of alkyl aromatic thioethers with calcium hexammine,[3] in which three or four aromatic rings are attach to a group 14 (IVA) metal or a group 15 (VA) atom, as shown below for group 14 metals.

$$(R\text{-}S\text{-}Ar)_3EX + 3\ Ca(NH_3)_6 \rightarrow (HS\text{-}Ar)_3EX + 3\ Ca(NH_2)_2 + 12\ NH_3 + 3\ RH$$

where R is an alkyl group, E is the group 14 metals and X could be any group such as Cl, Br, I, alkyl or metal-carbonyl fragments. Complexes which we think will have interesting properties are (*para*-$HSC_6H_4)_3SnX$, (*para*-$HSC_6H_4)_4Sn$, (*para*-$HSC_6H_4)_3SnMn(CO)_5$, *trans*-(*para*-$HSC_6H_4)_3SnMn(CO)_4[P($*para*-$HSC_6H_4)_3]$. The most important electronic properties of these complexes is that they are π-conjugated. The (*para*-$HSC_6H_4)_3SnX$ compound may be of great importance, especially when the X group is a halide, because it provides opportunity for many possible reaction pathways after the thiols are anchored onto metal surfaces, for reactions with Grignard reagents, lithium reagents or any other carbanion. It should be noted that the *trans* complex has two possible modes of orientations; either the phosphine or the tin group can anchor to the metal surface (Fig. 10.1). If both groups can be anchored onto the metal surfaces, then it may be used to create a "nanowire" as shown in Fig. 10.1(c). It should also be interesting to see if these groups would complex in a uniform, alternating or random mode.

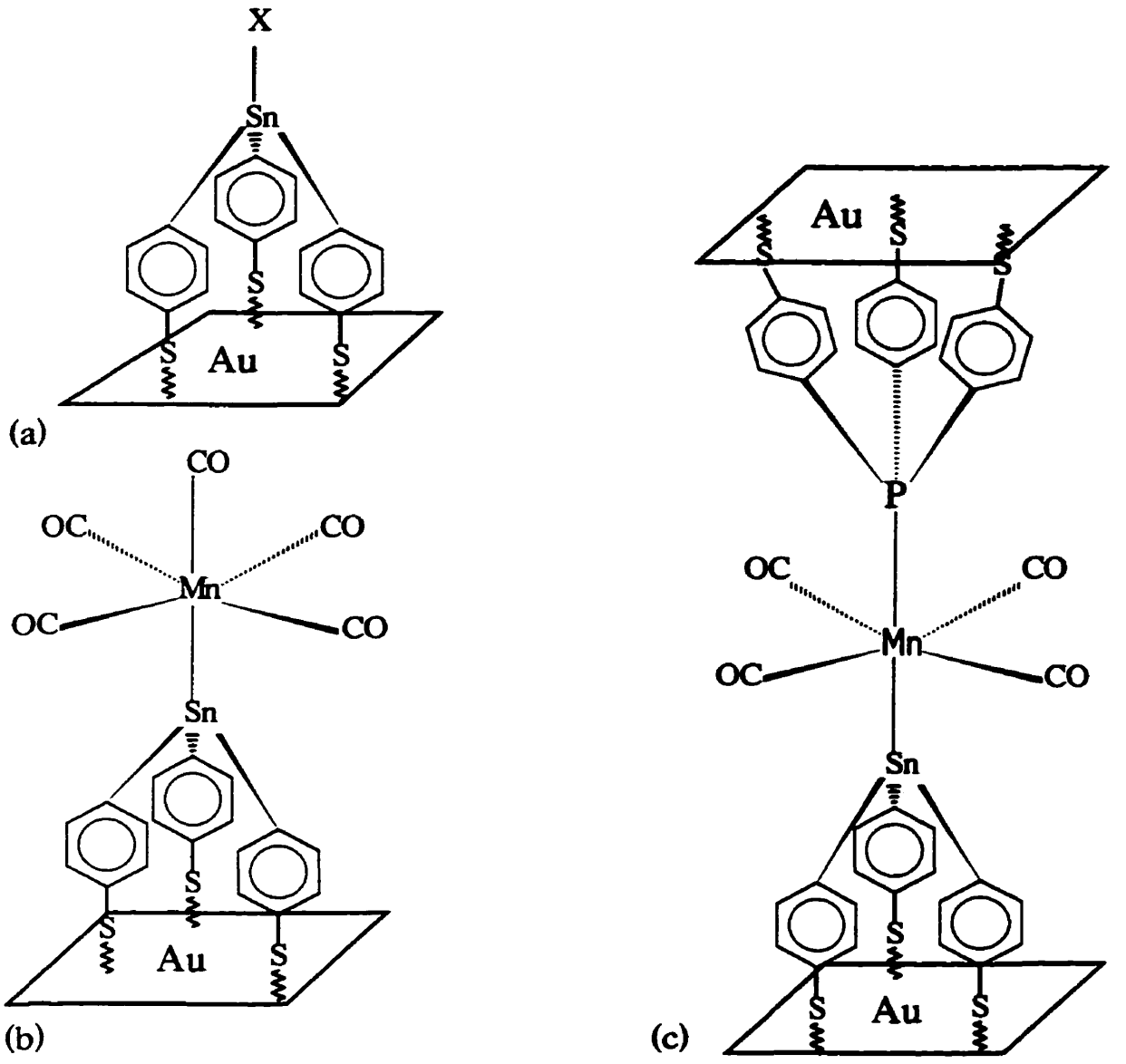

Figure 10.1. Possible schematic representations of tripod thiols interactions with gold, Au, surfaces.

(4) Solution and solid-state ^{31}P NMR spectroscopy were used to demonstrate structural changes in solution for Ni(II) bis(phosphine) complexes. Variable temperature ^{31}P NMR measurements of bis(tribenzylphosphine)nickel(II) halides in dichloromethane-d_2 and toluene-d_8 have revealed that there are two different isomers present in solution, whereas solid-state results indicate otherwise. The proposed mechanistic pathway and experimental data clearly indicated that the two solution structures are produced by dimerization of the complexes, where the halide nuclei act as the bridging ligands between the two nickel centres. However, the enthalpy, $\Delta H°$, the entropy, $\Delta S°$, and the Gibbs free energy, $\Delta G°$, for this conversion could not be determined due to significant temperature variation ($\pm$ 5 °C) on the Varian XL-300 instrument. These three quantities should be determined from more accurate measurements in order to determine the thermodynamic parameters. We believe that the same type of interaction is also responsible for the conversion of *trans*-$(Et_3P)_2PdX_2$ to the *cis*-isomers[4] and the *cis*-isomers of $(Cy_2PH)_2NiX_2$ (X = Cl, Br, I) to the trans complexes,[5] and should be studied for other nickel(II), palladium(II) and platinum(II) phosphine and halides complexes. We also believe that the unusually broad peaks observed in the solution ^{31}P NMR by Edwards *et at.*[6] for $[Bz(C_2H_5OC_2H_4)_2P]_2NiCl_2$ and $[Bz(C_2H_5OC_2H_4)_2P]_2$-Ni(Ph)Cl and Jarrett *et al.*[7] for (dppe)NiX_2 and (dppey)NiX_2 are due to dimerization.

References

(1) J. L. Slater, M. Pupp and R. K. Sheline, *J. Chem. Phys.*, **57**, 2105 (1972).

(2) S. J. Blunden, P. A. Cusack and R. Hill, *The Industrial Uses of Tin Chemicals*, Royal Society of Chemistry, Burlington House, London, England.

(3) J. Van Schotten, J. Knotnerus, H. Boer and PH. M. Duinker, *Rec. Trav. Chim.*, **77**, 346(1958).

(4) J. Chatt and R. G. Wilkins, *J. Chem. Soc.*, 273 (1952).

(5) R. A. Palmer and D. R. Whitcomb, *J. Magn. Reson.*, **39**, 371 (1979).

(6) S. J. Chadwell, S. M. Coles, P. G. Edwards, M. B Hursthouse and A. Imran, *Polyhedron*, **14**, 1057 (1995).

(7) P. S. Jarrett and P. J. Sadler, *Inorg. Chem.*, **30**, 2098 (1991).

APPENDIX I

Crystal Structures of some

Tertiary Phosphine Substituted

Benzyl(tetracarbonyl)manganese(I) Complexes

Structural Data for

cis-Benzyl(triphenylphosphine)(tetracarbonyl)manganese

cis-$(PhCH_2)(Ph_3P)Mn(CO)_4$

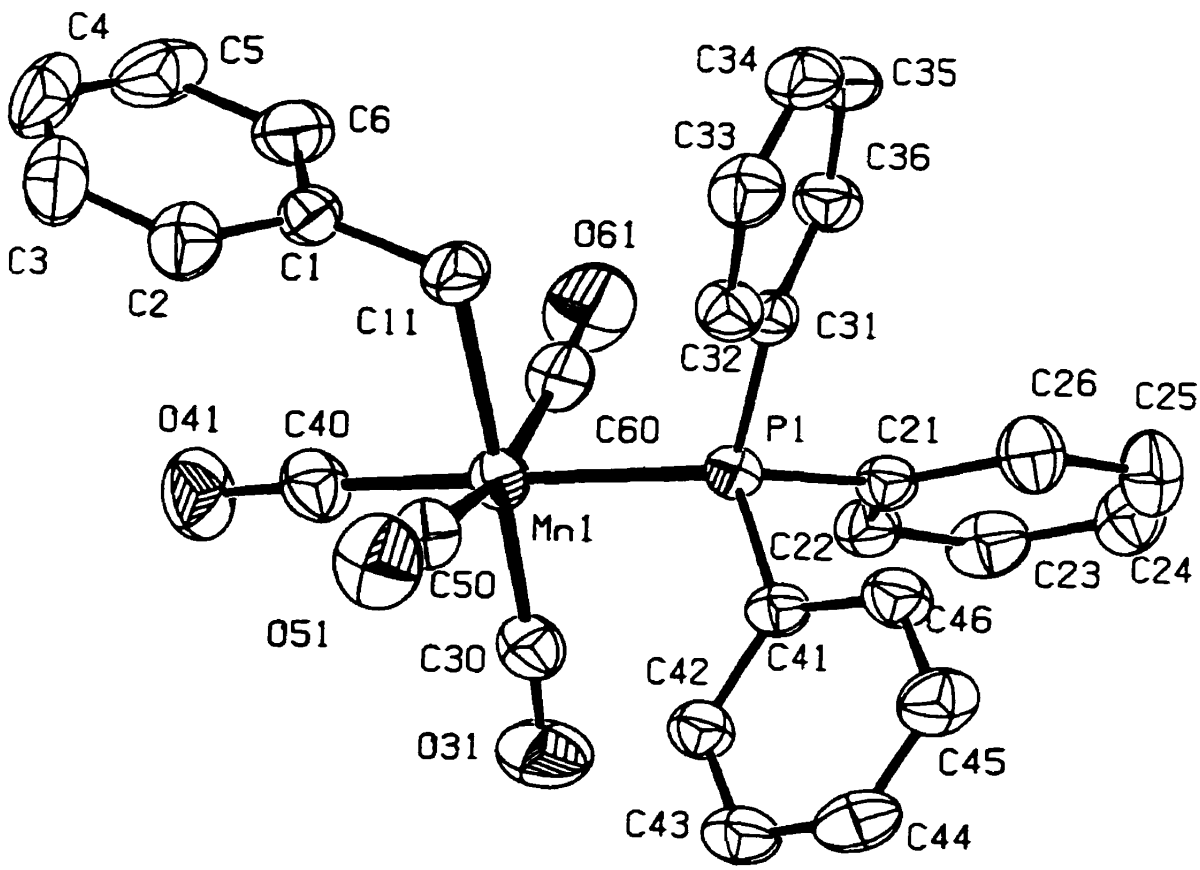

Crystal data for *cis*-$(PhCH_2)(Ph_3P)Mn(CO)_4$

Empirical Formula: C29 H22 O4 Mn P

Space group: Triclinic, P 1

Cell dimensions:

$a = 10.118\ (7)$Å

$b = 10.336\ (7)$Å

$c = 14.424\ (14)$Å

$\alpha = 71.63\ (6)°$

$\beta = 70.11\ (6)°$

$\gamma = 64.98\ (5)°$

Volume = 1259 (2)Å^3

FW = 520.38

Z = 2

$D_{calc} = 1.373$ g / cm^3

F(000) = 536

Mo Kα radiation

$\lambda = 0.70930$ Å

Cell parameters from 25 reflections

$2\theta = 37 - 45°$

$\mu = 0.621$ mm^{-1}

T = 295 (2) °K

Pale yellow block

0.50 × 0.40 × 0.25 mm

Data collection

Rigaku AFC –6S diffractometer

ω / 2θ scans

Absorption correction: *none*

$T_{min} = 1.0$, $T_{max} = 1.0$

3519 measured reflections

3296 independent reflections

2773 observed reflections [$I > 2\sigma(I)$]

$R_{int} = 0.014$

$\theta_{max} = 22.5°$

$h = -9 \rightarrow 10$

$k = 0 \rightarrow 11$

$l = -14 \rightarrow 15$

standard intensities show no variation over the course of collection.

Structure was solved by direct methods followed by a difference map.

Refinement

Refinement on F^2	317 parameters
$R(F^2 > 2\sigma(F^2)) = 0.0391$	H atoms riding,
$wR(F^2) = 0.0749$	C–H = 0.93 Å
GoF = 1.129	$(\Delta/\sigma) = -0.003$
57 atoms	$\Delta\rho_{max} = 0.253$ e/Å^3
3296 reflections	$\Delta\rho_{min} = -0.179$ e/Å^3

where

$$R = \Sigma(Fo-Fc) / \Sigma Fo$$

$$wR = [\Sigma(w(Fo^2-Fc^2)^2) / \Sigma[w(Fo^2)^2]]^{1/2}$$

$$GoF = [\Sigma(w(Fo^2-Fc^2)^2) / (\text{No. of refins - No. of params.})]^{1/2}$$

Table A1.1: Fractional atomic coordinates and equivalent isotropic displacement parameters (10^2 Å) for *cis*-$(Ph_2CH_2)(Ph_3P)Mn(CO)_4$.

	x	y	z	U_{eq}
Mn(1)	0.42672(4)	0.78957(4)	0.19517(3)	4.20(2)
P(1)	0.60335(6)	0.55217(6)	0.21374(4)	3.63(2)
O(31)	0.6617(3)	0.9188(2)	0.0930(2)	8.20(6)
O(41)	0.2087(3)	1.0910(2)	0.1683(2)	8.73(7)
O(51)	0.3816(3)	0.7472(2)	0.0158(2)	8.68(7)
O(61)	0.3834(2)	0.8049(3)	0.4054(2)	8.77(7)
C(30)	0.5733(3)	0.8645(3)	0.1334(2)	5.28(7)
C(40)	0.2902(3)	0.9733(3)	0.1792(2)	5.70(7)
C(50)	0.4033(3)	0.7631(3)	0.0830(2)	5.50(7)
C(60)	0.4059(3)	0.7969(3)	0.3242(2)	5.37(7)
C(21)	0.7360(2)	0.5091(2)	0.2890(2)	4.00(6)
C(22)	0.7576(3)	0.6182(3)	0.3119(2)	4.58(6)
C(23)	0.8653(3)	0.5855(3)	0.3619(2)	5.53(7)
C(24)	0.9545(3)	0.4436(3)	0.3891(2)	6.39(8)
C(25)	0.9350(3)	0.3339(3)	0.3670(2)	6.86(8)
C(26)	0.8260(3)	0.3662(3)	0.3187(2)	5.63(7)
C(41)	0.7326(2)	0.4918(2)	0.0979(2)	3.96(5)
C(42)	0.7574(3)	0.5906(3)	0.0091(2)	4.95(6)
C(43)	0.8614(3)	0.5439(3)	-0.0755(2)	5.84(7)
C(44)	0.9414(3)	0.3995(3)	-0.0731(2)	6.12(7)
C(45)	0.9185(3)	0.2993(3)	0.0139(2)	6.06(7)
C(46)	0.8147(3)	0.3454(3)	0.0985(2)	5.14(6)
C(31)	0.5190(2)	0.4120(2)	0.2723(2)	3.71(5)
C(32)	0.4767(3)	0.3603(3)	0.2139(2)	5.00(6)
C(33)	0.4026(3)	0.2622(3)	0.2579(2)	6.40(8)
C(34)	0.3705(3)	0.2148(3)	0.3603(2)	6.67(8)
C(35)	0.4096(3)	0.2665(3)	0.4191(2)	6.18(8)
C(36)	0.4836(3)	0.3647(3)	0.3761(2)	4.92(6)
C(11)	0.2424(3)	0.7026(3)	0.2710(2)	5.41(7)
C(1)	0.0887(3)	0.8148(2)	0.2866(2)	4.71(6)
C(2)	0.0079(3)	0.8688(3)	0.2141(2)	6.49(8)
C(3)	-0.1375(4)	0.9645(3)	0.2304(3)	8.36(10)
C(4)	-0.2044(4)	1.0097(3)	0.3191(4)	9.23(13)
C(5)	-0.1272(4)	0.9644(3)	0.3911(3)	8.69(11)
C(6)	0.0199(3)	0.8659(3)	0.3751(2)	6.46(8)

Table A1.2: Bond lengths (Å) and angles (in degrees) for *cis*-$(Ph_2CH_2)(Ph_3P)Mn(CO)_4$.

Mn(1)-C(30)	1.798(3)	Mn(1)-C(40)	1.814(3)
Mn(1)-C(60)	1.823(3)	Mn(1)-C(50)	1.828(3)
Mn(1)-C(11)	2.212(3)	Mn(1)-P(1)	2.343(2)
P(1)-C(31)	1.823(3)	P(1)-C(21)	1.833(3)
P(1)-C(41)	1.836(3)	O(31)-C(30)	1.148(3)
O(41)-C(40)	1.142(3)	O(51)-C(50)	1.136(3)
O(61)-C(60)	1.137(3)	C(21)-C(26)	1.386(3)
C(21)-C(22)	1.387(3)	C(22)-C(23)	1.375(4)
C(23)-C(24)	1.371(4)	C(24)-C(25)	1.372(4)
C(25)-C(26)	1.371(4)	C(41)-C(46)	1.383(3)
C(41)-C(42)	1.386(3)	C(42)-C(43)	1.378(4)
C(43)-C(44)	1.360(4)	C(44)-C(45)	1.374(4)
C(45)-C(46)	1.374(4)	C(31)-C(32)	1.379(3)
C(31)-C(36)	1.390(3)	C(32)-C(33)	1.380(4)
C(33)-C(34)	1.372(4)	C(34)-C(35)	1.360(4)
C(35)-C(36)	1.380(4)	C(11)-C(1)	1.488(3)
C(1)-C(2)	1.379(4)	C(1)-C(6)	1.380(4)
C(2)-C(3)	1.370(4)	C(3)-C(4)	1.355(5)
C(4)-C(5)	1.358(5)	C(5)-C(6)	1.392(4)
C(30)-Mn(1)-C(40)	88.61(14)	C(30)-Mn(1)-C(60)	98.74(13)
C(40)-Mn(1)-C(60)	89.28(14)	C(30)-Mn(1)-C(50)	97.57(13)
C(40)-Mn(1)-C(50)	90.32(14)	C(60)-Mn(1)-C(50)	163.67(12)
C(30)-Mn(1)-C(11)	178.65(10)	C(40)-Mn(1)-C(11)	90.04(12)
C(60)-Mn(1)-C(11)	81.15(12)	C(50)-Mn(1)-C(11)	82.53(13)
C(30)-Mn(1)-P(1)	91.29(11)	C(40)-Mn(1)-P(1)	179.27(9)
C(60)-Mn(1)-P(1)	91.45(11)	C(50)-Mn(1)-P(1)	88.98(11)
C(11)-Mn(1)-P(1)	90.06(9)	C(31)-P(1)-C(21)	103.64(12)
C(31)-P(1)-C(41)	102.77(12)	C(21)-P(1)-C(41)	101.00(12)
C(31)-P(1)-Mn(1)	113.56(9)	C(21)-P(1)-Mn(1)	117.13(9)
C(41)-P(1)-Mn(1)	116.72(10)	O(31)-C(30)-Mn(1)	176.7(2)
O(41)-C(40)-Mn(1)	177.3(2)	O(51)-C(50)-Mn(1)	176.6(3)
O(61)-C(60)-Mn(1)	175.7(2)	C(26)-C(21)-C(22)	117.7(2)
C(26)-C(21)-P(1)	120.8(2)	C(22)-C(21)-P(1)	121.3(2)
C(23)-C(22)-C(21)	121.0(2)	C(24)-C(23)-C(22)	120.2(2)
C(23)-C(24)-C(25)	119.7(3)	C(26)-C(25)-C(24)	120.1(3)
C(25)-C(26)-C(21)	121.3(3)	C(46)-C(41)-C(42)	117.9(2)
C(46)-C(41)-P(1)	120.5(2)	C(42)-C(41)-P(1)	121.5(2)
C(43)-C(42)-C(41)	120.8(2)	C(44)-C(43)-C(42)	120.3(3)
C(43)-C(44)-C(45)	120.0(3)	C(44)-C(45)-C(46)	119.8(3)
C(45)-C(46)-C(41)	121.1(2)	C(32)-C(31)-C(36)	118.5(2)
C(32)-C(31)-P(1)	119.8(2)	C(36)-C(31)-P(1)	121.5(2)
C(31)-C(32)-C(33)	120.5(2)	C(34)-C(33)-C(32)	120.3(3)
C(35)-C(34)-C(33)	119.9(3)	C(34)-C(35)-C(36)	120.4(3)
C(35)-C(36)-C(31)	120.3(2)	C(1)-C(11)-Mn(1)	115.1(2)
C(2)-C(1)-C(6)	117.4(3)	C(2)-C(1)-C(11)	121.3(3)
C(6)-C(1)-C(11)	121.3(3)	C(3)-C(2)-C(1)	121.8(3)
C(4)-C(3)-C(2)	119.8(3)	C(3)-C(4)-C(5)	120.5(3)
C(4)-C(5)-C(6)	119.6(3)	C(1)-C(6)-C(5)	120.8(3)

Table A1.3: Torsion angles (in degrees) for *cis*-$(Ph_2CH_2)(Ph_3P)Mn(CO)_4$.

C(30)-Mn(1)-P(1)-C(31)	-177.73(11)	C(40)-Mn(1)-P(1)-C(31)	-96(7)
C(60)-Mn(1)-P(1)-C(31)	83.49(13)	C(50)-Mn(1)-P(1)-C(31)	-80.19(13)
C(11)-Mn(1)-P(1)-C(31)	2.34(11)	C(30)-Mn(1)-P(1)-C(21)	61.43(13)
C(40)-Mn(1)-P(1)-C(21)	143(7)	C(60)-Mn(1)-P(1)-C(21)	-37.35(12)
C(50)-Mn(1)-P(1)-C(21)	158.98(12)	C(11)-Mn(1)-P(1)-C(21)	-118.50(12)
C(30)-Mn(1)-P(1)-C(41)	-58.43(13)	C(40)-Mn(1)-P(1)-C(41)	24(7)
C(60)-Mn(1)-P(1)-C(41)	-157.21(12)	C(50)-Mn(1)-P(1)-C(41)	39.11(13)
C(11)-Mn(1)-P(1)-C(41)	121.64(12)	C(40)-Mn(1)-C(30)-O(31)	-6(4)
C(60)-Mn(1)-C(30)-O(31)	-95(4)	C(50)-Mn(1)-C(30)-O(31)	85(4)
C(11)-Mn(1)-C(30)-O(31)	-9(8)	P(1)-Mn(1)-C(30)-O(31)	174(4)
C(30)-Mn(1)-C(40)-O(41)	-16(5)	C(60)-Mn(1)-C(40)-O(41)	82(5)
C(50)-Mn(1)-C(40)-O(41)	-114(5)	C(11)-Mn(1)-C(40)-O(41)	164(5)
P(1)-Mn(1)-C(40)-O(41)	-98(8)	C(30)-Mn(1)-C(50)-O(51)	-154(4)
C(40)-Mn(1)-C(50)-O(51)	-66(4)	C(60)-Mn(1)-C(50)-O(51)	23(4)
C(11)-Mn(1)-C(50)-O(51)	24(4)	P(1)-Mn(1)-C(50)-O(51)	115(4)
C(30)-Mn(1)-C(60)-O(61)	135(3)	C(40)-Mn(1)-C(60)-O(61)	47(3)
C(50)-Mn(1)-C(60)-O(61)	-42(3)	C(11)-Mn(1)-C(60)-O(61)	-44(3)
P(1)-Mn(1)-C(60)-O(61)	-133(3)	C(31)-P(1)-C(21)-C(26)	42.6(2)
C(41)-P(1)-C(21)-C(26)	-63.6(2)	Mn(1)-P(1)-C(21)-C(26)	168.5(2)
C(31)-P(1)-C(21)-C(22)	-142.2(2)	C(41)-P(1)-C(21)-C(22)	111.6(2)
Mn(1)-P(1)-C(21)-C(22)	-16.3(2)	C(26)-C(21)-C(22)-C(23)	0.3(3)
P(1)-C(21)-C(22)-C(23)	-175.1(2)	C(21)-C(22)-C(23)-C(24)	0.7(4)
C(22)-C(23)-C(24)-C(25)	-0.6(4)	C(23)-C(24)-C(25)-C(26)	-0.6(4)
C(24)-C(25)-C(26)-C(21)	1.6(4)	C(22)-C(21)-C(26)-C(25)	-1.4(4)
P(1)-C(21)-C(26)-C(25)	173.9(2)	C(31)-P(1)-C(41)-C(46)	-39.4(2)
C(21)-P(1)-C(41)-C(46)	67.5(2)	Mn(1)-P(1)-C(41)-C(46)	-164.3(2)
C(31)-P(1)-C(41)-C(42)	144.3(2)	C(21)-P(1)-C(41)-C(42)	-108.8(2)
Mn(1)-P(1)-C(41)-C(42)	19.4(2)	C(46)-C(41)-C(42)-C(43)	-0.3(4)
P(1)-C(41)-C(42)-C(43)	176.1(2)	C(41)-C(42)-C(43)-C(44)	0.0(4)
C(42)-C(43)-C(44)-C(45)	0.2(4)	C(43)-C(44)-C(45)-C(46)	-0.1(4)
C(44)-C(45)-C(46)-C(41)	-0.2(4)	C(42)-C(41)-C(46)-C(45)	0.4(4)
P(1)-C(41)-C(46)-C(45)	-176.0(2)	C(21)-P(1)-C(31)-C(32)	-146.9(2)
C(41)-P(1)-C(31)-C(32)	-42.0(2)	Mn(1)-P(1)-C(31)-C(32)	85.0(2)
C(21)-P(1)-C(31)-C(36)	39.0(2)	C(41)-P(1)-C(31)-C(36)	143.8(2)
Mn(1)-P(1)-C(31)-C(36)	-89.2(2)	C(36)-C(31)-C(32)-C(33)	-0.9(4)
P(1)-C(31)-C(32)-C(33)	-175.2(2)	C(31)-C(32)-C(33)-C(34)	-0.1(4)
C(32)-C(33)-C(34)-C(35)	1.0(4)	C(33)-C(34)-C(35)-C(36)	-1.0(4)
C(34)-C(35)-C(36)-C(31)	0.0(4)	C(32)-C(31)-C(36)-C(35)	0.9(3)
P(1)-C(31)-C(36)-C(35)	175.1(2)	C(30)-Mn(1)-C(11)-C(1)	0(5)
C(40)-Mn(1)-C(11)-C(1)	-3.7(2)	C(60)-Mn(1)-C(11)-C(1)	85.6(2)
C(50)-Mn(1)-C(11)-C(1)	-94.0(2)	P(1)-Mn(1)-C(11)-C(1)	177.0(2)
Mn(1)-C(11)-C(1)-C(2)	88.2(3)	Mn(1)-C(11)-C(1)-C(6)	-93.6(3)
C(6)-C(1)-C(2)-C(3)	-2.9(4)	C(11)-C(1)-C(2)-C(3)	175.4(2)
C(1)-C(2)-C(3)-C(4)	0.9(5)	C(2)-C(3)-C(4)-C(5)	2.0(5)
C(3)-C(4)-C(5)-C(6)	-2.7(5)	C(2)-C(1)-C(6)-C(5)	2.1(4)
C(11)-C(1)-C(6)-C(5)	-176.2(2)	C(4)-C(5)-C(6)-C(1)	0.6(5)

Table A1.4: Anisotropic thermal factors (10^2 Å^2) for *cis*-$(Ph_2CH_2)(Ph_3P)Mn(CO)_4$.

	U_{11}	U_{22}	U_{33}	U_{12}	U_{13}	U_{23}
Mn(1)	4.52(2)	3.73(2)	4.36(2)	-0.74(2)	-1.34(2)	-1.30(2)
P(1)	3.94(4)	3.60(3)	3.40(3)	-0.67(3)	-0.78(3)	-1.49(3)
O(31)	9.1(2)	8.1(2)	8.6(2)	-0.32(12)	-1.36(12)	-5.67(13)
O(41)	8.5(2)	3.95(12)	12.4(2)	-0.40(11)	-3.62(14)	-0.93(11)
O(51)	9.6(2)	10.6(2)	7.4(2)	-3.19(13)	-3.81(13)	-2.73(14)
O(61)	8.2(2)	12.1(2)	5.75(13)	-4.04(13)	-1.59(12)	-1.85(14)
C(30)	6.0(2)	4.7(2)	5.4(2)	-0.44(12)	-1.83(14)	-2.21(14)
C(40)	6.5(2)	4.1(2)	6.7(2)	-0.46(13)	-2.3(2)	-1.98(14)
C(50)	5.5(2)	5.1(2)	5.7(2)	-0.97(13)	-1.79(14)	-1.39(13)
C(60)	4.8(2)	5.1(2)	5.9(2)	-1.48(13)	-1.37(14)	-1.16(13)
C(21)	4.05(13)	4.43(14)	3.46(13)	-0.71(10)	-0.65(11)	-1.71(11)
C(22)	4.52(14)	4.9(2)	4.50(14)	-0.82(11)	-0.97(12)	-1.99(12)
C(23)	5.6(2)	7.1(2)	5.4(2)	-1.91(14)	-1.24(13)	-3.2(2)
C(24)	5.4(2)	8.7(2)	5.7(2)	-1.7(2)	-2.35(14)	-2.1(2)
C(25)	6.8(2)	6.5(2)	7.1(2)	-1.3(2)	-3.4(2)	-0.7(2)
C(26)	6.3(2)	5.0(2)	6.1(2)	-1.26(13)	-2.82(14)	-1.31(14)
C(41)	4.04(13)	4.66(14)	3.49(13)	-1.01(11)	-0.55(10)	-1.96(11)
C(42)	5.2(2)	5.0(2)	4.2(2)	-0.72(12)	-0.75(12)	-1.94(12)
C(43)	6.4(2)	7.2(2)	3.9(2)	-0.66(13)	-0.31(13)	-3.3(2)
C(44)	5.6(2)	8.2(2)	5.0(2)	-2.9(2)	0.69(13)	-3.2(2)
C(45)	5.9(2)	5.8(2)	6.0(2)	-2.6(2)	0.10(14)	-1.68(14)
C(46)	5.7(2)	4.7(2)	4.18(14)	-0.78(12)	-0.53(12)	-1.72(13)
C(31)	3.29(12)	3.47(12)	4.01(13)	-1.00(10)	-0.60(10)	-0.92(10)
C(32)	5.4(2)	5.1(2)	5.1(2)	-0.54(12)	-1.54(13)	-2.57(13)
C(33)	5.8(2)	6.1(2)	8.7(2)	-1.4(2)	-2.4(2)	-3.0(2)
C(34)	5.1(2)	5.7(2)	8.5(2)	-0.3(2)	-0.5(2)	-2.97(14)
C(35)	5.4(2)	5.8(2)	5.2(2)	-0.15(13)	0.67(13)	-2.16(14)
C(36)	5.2(2)	4.60(14)	4.3(2)	-0.91(11)	-0.49(12)	-1.74(12)
C(11)	4.4(2)	4.4(2)	6.7(2)	-0.87(12)	-0.77(13)	-1.48(12)
C(1)	4.22(14)	3.51(13)	6.0(2)	-0.72(12)	-0.97(13)	-1.33(11)
C(2)	6.2(2)	5.7(2)	8.2(2)	-1.4(2)	-2.5(2)	-2.1(2)
C(3)	6.6(2)	5.4(2)	13.6(3)	0.0(2)	-5.0(2)	-1.8(2)
C(4)	4.4(2)	4.1(2)	16.9(4)	-1.6(2)	-1.5(2)	-0.6(2)
C(5)	6.9(2)	6.5(2)	10.3(3)	-3.5(2)	2.6(2)	-2.6(2)
C(6)	6.1(2)	6.2(2)	6.3(2)	-1.3(2)	-0.2(2)	-2.4(2)

Structural Data for *cis*-Benzyl-

(*tri*-*p*-tolylphosphine)(tetracarbonyl)manganese(I)

cis-$(PhCH_2)[(p\text{-}CH_3C_6H_4)_3P]Mn(CO)_4$

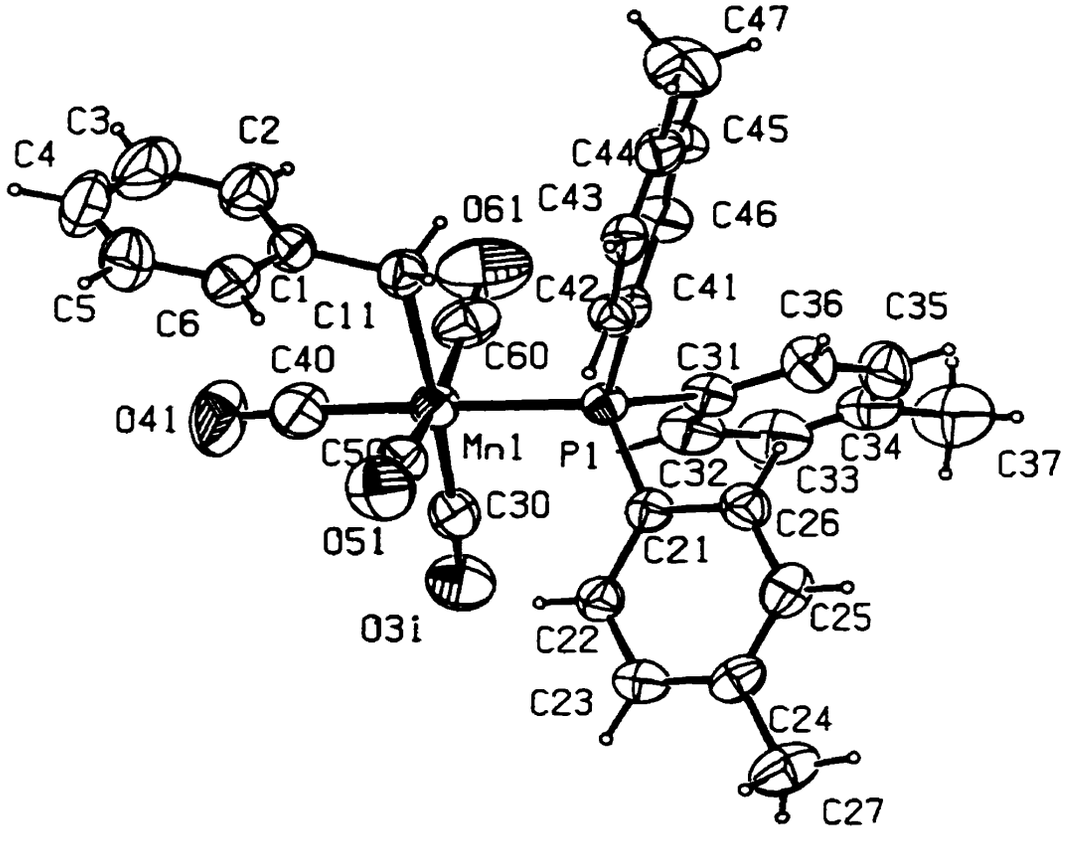

Crystal data for *cis*-$(PhCH_2)[(p\text{-}CH_3C_6H_4)_3P]Mn(CO)_4$

Empirical Formula: C32 H28 O4 Mn P

Space group: Triclinic, P 1

Cell dimensions:

a = 10.733 (2)Å

b = 10.992 (2)Å

c = 14.174 (2)Å

α = 96.71 (2)°

β = 93.05 (2)°

γ = 118.780 (10)°

Volume = 1444.1 (4)Å^3

FW = 562.45

Z = 2

D_{calc} = 1.294 g / cm^3

F(000) = 584

Mo Kα radiation

λ = 0.70930 Å

Cell parameters from 15 reflections

$2\theta = 27 - 33°$

μ = 0.546 mm^{-1}

T = 293 (2) °K

Colourless prism

0.46 × 0.35 × 0.12 mm

Data collection

Rigaku AFC –6S diffractometer

ω / 2θ scans

Absorption correction: *Psi scans*

T_{min} = 0.89, T_{max} = 1.0

10148 measured reflections

5074 independent reflections

3394 observed reflections [$I > 2\sigma(I)$]

R_{int} = 0.064

θ_{max} = 50.0°

h = -12 → 11

k = -13 → 13

l = -16 → 16

3 standard reflections were monitored every 200 reflections

Intensity decay: 0.64

Structure was solved by the direct methods followed by a difference map.

Refinement

Refinement on F^2	349 parameters
$R(F^2 > 2\sigma(F^2) = 0.0515$	H atoms riding,
$wR(F^2) = 0.1075$	C–H = 0.93 - 0.97 Å
GoF = 1.023	$(\Delta/\sigma) = 0.004$
66 atoms	$\Delta\rho_{max} = 0.241$ e/Å^3
5074 reflections	$\Delta\rho_{min} = -0.245$ e/Å^3

where

$R = \Sigma(Fo-Fc) / \Sigma Fo$

$wR = [\Sigma(w(Fo^2-Fc^2)^2) / \Sigma[w(Fo^2)^2]]^{1/2}$

$GoF = [\Sigma(w(Fo^2-Fc^2)^2) / (\text{No. of refins - No. of params.})]^{1/2}$

Table A1.5: Fractional atomic coordinates and equivalent isotropic displacement parameters (10^2 Å) for *cis*-$(Ph_2CH_2)[(p\text{-}CH_3C_6H_4)_3P]Mn(CO)_4$.

	x	y	z	U_{eq}
Mn(1)	0.07293(5)	0.33825(5)	0.29745(4)	4.23(2)
P(1)	0.29572(9)	0.53063(9)	0.28560(6)	3.27(2)
O(31)	-0.0500(3)	0.5148(3)	0.3721(2)	7.28(8)
O(41)	-0.2156(3)	0.0979(3)	0.3014(3)	10.80(13)
O(51)	0.0060(3)	0.3105(3)	0.0872(2)	7.54(9)
O(61)	0.1831(4)	0.3131(4)	0.4872(2)	10.29(12)
C(1)	0.0340(4)	0.0390(4)	0.2259(3)	4.76(9)
C(2)	-0.0013(4)	-0.0470(4)	0.2959(3)	6.60(11)
C(3)	-0.1092(6)	-0.1857(5)	0.2757(4)	8.5(2)
C(4)	-0.1850(5)	-0.2394(5)	0.1865(6)	9.7(2)
C(5)	-0.1538(5)	-0.1581(5)	0.1167(4)	8.7(2)
C(6)	-0.0441(4)	-0.0192(4)	0.1365(3)	6.22(11)
C(11)	0.1491(4)	0.1890(3)	0.2473(3)	4.83(9)
C(30)	0.0024(4)	0.4504(4)	0.3423(3)	4.99(9)
C(40)	-0.1029(5)	0.1878(4)	0.3009(3)	6.95(13)
C(50)	0.0301(4)	0.3241(4)	0.1680(3)	5.12(10)
C(60)	0.1409(5)	0.3258(4)	0.4158(3)	6.29(11)
C(21)	0.2947(3)	0.6536(3)	0.2089(2)	3.35(7)
C(22)	0.1729(3)	0.6637(3)	0.1873(2)	4.05(8)
C(23)	0.1778(4)	0.7686(4)	0.1405(2)	4.47(9)
C(24)	0.3031(4)	0.8682(3)	0.1140(2)	4.35(8)
C(25)	0.4249(4)	0.8582(4)	0.1340(2)	4.69(9)
C(26)	0.4216(4)	0.7524(3)	0.1808(2)	4.28(8)
C(27)	0.3074(5)	0.9858(4)	0.0651(3)	6.95(12)
C(31)	0.3972(3)	0.6552(3)	0.3947(2)	3.70(8)
C(32)	0.3268(4)	0.6742(4)	0.4690(2)	5.11(9)
C(33)	0.3996(5)	0.7828(5)	0.5457(3)	6.31(11)
C(34)	0.5442(5)	0.8726(4)	0.5522(3)	5.94(11)
C(35)	0.6152(4)	0.8523(4)	0.4795(3)	6.24(11)
C(36)	0.5431(4)	0.7461(4)	0.4013(3)	5.26(10)
C(37)	0.6222(6)	0.9903(5)	0.6371(3)	9.4(2)
C(41)	0.4195(3)	0.4782(3)	0.2371(2)	3.20(7)
C(42)	0.4172(3)	0.4480(3)	0.1383(2)	3.64(8)
C(43)	0.5035(3)	0.3976(3)	0.1022(2)	4.11(8)
C(44)	0.5956(4)	0.3773(3)	0.1611(3)	4.37(9)
C(45)	0.5948(4)	0.4032(4)	0.2587(3)	4.82(9)
C(46)	0.5074(3)	0.4519(3)	0.2966(2)	4.16(8)
C(47)	0.6971(4)	0.3311(5)	0.1222(3)	7.62(14)

Table A1.6: Bond lengths (Å) and angles (in degrees) for *cis*-$(Ph_2CH_2)[(p\text{-}CH_3C_6H_4)_3P]Mn(CO)_4$.

Mn(1)-C(30)	1.806(4)	Mn(1)-C(40)	1.823(4)
Mn(1)-C(50)	1.838(4)	Mn(1)-C(60)	1.840(5)
Mn(1)-C(11)	2.223(3)	Mn(1)-P(1)	2.3398(11)
P(1)-C(41)	1.820(3)	P(1)-C(31)	1.828(3)
P(1)-C(21)	1.835(3)	O(31)-C(30)	1.155(4)
O(41)-C(40)	1.137(4)	O(51)-C(50)	1.137(4)
O(61)-C(60)	1.137(5)	C(1)-C(6)	1.378(5)
C(1)-C(2)	1.391(5)	C(1)-C(11)	1.490(5)
C(2)-C(3)	1.382(6)	C(3)-C(4)	1.365(7)
C(4)-C(5)	1.358(7)	C(5)-C(6)	1.389(6)
C(21)-C(22)	1.385(4)	C(21)-C(26)	1.388(4)
C(22)-C(23)	1.377(4)	C(23)-C(24)	1.371(5)
C(24)-C(25)	1.381(5)	C(24)-C(27)	1.519(5)
C(25)-C(26)	1.392(5)	C(31)-C(32)	1.382(4)
C(31)-C(36)	1.384(5)	C(32)-C(33)	1.388(5)
C(33)-C(34)	1.371(6)	C(34)-C(35)	1.373(5)
C(34)-C(37)	1.519(5)	C(35)-C(36)	1.388(5)
C(41)-C(46)	1.385(4)	C(41)-C(42)	1.396(4)
C(42)-C(43)	1.380(4)	C(43)-C(44)	1.376(5)
C(44)-C(45)	1.380(5)	C(44)-C(47)	1.511(5)
C(45)-C(46)	1.387(4)		

C(30)-Mn(1)-C(40)	87.9(2)	C(30)-Mn(1)-C(50)	100.0(2)
C(40)-Mn(1)-C(50)	90.2(2)	C(30)-Mn(1)-C(60)	95.6(2)
C(40)-Mn(1)-C(60)	92.0(2)	C(50)-Mn(1)-C(60)	164.3(2)
C(30)-Mn(1)-C(11)	176.10(14)	C(40)-Mn(1)-C(11)	88.7(2)
C(50)-Mn(1)-C(11)	81.8(2)	C(60)-Mn(1)-C(11)	82.6(2)
C(30)-Mn(1)-P(1)	92.43(11)	C(40)-Mn(1)-P(1)	177.4(2)
C(50)-Mn(1)-P(1)	87.24(12)	C(60)-Mn(1)-P(1)	90.49(14)
C(11)-Mn(1)-P(1)	91.08(9)	C(41)-P(1)-C(31)	104.52(14)
C(41)-P(1)-C(21)	103.91(14)	C(31)-P(1)-C(21)	99.46(14)
C(41)-P(1)-Mn(1)	112.68(10)	C(31)-P(1)-Mn(1)	118.06(11)
C(21)-P(1)-Mn(1)	116.31(11)	C(6)-C(1)-C(2)	117.4(4)
C(6)-C(1)-C(11)	121.3(3)	C(2)-C(1)-C(11)	121.4(4)
C(3)-C(2)-C(1)	121.1(4)	C(4)-C(3)-C(2)	119.9(5)
C(5)-C(4)-C(3)	120.5(5)	C(4)-C(5)-C(6)	119.6(5)
C(1)-C(6)-C(5)	121.5(4)	C(1)-C(11)-Mn(1)	114.2(2)
O(31)-C(30)-Mn(1)	175.8(3)	O(41)-C(40)-Mn(1)	176.4(4)
O(51)-C(50)-Mn(1)	176.5(3)	O(61)-C(60)-Mn(1)	177.1(4)
C(22)-C(21)-C(26)	117.6(3)	C(22)-C(21)-P(1)	121.7(2)
C(26)-C(21)-P(1)	120.2(2)	C(23)-C(22)-C(21)	121.2(3)
C(24)-C(23)-C(22)	121.7(3)	C(23)-C(24)-C(25)	117.6(3)
C(23)-C(24)-C(27)	121.0(3)	C(25)-C(24)-C(27)	121.4(3)
C(24)-C(25)-C(26)	121.4(3)	C(21)-C(26)-C(25)	120.5(3)
C(32)-C(31)-C(36)	117.4(3)	C(32)-C(31)-P(1)	120.3(3)
C(36)-C(31)-P(1)	121.8(2)	C(31)-C(32)-C(33)	120.9(4)
C(34)-C(33)-C(32)	121.6(4)	C(33)-C(34)-C(35)	117.7(3)
C(33)-C(34)-C(37)	120.8(4)	C(35)-C(34)-C(37)	121.5(4)
C(34)-C(35)-C(36)	121.3(4)	C(31)-C(36)-C(35)	121.1(3)
C(46)-C(41)-C(42)	117.9(3)	C(46)-C(41)-P(1)	120.9(2)

C(42)-C(41)-P(1)	120.8(2)	C(43)-C(42)-C(41)	120.5(3)
C(44)-C(43)-C(42)	121.8(3)	C(43)-C(44)-C(45)	117.7(3)
C(43)-C(44)-C(47)	122.1(3)	C(45)-C(44)-C(47)	120.2(3)
C(44)-C(45)-C(46)	121.5(3)	C(41)-C(46)-C(45)	120.6(3)

Table A1.7: Torsion angles (in degrees) for *cis*-$(Ph_2CH_2)[(p\text{-}CH_3C_6H_4)_3P]Mn(CO)_4$.

C(30)-Mn(1)-P(1)-C(41)	-178.2(2)	C(31)-P(1)-C(21)-C(22)	-105.5(3)
C(40)-Mn(1)-P(1)-C(41)	-81(3)	Mn(1)-P(1)-C(21)-C(22)	22.4(3)
C(50)-Mn(1)-P(1)-C(41)	-78.2(2)	C(41)-P(1)-C(21)-C(26)	-41.6(3)
C(60)-Mn(1)-P(1)-C(41)	86.2(2)	C(31)-P(1)-C(21)-C(26)	66.1(3)
C(11)-Mn(1)-P(1)-C(41)	3.5(2)	Mn(1)-P(1)-C(21)-C(26)	-166.0(2)
C(30)-Mn(1)-P(1)-C(31)	59.8(2)	C(26)-C(21)-C(22)-C(23)	-0.5(5)
C(40)-Mn(1)-P(1)-C(31)	157(3)	P(1)-C(21)-C(22)-C(23)	171.3(2)
C(50)-Mn(1)-P(1)-C(31)	159.7(2)	C(21)-C(22)-C(23)-C(24)	-0.7(5)
C(60)-Mn(1)-P(1)-C(31)	-35.9(2)	C(22)-C(23)-C(24)-C(25)	1.5(5)
C(11)-Mn(1)-P(1)-C(31)	-118.5(2)	C(22)-C(23)-C(24)-C(27)	-178.1(3)
C(30)-Mn(1)-P(1)-C(21)	-58.3(2)	C(23)-C(24)-C(25)-C(26)	-1.1(5)
C(40)-Mn(1)-P(1)-C(21)	39(3)	C(27)-C(24)-C(25)-C(26)	178.5(3)
C(50)-Mn(1)-P(1)-C(21)	41.6(2)	C(22)-C(21)-C(26)-C(25)	0.9(5)
C(60)-Mn(1)-P(1)-C(21)	-154.0(2)	P(1)-C(21)-C(26)-C(25)	-171.1(2)
C(11)-Mn(1)-P(1)-C(21)	123.4(2)	C(24)-C(25)-C(26)-C(21)	0.0(5)
C(6)-C(1)-C(2)-C(3)	0.9(6)	C(41)-P(1)-C(31)-C(32)	-154.0(3)
C(11)-C(1)-C(2)-C(3)	179.3(4)	C(21)-P(1)-C(31)-C(32)	98.9(3)
C(1)-C(2)-C(3)-C(4)	-1.3(7)	Mn(1)-P(1)-C(31)-C(32)	-27.9(3)
C(2)-C(3)-C(4)-C(5)	0.9(8)	C(41)-P(1)-C(31)-C(36)	34.7(3)
C(3)-C(4)-C(5)-C(6)	-0.1(8)	C(21)-P(1)-C(31)-C(36)	-72.5(3)
C(2)-C(1)-C(6)-C(5)	0.0(6)	Mn(1)-P(1)-C(31)-C(36)	160.8(3)
C(11)-C(1)-C(6)-C(5)	-178.5(4)	C(36)-C(31)-C(32)-C(33)	1.6(5)
C(4)-C(5)-C(6)-C(1)	-0.4(7)	P(1)-C(31)-C(32)-C(33)	-170.1(3)
C(6)-C(1)-C(11)-Mn(1)	88.3(4)	C(31)-C(32)-C(33)-C(34)	-1.8(6)
C(2)-C(1)-C(11)-Mn(1)	-90.1(4)	C(32)-C(33)-C(34)-C(35)	0.4(6)
C(30)-Mn(1)-C(11)-C(1)	35(2)	C(32)-C(33)-C(34)-C(37)	-179.6(4)
C(40)-Mn(1)-C(11)-C(1)	6.8(3)	C(33)-C(34)-C(35)-C(36)	1.1(6)
C(50)-Mn(1)-C(11)-C(1)	-83.5(3)	C(37)-C(34)-C(35)-C(36)	-178.9(4)
C(60)-Mn(1)-C(11)-C(1)	99.0(3)	C(32)-C(31)-C(36)-C(35)	-0.2(5)
P(1)-Mn(1)-C(11)-C(1)	-170.6(3)	P(1)-C(31)-C(36)-C(35)	171.4(3)
C(40)-Mn(1)-C(30)-O(31)	11(5)	C(34)-C(35)-C(36)-C(31)	-1.2(6)
C(50)-Mn(1)-C(30)-O(31)	101(5)	C(31)-P(1)-C(41)-C(46)	41.2(3)
C(60)-Mn(1)-C(30)-O(31)	-81(5)	C(21)-P(1)-C(41)-C(46)	145.0(3)
C(11)-Mn(1)-C(30)-O(31)	-17(7)	Mn(1)-P(1)-C(41)-C(46)	-88.2(3)
P(1)-Mn(1)-C(30)-O(31)	-172(5)	C(31)-P(1)-C(41)-C(42)	-146.0(2)
C(30)-Mn(1)-C(40)-O(41)	40(7)	C(21)-P(1)-C(41)-C(42)	-42.2(3)
C(50)-Mn(1)-C(40)-O(41)	-60(7)	Mn(1)-P(1)-C(41)-C(42)	84.5(3)
C(60)-Mn(1)-C(40)-O(41)	135(7)	C(46)-C(41)-C(42)-C(43)	-1.9(4)
C(11)-Mn(1)-C(40)-O(41)	-142(7)	P(1)-C(41)-C(42)-C(43)	-174.8(2)
P(1)-Mn(1)-C(40)-O(41)	-58(8)	C(41)-C(42)-C(43)-C(44)	-1.0(5)
C(30)-Mn(1)-C(50)-O(51)	-174(6)	C(42)-C(43)-C(44)-C(45)	2.8(5)
C(40)-Mn(1)-C(50)-O(51)	-86(6)	C(42)-C(43)-C(44)-C(47)	-176.0(3)
C(60)-Mn(1)-C(50)-O(51)	12(6)	C(43)-C(44)-C(45)-C(46)	-1.8(5)
C(11)-Mn(1)-C(50)-O(51)	2(6)	C(47)-C(44)-C(45)-C(46)	177.0(3)
P(1)-Mn(1)-C(50)-O(51)	94(6)	C(42)-C(41)-C(46)-C(45)	2.9(5)
C(30)-Mn(1)-C(60)-O(61)	162(8)	P(1)-C(41)-C(46)-C(45)	175.8(3)
C(40)-Mn(1)-C(60)-O(61)	74(8)	C(44)-C(45)-C(46)-C(41)	-1.1(5)
C(50)-Mn(1)-C(60)-O(61)	-24(8)		
C(11)-Mn(1)-C(60)-O(61)	-14(8)		
P(1)-Mn(1)-C(60)-O(61)	-105(8)		
C(41)-P(1)-C(21)-C(22)	146.8(3)		

Table A1.8: Anisotropic thermal factors (10^2 Å^2) for *cis*-$(Ph_2CH_2)[(p\text{-}CH_3C_6H_4)_3P]$-$Mn(CO)_4$.

	U_{11}	U_{22}	U_{33}	U_{12}	U_{13}	U_{23}
Mn(1)	3.86(3)	3.99(3)	5.13(4)	1.01(3)	1.57(3)	1.99(3)
P(1)	3.30(5)	3.55(5)	3.14(5)	0.30(4)	0.67(4)	1.85(4)
O(31)	6.7(2)	8.2(2)	8.9(2)	0.6(2)	2.7(2)	5.2(2)
O(41)	5.8(2)	6.5(2)	19.3(4)	2.0(2)	6.2(2)	2.0(2)
O(51)	8.5(2)	8.1(2)	5.3(2)	-0.5(2)	-1.2(2)	4.1(2)
O(61)	15.1(3)	13.5(3)	6.4(2)	4.3(2)	2.2(2)	9.6(3)
C(1)	3.8(2)	4.0(2)	6.6(3)	0.9(2)	1.4(2)	1.9(2)
C(2)	6.5(3)	5.7(3)	8.0(3)	2.1(2)	2.1(2)	3.0(2)
C(3)	8.0(4)	6.2(3)	12.3(5)	4.6(3)	4.4(3)	3.4(3)
C(4)	5.9(3)	3.7(3)	17.9(7)	0.9(4)	2.5(4)	1.2(2)
C(5)	6.6(3)	5.3(3)	11.7(4)	-1.9(3)	-2.0(3)	2.0(3)
C(6)	6.5(3)	5.1(3)	7.2(3)	0.4(2)	0.2(2)	3.2(2)
C(11)	4.1(2)	3.9(2)	6.3(3)	0.8(2)	1.2(2)	1.8(2)
C(30)	4.1(2)	5.1(2)	6.0(3)	1.4(2)	1.6(2)	2.2(2)
C(40)	5.3(3)	5.6(3)	10.9(4)	1.6(2)	3.6(3)	3.1(2)
C(50)	4.0(2)	4.5(2)	6.6(3)	0.3(2)	0.1(2)	2.1(2)
C(60)	7.9(3)	6.3(3)	6.7(3)	2.3(2)	3.1(2)	4.6(2)
C(21)	3.8(2)	3.3(2)	3.1(2)	0.06(14)	0.72(14)	1.9(2)
C(22)	4.0(2)	3.9(2)	4.5(2)	1.0(2)	0.8(2)	1.9(2)
C(23)	5.0(2)	5.2(2)	4.1(2)	0.6(2)	0.3(2)	3.2(2)
C(24)	6.2(2)	3.8(2)	3.4(2)	0.3(2)	0.6(2)	2.8(2)
C(25)	5.3(2)	4.3(2)	4.3(2)	1.1(2)	1.6(2)	2.0(2)
C(26)	3.8(2)	4.6(2)	4.5(2)	0.6(2)	0.6(2)	2.2(2)
C(27)	9.1(3)	6.0(3)	7.4(3)	2.9(2)	2.3(3)	4.5(3)
C(31)	4.3(2)	4.5(2)	2.8(2)	0.1(2)	0.4(2)	2.7(2)
C(32)	5.8(2)	6.2(2)	4.2(2)	0.4(2)	0.9(2)	3.8(2)
C(33)	9.0(3)	8.5(3)	3.4(2)	-0.7(2)	0.7(2)	6.2(3)
C(34)	8.7(3)	6.2(3)	4.1(2)	-1.5(2)	-1.9(2)	5.4(3)
C(35)	5.9(3)	5.8(3)	5.8(3)	-1.4(2)	-1.0(2)	2.6(2)
C(36)	5.1(2)	6.0(2)	4.3(2)	-0.8(2)	0.2(2)	2.8(2)
C(37)	13.9(5)	9.5(4)	5.5(3)	-3.8(3)	-3.3(3)	7.8(4)
C(41)	2.7(2)	2.8(2)	3.5(2)	0.21(14)	0.38(14)	1.01(14)
C(42)	3.5(2)	3.8(2)	3.5(2)	0.4(2)	0.1(2)	1.8(2)
C(43)	4.2(2)	3.7(2)	3.8(2)	-0.3(2)	0.9(2)	1.7(2)
C(44)	4.1(2)	3.6(2)	5.4(2)	-0.4(2)	0.8(2)	2.0(2)
C(45)	4.3(2)	5.4(2)	5.6(3)	0.9(2)	0.1(2)	3.2(2)
C(46)	4.6(2)	5.1(2)	3.2(2)	0.5(2)	0.5(2)	2.7(2)
C(47)	7.0(3)	9.3(3)	8.0(3)	-1.4(3)	1.4(2)	5.7(3)

Structural Data for *cis*-Benzyl-

(*tris*(*p*-florophenyl)phosphine)(tetracarbonyl)manganese(I)

cis-$(PhCH_2)[(p\text{-}FC_6H_4)_3P]Mn(CO)_4$

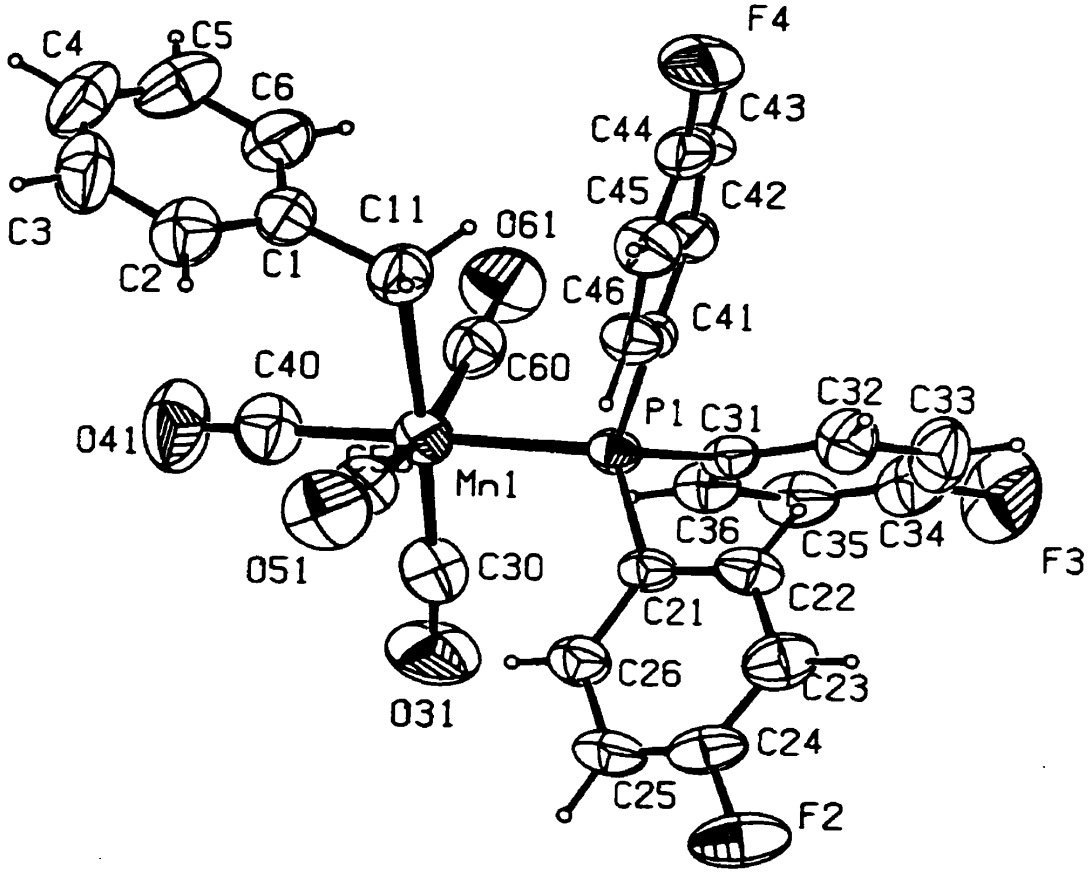

Crystal data for *cis*-$(PhCH_2)[(p\text{-}FC_6H_4)_3P]Mn(CO)_4$

Empirical Formula: C29 H19 O4 Mn P F3

Space group: Triclinic, P 1

Cell dimensions:

$a = 10.316$ (1)Å

$b = 10.344$ (2)Å

$c = 14.588$ (2)Å

$\alpha = 70.03$ (1)°

$\beta = 74.89$ (1)°

$\gamma = 64.04$ (1)°

Volume = 1304.1 (4)Å^3

FW = 574.37

Z = 2

$D_{calc} = 1.462$ g / cm^3

F(000) = 584

Cu Kα radiation

$\lambda = 1.54178$ Å

Cell parameters from 21 reflections

$2\theta = 45 - 60°$

$\mu = 5.185$ mm^{-1}

T = 295 (2) °K

Colourless prism

$0.37 \times 0.20 \times 0.05$ mm

Data collection

Rigaku AFC –6S diffractometer

ω / 2θ scans

Absorption correction: *Psi scans*

$T_{min} = 0.61$, $T_{max} = 1.0$

7198 measured reflections

3599 independent reflections

2672 observed reflections [$I > 2\sigma(I)$]

$R_{int} = 0.053$

$\theta_{max} = 60.0°$

$h = -12 \rightarrow 12$

$k = -16 \rightarrow 16$

$l = -12 \rightarrow 12$

3 standard reflections were monitored every 250 reflections

Intensity decay: 0.8

Structure was solved by the Patterson method.

Refinement

Refinement on F^2	344 parameters
$R(F^2 > 2\sigma(F^2)) = 0.045$	H atoms riding,
$wR(F^2) = 0.0884$	C–H = 0.93 - 0.97 Å
GoF = 1.036	$(\Delta/\sigma) = -0.001$
57 atoms	$\Delta\rho_{max} = 0.508$ e/Å^3
2672 reflections	$\Delta\rho_{min} = -0.377$ e/Å^3

where

$$R = \Sigma(Fo-Fc) / \Sigma Fo$$

$$wR = [\Sigma(w(Fo^2-Fc^2)^2) / \Sigma[w(Fo^2)^2]]^{1/2}$$

$$GoF = [\Sigma(w(Fo^2-Fc^2)^2) / (\text{No. of refins - No. of params.})]^{1/2}$$

Table A1.9: Fractional atomic coordinates and equivalent isotropic displacement parameters (10^2 Å) for *cis*-$(Ph_2CH_2)[(p\text{-}FC_6H_4)_3P]Mn(CO)_4$.

	x	y	z	U_{eq}
Mn(1)	0.49193(6)	0.07024(6)	0.20024(4)	4.24(2)
P(1)	0.30014(9)	0.29450(9)	0.21599(6)	3.48(2)
F(2)	0.0350(3)	0.7246(3)	-0.1401(2)	8.46(8)
F(3)	-0.2517(3)	0.2697(3)	0.4595(2)	10.48(10)
F(4)	0.5179(3)	0.6130(3)	0.3689(2)	8.07(8)
O(31)	0.3219(4)	-0.0092(4)	0.1094(2)	8.79(10)
O(41)	0.7288(3)	-0.2150(4)	0.1774(3)	9.86(11)
O(51)	0.6250(3)	0.2313(4)	0.0184(2)	8.47(10)
O(61)	0.4324(3)	-0.0718(4)	0.4126(2)	8.35(9)
C(1)	0.7776(4)	-0.0044(4)	0.2826(3)	4.88(9)
C(2)	0.8976(4)	-0.0197(5)	0.2118(3)	6.56(11)
C(3)	1.0329(5)	-0.1299(6)	0.2317(4)	7.87(14)
C(4)	1.0476(5)	-0.2274(5)	0.3217(5)	8.8(2)
C(5)	0.9316(6)	-0.2197(5)	0.3919(4)	8.5(2)
C(6)	0.7984(4)	-0.1087(5)	0.3736(3)	6.59(11)
C(11)	0.6337(4)	0.1181(4)	0.2643(3)	5.50(10)
C(30)	0.3831(4)	0.0249(4)	0.1456(3)	5.76(10)
C(40)	0.6395(5)	-0.1045(5)	0.1870(3)	6.21(11)
C(50)	0.5701(4)	0.1697(4)	0.0872(3)	5.30(10)
C(60)	0.4502(4)	-0.0184(4)	0.3300(3)	5.26(10)
C(21)	0.2256(3)	0.4276(4)	0.1032(2)	3.74(8)
C(22)	0.1356(4)	0.5745(4)	0.1035(3)	4.93(9)
C(23)	0.0722(4)	0.6748(4)	0.0208(3)	5.85(11)
C(24)	0.1003(4)	0.6263(4)	-0.0604(3)	5.48(10)
C(25)	0.1866(4)	0.4855(5)	-0.0645(3)	5.61(10)
C(26)	0.2508(4)	0.3845(4)	0.0186(3)	4.78(9)
C(31)	0.1345(3)	0.2829(4)	0.2975(2)	3.73(8)
C(32)	0.0297(4)	0.4048(4)	0.3281(3)	5.26(10)
C(33)	-0.1015(4)	0.4016(5)	0.3820(3)	6.99(12)
C(34)	-0.1242(4)	0.2738(5)	0.4054(3)	6.41(12)
C(35)	-0.0244(4)	0.1495(5)	0.3785(3)	5.63(10)
C(36)	0.1066(4)	0.1547(4)	0.3234(2)	4.74(9)
C(41)	0.3522(3)	0.4041(3)	0.2637(2)	3.35(8)
C(42)	0.3500(3)	0.3752(4)	0.3642(2)	3.99(8)
C(43)	0.4076(4)	0.4447(4)	0.3996(3)	4.86(9)
C(44)	0.4628(4)	0.5433(4)	0.3345(3)	4.97(9)
C(45)	0.4677(4)	0.5746(4)	0.2355(3)	5.30(10)
C(46)	0.4125(4)	0.5040(4)	0.2000(3)	4.42(8)

Table A1.10: Bond lengths (Å) and angles (in degrees) for *cis*-$(Ph_2CH_2)[(p\text{-}FC_6H_4)_3P]Mn(CO)_4$.

Mn(1)-C(30)	1.816(4)	Mn(1)-C(40)	1.816(4)
Mn(1)-C(50)	1.817(4)	Mn(1)-C(60)	1.829(4)
Mn(1)-C(11)	2.217(3)	Mn(1)-P(1)	2.3362(11)
P(1)-C(41)	1.824(3)	P(1)-C(31)	1.836(3)
P(1)-C(21)	1.839(3)	F(2)-C(24)	1.358(4)
F(3)-C(34)	1.356(4)	F(4)-C(44)	1.360(4)
O(31)-C(30)	1.140(4)	O(41)-C(40)	1.138(5)
O(51)-C(50)	1.148(4)	O(61)-C(60)	1.144(4)
C(1)-C(2)	1.378(5)	C(1)-C(6)	1.392(5)
C(1)-C(11)	1.487(5)	C(2)-C(3)	1.387(6)
C(3)-C(4)	1.352(7)	C(4)-C(5)	1.350(7)
C(5)-C(6)	1.371(6)	C(21)-C(26)	1.377(5)
C(21)-C(22)	1.392(5)	C(22)-C(23)	1.387(5)
C(23)-C(24)	1.355(5)	C(24)-C(25)	1.347(5)
C(25)-C(26)	1.395(5)	C(31)-C(32)	1.377(5)
C(31)-C(36)	1.385(4)	C(32)-C(33)	1.385(5)
C(33)-C(34)	1.357(6)	C(34)-C(35)	1.357(6)
C(35)-C(36)	1.394(5)	C(41)-C(46)	1.387(4)
C(41)-C(42)	1.388(4)	C(42)-C(43)	1.387(4)
C(43)-C(44)	1.353(5)	C(44)-C(45)	1.360(5)
C(45)-C(46)	1.379(4)		

C(30)-Mn(1)-C(40)	87.7(2)	C(30)-Mn(1)-C(50)	97.8(2)
C(40)-Mn(1)-C(50)	90.2(2)	C(30)-Mn(1)-C(60)	100.0(2)
C(40)-Mn(1)-C(60)	89.5(2)	C(50)-Mn(1)-C(60)	162.2(2)
C(30)-Mn(1)-C(11)	177.4(2)	C(40)-Mn(1)-C(11)	89.8(2)
C(50)-Mn(1)-C(11)	81.5(2)	C(60)-Mn(1)-C(11)	80.8(2)
C(30)-Mn(1)-P(1)	91.46(12)	C(40)-Mn(1)-P(1)	179.19(13)
C(50)-Mn(1)-P(1)	89.82(12)	C(60)-Mn(1)-P(1)	90.77(12)
C(11)-Mn(1)-P(1)	90.98(10)	C(41)-P(1)-C(31)	104.09(14)
C(41)-P(1)-C(21)	102.66(14)	C(31)-P(1)-C(21)	101.54(14)
C(41)-P(1)-Mn(1)	112.13(10)	C(31)-P(1)-Mn(1)	117.21(11)
C(21)-P(1)-Mn(1)	117.32(12)	C(2)-C(1)-C(6)	116.5(4)
C(2)-C(1)-C(11)	122.2(4)	C(6)-C(1)-C(11)	121.3(4)
C(1)-C(2)-C(3)	121.5(4)	C(4)-C(3)-C(2)	119.7(5)
C(5)-C(4)-C(3)	120.7(5)	C(4)-C(5)-C(6)	119.9(5)
C(5)-C(6)-C(1)	121.7(4)	C(1)-C(11)-Mn(1)	115.3(2)
O(31)-C(30)-Mn(1)	176.1(4)	O(41)-C(40)-Mn(1)	177.5(4)
O(51)-C(50)-Mn(1)	176.4(3)	O(61)-C(60)-Mn(1)	174.8(3)
C(26)-C(21)-C(22)	118.5(3)	C(26)-C(21)-P(1)	121.7(3)
C(22)-C(21)-P(1)	119.8(3)	C(23)-C(22)-C(21)	120.7(4)
C(24)-C(23)-C(22)	118.4(4)	C(25)-C(24)-C(23)	123.2(3)
C(25)-C(24)-F(2)	119.0(4)	C(23)-C(24)-F(2)	117.8(4)
C(24)-C(25)-C(26)	118.5(4)	C(21)-C(26)-C(25)	120.7(4)
C(32)-C(31)-C(36)	118.3(3)	C(32)-C(31)-P(1)	120.9(2)
C(36)-C(31)-P(1)	120.6(3)	C(31)-C(32)-C(33)	121.5(3)
C(34)-C(33)-C(32)	118.2(4)	F(3)-C(34)-C(33)	118.3(4)
F(3)-C(34)-C(35)	118.7(4)	C(33)-C(34)-C(35)	123.0(3)
C(34)-C(35)-C(36)	118.2(3)	C(31)-C(36)-C(35)	120.8(4)
C(46)-C(41)-C(42)	118.6(3)	C(46)-C(41)-P(1)	120.4(3)

C(42)-C(41)-P(1)	120.5(2)	C(43)-C(42)-C(41)	120.4(3)
C(44)-C(43)-C(42)	118.7(3)	C(43)-C(44)-C(45)	122.9(3)
C(43)-C(44)-F(4)	119.0(4)	C(45)-C(44)-F(4)	118.2(3)
C(44)-C(45)-C(46)	118.6(3)	C(45)-C(46)-C(41)	120.8(3)

Table A1.11: Torsion angles (in degrees) for *cis*-$(Ph_2CH_2)[(p\text{-}FC_6H_4)_3P]Mn(CO)_4$.

C(30)-Mn(1)-P(1)-C(41)	-176.3(2)	C(40)-Mn(1)-P(1)-C(41)	-169(10)
C(50)-Mn(1)-P(1)-C(41)	-78.5(2)	C(60)-Mn(1)-P(1)-C(41)	83.7(2)
C(11)-Mn(1)-P(1)-C(41)	3.0(2)	C(30)-Mn(1)-P(1)-C(31)	63.4(2)
C(40)-Mn(1)-P(1)-C(31)	70(10)	C(50)-Mn(1)-P(1)-C(31)	161.2(2)
C(60)-Mn(1)-P(1)-C(31)	-36.6(2)	C(11)-Mn(1)-P(1)-C(31)	-117.3(2)
C(30)-Mn(1)-P(1)-C(21)	-57.8(2)	C(40)-Mn(1)-P(1)-C(21)	-51(10)
C(50)-Mn(1)-P(1)-C(21)	39.9(2)	C(60)-Mn(1)-P(1)-C(21)	-157.8(2)
C(11)-Mn(1)-P(1)-C(21)	121.4(2)	C(6)-C(1)-C(2)-C(3)	-2.3(6)
C(11)-C(1)-C(2)-C(3)	176.6(4)	C(1)-C(2)-C(3)-C(4)	1.6(6)
C(2)-C(3)-C(4)-C(5)	0.9(7)	C(3)-C(4)-C(5)-C(6)	-2.6(7)
C(4)-C(5)-C(6)-C(1)	1.8(7)	C(2)-C(1)-C(6)-C(5)	0.6(6)
C(11)-C(1)-C(6)-C(5)	-178.3(4)	C(2)-C(1)-C(11)-Mn(1)	88.1(4)
C(6)-C(1)-C(11)-Mn(1)	-93.1(4)	C(30)-Mn(1)-C(11)-C(1)	-24(4)
C(40)-Mn(1)-C(11)-C(1)	-6.2(3)	C(50)-Mn(1)-C(11)-C(1)	-96.5(3)
C(60)-Mn(1)-C(11)-C(1)	83.3(3)	P(1)-Mn(1)-C(11)-C(1)	173.9(3)
C(40)-Mn(1)-C(30)-O(31)	-18(5)	C(50)-Mn(1)-C(30)-O(31)	72(5)
C(60)-Mn(1)-C(30)-O(31)	-107(5)	C(11)-Mn(1)-C(30)-O(31)	0(8)
P(1)-Mn(1)-C(30)-O(31)	162(5)	C(30)-Mn(1)-C(40)-O(41)	-3(9)
C(50)-Mn(1)-C(40)-O(41)	-101(9)	C(60)-Mn(1)-C(40)-O(41)	97(9)
C(11)-Mn(1)-C(40)-O(41)	178(100)	P(1)-Mn(1)-C(40)-O(41)	-10(19)
C(30)-Mn(1)-C(50)-O(51)	-161(6)	C(40)-Mn(1)-C(50)-O(51)	-73(6)
C(60)-Mn(1)-C(50)-O(51)	16(6)	C(11)-Mn(1)-C(50)-O(51)	17(6)
P(1)-Mn(1)-C(50)-O(51)	108(6)	C(30)-Mn(1)-C(60)-O(61)	170(4)
C(40)-Mn(1)-C(60)-O(61)	83(4)	C(50)-Mn(1)-C(60)-O(61)	-6(4)
C(11)-Mn(1)-C(60)-O(61)	-7(4)	P(1)-Mn(1)-C(60)-O(61)	-98(4)
C(41)-P(1)-C(21)-C(26)	141.0(3)	C(31)-P(1)-C(21)-C(26)	-111.5(3)
Mn(1)-P(1)-C(21)-C(26)	17.6(3)	C(41)-P(1)-C(21)-C(22)	-42.0(3)
C(31)-P(1)-C(21)-C(22)	65.5(3)	Mn(1)-P(1)-C(21)-C(22)	-165.4(2)
C(26)-C(21)-C(22)-C(23)	0.4(5)	P(1)-C(21)-C(22)-C(23)	-176.7(3)
C(21)-C(22)-C(23)-C(24)	-0.2(5)	C(22)-C(23)-C(24)-C(25)	0.1(6)
C(22)-C(23)-C(24)-F(2)	178.5(3)	C(23)-C(24)-C(25)-C(26)	-0.3(6)
F(2)-C(24)-C(25)-C(26)	-178.7(3)	C(22)-C(21)-C(26)-C(25)	-0.6(5)
P(1)-C(21)-C(26)-C(25)	176.4(3)	C(24)-C(25)-C(26)-C(21)	0.5(5)
C(41)-P(1)-C(31)-C(32)	41.2(3)	C(21)-P(1)-C(31)-C(32)	-65.2(3)
Mn(1)-P(1)-C(31)-C(32)	165.6(3)	C(41)-P(1)-C(31)-C(36)	-143.9(3)
C(21)-P(1)-C(31)-C(36)	109.7(3)	Mn(1)-P(1)-C(31)-C(36)	-19.5(3)
C(36)-C(31)-C(32)-C(33)	-1.1(6)	P(1)-C(31)-C(32)-C(33)	174.0(3)
C(31)-C(32)-C(33)-C(34)	0.8(6)	C(32)-C(33)-C(34)-F(3)	178.9(4)
C(32)-C(33)-C(34)-C(35)	0.2(7)	F(3)-C(34)-C(35)-C(36)	-179.6(3)
C(33)-C(34)-C(35)-C(36)	-0.8(6)	C(32)-C(31)-C(36)-C(35)	0.3(5)
P(1)-C(31)-C(36)-C(35)	-174.7(3)	C(34)-C(35)-C(36)-C(31)	0.6(6)
C(31)-P(1)-C(41)-C(46)	-143.8(3)	C(21)-P(1)-C(41)-C(46)	-38.3(3)
Mn(1)-P(1)-C(41)-C(46)	88.5(3)	C(31)-P(1)-C(41)-C(42)	44.6(3)
C(21)-P(1)-C(41)-C(42)	150.2(3)	Mn(1)-P(1)-C(41)-C(42)	-83.0(3)
C(46)-C(41)-C(42)-C(43)	-0.2(5)	P(1)-C(41)-C(42)-C(43)	171.4(2)
C(41)-C(42)-C(43)-C(44)	1.4(5)	C(42)-C(43)-C(44)-C(45)	-1.7(5)
C(42)-C(43)-C(44)-F(4)	179.3(3)	C(43)-C(44)-C(45)-C(46)	0.7(6)
F(4)-C(44)-C(45)-C(46)	179.7(3)	C(44)-C(45)-C(46)-C(41)	0.6(5)
C(42)-C(41)-C(46)-C(45)	-0.8(5)	P(1)-C(41)-C(46)-C(45)	-172.5(3)

Table A1.12: Anisotropic thermal factors (10^2 Å^2) for *cis*-$(Ph_2CH_2)[(p\text{-}FC_6H_4)_3P]$-$Mn(CO)_4$.

	U_{11}	U_{22}	U_{33}	U_{12}	U_{13}	U_{23}
Mn(1)	4.43(3)	4.27(3)	4.12(4)	-1.17(3)	-0.14(3)	-1.94(3)
P(1)	3.91(5)	4.05(5)	2.84(5)	-0.68(4)	-0.38(4)	-2.05(4)
F(2)	11.8(2)	8.6(2)	5.7(2)	1.88(13)	-5.2(2)	-5.2(2)
F(3)	5.8(2)	14.1(3)	11.0(2)	-2.7(2)	2.50(14)	-5.9(2)
F(4)	8.7(2)	10.2(2)	9.3(2)	-4.7(2)	-1.97(14)	-5.2(2)
O(31)	10.4(2)	10.5(2)	10.0(3)	-4.7(2)	-1.6(2)	-6.3(2)
O(41)	7.5(2)	6.8(2)	15.0(3)	-5.4(2)	-0.7(2)	-1.0(2)
O(51)	8.7(2)	10.1(2)	6.1(2)	-0.2(2)	0.8(2)	-5.6(2)
O(61)	9.4(2)	8.8(2)	5.0(2)	0.7(2)	-0.8(2)	-3.9(2)
C(1)	4.6(2)	4.4(2)	6.0(3)	-1.8(2)	-1.0(2)	-1.7(2)
C(2)	5.7(3)	7.0(3)	7.9(3)	-2.1(2)	-0.5(2)	-3.4(2)
C(3)	4.5(3)	7.9(3)	12.3(5)	-5.5(3)	0.6(3)	-2.2(2)
C(4)	5.7(3)	5.4(3)	15.8(6)	-3.5(3)	-4.8(4)	-0.2(2)
C(5)	7.7(3)	7.5(3)	9.3(4)	0.4(3)	-4.6(3)	-1.9(3)
C(6)	5.8(3)	7.0(3)	6.4(3)	-0.9(2)	-1.8(2)	-2.1(2)
C(11)	5.1(2)	5.0(2)	6.6(3)	-1.9(2)	-1.4(2)	-1.5(2)
C(30)	6.2(2)	5.2(2)	5.8(3)	-1.7(2)	0.1(2)	-2.5(2)
C(40)	6.3(3)	5.2(2)	7.8(3)	-2.3(2)	-0.5(2)	-2.5(2)
C(50)	5.3(2)	5.6(2)	5.0(3)	-1.8(2)	-0.5(2)	-2.0(2)
C(60)	4.9(2)	4.5(2)	5.8(3)	-1.1(2)	-1.1(2)	-1.3(2)
C(21)	4.2(2)	5.0(2)	2.5(2)	-0.4(2)	-0.55(14)	-2.6(2)
C(22)	6.4(2)	5.3(2)	3.4(2)	-0.7(2)	-1.3(2)	-2.4(2)
C(23)	6.7(3)	4.9(2)	5.6(3)	0.1(2)	-2.3(2)	-2.2(2)
C(24)	6.7(3)	6.6(3)	3.9(3)	0.9(2)	-2.3(2)	-4.0(2)
C(25)	7.2(3)	7.8(3)	3.2(2)	-1.1(2)	-1.1(2)	-4.1(2)
C(26)	5.2(2)	5.9(2)	3.6(2)	-1.1(2)	-0.6(2)	-2.6(2)
C(31)	3.6(2)	4.9(2)	2.9(2)	-0.5(2)	-0.70(14)	-2.0(2)
C(32)	4.6(2)	5.5(2)	5.2(3)	-0.9(2)	0.1(2)	-2.2(2)
C(33)	4.3(2)	8.0(3)	7.1(3)	-2.1(2)	0.7(2)	-1.8(2)
C(34)	4.2(2)	9.5(3)	5.7(3)	-0.9(2)	0.2(2)	-4.0(2)
C(35)	6.1(2)	7.4(3)	4.8(2)	-0.6(2)	-0.8(2)	-4.6(2)
C(36)	5.2(2)	5.7(2)	4.0(2)	-0.7(2)	-0.9(2)	-3.0(2)
C(41)	3.1(2)	3.7(2)	3.0(2)	-0.83(14)	-0.37(13)	-1.19(14)
C(42)	3.8(2)	4.5(2)	3.3(2)	-0.7(2)	-0.4(2)	-1.6(2)
C(43)	4.9(2)	6.6(2)	3.5(2)	-2.3(2)	-1.1(2)	-1.6(2)
C(44)	4.3(2)	5.4(2)	6.3(3)	-2.5(2)	-1.3(2)	-1.9(2)
C(45)	5.6(2)	5.9(2)	5.8(3)	-1.6(2)	-0.3(2)	-3.6(2)
C(46)	5.2(2)	5.0(2)	3.7(2)	-0.8(2)	-0.6(2)	-2.8(2)

Structural Data for *cis*-Benzyl-(*tri*-cyclohexylphosphine)(tetracarbonyl)manganese(I)

cis-$(PhCH_2)[(C_6H_{11})_3P]Mn(CO)_4$

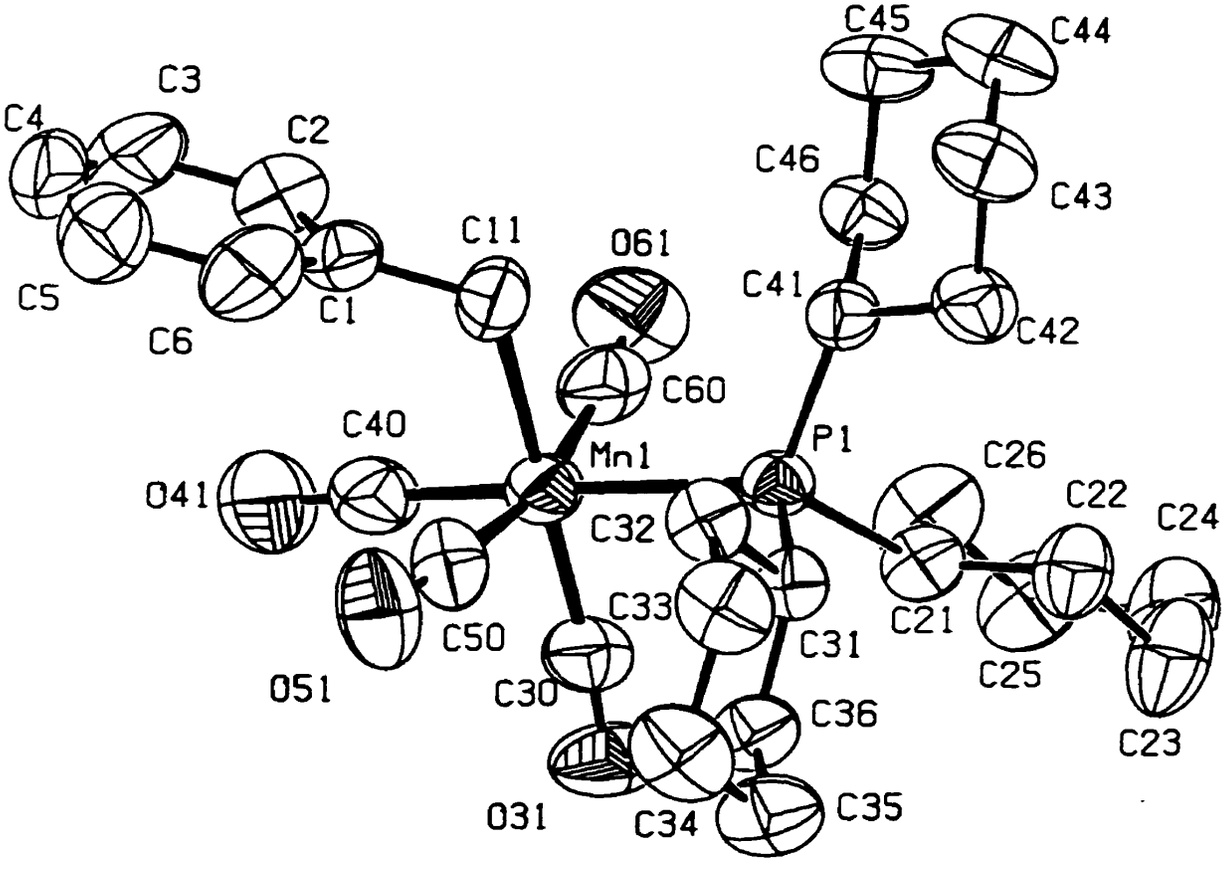

Crystal data for *cis*-$(PhCH_2)[(C_6H_{11})_3P]Mn(CO)_4$

Empirical Formula: C29 H40 O4 Mn P

Space group: monoclinic, P21/n

Cell dimensions:

$a = 11.155$ (3)Å

$b = 24.500$ (3)Å

$c = 11.951$ (4)Å

$\alpha = 90°$

$\beta = 117.72$ (2)°

$\gamma = 90°$

Volume = 2891.3 (13)Å^3

FW = 538.52

Z = 4

$D_{calc} = 1.237$ g / cm^3

F(000) = 1144

Mo Kα radiation

$\lambda = 0.70930$ Å

Cell parameters from 24 reflections

$2\theta = 28 - 30°$

$\mu = 0.542$ mm^{-1}

T = 293 (2) °K

Colourless prism

0.51 × 0.48 × 0.29 mm

Data collection

Rigaku AFC –6S diffractometer

ω / 2θ scans

Absorption correction: *Psi scans*

$T_{min} = 0.82$, $T_{max} = 1.0$

7849 measured reflections

3775 independent reflections

2218 observed reflections [$I > 2\sigma(I)$]

$R_{int} = 0.073$

$\theta_{max} = 45.0°$

$h = -12 \rightarrow 10$

$k = 0 \rightarrow 26$

$l = 0 \rightarrow 12$

3 standard reflections were monitored every 200 reflections

Intensity decay: 1.30

Structure was solved by the direct methods followed by a difference map.

Refinement

Refinement on F^2	317 parameters
$R(F^2 > 2\sigma(F^2)) = 0.0665$	H atoms riding,
$wR(F^2) = 0.1357$	C–H = 0.93 - 0.97 Å
GoF = 1.041	$(\Delta/\sigma) = -0.004$
75 atoms	$\Delta\rho_{max} = 0.212$ e/Å^3
3775 reflections	$\Delta\rho_{min} = -0.240$ e/Å^3

where

$R = \Sigma(Fo-Fc) / \Sigma Fo$

$wR = [\Sigma(w(Fo^2-Fc^2)^2) / \Sigma[w(Fo^2)^2]]^{1/2}$

$GoF = [\Sigma(w(Fo^2-Fc^2)^2) / (\text{No. of refins - No. of params.})]^{1/2}$

Table A1.13: Fractional atomic coordinates and equivalent isotropic displacement parameters (10^2 Å) for *cis*-$(Ph_2CH_2)[(C_6H_{11})_3P]Mn(CO)_4$.

	x	y	z	U_{eq}
Mn(1)	0.44443(9)	0.12291(4)	0.16181(8)	5.59(4)
P(1)	0.6564(2)	0.11250(6)	0.35010(14)	4.56(5)
O(51)	0.3785(5)	0.0061(2)	0.0950(5)	10.1(2)
O(41)	0.1917(6)	0.1427(2)	-0.0737(5)	11.2(2)
O(61)	0.4192(5)	0.2402(2)	0.2084(5)	9.9(2)
O(31)	0.5896(5)	0.1326(2)	0.0091(4)	8.7(2)
C(30)	0.5372(7)	0.1297(3)	0.0713(6)	6.2(2)
C(40)	0.2877(8)	0.1344(3)	0.0186(7)	7.3(2)
C(50)	0.4116(7)	0.0504(3)	0.1264(6)	7.0(2)
C(60)	0.4355(6)	0.1944(3)	0.1941(6)	7.0(2)
C(1)	0.1891(7)	0.0998(3)	0.2042(6)	6.3(2)
C(2)	0.0974(8)	0.1426(3)	0.1512(7)	8.7(2)
C(3)	-0.0401(9)	0.1343(4)	0.0860(8)	10.6(3)
C(4)	-0.0903(10)	0.0837(6)	0.0711(8)	10.9(4)
C(5)	-0.0055(11)	0.0405(5)	0.1204(9)	11.8(3)
C(6)	0.1336(8)	0.0485(3)	0.1867(7)	9.2(2)
C(11)	0.3392(6)	0.1085(3)	0.2762(6)	7.2(2)
C(21)	0.7940(6)	0.1549(2)	0.3477(5)	5.2(2)
C(22)	0.9351(6)	0.1483(3)	0.4597(6)	7.0(2)
C(23)	1.0418(7)	0.1785(3)	0.4365(7)	9.4(3)
C(24)	1.0083(8)	0.2363(3)	0.4021(7)	9.4(2)
C(25)	0.8703(8)	0.2435(3)	0.2951(7)	8.6(2)
C(26)	0.7609(7)	0.2139(2)	0.3152(7)	8.4(2)
C(31)	0.7292(6)	0.0433(2)	0.3733(5)	4.5(2)
C(32)	0.6478(6)	0.0005(2)	0.4045(5)	6.0(2)
C(33)	0.7132(7)	-0.0566(2)	0.4249(6)	7.4(2)
C(34)	0.7305(8)	-0.0733(2)	0.3108(7)	8.4(2)
C(35)	0.8164(7)	-0.0330(2)	0.2846(6)	7.8(2)
C(36)	0.7528(6)	0.0245(2)	0.2632(6)	6.2(2)
C(41)	0.6507(6)	0.1247(2)	0.5012(5)	4.9(2)
C(42)	0.7702(6)	0.1055(2)	0.6246(5)	6.4(2)
C(43)	0.7306(7)	0.1066(3)	0.7314(5)	7.6(2)
C(44)	0.6874(8)	0.1629(3)	0.7498(6)	8.2(2)
C(45)	0.5749(7)	0.1845(2)	0.6269(6)	7.1(2)
C(46)	0.6125(6)	0.1826(2)	0.5198(5)	5.9(2)

Table A1.14: Bond lengths (Å) and angles (in degrees) for *cis*-$(Ph_2CH_2)[(C_6H_{11})_3P]$-$Mn(CO)_4$.

Mn(1)-C(60)	1.806(8)	Mn(1)-C(40)	1.812(8)
Mn(1)-C(30)	1.820(7)	Mn(1)-C(50)	1.823(7)
Mn(1)-C(11)	2.206(6)	Mn(1)-P(1)	2.402(2)
P(1)-C(31)	1.845(5)	P(1)-C(41)	1.860(5)
P(1)-C(21)	1.865(5)	O(51)-C(50)	1.153(7)
O(41)-C(40)	1.143(7)	O(61)-C(60)	1.162(7)
O(31)-C(30)	1.142(7)	C(1)-C(6)	1.375(9)
C(1)-C(2)	1.394(9)	C(1)-C(11)	1.499(8)
C(2)-C(3)	1.375(10)	C(3)-C(4)	1.339(11)
C(4)-C(5)	1.357(12)	C(5)-C(6)	1.390(11)
C(21)-C(26)	1.496(7)	C(21)-C(22)	1.528(7)
C(22)-C(23)	1.533(8)	C(23)-C(24)	1.473(9)
C(24)-C(25)	1.485(9)	C(25)-C(26)	1.532(8)
C(31)-C(36)	1.527(7)	C(31)-C(32)	1.542(7)
C(32)-C(33)	1.543(7)	C(33)-C(34)	1.519(8)
C(34)-C(35)	1.505(8)	C(35)-C(36)	1.545(7)
C(41)-C(46)	1.529(7)	C(41)-C(42)	1.531(7)
C(42)-C(43)	1.532(8)	C(43)-C(44)	1.511(8)
C(44)-C(45)	1.516(8)	C(45)-C(46)	1.522(7)
C(60)-Mn(1)-C(40)	85.8(3)	C(60)-Mn(1)-C(30)	98.1(3)
C(40)-Mn(1)-C(30)	89.4(3)	C(60)-Mn(1)-C(50)	165.8(3)
C(40)-Mn(1)-C(50)	86.0(3)	C(30)-Mn(1)-C(50)	93.4(3)
C(60)-Mn(1)-C(11)	85.7(3)	C(40)-Mn(1)-C(11)	93.0(3)
C(30)-Mn(1)-C(11)	175.6(3)	C(50)-Mn(1)-C(11)	83.2(3)
C(60)-Mn(1)-P(1)	91.8(2)	C(40)-Mn(1)-P(1)	176.9(2)
C(30)-Mn(1)-P(1)	89.0(2)	C(50)-Mn(1)-P(1)	96.8(2)
C(11)-Mn(1)-P(1)	88.7(2)	C(31)-P(1)-C(41)	102.3(2)
C(31)-P(1)-C(21)	101.9(2)	C(41)-P(1)-C(21)	109.0(3)
C(31)-P(1)-Mn(1)	114.3(2)	C(41)-P(1)-Mn(1)	115.4(2)
C(21)-P(1)-Mn(1)	112.6(2)	O(31)-C(30)-Mn(1)	176.2(6)
O(41)-C(40)-Mn(1)	177.2(6)	O(51)-C(50)-Mn(1)	173.3(6)
O(61)-C(60)-Mn(1)	174.7(6)	C(6)-C(1)-C(2)	115.8(7)
C(6)-C(1)-C(11)	121.4(7)	C(2)-C(1)-C(11)	122.7(7)
C(3)-C(2)-C(1)	122.4(8)	C(4)-C(3)-C(2)	120.0(9)
C(3)-C(4)-C(5)	120.1(10)	C(4)-C(5)-C(6)	120.4(10)
C(1)-C(6)-C(5)	121.3(8)	C(1)-C(11)-Mn(1)	116.1(4)
C(26)-C(21)-C(22)	111.0(5)	C(26)-C(21)-P(1)	115.9(4)
C(22)-C(21)-P(1)	116.6(4)	C(21)-C(22)-C(23)	111.1(5)
C(24)-C(23)-C(22)	113.4(6)	C(23)-C(24)-C(25)	112.4(6)
C(24)-C(25)-C(26)	113.0(6)	C(21)-C(26)-C(25)	112.3(5)
C(36)-C(31)-C(32)	11.1(4)	C(36)-C(31)-P(1)	112.8(4)
C(32)-C(31)-P(1)	113.2(4)	C(31)-C(32)-C(33)	111.5(5)
C(34)-C(33)-C(32)	110.5(5)	C(35)-C(34)-C(33)	111.7(5)
C(34)-C(35)-C(36)	110.1(5)	C(31)-C(36)-C(35)	112.5(5)
C(46)-C(41)-C(42)	108.8(5)	C(46)-C(41)-P(1)	115.3(4)
C(42)-C(41)-P(1)	118.6(4)	C(41)-C(42)-C(43)	109.7(5)
C(44)-C(43)-C(42)	111.8(5)	C(43)-C(44)-C(45)	110.8(5)
C(44)-C(45)-C(46)	112.1(5)	C(45)-C(46)-C(41)	110.8(5)
C(45)-C(46)-H(46A)	109.5(3)		

Table A1.15: Torsion angles (in degrees) for *cis*-$(Ph_2CH_2)[(C_6H_{11})_3P]Mn(CO)_4$.

C(60)-Mn(1)-P(1)-C(31)	-178.5(3)	C(40)-Mn(1)-C(11)-C(1)	13.2(5)
C(40)-Mn(1)-P(1)-C(31)	-140(4)	C(30)-Mn(1)-C(11)-C(1)	-111(3)
C(30)-Mn(1)-P(1)-C(31)	-80.4(3)	C(50)-Mn(1)-C(11)-C(1)	-72.4(5)
C(50)-Mn(1)-P(1)-C(31)	12.9(3)	P(1)-Mn(1)-C(11)-C(1)	-169.3(5)
C(11)-Mn(1)-P(1)-C(31)	95.9(3)	C(31)-P(1)-C(21)-C(26)	173.2(5)
C(60)-Mn(1)-P(1)-C(41)	63.3(3)	C(41)-P(1)-C(21)-C(26)	-79.1(5)
C(40)-Mn(1)-P(1)-C(41)	102(4)	Mn(1)-P(1)-C(21)-C(26)	50.3(5)
C(30)-Mn(1)-P(1)-C(41)	161.4(3)	C(31)-P(1)-C(21)-C(22)	-53.3(5)
C(50)-Mn(1)-P(1)-C(41)	-105.3(3)	C(41)-P(1)-C(21)-C(22)	54.3(5)
C(11)-Mn(1)-P(1)-C(41)	-22.4(3)	Mn(1)-P(1)-C(21)-C(22)	-176.2(4)
C(60)-Mn(1)-P(1)-C(21)	-62.8(3)	C(26)-C(21)-C(22)-C(23)	-53.0(7)
C(40)-Mn(1)-P(1)-C(21)	-24(4)	P(1)-C(21)-C(22)-C(23)	171.4(5)
C(30)-Mn(1)-P(1)-C(21)	35.3(3)	C(21)-C(22)-C(23)-C(24)	53.1(8)
C(50)-Mn(1)-P(1)-C(21)	128.6(3)	C(22)-C(23)-C(24)-C(25)	-52.2(9)
C(11)-Mn(1)-P(1)-C(21)	-148.4(3)	C(23)-C(24)-C(25)-C(26)	51.3(9)
C(60)-Mn(1)-C(30)-O(31)	-121(8)	C(22)-C(21)-C(26)-C(25)	53.0(7)
C(40)-Mn(1)-C(30)-O(31)	-35(8)	P(1)-C(21)-C(26)-C(25)	-171.1(5)
C(50)-Mn(1)-C(30)-O(31)	51(8)	C(24)-C(25)-C(26)-C(21)	-52.5(8)
C(11)-Mn(1)-C(30)-O(31)	89(9)	C(41)-P(1)-C(31)-C(36)	-176.6(4)
P(1)-Mn(1)-C(30)-O(31)	148(8)	C(21)-P(1)-C(31)-C(36)	-63.8(4)
C(60)-Mn(1)-C(40)-O(41)	72(14)	Mn(1)-P(1)-C(31)-C(36)	58.0(4)
C(30)-Mn(1)-C(40)-O(41)	-26(14)	C(41)-P(1)-C(31)-C(32)	56.2(4)
C(50)-Mn(1)-C(40)-O(41)	-119(14)	C(21)-P(1)-C(31)-C(32)	168.9(4)
C(11)-Mn(1)-C(40)-O(41)	158(14)	Mn(1)-P(1)-C(31)-C(32)	-69.3(4)
P(1)-Mn(1)-C(40)-O(41)	34(17)	C(36)-C(31)-C(32)-C(33)	52.6(6)
C(60)-Mn(1)-C(50)-O(51)	44(6)	P(1)-C(31)-C(32)-C(33)	-179.2(4)
C(40)-Mn(1)-C(50)-O(51)	-11(5)	C(31)-C(32)-C(33)-C(34)	-55.2(7)
C(30)-Mn(1)-C(50)-O(51)	-100(5)	C(32)-C(33)-C(34)-C(35)	58.4(8)
C(11)-Mn(1)-C(50)-O(51)	83(5)	C(33)-C(34)-C(35)-C(36)	-57.9(7)
P(1)-Mn(1)-C(50)-O(51)	171(5)	C(32)-C(31)-C(36)-C(35)	-52.8(7)
C(40)-Mn(1)-C(60)-O(61)	20(7)	P(1)-C(31)-C(36)-C(35)	178.9(4)
C(30)-Mn(1)-C(60)-O(61)	109(7)	C(34)-C(35)-C(36)-C(31)	55.3(7)
C(50)-Mn(1)-C(60)-O(61)	-35(7)	C(31)-P(1)-C(41)-C(46)	171.9(4)
C(11)-Mn(1)-C(60)-O(61)	-73(7)	C(21)-P(1)-C(41)-C(46)	64.5(5)
P(1)-Mn(1)-C(60)-O(61)	-162(7)	Mn(1)-P(1)-C(41)-C(46)	-63.4(5)
C(6)-C(1)-C(2)-C(3)	0.4(10)	C(31)-P(1)-C(41)-C(42)	40.3(5)
C(11)-C(1)-C(2)-C(3)	-179.5(7)	C(21)-P(1)-C(41)-C(42)	-67.0(5)
C(1)-C(2)-C(3)-C(4)	-0.3(12)	Mn(1)-P(1)-C(41)-C(42)	165.1(4)
C(2)-C(3)-C(4)-C(5)	0.0(14)	C(46)-C(41)-C(42)-C(43)	59.4(6)
C(3)-C(4)-C(5)-C(6)	0.1(14)	P(1)-C(41)-C(42)-C(43)	-166.2(4)
C(2)-C(1)-C(6)-C(5)	-0.2(11)	C(41)-C(42)-C(43)-C(44)	-58.3(7)
C(11)-C(1)-C(6)-C(5)	179.7(7)	C(42)-C(43)-C(44)-C(45)	54.6(8)
C(4)-C(5)-C(6)-C(1)	0.0(13)	C(43)-C(44)-C(45)-C(46)	-53.6(7)
C(6)-C(1)-C(11)-Mn(1)	101.6(7)	C(44)-C(45)-C(46)-C(41)	56.4(7)
C(2)-C(1)-C(11)-Mn(1)	-78.5(7)	C(42)-C(41)-C(46)-C(45)	-58.8(6)
C(60)-Mn(1)-C(11)-C(1)	98.8(5)	P(1)-C(41)-C(46)-C(45)	165.1(4)

Table A1.16: Anisotropic thermal factors (10^2 Å^2) for *cis*-$(Ph_2CH_2)[(C_6H_{11})_3P]Mn(CO)_4$.

	U_{11}	U_{22}	U_{33}	U_{12}	U_{13}	U_{23}
Mn(1)	5.17(6)	6.75(7)	4.86(6)	0.19(5)	2.36(5)	0.50(5)
P(1)	4.87(10)	4.67(10)	4.45(9)	0.03(7)	2.42(8)	-0.16(8)
O(51)	9.3(4)	7.9(4)	9.8(4)	-1.2(3)	1.7(3)	-2.4(3)
O(41)	8.3(4)	16.2(5)	6.5(3)	0.3(3)	1.2(3)	2.5(4)
O(61)	10.8(4)	8.3(4)	9.6(4)	1.2(3)	3.7(3)	4.1(3)
O(31)	10.1(4)	10.8(4)	8.0(3)	1.8(3)	6.4(3)	2.1(3)
C(30)	6.6(5)	7.3(5)	4.7(4)	1.2(3)	2.5(4)	1.9(4)
C(40)	7.3(5)	9.3(5)	5.4(4)	0.2(4)	3.0(4)	1.1(4)
C(50)	6.5(5)	7.3(5)	5.9(5)	-0.1(4)	1.9(4)	-0.9(4)
C(60)	5.9(5)	8.4(5)	6.2(5)	1.7(4)	2.5(4)	2.6(4)
C(1)	5.7(5)	8.3(5)	5.8(4)	0.0(4)	3.3(4)	0.2(4)
C(2)	7.2(6)	10.5(6)	8.9(6)	-1.3(5)	4.3(5)	0.1(5)
C(3)	6.3(7)	15.8(10)	9.9(7)	-1.2(6)	4.0(6)	2.3(6)
C(4)	5.3(6)	21.1(13)	5.7(5)	-1.9(7)	2.1(5)	-1.4(8)
C(5)	9.6(8)	17.0(11)	10.5(8)	-3.4(7)	6.1(7)	-6.6(7)
C(6)	8.2(7)	9.7(6)	10.9(6)	1.4(5)	5.3(5)	-0.1(5)
C(11)	4.8(4)	10.9(6)	5.7(4)	0.0(4)	2.1(4)	-1.3(4)
C(21)	5.8(4)	4.5(4)	5.9(4)	0.9(3)	3.2(4)	-0.4(3)
C(22)	6.3(5)	6.7(4)	7.8(5)	0.7(4)	3.1(4)	-1.5(4)
C(23)	6.8(5)	9.6(6)	10.7(6)	2.7(5)	3.0(5)	-2.1(4)
C(24)	8.9(6)	8.7(6)	10.7(6)	0.7(5)	4.7(5)	-3.6(5)
C(25)	9.3(6)	6.6(5)	11.8(6)	2.4(4)	6.4(6)	-0.7(4)
C(26)	9.4(6)	4.0(4)	12.7(6)	1.7(4)	6.0(5)	-0.3(4)
C(31)	4.7(4)	3.9(3)	4.7(3)	0.2(3)	1.9(3)	-0.1(3)
C(32)	6.9(5)	4.7(4)	6.4(4)	0.5(3)	3.0(4)	-0.5(3)
C(33)	9.7(6)	4.1(4)	8.6(5)	0.4(4)	4.5(5)	-0.8(4)
C(34)	11.1(6)	4.2(4)	9.2(6)	0.0(4)	4.1(5)	1.2(4)
C(35)	9.6(6)	5.0(4)	10.4(6)	0.0(4)	6.0(5)	1.0(4)
C(36)	6.6(5)	4.8(4)	8.1(5)	0.0(3)	4.2(4)	0.0(3)
C(41)	4.5(4)	6.0(4)	4.3(3)	0.2(3)	2.0(3)	-0.4(3)
C(42)	6.8(5)	7.3(4)	4.9(4)	0.4(3)	2.4(4)	0.4(4)
C(43)	10.5(6)	7.9(5)	4.8(4)	1.2(3)	4.0(4)	0.7(4)
C(44)	13.9(7)	5.8(5)	6.8(5)	-0.6(4)	6.4(5)	-0.7(4)
C(45)	10.7(6)	4.9(4)	8.5(5)	-0.9(4)	6.8(5)	0.0(4)
C(46)	6.9(4)	5.2(4)	5.7(4)	-0.5(3)	3.1(4)	-0.4(3)

APPENDIX II

Crystal Structures of some Group 14 (IVA) (Pentatacarbonyl)manganese(I) Complexes

Structural Data for

Triphenylsilyl(pentacarbonyl)manganese(I)

$Ph_3SiMn(CO)_5$

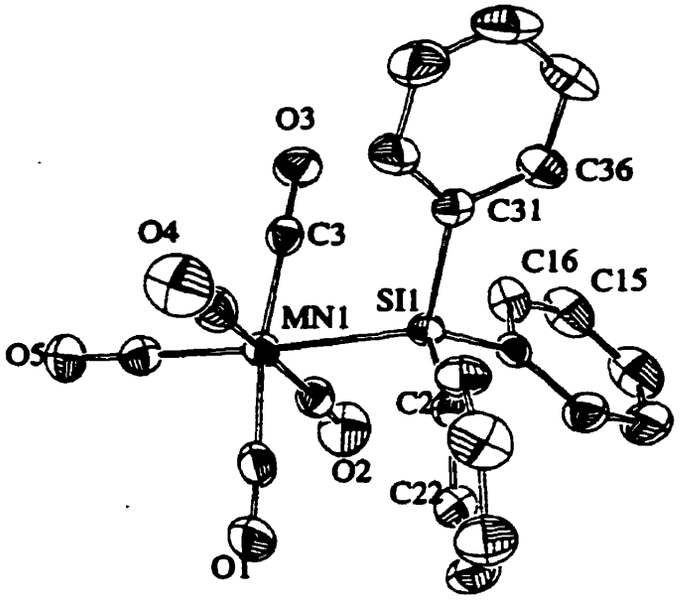

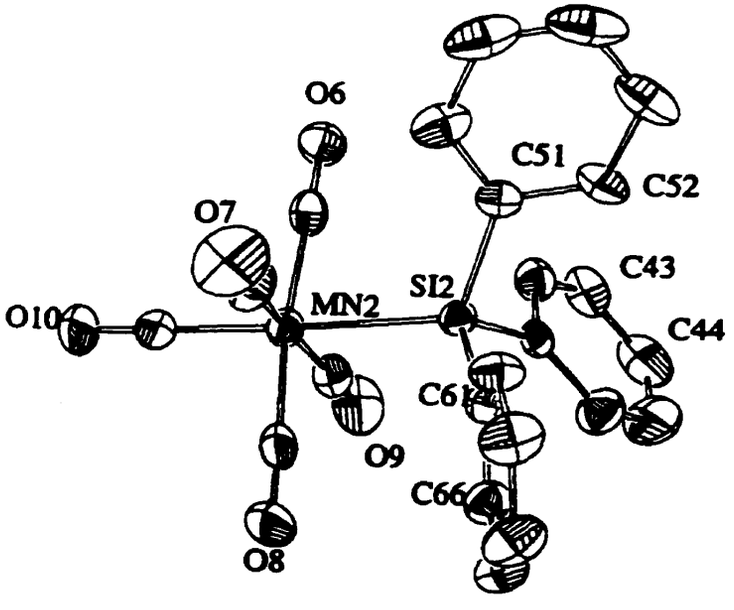

Crystal data for $Ph_3SiMn(CO)_5$

Empirical Formula: C23 H15 O5 Mn Si

Space group: Triclinic, P 1

Cell dimensions:

a = 11.380 (2)Å

b = 11.541 (2)Å

c = 17.111 (3)Å

α = 104.95 (2)°

β = 98.20 (2)°

γ = 91.10 (2)°

Volume = 2145.4 (6)Å^3

FW = 454.36

Z = 4

D_{calc} = 1.407 g / cm^3

F(000) = 928

Mo Kα radiation

λ = 0.70930 Å

Cell parameters from 24 reflections

2θ = 28 - 34°

μ = 0.702 mm^{-1}

T = 295 (2) °K

colourless plate

0.45 × 0.36 × 0.10 mm

Data collection

Rigaku AFC –6S diffractometer

ω / 2θ scans

Absorption correction: *psi scan*

T_{min} = 0.86, T_{max} = 1.0

15186 measured reflections

7558 independent reflections

3921 observed reflections [$I > 2\sigma(I)$]

R_{int} = 0.071

θ_{max} = 25.0°

$h = 0 \rightarrow 13$

$k = -13 \rightarrow 13$

$l = -20 \rightarrow 19$

3 standard reflections were monitored every 200 reflections

Intensity decay: 1.2 %

Structure was solved by direct methods followed by a difference map.

Refinement

Refinement on F^2	542 parameters
$R(F^2 > 2\sigma(F^2)) = 0.069$	H atoms riding,
$wR(F^2) = 0.1078$	C–H = 0.93 Å
GoF = 0.918	$(\Delta/\sigma) = -0.008$
90 atoms	$\Delta\rho_{max} = 0.364$ e/Å^3
7558 reflections	$\Delta\rho_{min} = -0.302$ e/Å^3

where

$R = \Sigma(Fo-Fc) / \Sigma Fo$

$wR = [\Sigma(w(Fo^2-Fc^2)^2) / \Sigma[w(Fo^2)^2]]^{1/2}$

$GoF = [\Sigma(w(Fo^2-Fc^2)^2) / (\text{No. of refins - No. of params.})]^{1/2}$

Table A2.1: Fractional atomic coordinates and equivalent isotropic displacement parameters (10^2 Å) for $Ph_3SiMn(CO)_5$.

	x	y	z	U_{eq}
Mn(1)	0.08448(7)	0.81747(7)	0.35305(5)	4.03(2)
Si(1)	0.21406(13)	0.75672(12)	0.24405(9)	3.57(4)
O(1)	0.0767(4)	1.0625(4)	0.3264(3)	8.0(2)
O(2)	0.3028(4)	0.9104(4)	0.4741(3)	8.2(2)
O(3)	0.1139(3)	0.5644(3)	0.3606(3)	6.56(12)
O(4)	-0.1250(4)	0.7524(4)	0.2221(3)	9.6(2)
O(5)	-0.0768(4)	0.8694(4)	0.4782(3)	7.05(13)
C(1)	0.0812(5)	0.9682(6)	0.3357(4)	5.7(2)
C(2)	0.2215(5)	0.8715(5)	0.4276(3)	5.1(2)
C(3)	0.1034(4)	0.6602(5)	0.3573(3)	4.4(2)
C(4)	-0.0437(5)	0.7739(5)	0.2701(4)	6.0(2)
C(5)	-0.0138(5)	0.8511(5)	0.4307(4)	5.2(2)
C(11)	0.3753(4)	0.7656(4)	0.2920(3)	3.89(13)
C(12)	0.4629(5)	0.8346(5)	0.2733(4)	5.8(2)
C(13)	0.5803(6)	0.8381(6)	0.3095(5)	8.3(2)
C(14)	0.6125(6)	0.7710(7)	0.3646(5)	8.6(3)
C(15)	0.5280(6)	0.7003(6)	0.3825(4)	7.1(2)
C(16)	0.4115(5)	0.6976(5)	0.3464(3)	5.2(2)
C(21)	0.1940(4)	0.8552(4)	0.1715(3)	3.77(13)
C(22)	0.2327(4)	0.9756(5)	0.1950(3)	4.8(2)
C(23)	0.2159(5)	1.0495(5)	0.1423(4)	6.1(2)
C(24)	0.1598(5)	1.0019(6)	0.0634(4)	7.1(2)
C(25)	0.1206(6)	0.8838(6)	0.0377(4)	7.3(2)
C(26)	0.1373(5)	0.8105(5)	0.0905(3)	5.6(2)
C(31)	0.1819(5)	0.5960(4)	0.1793(3)	4.26(14)
C(32)	0.0700(5)	0.5441(5)	0.1469(4)	7.1(2)
C(33)	0.0503(7)	0.4292(6)	0.0967(4)	8.9(2)
C(34)	0.1438(8)	0.3620(6)	0.0778(4)	8.3(2)
C(35)	0.2561(7)	0.4095(6)	0.1081(4)	7.5(2)
C(36)	0.2751(5)	0.5258(5)	0.1589(3)	5.6(2)
Mn(2)	0.15691(7)	0.68726(8)	0.64892(5)	4.49(3)
Si(2)	0.34065(13)	0.74923(13)	0.75216(9)	3.82(4)
O(6)	0.1803(3)	0.9371(4)	0.6318(2)	6.32(12)
O(7)	0.0311(4)	0.7567(5)	0.7941(3)	10.9(2)
O(8)	0.1628(4)	0.4397(4)	0.6706(3)	9.7(2)
O(9)	0.3129(4)	0.6021(4)	0.5222(3)	9.0(2)
O(10)	-0.0677(4)	0.6265(4)	0.5307(3)	8.03(14)
C(6)	0.1713(5)	0.8421(5)	0.6391(3)	4.8(2)
C(7)	0.0789(5)	0.7318(6)	0.7378(4)	6.5(2)
C(8)	0.1622(5)	0.5361(6)	0.6650(4)	6.4(2)
C(9)	0.2543(5)	0.6355(5)	0.5708(4)	5.8(2)
C(10)	0.0182(5)	0.6495(5)	0.5758(4)	5.6(2)
C(41)	0.4746(4)	0.7444(5)	0.6988(3)	4.10(13)
C(42)	0.4861(5)	0.8225(5)	0.6502(3)	5.6(2)
C(43)	0.5792(6)	0.8237(6)	0.6080(4)	7.0(2)
C(44)	0.6675(7)	0.7463(7)	0.6130(5)	8.8(3)
C(45)	0.6606(6)	0.6682(7)	0.6612(5)	9.8(3)
C(46)	0.5663(5)	0.6672(5)	0.7040(4)	6.8(2)

C(51)	0.3484(5)	0.9083(4)	0.8196(3)	4.41(14)
C(52)	0.4607(5)	0.9544(5)	0.8606(3)	6.2(2)
C(53)	0.4786(7)	1.0668(6)	0.9149(4)	8.4(2)
C(54)	0.3865(9)	1.1372(6)	0.9290(4)	9.3(3)
C(55)	0.2731(8)	1.0963(7)	0.8904(4)	9.0(3)
C(56)	0.2554(6)	0.9815(6)	0.8361(3)	6.8(2)
C(61)	0.3550(4)	0.6504(5)	0.8244(3)	4.26(14)
C(62)	0.3312(5)	0.6930(5)	0.9046(3)	5.8(2)
C(63)	0.3344(5)	0.6205(6)	0.9573(4)	7.3(2)
C(64)	0.3631(6)	0.5031(6)	0.9321(4)	7.9(2)
C(65)	0.3874(5)	0.4583(6)	0.8543(4)	7.0(2)
C(66)	0.3840(5)	0.5304(5)	0.8014(4)	5.5(2)

Table A2.2: Bond lengths (Å) and angles (in degrees) for $Ph_3SiMn(CO)_5$.

Mn(1)-C(1)	1.839(6)	Mn(2)-C(7)	1.834(7)
Mn(1)-C(4)	1.846(6)	Mn(2)-C(8)	1.835(6)
Mn(1)-C(3)	1.850(6)	Mn(2)-C(10)	1.837(6)
Mn(1)-C(2)	1.852(6)	Mn(2)-C(6)	1.844(6)
Mn(1)-Si(1)	2.509(2)	Mn(2)-C(9)	1.846(6)
Mn(1)-C(5)	1.827(6)	Mn(2)-Si(2)	2.498(2)
Si(1)-C(21)	1.882(5)	Si(2)-C(61)	1.879(5)
Si(1)-C(11)	1.890(5)	Si(2)-C(41)	1.880(5)
Si(1)-C(31)	1.898(5)	Si(2)-C(51)	1.892(5)
O(1)-C(1)	1.141(6)	O(6)-C(6)	1.139(6)
O(2)-C(2)	1.132(6)	O(7)-C(7)	1.149(6)
O(3)-C(3)	1.130(5)	O(8)-C(8)	1.142(6)
O(4)-C(4)	1.123(6)	O(9)-C(9)	1.135(6)
O(5)-C(5)	1.142(5)	O(10)-C(10)	1.136(6)
C(11)-C(12)	1.386(6)	C(41)-C(42)	1.390(7)
C(11)-C(16)	1.389(6)	C(41)-C(46)	1.394(7)
C(12)-C(13)	1.386(7)	C(42)-C(43)	1.367(7)
C(12)-H(12)	0.93	C(42)-H(42)	0.93
C(13)-C(14)	1.382(9)	C(43)-C(44)	1.366(8)
C(13)-H(13)	0.93	C(43)-H(43)	0.93
C(14)-C(15)	1.368(8)	C(44)-C(45)	1.378(9)
C(14)-H(14)	0.93	C(44)-H(44)	0.93
C(15)-C(16)	1.376(7)	C(45)-C(46)	1.385(8)
C(15)-H(15)	0.93	C(45)-H(45)	0.93
C(16)-H(16)	0.93	C(46)-H(46)	0.93
C(21)-C(22)	1.387(6)	C(51)-C(56)	1.382(7)
C(21)-C(26)	1.402(6)	C(51)-C(52)	1.391(7)
C(22)-C(23)	1.390(7)	C(52)-C(53)	1.379(7)
C(22)-H(22)	0.93	C(52)-H(52)	0.93
C(23)-C(24)	1.374(7)	C(53)-C(54)	1.350(8)
C(23)-H(23)	0.93	C(53)-H(53)	0.93
C(24)-C(25)	1.365(7)	C(54)-C(55)	1.377(9)
C(24)-H(24)	0.93	C(54)-H(54)	0.93
C(25)-C(26)	1.386(7)	C(55)-C(56)	1.400(8)
C(25)-H(25)	0.93	C(55)-H(55)	0.93
C(26)-H(26)	0.93	C(56)-H(56)	0.93
C(31)-C(32)	1.373(7)	C(61)-C(66)	1.398(6)
C(31)-C(36)	1.377(6)	C(61)-C(62)	1.401(6)
C(32)-C(33)	1.376(7)	C(62)-C(63)	1.377(7)
C(32)-H(32)	0.93	C(62)-H(62)	0.93
C(33)-C(34)	1.355(8)	C(63)-C(64)	1.373(7)
C(33)-H(33)	0.93	C(63)-H(63)	0.93
C(34)-C(35)	1.357(8)	C(64)-C(65)	1.367(7)
C(34)-H(34)	0.93	C(64)-H(64)	0.93
C(35)-C(36)	1.392(7)	C(65)-C(66)	1.377(7)
C(35)-H(35)	0.93	C(65)-H(65)	0.93
C(36)-H(36)	0.93	C(66)-H(66)	0.93

C(5)-Mn(1)-C(1)	94.2(2)
C(5)-Mn(1)-C(4)	91.4(3)
C(1)-Mn(1)-C(4)	87.0(3)
C(5)-Mn(1)-C(3)	95.1(2)
C(1)-Mn(1)-C(3)	170.7(2)
C(4)-Mn(1)-C(3)	92.5(2)
C(5)-Mn(1)-C(2)	94.0(2)
C(1)-Mn(1)-C(2)	87.6(3)
C(4)-Mn(1)-C(2)	172.6(3)
C(3)-Mn(1)-C(2)	92.0(2)
C(5)-Mn(1)-Si(1)	176.1(2)
C(1)-Mn(1)-Si(1)	89.2(2)
C(4)-Mn(1)-Si(1)	86.8(2)
C(3)-Mn(1)-Si(1)	81.5(2)
C(2)-Mn(1)-Si(1)	88.0(2)
C(21)-Si(1)-C(11)	110.0(2)
C(21)-Si(1)-C(31)	106.6(2)
C(11)-Si(1)-C(31)	105.3(2)
C(21)-Si(1)-Mn(1)	110.7(2)
C(11)-Si(1)-Mn(1)	110.2(2)
C(31)-Si(1)-Mn(1)	113.8(2)
O(1)-C(1)-Mn(1)	178.0(5)
O(2)-C(2)-Mn(1)	176.3(5)
O(3)-C(3)-Mn(1)	179.1(5)
O(4)-C(4)-Mn(1)	176.1(6)
O(5)-C(5)-Mn(1)	178.3(5)
C(12)-C(11)-C(16)	117.0(5)
C(12)-C(11)-Si(1)	122.9(4)
C(16)-C(11)-Si(1)	120.1(4)
C(13)-C(12)-C(11)	121.1(6)
C(13)-C(12)-H(12)	119.4(4)
C(11)-C(12)-H(12)	119.4(3)
C(14)-C(13)-C(12)	120.2(7)
C(14)-C(13)-H(13)	119.9(4)
C(12)-C(13)-H(13)	119.9(4)
C(15)-C(14)-C(13)	119.6(7)
C(15)-C(14)-H(14)	120.2(4)
C(13)-C(14)-H(14)	120.2(4)
C(14)-C(15)-C(16)	119.8(7)
C(14)-C(15)-H(15)	120.1(4)
C(16)-C(15)-H(15)	120.1(4)
C(15)-C(16)-C(11)	122.3(6)
C(15)-C(16)-H(16)	118.9(4)
C(11)-C(16)-H(16)	118.9(3)
C(22)-C(21)-C(26)	116.4(5)
C(22)-C(21)-Si(1)	122.2(4)
C(26)-C(21)-Si(1)	121.4(4)
C(21)-C(22)-C(23)	122.6(5)
C(21)-C(22)-H(22)	118.7(3)
C(23)-C(22)-H(22)	118.7(3)
C(24)-C(23)-C(22)	119.1(6)
C(24)-C(23)-H(23)	120.4(4)
C(22)-C(23)-H(23)	120.4(3)
C(25)-C(24)-C(23)	120.2(6)
C(25)-C(24)-H(24)	119.9(4)
C(23)-C(24)-H(24)	119.9(4)
C(24)-C(25)-C(26)	120.5(6)
C(24)-C(25)-H(25)	119.8(4)
C(26)-C(25)-H(25)	119.8(4)
C(25)-C(26)-C(21)	121.3(5)
C(25)-C(26)-H(26)	119.4(4)
C(21)-C(26)-H(26)	119.4(3)
C(32)-C(31)-C(36)	116.0(5)
C(32)-C(31)-Si(1)	124.5(4)
C(36)-C(31)-Si(1)	119.4(4)
C(31)-C(32)-C(33)	122.8(6)
C(31)-C(32)-H(32)	118.6(3)
C(33)-C(32)-H(32)	118.6(4)
C(34)-C(33)-C(32)	119.9(7)
C(34)-C(33)-H(33)	120.0(4)
C(32)-C(33)-H(33)	120.0(4)
C(33)-C(34)-C(35)	119.4(7)
C(33)-C(34)-H(34)	120.3(4)
C(35)-C(34)-H(34)	120.3(4)
C(34)-C(35)-C(36)	120.3(6)
C(34)-C(35)-H(35)	119.9(4)
C(36)-C(35)-H(35)	119.9(4)
C(31)-C(36)-C(35)	121.5(6)
C(31)-C(36)-H(36)	119.2(3)
C(35)-C(36)-H(36)	119.2(4)
C(7)-Mn(2)-C(8)	88.2(3)
C(7)-Mn(2)-C(10)	93.3(3)
C(8)-Mn(2)-C(10)	93.2(3)
C(7)-Mn(2)-C(6)	93.2(3)
C(8)-Mn(2)-C(6)	172.7(2)
C(10)-Mn(2)-C(6)	93.8(2)
C(7)-Mn(2)-C(9)	170.9(3)
C(8)-Mn(2)-C(9)	86.8(3)
C(10)-Mn(2)-C(9)	94.6(3)
C(6)-Mn(2)-C(9)	90.8(3)
C(7)-Mn(2)-Si(2)	84.4(2)
C(8)-Mn(2)-Si(2)	89.0(2)
C(10)-Mn(2)-Si(2)	176.8(2)
C(6)-Mn(2)-Si(2)	84.1(2)
C(9)-Mn(2)-Si(2)	87.8(2)
C(61)-Si(2)-C(41)	111.3(2)
C(61)-Si(2)-C(51)	105.4(2)
C(41)-Si(2)-C(51)	104.1(2)
C(61)-Si(2)-Mn(2)	110.4(2)
C(41)-Si(2)-Mn(2)	109.9(2)
C(51)-Si(2)-Mn(2)	115.6(2)
O(6)-C(6)-Mn(2)	178.9(5)
O(7)-C(7)-Mn(2)	178.0(6)
O(8)-C(8)-Mn(2)	176.3(6)
O(9)-C(9)-Mn(2)	178.8(6)
O(10)-C(10)-Mn(2)	179.7(5)
C(42)-C(41)-C(46)	115.9(5)
C(42)-C(41)-Si(2)	119.4(4)

C(46)-C(41)-Si(2)	124.7(5)	C(53)-C(54)-H(54)	119.9(5)
C(43)-C(42)-C(41)	123.3(6)	C(55)-C(54)-H(54)	119.9(5)
C(43)-C(42)-H(42)	118.3(4)	C(54)-C(55)-C(56)	119.0(7)
C(41)-C(42)-H(42)	118.3(3)	C(54)-C(55)-H(55)	120.5(5)
C(44)-C(43)-C(42)	120.0(7)	C(56)-C(55)-H(55)	120.5(4)
C(44)-C(43)-H(43)	120.0(5)	C(51)-C(56)-C(55)	122.0(6)
C(42)-C(43)-H(43)	120.0(4)	C(51)-C(56)-H(56)	119.0(4)
C(43)-C(44)-C(45)	118.7(7)	C(55)-C(56)-H(56)	119.0(4)
C(43)-C(44)-H(44)	120.6(5)	C(66)-C(61)-C(62)	116.1(5)
C(45)-C(44)-H(44)	120.6(5)	C(66)-C(61)-Si(2)	123.1(4)
C(44)-C(45)-C(46)	121.2(7)	C(62)-C(61)-Si(2)	120.7(4)
C(44)-C(45)-H(45)	119.4(5)	C(63)-C(62)-C(61)	121.9(5)
C(46)-C(45)-H(45)	119.4(4)	C(63)-C(62)-H(62)	119.0(4)
C(45)-C(46)-C(41)	120.8(6)	C(61)-C(62)-H(62)	119.0(3)
C(45)-C(46)-H(46)	119.6(4)	C(64)-C(63)-C(62)	120.0(6)
C(41)-C(46)-H(46)	119.6(4)	C(64)-C(63)-H(63)	120.0(4)
C(56)-C(51)-C(52)	116.3(5)	C(62)-C(63)-H(63)	120.0(4)
C(56)-C(51)-Si(2)	127.8(5)	C(65)-C(64)-C(63)	119.8(6)
C(52)-C(51)-Si(2)	115.8(4)	C(65)-C(64)-H(64)	120.1(4)
C(53)-C(52)-C(51)	122.0(6)	C(63)-C(64)-H(64)	120.1(4)
C(53)-C(52)-H(52)	119.0(4)	C(64)-C(65)-C(66)	120.4(6)
C(51)-C(52)-H(52)	119.0(3)	C(64)-C(65)-H(65)	119.8(4)
C(54)-C(53)-C(52)	120.5(7)	C(66)-C(65)-H(65)	119.8(4)
C(54)-C(53)-H(53)	119.8(5)	C(65)-C(66)-C(61)	121.8(6)
C(52)-C(53)-H(53)	119.8(4)	C(65)-C(66)-H(66)	119.1(4)
C(53)-C(54)-C(55)	120.2(7)	C(61)-C(66)-H(66)	119.1(3)

Table A2.3: Torsion angles (in degrees) for $Ph_3SiMn(CO)_5$.

C(6)-Mn(2)-C(8)-O(8)	-133(8)	C(41)-Si(2)-C(51)-C(56)	141.3(5)
C(9)-Mn(2)-C(8)-O(8)	-61(9)	Mn(2)-Si(2)-C(51)-C(56)	20.7(5)
Si(2)-Mn(2)-C(8)-O(8)	-149(9)	C(61)-Si(2)-C(51)-C(52)	74.8(4)
C(7)-Mn(2)-C(9)-O(9)	107(27)	C(41)-Si(2)-C(51)-C(52)	-42.3(5)
C(8)-Mn(2)-C(9)-O(9)	50(27)	Mn(2)-Si(2)-C(51)-C(52)	-162.9(4)
C(10)-Mn(2)-C(9)-O(9)	-43(27)	C(56)-C(51)-C(52)-C(53)	0.1(8)
C(6)-Mn(2)-C(9)-O(9)	-137(27)	Si(2)-C(51)-C(52)-C(53)	-176.6(5)
Si(2)-Mn(2)-C(9)-O(9)	139(27)	C(51)-C(52)-C(53)-C(54)	-1.2(10)
C(7)-Mn(2)-C(10)-O(10)	58(100)	C(52)-C(53)-C(54)-C(55)	1.4(11)
C(8)-Mn(2)-C(10)-O(10)	147(100)	C(53)-C(54)-C(55)-C(56)	-0.6(11)
C(6)-Mn(2)-C(10)-O(10)	-35(100)	C(52)-C(51)-C(56)-C(55)	0.7(8)
C(9)-Mn(2)-C(10)-O(10)	-126(100)	Si(2)-C(51)-C(56)-C(55)	177.1(5)
Si(2)-Mn(2)-C(10)-O(10)	13(100)	C(54)-C(55)-C(56)-C(51)	-0.6(10)
C(61)-Si(2)-C(41)-C(42)	-172.6(4)	C(41)-Si(2)-C(61)-C(66)	-50.8(5)
C(51)-Si(2)-C(41)-C(42)	-59.5(5)	C(51)-Si(2)-C(61)-C(66)	-163.0(4)
Mn(2)-Si(2)-C(41)-C(42)	64.9(4)	Mn(2)-Si(2)-C(61)-C(66)	71.5(5)
C(61)-Si(2)-C(41)-C(46)	7.2(5)	C(41)-Si(2)-C(61)-C(62)	132.3(4)
C(51)-Si(2)-C(41)-C(46)	120.3(5)	C(51)-Si(2)-C(61)-C(62)	20.1(5)
Mn(2)-Si(2)-C(41)-C(46)	-115.3(4)	Mn(2)-Si(2)-C(61)-C(62)	-105.5(4)
C(46)-C(41)-C(42)-C(43)	1.5(8)	C(66)-C(61)-C(62)-C(63)	-0.9(8)
Si(2)-C(41)-C(42)-C(43)	-178.7(4)	Si(2)-C(61)-C(62)-C(63)	176.2(5)
C(41)-C(42)-C(43)-C(44)	-0.7(9)	C(61)-C(62)-C(63)-C(64)	0.9(10)
C(42)-C(43)-C(44)-C(45)	-0.1(10)	C(62)-C(63)-C(64)-C(65)	-0.5(10)
C(43)-C(44)-C(45)-C(46)	0.1(12)	C(63)-C(64)-C(65)-C(66)	0.3(10)
C(44)-C(45)-C(46)-C(41)	0.8(11)	C(64)-C(65)-C(66)-C(61)	-0.4(9)
C(42)-C(41)-C(46)-C(45)	-1.5(8)	C(62)-C(61)-C(66)-C(65)	0.7(8)
Si(2)-C(41)-C(46)-C(45)	178.7(5)	Si(2)-C(61)-C(66)-C(65)	-176.3(4)
C(61)-Si(2)-C(51)-C(56)	-101.5(5)		

Table A2.4: Anisotropic thermal factors (10^2 Å^2) for $Ph_3SiMn(CO)_5$.

	U_{11}	U_{22}	U_{33}	U_{12}	U_{13}	U_{23}
Mn(1)	4.07(5)	3.93(5)	4.32(6)	1.35(4)	0.90(4)	0.51(4)
Si(1)	3.85(9)	3.30(9)	3.31(9)	0.59(7)	0.24(7)	0.02(7)
O(1)	9.3(4)	5.6(3)	11.2(4)	3.9(3)	5.1(3)	2.6(3)
O(2)	6.9(3)	9.9(4)	5.7(3)	-0.7(3)	-0.7(2)	-1.3(3)
O(3)	6.2(3)	4.9(3)	9.5(3)	3.6(3)	1.1(2)	0.9(2)
O(4)	7.5(4)	11.0(4)	9.1(4)	2.9(3)	-3.1(3)	1.5(3)
O(5)	7.1(3)	7.5(3)	7.2(3)	1.8(3)	3.5(3)	0.9(2)
C(1)	5.6(4)	5.9(4)	6.4(4)	2.0(4)	2.7(3)	1.7(3)
C(2)	5.3(4)	5.3(4)	4.2(4)	0.3(3)	1.3(3)	0.1(3)
C(3)	4.0(3)	5.0(4)	4.2(4)	0.9(3)	0.5(3)	0.0(3)
C(4)	5.4(4)	6.1(4)	6.7(5)	2.0(4)	0.6(4)	1.6(3)
C(5)	4.8(4)	5.1(4)	6.1(4)	1.8(3)	1.1(3)	0.5(3)
C(11)	3.6(3)	3.7(3)	3.8(3)	-0.1(3)	0.5(3)	0.3(3)
C(12)	4.5(4)	5.0(4)	7.8(5)	1.8(3)	0.3(3)	0.0(3)
C(13)	4.6(5)	6.2(5)	13.1(7)	1.1(5)	1.0(4)	-1.0(4)
C(14)	4.5(5)	8.6(6)	10.0(6)	-1.0(5)	-1.7(4)	1.4(4)
C(15)	6.3(5)	7.9(5)	6.1(5)	0.6(4)	-0.8(4)	2.3(4)
C(16)	4.8(4)	6.6(4)	4.1(4)	1.3(3)	0.2(3)	1.4(3)
C(21)	3.6(3)	3.4(3)	4.2(3)	0.9(3)	0.3(3)	0.2(2)
C(22)	5.3(4)	5.1(4)	3.6(3)	0.8(3)	0.3(3)	-0.4(3)
C(23)	6.7(4)	4.6(4)	7.5(5)	2.6(4)	1.0(4)	-0.5(3)
C(24)	8.4(5)	6.5(5)	7.2(5)	3.4(4)	0.3(4)	0.7(4)
C(25)	10.3(6)	8.1(5)	3.6(4)	2.2(4)	0.0(4)	1.5(4)
C(26)	6.5(4)	4.6(4)	5.2(4)	1.3(3)	-0.6(3)	-0.2(3)
C(31)	5.2(4)	4.3(4)	3.5(3)	1.5(3)	0.4(3)	0.0(3)
C(32)	6.4(5)	4.7(4)	8.6(5)	-0.9(4)	1.1(4)	-0.6(3)
C(33)	9.4(6)	6.7(5)	8.7(6)	-0.8(4)	0.5(5)	-2.7(5)
C(34)	13.4(8)	4.0(4)	6.4(5)	-0.1(4)	0.7(5)	-1.6(5)
C(35)	10.4(6)	5.1(5)	6.6(5)	0.4(4)	1.5(4)	3.0(4)
C(36)	6.4(4)	5.1(4)	4.7(4)	0.6(3)	0.3(3)	0.9(3)
Mn(2)	3.75(5)	4.81(6)	5.11(6)	2.01(5)	0.04(4)	0.08(4)
Si(2)	3.92(9)	3.81(9)	3.51(9)	0.74(8)	0.22(7)	0.56(7)
O(6)	6.4(3)	5.6(3)	7.6(3)	2.9(3)	1.0(2)	-0.2(2)
O(7)	11.5(4)	14.9(5)	8.8(4)	5.4(4)	5.5(3)	2.5(4)
O(8)	8.1(3)	5.7(3)	15.0(5)	4.9(3)	-2.9(3)	-1.6(3)
O(9)	7.9(4)	11.4(4)	6.0(3)	-1.2(3)	2.1(3)	0.3(3)
O(10)	5.4(3)	8.1(3)	9.8(4)	2.9(3)	-2.5(3)	-0.4(3)
C(6)	4.0(3)	6.4(4)	3.9(4)	1.5(3)	0.2(3)	0.0(3)
C(7)	5.1(4)	8.0(5)	7.5(5)	3.9(4)	0.9(4)	1.3(4)
C(8)	4.1(4)	6.2(5)	8.5(5)	2.7(4)	-1.5(3)	-0.9(3)
C(9)	4.9(4)	5.8(4)	6.1(5)	0.8(4)	-0.2(3)	-0.1(3)
C(10)	4.4(4)	5.0(4)	7.5(5)	2.1(4)	0.4(3)	0.3(3)
C(41)	3.7(3)	4.2(3)	3.5(3)	0.0(3)	-0.5(3)	-0.2(3)
C(42)	4.5(4)	6.1(4)	5.9(4)	1.0(3)	0.9(3)	-0.4(3)
C(43)	6.6(5)	7.9(5)	5.8(5)	1.1(4)	0.7(4)	-1.5(4)
C(44)	7.7(6)	8.2(6)	9.2(6)	-1.4(5)	4.0(5)	-1.7(5)
C(45)	6.7(5)	8.4(6)	14.2(8)	1.1(6)	4.2(5)	2.7(5)
C(46)	5.4(4)	7.2(5)	8.2(5)	2.3(4)	1.8(4)	1.4(4)
C(51)	6.1(4)	3.9(3)	3.7(3)	1.4(3)	1.6(3)	0.5(3)

C(52)	7.5(5)	4.1(4)	5.9(4)	-0.4(3)	1.0(4)	-1.0(3)
C(53)	12.1(7)	5.7(5)	5.8(5)	-0.7(4)	0.9(4)	-3.2(5)
C(54)	17.5(9)	4.2(5)	5.8(5)	0.2(4)	2.9(6)	1.6(6)
C(55)	14.2(8)	7.5(6)	6.4(5)	2.3(5)	3.7(5)	5.8(5)
C(56)	9.4(5)	6.7(5)	4.7(4)	1.5(4)	1.5(4)	2.9(4)
C(61)	4.3(3)	4.3(4)	4.0(4)	1.2(3)	-0.4(3)	0.3(3)
C(62)	8.2(5)	4.5(4)	5.0(4)	1.6(3)	1.4(3)	1.1(3)
C(63)	10.1(6)	7.8(5)	5.0(4)	3.0(4)	2.1(4)	1.9(4)
C(64)	10.0(6)	7.9(6)	7.6(5)	5.7(5)	0.9(4)	1.9(4)
C(65)	7.5(5)	5.6(4)	8.1(5)	2.3(4)	1.1(4)	1.7(4)
C(66)	6.1(4)	5.3(4)	4.9(4)	1.4(3)	0.1(3)	1.0(3)

Structural Data for

Bis[(pentacarbonyl)manganese]diphenyltin

$[(CO)_5Mn]_2SnPh_2$

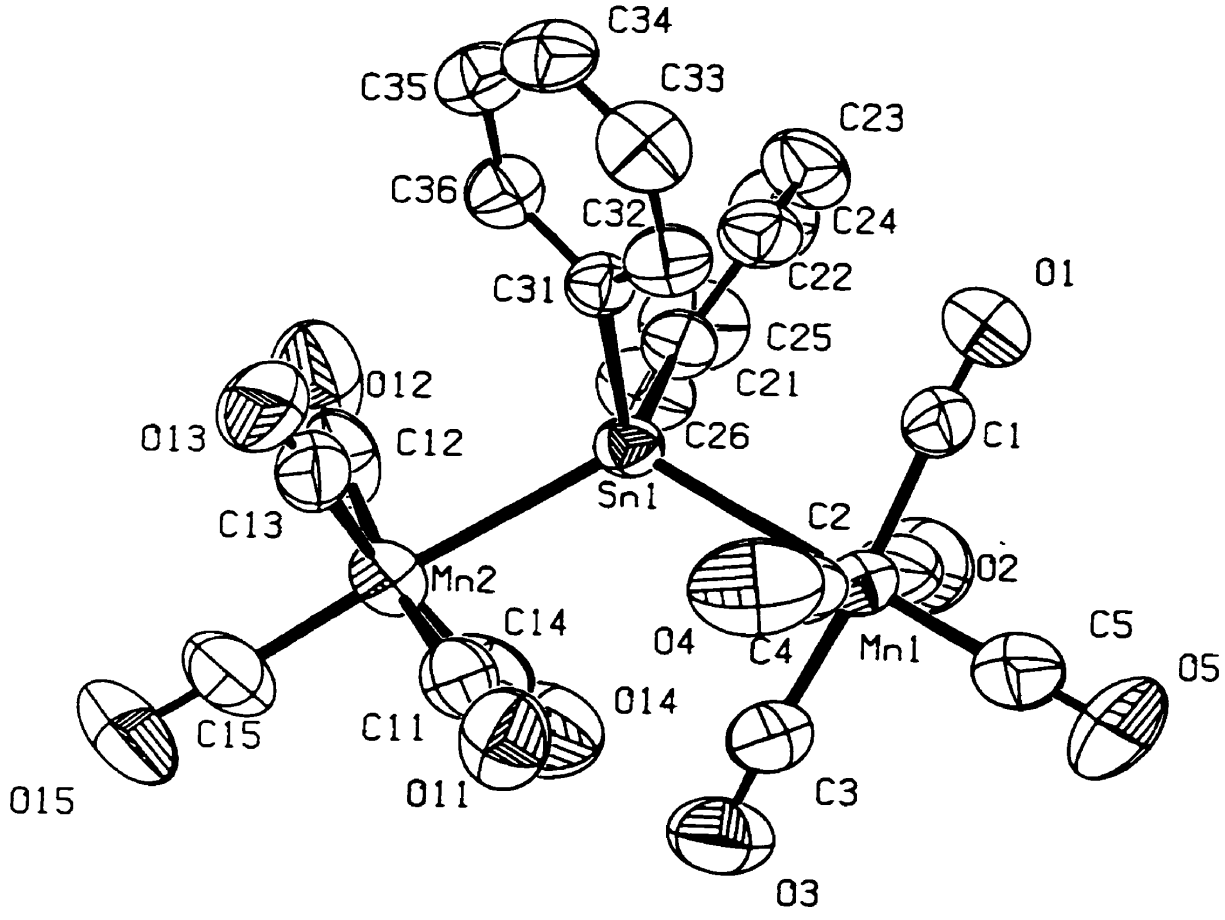

Crystallographic data for $[(CO)_5Mn]_2SnPh_2$

Empirical Formula: C22 H10 O10 Sn Mn2

Space group: Monoclinic, P $2_1/a$

Cell dimensions:

$a = 15.352\ (7)$Å

$b = 9.696\ (3)$Å

$c = 16.742\ (7)$Å

$\alpha = 90°$

$\beta = 93.48\ (4)°$

$\gamma = 90°$

Volume = 2488 (2)Å^3

FW = 662.87

Z = 4

$D_{calc} = 1.770$ g / cm^3

F(000) = 1288

Mo Kα radiation

$\lambda = 0.70930$ Å

Cell parameters from 18 reflections

$2\theta = 28 - 32°$

$\mu = 2.048$ mm^{-1}

T = 293 (2) °K

Colourless plate

0.35 × 0.40 × 0.20 mm

Data collection

Rigaku AFC –6S diffractometer

ω / 2θ scans

Absorption correction: *psi scans*

$T_{min} = 0.69$, $T_{max} = 1.0$

8907 measured reflections

4398 independent reflections

2961 observed reflections [$I > 2\sigma(I)$]

$R_{int} = 0.087$

$\theta_{max} = 25.0°$

$h = -18 \rightarrow 18$

$k = 0 \rightarrow 11$

$l = -19 \rightarrow 19$

3 standard reflections were monitored every 200 reflections

Intensity decay: 0.016 %

Structure was solved by the Patterson method.

Refinement

Refinement on F^2	317 parameters
$R(F^2 > 2\sigma(F^2)) = 0.0485$	H atoms riding,
$wR(F^2) = 0.1027$	C–H = 0.93 Å
GoF = 1.036	$(\Delta/\sigma) = 0.001$
57 atoms	$\Delta\rho_{max} = 0.803$ e/Å^3
4398 reflections	$\Delta\rho_{min} = -0.653$ e/Å^3

where

$$R = \Sigma(Fo-Fc) / \Sigma Fo$$

$$wR = [\Sigma(w(Fo^2-Fc^2)^2) / \Sigma[w(Fo^2)^2]]^{1/2}$$

$$GoF = [\Sigma(w(Fo^2-Fc^2)^2) / (\text{No. of refins - No. of params.})]^{1/2}$$

Table A2.5: Fractional atomic coordinates and equivalent isotropic displacement parameters (10^2 Å) for $[(CO)_5Mn]_2SnPh_2$.

	x	y	z	U_{eq}
Sn(1)	0.34122(3)	0.01046(4)	0.25169(2)	4.57(2)
Mn(1)	0.22224(7)	0.17659(11)	0.17334(6)	6.39(3)
Mn(2)	0.42402(7)	-0.17623(10)	0.16297(6)	6.28(3)
O(1)	0.2307(4)	0.3377(6)	0.3260(3)	9.1(2)
O(2)	0.0919(4)	-0.0195(7)	0.2332(4)	11.1(2)
O(3)	0.2185(4)	0.0047(7)	0.0269(3)	10.6(2)
O(4)	0.3737(5)	0.3396(7)	0.1209(4)	11.9(2)
O(5)	0.0858(6)	0.3520(9)	0.0951(5)	20.1(5)
O(11)	0.2453(5)	-0.2767(8)	0.1149(4)	12.6(2)
O(12)	0.4264(5)	-0.3530(7)	0.3084(4)	13.3(3)
O(13)	0.5941(4)	-0.0609(7)	0.2267(4)	10.1(2)
O(14)	0.4150(3)	0.0459(6)	0.0398(3)	9.4(2)
O(15)	0.5128(5)	-0.3778(7)	0.0615(4)	13.4(3)
C(1)	0.2284(5)	0.2750(8)	0.2697(4)	6.7(2)
C(2)	0.1419(5)	0.0563(10)	0.2119(5)	8.3(2)
C(3)	0.2233(5)	0.0711(9)	0.0834(5)	7.7(2)
C(4)	0.3148(6)	0.2748(8)	0.1392(4)	8.2(2)
C(5)	0.1385(7)	0.2862(11)	0.1262(5)	11.1(3)
C(11)	0.3140(6)	-0.2387(9)	0.1326(4)	8.1(2)
C(12)	0.4253(5)	-0.2863(8)	0.2520(5)	8.5(2)
C(13)	0.5279(5)	-0.1030(8)	0.2026(4)	7.3(2)
C(14)	0.4185(4)	-0.0404(8)	0.0862(4)	6.6(2)
C(15)	0.4781(6)	-0.3006(9)	0.1000(5)	9.2(3)
C(21)	0.2713(4)	-0.0905(6)	0.3447(3)	5.1(2)
C(22)	0.2566(4)	-0.0182(6)	0.4136(4)	5.7(2)
C(23)	0.2062(5)	-0.0725(8)	0.4718(4)	7.1(2)
C(24)	0.1685(5)	-0.1984(8)	0.4624(5)	8.2(2)
C(25)	0.1815(5)	-0.2716(8)	0.3952(5)	8.6(2)
C(26)	0.2331(5)	-0.2195(8)	0.3359(4)	7.6(2)
C(31)	0.4364(4)	0.1263(6)	0.3255(3)	4.78(14)
C(32)	0.4504(4)	0.2674(7)	0.3250(4)	6.1(2)
C(33)	0.5109(5)	0.3301(7)	0.3782(5)	7.4(2)
C(34)	0.5603(4)	0.2525(8)	0.4321(4)	7.0(2)
C(35)	0.5491(4)	0.1136(8)	0.4332(4)	6.6(2)
C(36)	0.4876(4)	0.0487(7)	0.3811(4)	5.7(2)

Table A2.6: Bond lengths (Å) and angles (°) for $[(CO)_5Mn]_2SnPh_2$.

Sn(1)-C(31)	2.169(6)	Sn(1)-C(21)	2.178(6)
Sn(1)-Mn(2)	2.7071(13)	Sn(1)-Mn(1)	2.7130(14)
Mn(1)-C(5)	1.812(9)	Mn(1)-C(3)	1.822(8)
Mn(1)-C(4)	1.831(10)	Mn(1)-C(2)	1.843(9)
Mn(1)-C(1)	1.872(8)	Mn(2)-C(13)	1.833(9)
Mn(2)-C(12)	1.833(9)	Mn(2)-C(15)	1.833(8)
Mn(2)-C(11)	1.837(8)	Mn(2)-C(14)	1.839(8)
O(1)-C(1)	1.121(7)	O(2)-C(2)	1.135(9)
O(3)-C(3)	1.143(8)	O(4)-C(4)	1.156(9)
O(5)-C(5)	1.132(9)	O(11)-C(11)	1.138(9)
O(12)-C(12)	1.143(8)	O(13)-C(13)	1.145(8)
O(14)-C(14)	1.140(8)	O(15)-C(15)	1.141(8)
C(21)-C(22)	1.379(8)	C(21)-C(26)	1.385(9)
C(22)-C(23)	1.385(8)	C(23)-C(24)	1.356(10)
C(24)-C(25)	1.355(10)	C(25)-C(26)	1.401(9)
C(31)-C(32)	1.385(8)	C(31)-C(36)	1.401(8)
C(32)-C(33)	1.388(9)	C(33)-C(34)	1.369(9)
C(34)-C(35)	1.358(10)	C(35)-C(36)	1.395(8)

C(31)-Sn(1)-C(21)	99.8(2)	C(31)-Sn(1)-Mn(2)	109.6(2)
C(21)-Sn(1)-Mn(2)	111.1(2)	C(31)-Sn(1)-Mn(1)	112.3(2)
C(21)-Sn(1)-Mn(1)	105.4(2)	Mn(2)-Sn(1)-Mn(1)	117.16(4)
C(5)-Mn(1)-C(3)	90.6(4)	C(5)-Mn(1)-C(4)	95.9(4)
C(3)-Mn(1)-C(4)	89.3(3)	C(5)-Mn(1)-C(2)	93.0(4)
C(3)-Mn(1)-C(2)	88.5(4)	C(4)-Mn(1)-C(2)	170.9(4)
C(5)-Mn(1)-C(1)	94.2(3)	C(3)-Mn(1)-C(1)	175.1(3)
C(4)-Mn(1)-C(1)	90.2(3)	C(2)-Mn(1)-C(1)	91.2(3)
C(5)-Mn(1)-Sn(1)	176.4(3)	C(3)-Mn(1)-Sn(1)	91.5(2)
C(4)-Mn(1)-Sn(1)	87.0(2)	C(2)-Mn(1)-Sn(1)	84.3(3)
C(1)-Mn(1)-Sn(1)	83.6(2)	C(13)-Mn(2)-C(12)	88.0(4)
C(13)-Mn(2)-C(15)	92.8(4)	C(12)-Mn(2)-C(15)	95.8(3)
C(13)-Mn(2)-C(11)	173.3(3)	C(12)-Mn(2)-C(11)	89.9(4)
C(15)-Mn(2)-C(11)	93.7(4)	C(13)-Mn(2)-C(14)	88.7(3)
C(12)-Mn(2)-C(14)	169.6(3)	C(15)-Mn(2)-C(14)	94.1(3)
C(11)-Mn(2)-C(14)	92.3(3)	C(13)-Mn(2)-Sn(1)	88.3(2)
C(12)-Mn(2)-Sn(1)	85.7(2)	C(15)-Mn(2)-Sn(1)	178.2(3)
C(11)-Mn(2)-Sn(1)	85.3(2)	C(14)-Mn(2)-Sn(1)	84.3(2)
O(1)-C(1)-Mn(1)	177.6(6)	O(2)-C(2)-Mn(1)	177.8(7)
O(3)-C(3)-Mn(1)	175.7(7)	O(4)-C(4)-Mn(1)	177.0(7)
O(5)-C(5)-Mn(1)	178.0(9)	O(11)-C(11)-Mn(2)	179.0(7)
O(12)-C(12)-Mn(2)	178.8(8)	O(13)-C(13)-Mn(2)	177.9(7)
O(14)-C(14)-Mn(2)	178.5(7)	O(15)-C(15)-Mn(2)	179.1(8)
C(22)-C(21)-C(26)	117.3(6)	C(22)-C(21)-Sn(1)	118.8(4)
C(26)-C(21)-Sn(1)	123.6(5)	C(21)-C(22)-C(23)	121.4(6)
C(24)-C(23)-C(22)	120.9(7)	C(25)-C(24)-C(23)	119.0(7)
C(24)-C(25)-C(26)	121.1(7)	C(21)-C(26)-C(25)	120.2(7)
C(32)-C(31)-C(36)	117.0(6)	C(32)-C(31)-Sn(1)	127.4(5)
C(36)-C(31)-Sn(1)	115.6(4)	C(31)-C(32)-C(33)	121.8(6)
C(34)-C(33)-C(32)	120.3(6)	C(35)-C(34)-C(33)	119.2(7)
C(34)-C(35)-C(36)	121.4(7)	C(35)-C(36)-C(31)	120.3(6)

Table A2.7: Torsion angles (in degrees) for $[(CO)_5Mn]_2SnPh_2$.

C(31)-Sn(1)-Mn(1)-C(5)	-92(5)	C(21)-Sn(1)-Mn(1)-C(5)	15(5)
Mn(2)-Sn(1)-Mn(1)-C(5)	140(5)	C(31)-Sn(1)-Mn(1)-C(3)	140.3(3)
C(21)-Sn(1)-Mn(1)-C(3)	-112.1(3)	Mn(2)-Sn(1)-Mn(1)-C(3)	12.1(3)
C(31)-Sn(1)-Mn(1)-C(4)	51.1(3)	C(21)-Sn(1)-Mn(1)-C(4)	158.7(3)
Mn(2)-Sn(1)-Mn(1)-C(4)	-77.1(2)	C(31)-Sn(1)-Mn(1)-C(2)	-131.4(3)
C(21)-Sn(1)-Mn(1)-C(2)	-23.7(3)	Mn(2)-Sn(1)-Mn(1)-C(2)	100.5(2)
C(31)-Sn(1)-Mn(1)-C(1)	-39.5(3)	C(21)-Sn(1)-Mn(1)-C(1)	68.2(3)
Mn(2)-Sn(1)-Mn(1)-C(1)	-167.7(2)	C(31)-Sn(1)-Mn(2)-C(13)	-4.9(3)
C(21)-Sn(1)-Mn(2)-C(13)	-114.2(3)	Mn(1)-Sn(1)-Mn(2)-C(13)	124.5(2)
C(31)-Sn(1)-Mn(2)-C(12)	83.2(3)	C(21)-Sn(1)-Mn(2)-C(12)	-26.1(3)
Mn(1)-Sn(1)-Mn(2)-C(12)	-147.4(3)	C(31)-Sn(1)-Mn(2)-C(15)	-129(9)
C(21)-Sn(1)-Mn(2)-C(15)	122(9)	Mn(1)-Sn(1)-Mn(2)-C(15)	1(9)
C(31)-Sn(1)-Mn(2)-C(11)	173.5(3)	C(21)-Sn(1)-Mn(2)-C(11)	64.1(3)
Mn(1)-Sn(1)-Mn(2)-C(11)	-57.1(3)	C(31)-Sn(1)-Mn(2)-C(14)	-93.8(3)
C(21)-Sn(1)-Mn(2)-C(14)	156.9(3)	Mn(1)-Sn(1)-Mn(2)-C(14)	35.6(2)
C(5)-Mn(1)-C(1)-O(1)	-17(16)	C(3)-Mn(1)-C(1)-O(1)	163(14)
C(4)-Mn(1)-C(1)-O(1)	79(16)	C(2)-Mn(1)-C(1)-O(1)	-110(16)
Sn(1)-Mn(1)-C(1)-O(1)	166(16)	C(5)-Mn(1)-C(2)-O(2)	74(21)
C(3)-Mn(1)-C(2)-O(2)	-16(21)	C(4)-Mn(1)-C(2)-O(2)	-92(20)
C(1)-Mn(1)-C(2)-O(2)	169(21)	Sn(1)-Mn(1)-C(2)-O(2)	-108(21)
C(5)-Mn(1)-C(3)-O(3)	-48(10)	C(4)-Mn(1)-C(3)-O(3)	-144(10)
C(2)-Mn(1)-C(3)-O(3)	45(10)	C(1)-Mn(1)-C(3)-O(3)	132(9)
Sn(1)-Mn(1)-C(3)-O(3)	130(10)	C(5)-Mn(1)-C(4)-O(4)	100(15)
C(3)-Mn(1)-C(4)-O(4)	-170(15)	C(2)-Mn(1)-C(4)-O(4)	-94(15)
C(1)-Mn(1)-C(4)-O(4)	5(15)	Sn(1)-Mn(1)-C(4)-O(4)	-78(15)
C(3)-Mn(1)-C(5)-O(5)	14(30)	C(4)-Mn(1)-C(5)-O(5)	103(30)
C(2)-Mn(1)-C(5)-O(5)	-75(30)	C(1)-Mn(1)-C(5)-O(5)	-166(30)
Sn(1)-Mn(1)-C(5)-O(5)	-114(28)	C(13)-Mn(2)-C(11)-O(11)	-15(52)
C(12)-Mn(2)-C(11)-O(11)	57(50)	C(15)-Mn(2)-C(11)-O(11)	152(50)
C(14)-Mn(2)-C(11)-O(11)	-113(50)	Sn(1)-Mn(2)-C(11)-O(11)	-29(50)
C(13)-Mn(2)-C(12)-O(12)	52(38)	C(15)-Mn(2)-C(12)-O(12)	144(38)
C(11)-Mn(2)-C(12)-O(12)	-122(38)	C(14)-Mn(2)-C(12)-O(12)	-20(40)
Sn(1)-Mn(2)-C(12)-O(12)	-37(38)	C(12)-Mn(2)-C(13)-O(13)	75(19)
C(15)-Mn(2)-C(13)-O(13)	-21(19)	C(11)-Mn(2)-C(13)-O(13)	146(17)
C(14)-Mn(2)-C(13)-O(13)	-115(19)	Sn(1)-Mn(2)-C(13)-O(13)	161(19)
C(13)-Mn(2)-C(14)-O(14)	-63(24)	C(12)-Mn(2)-C(14)-O(14)	9(25)
C(15)-Mn(2)-C(14)-O(14)	-155(24)	C(11)-Mn(2)-C(14)-O(14)	111(24)
Sn(1)-Mn(2)-C(14)-O(14)	26(24)	C(13)-Mn(2)-C(15)-O(15)	24(55)
C(12)-Mn(2)-C(15)-O(15)	-64(55)	C(11)-Mn(2)-C(15)-O(15)	-154(55)
C(14)-Mn(2)-C(15)-O(15)	113(55)	Sn(1)-Mn(2)-C(15)-O(15)	148(49)
C(31)-Sn(1)-C(21)-C(22)	37.8(5)	Mn(2)-Sn(1)-C(21)-C(22)	153.4(4)
Mn(1)-Sn(1)-C(21)-C(22)	-78.7(5)	C(31)-Sn(1)-C(21)-C(26)	-148.6(6)
Mn(2)-Sn(1)-C(21)-C(26)	-33.0(6)	Mn(1)-Sn(1)-C(21)-C(26)	94.9(6)
C(26)-C(21)-C(22)-C(23)	0.3(10)	Sn(1)-C(21)-C(22)-C(23)	174.3(5)
C(21)-C(22)-C(23)-C(24)	-0.7(11)	C(22)-C(23)-C(24)-C(25)	0.5(12)
C(23)-C(24)-C(25)-C(26)	0.3(13)	C(22)-C(21)-C(26)-C(25)	0.4(11)
Sn(1)-C(21)-C(26)-C(25)	-173.3(6)	C(24)-C(25)-C(26)-C(21)	-0.7(13)
C(21)-Sn(1)-C(31)-C(32)	-123.1(5)	Mn(2)-Sn(1)-C(31)-C(32)	120.1(5)
Mn(1)-Sn(1)-C(31)-C(32)	-11.9(6)	C(21)-Sn(1)-C(31)-C(36)	55.0(5)
Mn(2)-Sn(1)-C(31)-C(36)	-61.8(5)	Mn(1)-Sn(1)-C(31)-C(36)	166.2(4)
C(36)-C(31)-C(32)-C(33)	-1.2(9)	Sn(1)-C(31)-C(32)-C(33)	176.9(5)

C(31)-C(32)-C(33)-C(34)	1.3(10)	C(32)-C(33)-C(34)-C(35)	-0.3(11)
C(33)-C(34)-C(35)-C(36)	-0.7(11)	C(34)-C(35)-C(36)-C(31)	0.8(10)
C(32)-C(31)-C(36)-C(35)	0.2(9)	Sn(1)-C(31)-C(36)-C(35)	-178.1(5)

Table A2.8: Anisotropic thermal factors (10^2 Å^2) for $[(CO)_5Mn]_2SnPh_2$.

	U_{11}	U_{22}	U_{33}	U_{12}	U_{13}	U_{23}
Sn(1)	4.55(2)	5.00(3)	4.17(2)	0.12(2)	0.45(2)	-0.15(2)
Mn(1)	6.03(6)	8.51(8)	4.57(6)	0.02(5)	-0.20(5)	1.93(6)
Mn(2)	6.64(7)	6.21(7)	6.10(7)	-0.86(5)	1.27(5)	0.57(5)
O(1)	10.1(4)	10.4(4)	6.7(3)	-1.9(3)	0.9(3)	2.1(3)
O(2)	6.3(4)	16.3(6)	10.8(5)	-2.2(4)	1.4(3)	-2.4(4)
O(3)	9.1(4)	14.9(6)	7.6(4)	-3.3(4)	-0.4(3)	0.1(4)
O(4)	14.8(6)	11.7(5)	9.1(4)	3.0(4)	0.9(4)	-3.6(5)
O(5)	22.9(9)	23.6(10)	12.8(6)	-0.7(6)	-6.8(6)	16.4(8)
O(11)	10.8(5)	15.7(6)	11.3(5)	-3.5(4)	0.6(4)	-5.1(5)
O(12)	16.1(6)	11.0(5)	13.3(6)	5.3(4)	5.5(5)	5.3(5)
O(13)	6.6(4)	13.3(5)	10.2(5)	-0.2(4)	-0.7(3)	0.7(4)
O(14)	7.7(4)	11.5(5)	9.2(4)	2.6(4)	3.0(3)	1.0(3)
O(15)	16.3(6)	12.8(5)	11.4(5)	-4.9(5)	3.4(5)	4.2(5)
C(1)	6.7(5)	8.3(5)	5.2(4)	0.8(4)	0.5(4)	2.0(4)
C(2)	5.1(4)	13.8(7)	6.0(5)	-1.8(5)	0.2(4)	-0.2(5)
C(3)	6.7(5)	10.8(6)	5.7(5)	-0.5(4)	-0.5(4)	1.5(4)
C(4)	12.0(7)	6.9(5)	5.4(5)	1.1(4)	-1.0(5)	0.3(5)
C(5)	14.0(9)	13.1(8)	6.1(5)	-0.6(5)	-0.8(5)	5.5(7)
C(11)	8.4(6)	9.4(6)	6.6(5)	-2.2(4)	1.2(4)	-2.2(5)
C(12)	9.6(6)	6.5(5)	9.8(6)	0.2(5)	3.3(5)	2.1(4)
C(13)	6.9(5)	8.1(5)	6.9(5)	0.5(4)	1.1(4)	1.6(4)
C(14)	5.0(4)	8.4(5)	6.4(5)	0.0(4)	1.9(4)	0.2(4)
C(15)	11.6(7)	8.9(6)	7.2(5)	-1.9(5)	2.4(5)	1.3(5)
C(21)	5.3(4)	5.6(4)	4.6(4)	0.9(3)	1.1(3)	-0.1(3)
C(22)	6.8(4)	5.8(4)	4.6(4)	0.4(3)	0.5(3)	-0.1(3)
C(23)	9.5(6)	7.2(5)	5.0(4)	0.9(4)	2.5(4)	1.0(4)
C(24)	8.0(5)	9.5(6)	7.6(6)	3.1(5)	3.3(4)	0.9(5)
C(25)	9.2(6)	7.9(5)	8.8(6)	1.8(5)	1.9(5)	-3.5(5)
C(26)	7.8(5)	7.9(5)	7.2(5)	-0.1(4)	2.2(4)	-2.3(4)
C(31)	4.9(3)	5.1(4)	4.3(3)	0.3(3)	0.3(3)	0.1(3)
C(32)	6.5(4)	6.4(4)	5.3(4)	0.9(3)	0.5(3)	-1.0(4)
C(33)	8.0(5)	5.6(4)	8.9(6)	-0.4(4)	1.1(4)	-2.1(4)
C(34)	5.5(4)	9.3(6)	6.1(5)	-0.4(4)	-0.4(4)	-2.6(4)
C(35)	5.8(4)	8.0(5)	5.9(4)	0.3(4)	-0.7(3)	-0.7(4)
C(36)	5.9(4)	5.4(4)	5.8(4)	0.3(3)	0.1(3)	-0.2(3)

Structural Data for

Tris(*p*-tolyl)tin(pentacarbonyl)manganese(I)

$(p\text{-}CH_3C_6H_4)_3SnMn(CO)_5$

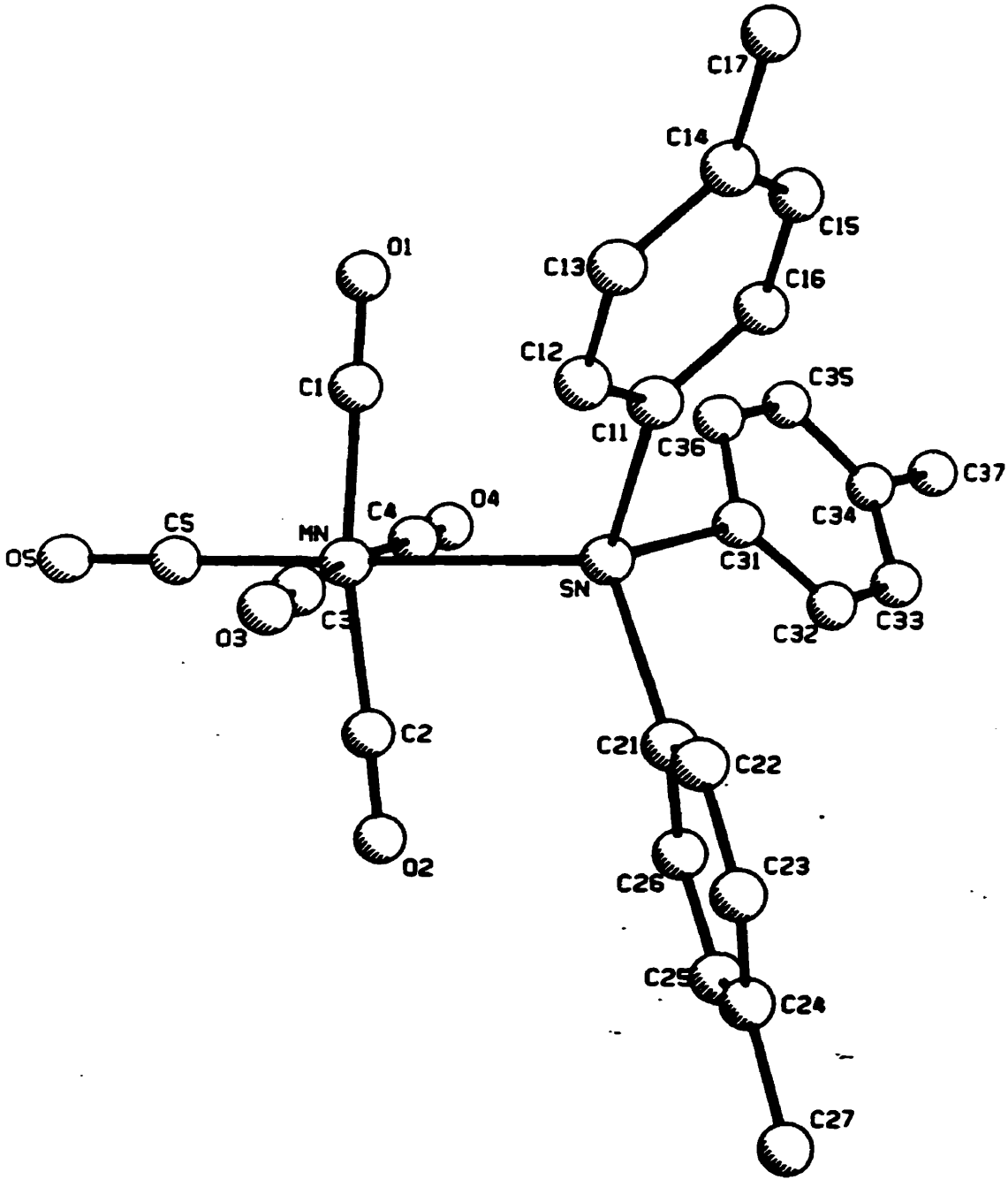

Crystal data for $(p\text{-}CH_3C_6H_4)_2SnMn(CO)_5$

Empirical Formula: C26 H21 O5 Sn Mn

Space group: Triclinic, P 1

Cell dimensions:

$a = 8.815\ (2)$Å

$b = 11.160\ (3)$Å

$c = 13.689\ (2)$Å

$\alpha = 98.28\ (2)°$

$\beta = 91.11\ (2)°$

$\gamma = 106.31\ (2)°$

Volume = 1276.4 (4)Å^3

FW = 587.06

Z = 2

$D_{calc} = 1.527$ g / cm^3

F(000) = 584

Mo Kα radiation

$\lambda = 0.70930$ Å

Cell parameters from 25 reflections

$2\theta = 28 - 35°$

$\mu = 1.505$ mm^{-1}

T = 295 (2) °K

Colourless block

0.36 × 0.18 × 0.13 mm

Data collection

Rigaku AFC –6S diffractometer

ω / 2θ scans

Absorption correction: *Azimuthal scans*

$T_{min} = 0.67$, $T_{max} = 0.71$

9016 measured reflections

4508 independent reflections

3314 observed reflections [$I > 2\sigma(I)$]

$R_{int} = 0.0250$

$\theta_{max} = 50.0°$

$h = -10 \rightarrow 10$

$k = -13 \rightarrow 13$

$l = -16 \rightarrow 16$

3 standard reflections were monitored every 200 reflections

Intensity decay: 0.9 %

Structure was solved by the Patterson method.

Refinement

Refinement on F^2	302 parameters
$R(F^2 > 2\sigma(F^2)) = 0.040$	H atoms riding,
$wR(F^2) = 0.0723$	C–H = 0.93 - 0.97 Å
GoF = 1.044	$(\Delta/\sigma) = 0.005$
54 atoms	$\Delta\rho_{max} = 0.396$ e/Å^3
4508 reflections	$\Delta\rho_{min} = -0.399$ e/Å^3

where

$R = \Sigma(Fo-Fc) / \Sigma Fo$

$wR = [\Sigma(w(Fo-Fc)^2) / \Sigma wFo^2]^{1/2}$

GoF = [Σ(w(Fo-Fc)^2) / (No. of refins - No. of params.)

Table A2.9: Fractional atomic coordinates and equivalent isotropic displacement parameters (10^2 Å) for $(p\text{-}CH_3C_6H_5)_3SnMn(CO)_5$.

	x	y	z	U_{eq}
Sn	0.09138(4)	-0.18048(3)	0.21038(2)	5.175(13)
Mn	-0.19778(8)	-0.34927(6)	0.18056(5)	6.03(2)
O(1)	-0.1482(5)	-0.3754(4)	0.3908(3)	10.91(14)
O(2)	-0.0193(5)	-0.5341(4)	0.1132(3)	10.53(14)
O(3)	-0.2033(5)	-0.2839(5)	-0.0225(3)	11.6(2)
O(4)	-0.3382(4)	-0.1398(4)	0.2472(3)	9.61(12)
O(5)	-0.5150(5)	-0.5348(4)	0.1523(4)	14.1(2)
C(1)	-0.1662(6)	-0.3666(5)	0.3096(4)	7.21(14)
C(2)	-0.0872(6)	-0.4634(5)	0.1386(4)	7.41(14)
C(3)	-0.1991(6)	-0.3086(5)	0.0551(4)	8.0(2)
C(4)	-0.2813(6)	-0.2177(5)	0.2220(4)	6.95(13)
C(5)	-0.3918(7)	-0.4638(6)	0.1626(4)	9.1(2)
C(11)	0.2428(5)	-0.2276(4)	0.3144(3)	5.13(11)
C(12)	0.2798(6)	-0.3409(4)	0.3048(3)	6.89(13)
C(13)	0.3768(6)	-0.3664(5)	0.3755(4)	7.31(14)
C(14)	0.4387(6)	-0.2817(5)	0.4590(3)	6.53(13)
C(15)	0.4026(6)	-0.1688(5)	0.4695(3)	7.21(14)
C(16)	0.3072(5)	-0.1424(4)	0.3983(3)	6.64(13)
C(17)	0.5417(6)	-0.3094(5)	0.5373(4)	9.7(2)
C(21)	0.0726(5)	0.0038(4)	0.2717(3)	5.13(11)
C(22)	0.1272(5)	0.1082(4)	0.2255(3)	5.91(12)
C(23)	0.1022(6)	0.2225(4)	0.2621(3)	6.58(13)
C(24)	0.0206(5)	0.2370(4)	0.3451(3)	5.99(12)
C(25)	-0.0289(6)	0.1353(4)	0.3938(3)	6.64(13)
C(26)	-0.0049(6)	0.0198(4)	0.3579(3)	6.40(13)
C(27)	-0.0171(7)	0.3600(5)	0.3812(4)	9.3(2)
C(31)	0.2096(5)	-0.1645(4)	0.0753(3)	5.35(11)
C(32)	0.3384(5)	-0.2097(4)	0.0571(3)	6.81(13)
C(33)	0.4112(6)	-0.2019(5)	-0.0321(4)	7.8(2)
C(34)	0.3592(5)	-0.1474(4)	-0.1048(3)	6.53(13)
C(35)	0.2322(6)	-0.1014(5)	-0.0870(4)	7.01(13)
C(36)	0.1592(5)	-0.1102(4)	0.0008(3)	6.46(13)
C(37)	0.4357(6)	-0.1421(6)	-0.2028(4)	9.6(2)

Table A2.10: Bond lengths (Å) and angles (°) for $(p\text{-}CH_3C_6H_5)_3SnMn(CO)_5$.

Sn-C(31)	2.145(4)	Sn-C(11)	2.150(4)
Sn-C(21)	2.159(4)	Sn-Mn	2.6932(11)
Mn-C(5)	1.812(7)	Mn-C(1)	1.829(5)
Mn-C(3)	1.839(6)	Mn-C(4)	1.845(5)
Mn-C(2)	1.847(5)	O(1)-C(1)	1.141(5)
O(2)-C(2)	1.138(5)	O(3)-C(3)	1.137(6)
O(4)-C(4)	1.137(5)	O(5)-C(5)	1.143(6)
C(11)-C(16)	1.380(6)	C(11)-C(12)	1.381(5)
C(12)-C(13)	1.391(6)	C(12)-H(12)	0.93
C(13)-C(14)	1.368(6)	C(13)-H(13)	0.93
C(14)-C(15)	1.373(6)	C(14)-C(17)	1.512(6)
C(15)-C(16)	1.391(6)	C(15)-H(15)	0.93
C(16)-H(16)	0.93	C(17)-H(17A)	0.96
C(17)-H(17B)	0.96	C(17)-H(17C)	0.96
C(21)-C(22)	1.379(6)	C(21)-C(26)	1.389(6)
C(22)-C(23)	1.380(6)	C(22)-H(22)	0.93
C(23)-C(24)	1.371(6)	C(23)-H(23)	0.93
C(24)-C(25)	1.368(6)	C(24)-C(27)	1.519(6)
C(25)-C(26)	1.387(6)	C(25)-H(25)	0.93
C(26)-H(26)	0.93	C(27)-H(27A)	0.96
C(27)-H(27B)	0.96	C(27)-H(27C)	0.96
C(31)-C(32)	1.379(5)	C(31)-C(36)	1.385(5)
C(32)-C(33)	1.393(6)	C(32)-H(32)	0.93
C(33)-C(34)	1.372(6)	C(33)-H(33)	0.93
C(34)-C(35)	1.369(6)	C(34)-C(37)	1.514(6)
C(35)-C(36)	1.377(6)	C(35)-H(35)	0.93
C(36)-H(36)	0.93	C(37)-H(37A)	0.96
C(37)-H(37B)	0.96	C(37)-H(37C)	0.96
C(31)-Sn-C(11)	107.7(2)	C(31)-Sn-C(21)	108.2(2)
C(11)-Sn-C(21)	106.0(2)	C(31)-Sn-Mn	111.66(11)
C(11)-Sn-Mn	112.63(12)	C(21)-Sn-Mn	110.34(11)
C(5)-Mn-C(1)	94.8(3)	C(5)-Mn-C(3)	94.8(3)
C(1)-Mn-C(3)	170.2(2)	C(5)-Mn-C(4)	92.5(2)
C(1)-Mn-C(4)	89.6(2)	C(3)-Mn-C(4)	88.3(2)
C(5)-Mn-C(2)	95.5(2)	C(1)-Mn-C(2)	91.1(2)
C(3)-Mn-C(2)	89.6(2)	C(4)-Mn-C(2)	171.8(2)
C(5)-Mn-Sn	179.0(2)	C(1)-Mn-Sn	84.2(2)
C(3)-Mn-Sn	86.2(2)	C(4)-Mn-Sn	87.7(2)
C(2)-Mn-Sn	84.3(2)	O(1)-C(1)-Mn	178.4(4)
O(2)-C(2)-Mn	179.6(5)	O(3)-C(3)-Mn	178.5(5)
O(4)-C(4)-Mn	177.5(5)	O(5)-C(5)-Mn	178.9(5)
C(16)-C(11)-C(12)	115.9(4)	C(16)-C(11)-Sn	119.6(3)
C(12)-C(11)-Sn	124.4(3)	C(11)-C(12)-C(13)	121.7(4)
C(11)-C(12)-H(12)	119.2	C(13)-C(12)-H(12)	119.2
C(14)-C(13)-C(12)	121.9(4)	C(14)-C(13)-H(13)	119.1
C(12)-C(13)-H(13)	119.1	C(13)-C(14)-C(15)	117.0(4)
C(13)-C(14)-C(17)	122.3(4)	C(15)-C(14)-C(17)	120.6(5)
C(14)-C(15)-C(16)	121.2(4)	C(14)-C(15)-H(15)	119.4
C(16)-C(15)-H(15)	119.4	C(11)-C(16)-C(15)	122.3(4)

C(11)-C(16)-H(16)	118.9	C(15)-C(16)-H(16)	118.9
C(14)-C(17)-H(17A)	109.5	C(14)-C(17)-H(17B)	109.5
H(17A)-C(17)-H(17B)	109.5	C(14)-C(17)-H(17C)	109.5
H(17A)-C(17)-H(17C)	109.5	H(17B)-C(17)-H(17C)	109.5
C(22)-C(21)-C(26)	117.0(4)	C(22)-C(21)-Sn	122.5(3)
C(26)-C(21)-Sn	120.4(3)	C(21)-C(22)-C(23)	121.3(4)
C(21)-C(22)-H(22)	119.4	C(23)-C(22)-H(22)	119.4
C(24)-C(23)-C(22)	121.7(4)	C(24)-C(23)-H(23)	119.2
C(22)-C(23)-H(23)	119.2	C(25)-C(24)-C(23)	117.6(4)
C(25)-C(24)-C(27)	120.8(4)	C(23)-C(24)-C(27)	121.7(4)
C(24)-C(25)-C(26)	121.4(4)	C(24)-C(25)-H(25)	119.3
C(26)-C(25)-H(25)	119.3	C(25)-C(26)-C(21)	121.0(4)
C(25)-C(26)-H(26)	119.5	C(21)-C(26)-H(26)	119.5
C(24)-C(27)-H(27A)	109.5	C(24)-C(27)-H(27B)	109.5
H(27A)-C(27)-H(27B)	109.5	C(24)-C(27)-H(27C)	109.5
H(27A)-C(27)-H(27C)	109.5	H(27B)-C(27)-H(27C)	109.5
C(32)-C(31)-C(36)	116.3(4)	C(32)-C(31)-Sn	121.9(3)
C(36)-C(31)-Sn	121.9(3)	C(31)-C(32)-C(33)	121.2(4)
C(31)-C(32)-H(32)	119.4	C(33)-C(32)-H(32)	119.4
C(34)-C(33)-C(32)	121.4(4)	C(34)-C(33)-H(33)	119.3
C(32)-C(33)-H(33)	119.3	C(35)-C(34)-C(33)	117.7(4)
C(35)-C(34)-C(37)	120.9(5)	C(33)-C(34)-C(37)	121.4(4)
C(34)-C(35)-C(36)	120.9(4)	C(34)-C(35)-H(35)	119.5
C(36)-C(35)-H(35)	119.5	C(35)-C(36)-C(31)	122.4(4)
C(35)-C(36)-H(36)	118.8	C(31)-C(36)-H(36)	118.8
C(34)-C(37)-H(37A)	109.5	C(34)-C(37)-H(37B)	109.5
H(37A)-C(37)-H(37B)	109.5	C(34)-C(37)-H(37C)	109.5
H(37A)-C(37)-H(37C)	109.5	H(37B)-C(37)-H(37C)	109.5

Table A2.11: Torsion angles (in degrees) for (p-$CH_3C_6H_5$)$_3$SnMn(CO)$_5$.

C(31)-Sn-Mn-C(5)	141(9)	C(11)-Sn-Mn-C(5)	19(9)
C(21)-Sn-Mn-C(5)	-99(9)	C(31)-Sn-Mn-C(1)	153.2(2)
C(11)-Sn-Mn-C(1)	31.8(2)	C(21)-Sn-Mn-C(1)	-86.4(2)
C(31)-Sn-Mn-C(3)	-28.5(2)	C(11)-Sn-Mn-C(3)	-149.9(2)
C(21)-Sn-Mn-C(3)	91.9(2)	C(31)-Sn-Mn-C(4)	-117.0(2)
C(11)-Sn-Mn-C(4)	121.6(2)	C(21)-Sn-Mn-C(4)	3.4(2)
C(31)-Sn-Mn-C(2)	61.5(2)	C(11)-Sn-Mn-C(2)	-59.9(2)
C(21)-Sn-Mn-C(2)	-178.1(2)	C(31)-Sn-C(11)-C(16)	114.2(4)
C(21)-Sn-C(11)-C(16)	-1.5(4)	Mn-Sn-C(11)-C(16)	-122.2(3)
C(31)-Sn-C(11)-C(12)	-67.2(4)	C(21)-Sn-C(11)-C(12)	177.1(4)
Mn-Sn-C(11)-C(12)	56.4(4)	C(16)-C(11)-C(12)-C(13)	-0.3(7)
Sn-C(11)-C(12)-C(13)	-179.0(4)	C(11)-C(12)-C(13)-C(14)	1.0(8)
C(12)-C(13)-C(14)-C(15)	-0.8(8)	C(12)-C(13)-C(14)-C(17)	178.8(5)
C(13)-C(14)-C(15)-C(16)	0.1(8)	C(17)-C(14)-C(15)-C(16)	-179.6(5)
C(12)-C(11)-C(16)-C(15)	-0.5(7)	Sn-C(11)-C(16)-C(15)	178.3(4)
C(14)-C(15)-C(16)-C(11)	0.6(8)	C(31)-Sn-C(21)-C(22)	1.5(4)
C(11)-Sn-C(21)-C(22)	116.8(3)	Mn-Sn-C(21)-C(22)	-121.0(3)
C(31)-Sn-C(21)-C(26)	177.5(3)	C(11)-Sn-C(21)-C(26)	-67.1(4)
Mn-Sn-C(21)-C(26)	55.1(3)	C(26)-C(21)-C(22)-C(23)	-1.6(6)
Sn-C(21)-C(22)-C(23)	174.6(3)	C(21)-C(22)-C(23)-C(24)	-0.8(7)
C(22)-C(23)-C(24)-C(25)	3.1(7)	C(22)-C(23)-C(24)-C(27)	-175.6(4)
C(23)-C(24)-C(25)-C(26)	-3.2(7)	C(27)-C(24)-C(25)-C(26)	175.5(5)
C(24)-C(25)-C(26)-C(21)	0.9(7)	C(22)-C(21)-C(26)-C(25)	1.5(7)
Sn-C(21)-C(26)-C(25)	-174.8(3)	C(11)-Sn-C(31)-C(32)	14.7(4)
C(21)-Sn-C(31)-C(32)	128.8(4)	Mn-Sn-C(31)-C(32)	-109.5(4)
C(11)-Sn-C(31)-C(36)	-166.5(4)	C(21)-Sn-C(31)-C(36)	-52.3(4)
Mn-Sn-C(31)-C(36)	69.4(4)	C(36)-C(31)-C(32)-C(33)	-0.8(7)
Sn-C(31)-C(32)-C(33)	178.1(4)	C(31)-C(32)-C(33)-C(34)	1.0(8)
C(32)-C(33)-C(34)-C(35)	-0.4(8)	C(32)-C(33)-C(34)-C(37)	-178.4(5)
C(33)-C(34)-C(35)-C(36)	-0.2(7)	C(37)-C(34)-C(35)-C(36)	177.7(5)
C(34)-C(35)-C(36)-C(31)	0.3(8)	C(32)-C(31)-C(36)-C(35)	0.2(7)
Sn-C(31)-C(36)-C(35)	-178.8(4)		

Table A2.12: Anisotropic thermal factors (10^2 Å^2) for (p-$CH_3C_6H_5)_3SnMn(CO)_5$.

	U_{11}	U_{22}	U_{33}	U_{12}	U_{13}	U_{23}
Sn	5.56(2)	5.43(2)	5.00(2)	0.632(13)	-0.292(13)	2.48(2)
Mn	5.78(5)	6.16(5)	5.95(4)	0.08(4)	-0.07(3)	1.86(4)
O(1)	15.3(4)	12.9(4)	6.8(3)	3.1(2)	1.7(3)	6.8(3)
O(2)	12.9(4)	9.6(3)	9.9(3)	-1.5(2)	0.4(3)	6.1(3)
O(3)	9.5(3)	18.5(5)	6.9(3)	2.6(3)	-1.4(2)	3.8(3)
O(4)	8.3(3)	8.5(3)	13.0(3)	1.3(2)	0.8(2)	4.3(2)
O(5)	8.1(3)	10.8(4)	19.4(5)	-4.6(3)	1.7(3)	-0.6(3)
C(1)	8.7(4)	6.6(3)	6.9(3)	0.5(3)	0.7(3)	3.3(3)
C(2)	7.9(4)	7.0(4)	6.6(3)	-0.7(3)	-0.3(3)	1.8(3)
C(3)	6.4(3)	10.7(4)	6.8(4)	0.4(3)	-0.9(3)	2.6(3)
C(4)	5.8(3)	7.0(3)	8.0(4)	1.3(3)	0.1(3)	1.7(3)
C(5)	8.0(4)	8.5(4)	9.8(4)	-2.0(3)	0.8(3)	2.4(4)
C(11)	5.0(3)	6.0(3)	4.9(3)	1.1(2)	-0.2(2)	2.2(2)
C(12)	8.5(4)	6.5(3)	5.9(3)	0.3(2)	-1.6(3)	3.0(3)
C(13)	9.0(4)	6.6(3)	7.7(3)	1.7(3)	-0.8(3)	4.2(3)
C(14)	7.1(3)	8.2(4)	5.5(3)	2.1(3)	0.0(2)	3.7(3)
C(15)	7.9(4)	7.6(4)	6.0(3)	0.0(3)	-2.2(3)	2.6(3)
C(16)	7.5(3)	6.2(3)	7.0(3)	0.6(3)	-0.9(3)	3.4(3)
C(17)	11.2(5)	12.2(5)	7.8(4)	2.2(3)	-1.9(3)	6.4(4)
C(21)	5.3(3)	5.8(3)	4.9(3)	0.7(2)	-0.1(2)	2.7(2)
C(22)	6.6(3)	5.9(3)	5.5(3)	0.8(2)	0.5(2)	2.3(2)
C(23)	8.1(4)	5.3(3)	6.7(3)	1.9(2)	0.0(3)	2.0(3)
C(24)	7.3(3)	5.7(3)	5.6(3)	0.5(2)	-0.5(2)	3.0(3)
C(25)	8.4(4)	7.0(3)	5.3(3)	0.5(3)	1.3(2)	3.5(3)
C(26)	8.4(4)	5.7(3)	6.0(3)	2.0(2)	1.5(3)	2.7(3)
C(27)	13.1(5)	7.1(4)	9.1(4)	0.3(3)	0.7(4)	5.3(4)
C(31)	5.2(3)	5.9(3)	5.2(3)	0.4(2)	0.0(2)	2.3(2)
C(32)	6.0(3)	8.4(4)	6.7(3)	0.5(3)	-0.9(3)	3.7(3)
C(33)	6.0(3)	11.0(4)	7.3(4)	-0.7(3)	0.4(3)	4.8(3)
C(34)	5.5(3)	7.1(3)	6.3(3)	-0.3(3)	0.1(2)	1.3(3)
C(35)	6.3(3)	8.8(4)	6.9(3)	2.7(3)	0.8(3)	3.0(3)
C(36)	6.2(3)	7.6(3)	7.0(3)	2.1(3)	1.0(3)	3.8(3)
C(37)	8.8(4)	13.3(5)	7.2(4)	1.7(3)	2.5(3)	3.6(4)

Structural Analysis of

Tris(*p*-Anisol)tin(pentacarbonyl)manganese(I)

$(p\text{-}CH_3OC_6H_4)_3SnMn(CO)_5$

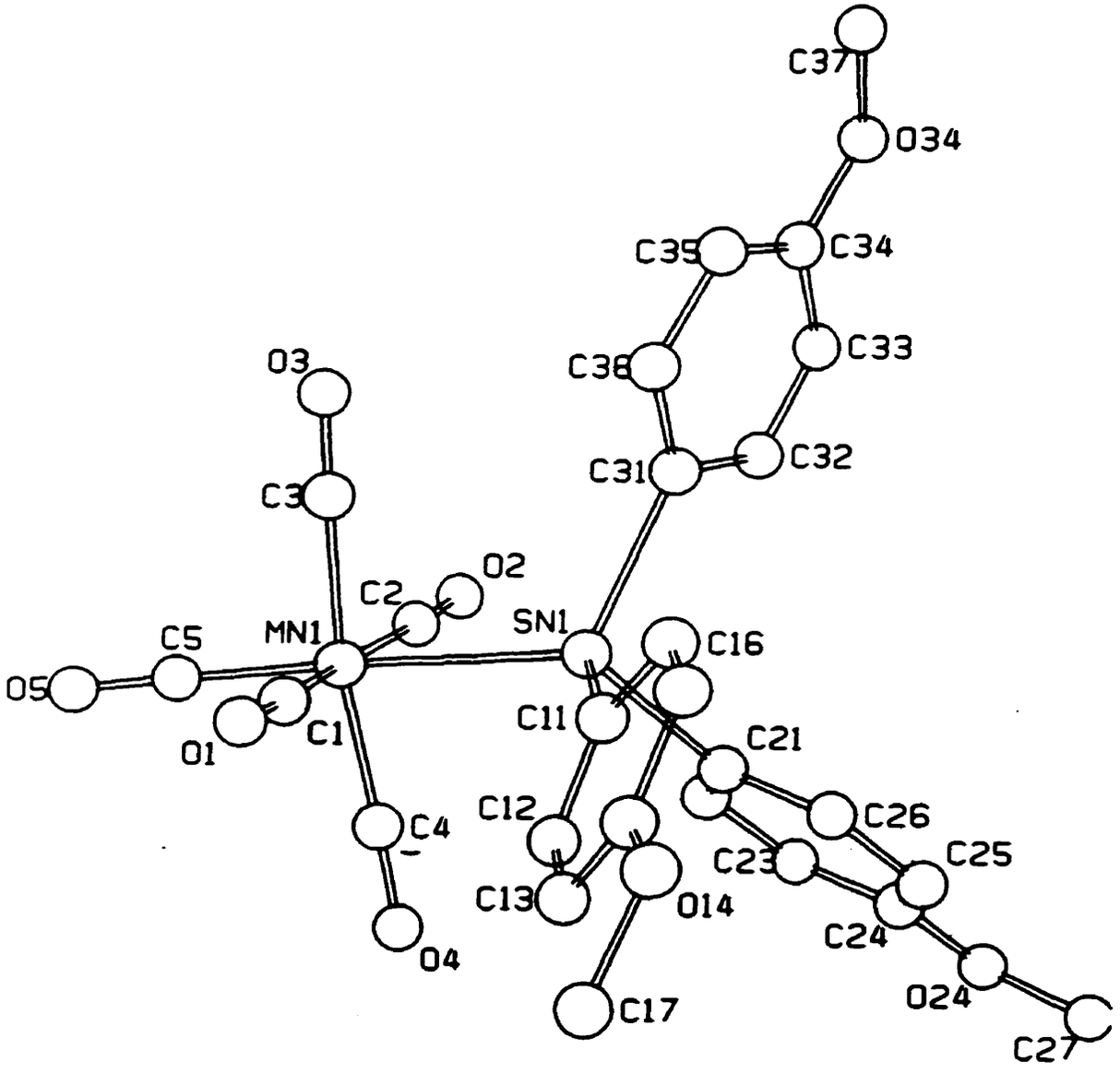

Crystal data for $(p\text{-}CH_3OC_6H_4)_2SnMn(CO)_5$

Empirical Formula: C26 H21 O8 Sn Mn

Space group: Monoclinic, $P2_1/c$

Cell dimensions:

$a = 14.096\ (2)$Å

$b = 11.161\ (2)$Å

$c = 17.000\ (10)$Å

$\alpha = 90°$

$\beta = 91.71\ (2)°$

$\gamma = 90°$

Volume = 2673 (2)Å^3

FW = 635.06

Z = 4

$D_{calc} = 1.578$ g / cm^3

F(000) = 1264

Mo Kα radiation

$\lambda = 0.7093$ Å

Cell parameters from 21 reflections

$2\theta = 26 - 30°$

$\mu = 1.452$ mm^{-1}

T = 295 (2) °K

Colourless thick plate

$0.35 \times 0.22 \times 0.12$ mm

Data collection

Rigaku AFC –6S diffractometer

ω / 2θ scans

Absorption correction: *Psi scans*

$T_{min} = 0.64$, $T_{max} = 0.76$

9414 measured reflections

4716 independent reflections

2891 observed reflections [$I > 2\sigma(I)$]

$R_{int} = 0.083$

$\theta_{max} = 50.0°$

$h = -17 \rightarrow 17$

$k = 0 \rightarrow 13$

$l = -20 \rightarrow 20$

3 standard reflections were monitored every 250 reflections

Intensity decay: 0.6 %

Structure was solved by the heavy atom method.

Refinement

Refinement on F^2	323 parameters
$R(F^2 > 2\sigma(F^2) = 0.0546$	H atoms riding,
$wR(F^2) = 0.0918$	C–H = 0.93 - 0.97 Å
GoF = 1.023	$(\Delta/\sigma) = 0.002$
57 atoms	$\Delta\rho_{max} = 0.570$ e/Å^3
4716 reflections	$\Delta\rho_{min} = -0.595$ e/Å^3

where

$R = \Sigma(Fo-Fc) / \Sigma Fo$

$wR = [\Sigma(w(Fo-Fc)^2) / \Sigma wFo^2]^{1/2}$

GoF = [Σ(w(Fo-Fc)^2) / (No. of refins - No. of params.)

Table A2.13: Fractional atomic coordinates and equivalent isotropic displacement parameters (10^2 Å) for $(p\text{-}CH_3OC_6H_4)_3SnMn(CO)_5$.

	x	y	z	U_{eq}
Sn	0.70314(3)	0.73946(4)	0.52741(3)	4.40(2)
Mn	0.68048(7)	0.84336(9)	0.38672(6)	4.92(3)
O(1)	0.4755(4)	0.7813(7)	0.3973(4)	12.2(3)
O(2)	0.6384(5)	1.0645(5)	0.4785(3)	9.9(2)
O(3)	0.8895(4)	0.8771(6)	0.4000(4)	9.9(2)
O(4)	0.7116(4)	0.6027(5)	0.3179(3)	8.3(2)
O(5)	0.6667(5)	0.9543(5)	0.2302(4)	10.4(2)
O(14)	0.3457(4)	0.7712(5)	0.7411(3)	7.8(2)
O(24)	0.8533(4)	0.2066(4)	0.5024(3)	7.5(2)
O(34)	1.0039(4)	0.9779(5)	0.7646(3)	8.4(2)
C(1)	0.5529(6)	0.8051(8)	0.3927(4)	7.2(2)
C(2)	0.6562(5)	0.9813(7)	0.4429(4)	6.4(2)
C(3)	0.8094(6)	0.8660(7)	0.3960(4)	6.5(2)
C(4)	0.7020(5)	0.6949(7)	0.3460(5)	6.2(2)
C(5)	0.6708(6)	0.9128(7)	0.2907(5)	7.3(2)
C(11)	0.5772(4)	0.7447(6)	0.5951(4)	4.6(2)
C(12)	0.5719(5)	0.8295(6)	0.6538(4)	5.2(2)
C(13)	0.4945(5)	0.8351(7)	0.7033(4)	6.2(2)
C(14)	0.4197(5)	0.7567(7)	0.6909(4)	5.5(2)
C(15)	0.4217(5)	0.6731(6)	0.6327(4)	5.9(2)
C(16)	0.5003(5)	0.6683(6)	0.5841(4)	5.4(2)
C(17)	0.2717(4)	0.6863(6)	0.7385(6)	12.8(4)
C(21)	0.7517(3)	0.5572(4)	0.5185(3)	4.2(2)
C(22)	0.8333(3)	0.5337(4)	0.4778(3)	5.8(2)
C(23)	0.8691(5)	0.4188(7)	0.4700(4)	5.7(2)
C(24)	0.8236(5)	0.3244(6)	0.5040(4)	5.3(2)
C(25)	0.7409(5)	0.3451(6)	0.5438(4)	5.2(2)
C(26)	0.7067(5)	0.4607(6)	0.5504(4)	4.8(2)
C(27)	0.9341(6)	0.1782(7)	0.4592(5)	9.7(3)
C(31)	0.8085(4)	0.8222(6)	0.6049(4)	4.6(2)
C(32)	0.8301(5)	0.9440(6)	0.6052(4)	5.3(2)
C(33)	0.8953(5)	0.9914(6)	0.6587(4)	5.6(2)
C(34)	0.9405(5)	0.9214(7)	0.7139(4)	5.8(2)
C(35)	0.9214(5)	0.7998(7)	0.7136(4)	6.2(2)
C(36)	0.8558(4)	0.7515(7)	0.6600(4)	5.7(2)
C(37)	1.0545(6)	0.9086(9)	0.8189(5)	10.8(3)

Table A2.14: Bond lengths (Å) and angles (°) for (p-$CH_3OC_6H_4$)$_3$SnMn(CO)$_5$.

Sn-C(11)	2.144(6)	Sn-C(21)	2.153(4)
Sn-C(31)	2.163(6)	Sn-Mn	2.669(2)
Mn-C(5)	1.808(9)	Mn-C(4)	1.824(8)
Mn-C(3)	1.837(8)	Mn-C(2)	1.849(8)
Mn-C(1)	1.854(9)	O(1)-C(1)	1.129(8)
O(2)-C(2)	1.140(8)	O(3)-C(3)	1.136(8)
O(4)-C(4)	1.144(8)	O(5)-C(5)	1.129(8)
O(14)-C(14)	1.377(7)	O(14)-C(17)	1.409(6)
O(24)-C(24)	1.379(8)	O(24)-C(27)	1.410(8)
O(34)-C(34)	1.376(8)	O(34)-C(37)	1.387(9)
C(11)-C(12)	1.380(9)	C(11)-C(16)	1.388(8)
C(12)-C(13)	1.399(9)	C(12)-H(12)	0.93
C(13)-C(14)	1.381(9)	C(13)-H(13)	0.93
C(14)-C(15)	1.360(9)	C(15)-C(16)	1.403(8)
C(15)-H(15)	0.93	C(16)-H(16)	0.93
C(17)-H(17A)	0.96	C(17)-H(17B)	0.96
C(17)-H(17C)	0.96	C(21)-C(26)	1.370(7)
C(21)-C(22)	1.38	C(22)-C(23)	1.386(8)
C(22)-H(22)	0.93	C(23)-C(24)	1.371(9)
C(23)-H(23)	0.93	C(24)-C(25)	1.385(8)
C(25)-C(26)	1.383(8)	C(25)-H(25)	0.93
C(26)-H(26)	0.93	C(27)-H(27A)	0.96
C(27)-H(27B)	0.96	C(27)-H(27C)	0.96
C(31)-C(36)	1.381(8)	C(31)-C(32)	1.393(8)
C(32)-C(33)	1.379(8)	C(32)-H(32)	0.93
C(33)-C(34)	1.364(9)	C(33)-H(33)	0.93
C(34)-C(35)	1.384(9)	C(35)-C(36)	1.388(9)
C(35)-H(35)	0.93	C(36)-H(36)	0.93
C(37)-H(37A)	0.96	C(37)-H(37B)	0.96
C(37)-H(37C)	0.96		
C(11)-Sn-C(21)	109.5(2)	C(11)-Sn-C(31)	103.0(2)
C(21)-Sn-C(31)	103.5(2)	C(11)-Sn-Mn	113.0(2)
C(21)-Sn-Mn	112.15(12)	C(31)-Sn-Mn	115.0(2)
C(5)-Mn-C(4)	93.2(3)	C(5)-Mn-C(3)	93.8(4)
C(4)-Mn-C(3)	89.0(3)	C(5)-Mn-C(2)	95.7(3)
C(4)-Mn-C(2)	170.9(3)	C(3)-Mn-C(2)	92.2(3)
C(5)-Mn-C(1)	95.8(4)	C(4)-Mn-C(1)	89.1(4)
C(3)-Mn-C(1)	170.3(4)	C(2)-Mn-C(1)	88.2(3)
C(5)-Mn-Sn	177.4(3)	C(4)-Mn-Sn	85.9(2)
C(3)-Mn-Sn	83.8(2)	C(2)-Mn-Sn	85.3(2)
C(1)-Mn-Sn	86.7(3)	C(14)-O(14)-C(17)	118.3(5)
C(24)-O(24)-C(27)	118.4(6)	C(34)-O(34)-C(37)	118.2(7)
O(1)-C(1)-Mn	179.1(8)	O(2)-C(2)-Mn	177.6(8)
O(3)-C(3)-Mn	177.8(8)	O(4)-C(4)-Mn	176.5(7)
O(5)-C(5)-Mn	178.2(8)	C(12)-C(11)-C(16)	117.4(6)
C(12)-C(11)-Sn	118.1(5)	C(16)-C(11)-Sn	124.5(5)
C(11)-C(12)-C(13)	121.7(6)	C(11)-C(12)-H(12)	119.1
C(13)-C(12)-H(12)	119.1	C(14)-C(13)-C(12)	119.1(7)
C(14)-C(13)-H(13)	120.5	C(12)-C(13)-H(13)	120.5
C(15)-C(14)-O(14)	124.3(7)	C(15)-C(14)-C(13)	120.8(6)

O(14)-C(14)-C(13)	114.8(7)	C(14)-C(15)-C(16)	119.3(7)
C(14)-C(15)-H(15)	120.3	C(16)-C(15)-H(15)	120.3
C(11)-C(16)-C(15)	121.6(6)	C(11)-C(16)-H(16)	119.2
C(15)-C(16)-H(16)	119.2	O(14)-C(17)-H(17A)	109.5
O(14)-C(17)-H(17B)	109.5	H(17A)-C(17)-H(17B)	109.5
O(14)-C(17)-H(17C)	109.5	H(17A)-C(17)-H(17C)	109.5
H(17B)-C(17)-H(17C)	109.5	C(26)-C(21)-C(22)	116.8(3)
C(26)-C(21)-Sn	124.2(4)	C(22)-C(21)-Sn	119.01(11)
C(21)-C(22)-C(23)	122.2(3)	C(21)-C(22)-H(22)	118.9
C(23)-C(22)-H(22)	118.9	C(24)-C(23)-C(22)	119.7(6)
C(24)-C(23)-H(23)	120.2	C(22)-C(23)-H(23)	120.2
C(23)-C(24)-O(24)	125.3(6)	C(23)-C(24)-C(25)	119.3(6)
O(24)-C(24)-C(25)	115.4(7)	C(26)-C(25)-C(24)	119.7(6)
C(26)-C(25)-H(25)	120.1	C(24)-C(25)-H(25)	120.1
C(21)-C(26)-C(25)	122.3(6)	C(21)-C(26)-H(26)	118.8
C(25)-C(26)-H(26)	118.8	O(24)-C(27)-H(27A)	109.5
O(24)-C(27)-H(27B)	109.5	H(27A)-C(27)-H(27B)	109.5
O(24)-C(27)-H(27C)	109.5	H(27A)-C(27)-H(27C)	109.5
H(27B)-C(27)-H(27C)	109.5	C(36)-C(31)-C(32)	117.0(6)
C(36)-C(31)-Sn	118.6(5)	C(32)-C(31)-Sn	124.4(5)
C(33)-C(32)-C(31)	121.2(7)	C(33)-C(32)-H(32)	119.4
C(31)-C(32)-H(32)	119.4	C(34)-C(33)-C(32)	121.5(7)
C(34)-C(33)-H(33)	119.2	C(32)-C(33)-H(33)	119.2
C(33)-C(34)-O(34)	116.7(7)	C(33)-C(34)-C(35)	118.2(7)
O(34)-C(34)-C(35)	125.0(7)	C(34)-C(35)-C(36)	120.6(7)
C(34)-C(35)-H(35)	119.7	C(36)-C(35)-H(35)	119.7
C(31)-C(36)-C(35)	121.5(7)	C(31)-C(36)-H(36)	119.2
C(35)-C(36)-H(36)	119.2	O(34)-C(37)-H(37A)	109.5
O(34)-C(37)-H(37B)	109.5	H(37A)-C(37)-H(37B)	109.47
O(34)-C(37)-H(37C)	109.5	H(37A)-C(37)-H(37C)	109.5
H(37B)-C(37)-H(37C)	109.5		

Table A2.15: Torsion angles (in degrees) for $(p\text{-}CH_3OC_6H_4)_3SnMn(CO)_5$.

C(11)-Sn-Mn-C(5)	174(6)	C(21)-Sn-Mn-C(5)	-62(6)
C(31)-Sn-Mn-C(5)	56(6)	C(11)-Sn-Mn-C(4)	-116.2(3)
C(21)-Sn-Mn-C(4)	8.1(3)	C(31)-Sn-Mn-C(4)	125.9(3)
C(11)-Sn-Mn-C(3)	154.4(3)	C(21)-Sn-Mn-C(3)	-81.3(3)
C(31)-Sn-Mn-C(3)	36.5(3)	C(11)-Sn-Mn-C(2)	61.6(3)
C(21)-Sn-Mn-C(2)	-174.1(3)	C(31)-Sn-Mn-C(2)	-56.3(3)
C(11)-Sn-Mn-C(1)	-26.9(3)	C(21)-Sn-Mn-C(1)	97.4(3)
C(31)-Sn-Mn-C(1)	-144.8(3)	C(21)-Sn-C(11)-C(12)	132.9(5)
C(31)-Sn-C(11)-C(12)	23.3(5)	Mn-Sn-C(11)-C(12)	-101.3(5)
C(21)-Sn-C(11)-C(16)	-47.0(6)	C(31)-Sn-C(11)-C(16)	-156.5(5)
Mn-Sn-C(11)-C(16)	78.8(6)	C(16)-C(11)-C(12)-C(13)	3.2(10)
Sn-C(11)-C(12)-C(13)	-176.7(5)	C(11)-C(12)-C(13)-C(14)	-2.6(10)
C(17)-O(14)-C(14)-C(15)	7.4(11)	C(17)-O(14)-C(14)-C(13)	-172.8(8)
C(12)-C(13)-C(14)-C(15)	1.5(11)	C(12)-C(13)-C(14)-O(14)	-178.3(6)
O(14)-C(14)-C(15)-C(16)	178.7(6)	C(13)-C(14)-C(15)-C(16)	-1.0(11)
C(12)-C(11)-C(16)-C(15)	-2.7(10)	Sn-C(11)-C(16)-C(15)	177.2(5)
C(14)-C(15)-C(16)-C(11)	1.7(11)	C(11)-Sn-C(21)-C(26)	1.2(5)
C(31)-Sn-C(21)-C(26)	110.5(5)	Mn-Sn-C(21)-C(26)	-125.1(4)
C(11)-Sn-C(21)-C(22)	-179.1(2)	C(31)-Sn-C(21)-C(22)	-69.8(2)
Mn-Sn-C(21)-C(22)	54.64(10)	C(26)-C(21)-C(22)-C(23)	-0.7(4)
Sn-C(21)-C(22)-C(23)	179.6(5)	C(21)-C(22)-C(23)-C(24)	-0.7(8)
C(22)-C(23)-C(24)-O(24)	-178.1(6)	C(22)-C(23)-C(24)-C(25)	1.7(11)
C(27)-O(24)-C(24)-C(23)	-3.5(11)	C(27)-O(24)-C(24)-C(25)	176.6(7)
C(23)-C(24)-C(25)-C(26)	-1.5(11)	O(24)-C(24)-C(25)-C(26)	178.4(6)
C(22)-C(21)-C(26)-C(25)	0.9(7)	Sn-C(21)-C(26)-C(25)	-179.4(5)
C(24)-C(25)-C(26)-C(21)	0.1(10)	C(11)-Sn-C(31)-C(36)	85.6(5)
C(21)-Sn-C(31)-C(36)	-28.4(6)	Mn-Sn-C(31)-C(36)	-151.0(5)
C(11)-Sn-C(31)-C(32)	-92.0(6)	C(21)-Sn-C(31)-C(32)	153.9(6)
Mn-Sn-C(31)-C(32)	31.3(6)	C(36)-C(31)-C(32)-C(33)	-0.5(10)
Sn-C(31)-C(32)-C(33)	177.1(5)	C(31)-C(32)-C(33)-C(34)	-0.7(11)
C(32)-C(33)-C(34)-O(34)	-179.7(6)	C(32)-C(33)-C(34)-C(35)	1.9(11)
C(37)-O(34)-C(34)-C(33)	-176.9(7)	C(37)-O(34)-C(34)-C(35)	1.3(12)
C(33)-C(34)-C(35)-C(36)	-1.9(11)	O(34)-C(34)-C(35)-C(36)	179.9(7)
C(32)-C(31)-C(36)-C(35)	0.5(10)	Sn-C(31)-C(36)-C(35)	-177.3(5)
C(34)-C(35)-C(36)-C(31)	0.7(11)		

Table A2.16: Anisotropic thermal factors (10^2 Å^2) for $(p\text{-}CH_3OC_6H_4)_3SnMn(CO)_5$.

	U_{11}	U_{22}	U_{33}	U_{12}	U_{13}	U_{23}
Sn	4.39(3)	4.15(3)	4.66(3)	-0.08(3)	0.01(2)	-0.11(3)
Mn	5.37(7)	4.72(7)	4.66(6)	0.02(5)	0.08(5)	0.30(5)
O(1)	5.7(4)	22.3(9)	8.8(4)	-2.0(5)	0.0(3)	-2.2(5)
O(2)	13.8(6)	7.2(4)	8.5(4)	-2.8(4)	-1.9(4)	3.9(4)
O(3)	6.1(4)	13.0(6)	10.8(5)	-1.0(4)	0.8(4)	-3.1(4)
O(4)	11.6(5)	6.4(4)	6.9(4)	-1.4(3)	-0.8(3)	1.0(4)
O(5)	17.2(7)	7.1(4)	6.8(4)	0.2(4)	0.4(4)	2.2(4)
O(14)	6.3(3)	8.1(4)	9.0(4)	-2.1(3)	3.0(3)	0.0(3)
O(24)	6.6(4)	5.0(3)	11.0(5)	0.7(3)	2.3(3)	1.1(3)
O(34)	8.1(4)	8.8(4)	8.1(4)	-0.3(3)	-3.3(3)	-1.3(3)
C(1)	6.0(5)	9.8(7)	5.8(5)	-1.8(4)	-0.1(4)	0.0(5)
C(2)	7.9(6)	5.9(5)	5.2(5)	-0.5(4)	-1.4(4)	1.3(4)
C(3)	6.8(5)	6.4(5)	6.3(5)	-0.3(4)	0.6(4)	-1.4(5)
C(4)	6.4(5)	5.2(5)	6.9(6)	-0.2(4)	-0.8(4)	0.1(4)
C(5)	10.1(7)	5.4(5)	6.2(6)	0.0(5)	-0.3(5)	1.0(5)
C(11)	4.4(4)	4.4(4)	5.0(4)	0.1(4)	0.1(3)	0.0(4)
C(12)	4.5(4)	5.6(5)	5.5(4)	0.1(4)	-0.1(4)	-0.5(4)
C(13)	6.0(5)	6.3(5)	6.3(5)	-1.3(4)	0.1(4)	0.2(4)
C(14)	4.9(4)	5.9(5)	5.8(4)	-0.6(4)	0.7(3)	0.5(4)
C(15)	5.3(5)	5.8(5)	6.6(5)	-0.2(4)	0.9(4)	-0.7(4)
C(16)	5.3(5)	6.3(5)	4.7(4)	-1.6(4)	0.3(4)	0.0(4)
C(17)	8.4(7)	13.9(9)	16.6(10)	-6.5(8)	7.5(7)	-3.8(7)
C(21)	4.9(4)	4.0(4)	3.8(4)	0.3(3)	-0.2(3)	-0.2(3)
C(22)	5.9(5)	4.4(4)	7.2(5)	1.8(4)	1.8(4)	-0.2(4)
C(23)	4.3(4)	6.9(5)	6.0(5)	1.2(4)	1.8(4)	1.0(4)
C(24)	4.8(5)	4.8(5)	6.3(5)	-0.1(4)	0.3(4)	0.9(4)
C(25)	5.3(4)	4.0(4)	6.3(5)	0.8(4)	1.4(4)	-0.3(4)
C(26)	4.5(4)	5.1(4)	4.9(4)	0.1(3)	1.2(3)	-0.4(4)
C(27)	9.0(7)	7.0(6)	13.4(9)	-0.6(6)	3.5(6)	2.1(5)
C(31)	4.2(4)	4.0(4)	5.4(4)	0.1(3)	-0.4(3)	-0.2(3)
C(32)	5.3(4)	4.7(4)	5.7(5)	0.5(4)	-1.3(4)	0.3(4)
C(33)	6.0(5)	4.9(4)	6.0(5)	-0.3(4)	-0.1(4)	-0.7(4)
C(34)	5.6(5)	6.0(5)	5.6(5)	-0.7(4)	-0.9(4)	-0.7(4)
C(35)	5.7(5)	6.8(5)	5.9(5)	0.7(4)	-0.6(4)	-0.1(4)
C(36)	5.8(4)	5.5(4)	5.8(4)	-0.1(4)	-0.4(4)	-0.6(4)
C(37)	11.2(8)	11.9(8)	8.9(7)	-0.7(6)	-4.5(6)	-1.0(7)

Structural Analysis of

Tris(*p*-Thioanisol)tin(pentacarbonyl)manganese(I)

$(p\text{-}CH_3SC_6H_4)_3SnMn(CO)_5$

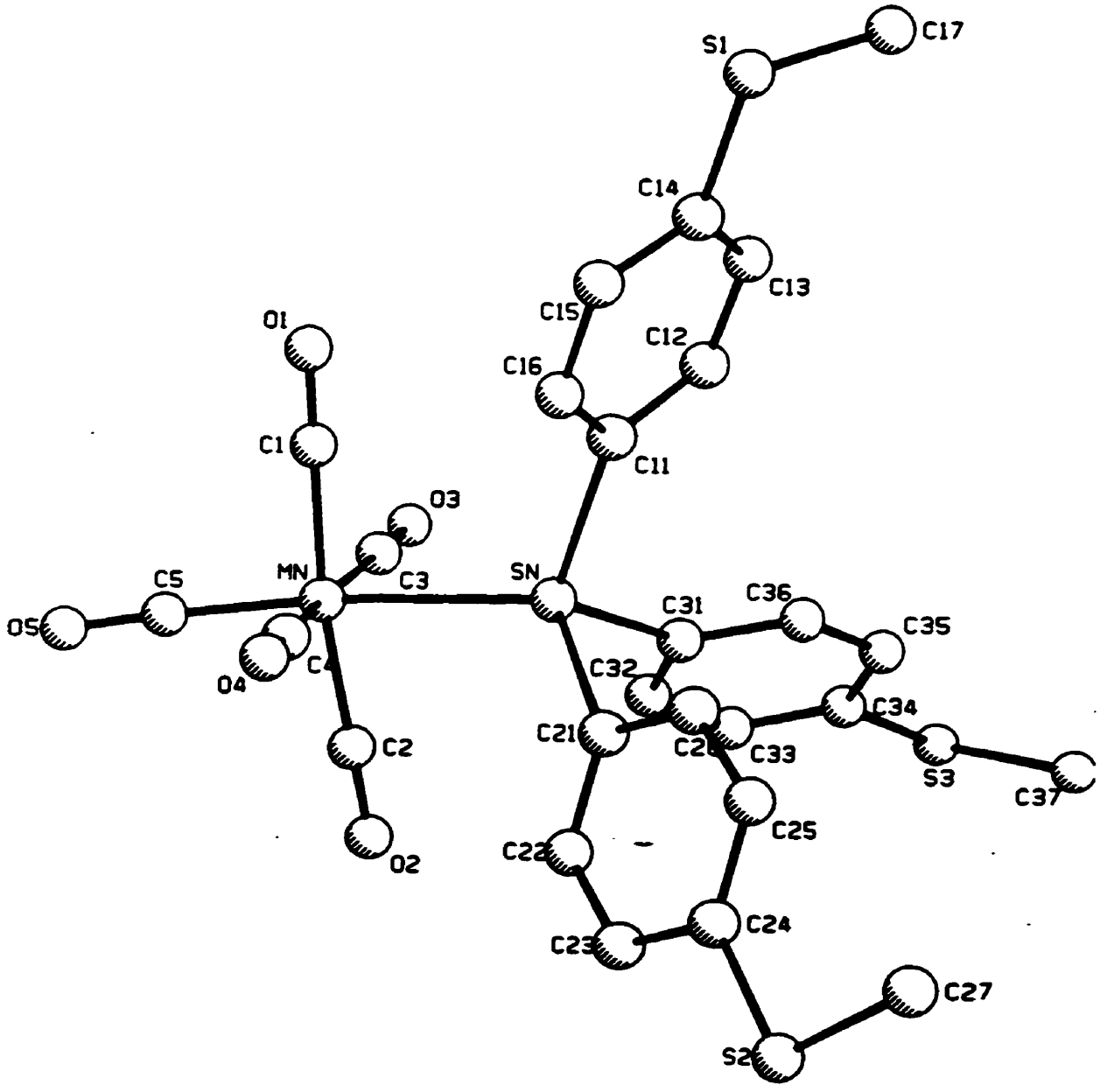

Crystal data for $(p\text{-}CH_3SC_6H_4)_3SnMn(CO)_5$

Empirical Formula: C26 H21 O4 S3 Sn Mn

Space group: Monoclinic, $P2_1/n$

Cell dimensions:

$a = 10.966\ (1)$Å

$b = 21.229\ (2)$Å

$c = 12.297\ (3)$Å

$\alpha = 90°$

$\beta = 101.22\ (1)°$

$\gamma = 90°$

Volume = 2808.0 (8)Å^3

FW = 683.24

Z = 4

$D_{calc} = 1.616$ g / cm^3

F(000) = 1360

Mo Kα radiation

$\lambda = 0.7093$ Å

Cell parameters from 23 reflections

$2\theta = 25 - 30°$

$\mu = 1.596$ mm^{-1}

T = 295 (2) °K

Colourless block

$0.45 \times 0.25 \times 0.22$ mm

Data collection

Rigaku AFC –6S diffractometer

ω / 2θ scans

Absorption correction: *Psi scans*

$T_{min} = 0.66$, $T_{max} = 0.57$

9864 measured reflections

4961 independent reflections

3188 observed reflections [$I > 2\sigma(I)$]

$R_{int} = 0.077$

$\theta_{max} = 50.0°$

$h = -13 \rightarrow 13$

$k = 0 \rightarrow 25$

$l = -15 \rightarrow 15$

3 standard reflections were monitored every 250 reflections

Intensity decay: 0.7 %

Structure was solved by the Patterson method.

Refinement

Refinement on F^2	329 parameters
$R(F^2 > 2\sigma(F^2)) = 0.0544$	H atoms riding,
$wR(F^2) = 0.1079$	C–H = 0.93 - 0.97 Å
GoF = 1.037	$(\Delta/\sigma) = -0.003$
57 atoms	$\Delta\rho_{max} = 0.522$ e/Å^3
4961 reflections	$\Delta\rho_{min} = -0.673$ e/Å^3

where

$R = \Sigma(Fo-Fc) / \Sigma Fo$

$wR = [\Sigma(w(Fo-Fc)^2) / \Sigma wFo^2]^{1/2}$

GoF = [Σ(w(Fo-Fc)^2) / (No. of refins - No. of params.)

Table A2.17: Fractional atomic coordinates and equivalent isotropic displacement parameters (10^2 Å) for $(p\text{-}CH_3SC_6H_4)_3SnMn(CO)_5$.

	x	y	z	U_{eq}
Sn	0.08026(5)	0.13260(2)	0.21754(4)	3.74(2)
Mn	-0.08421(10)	0.04537(5)	0.24730(9)	3.91(3)
S(2)	0.0695(2)	0.19783(12)	-0.3188(2)	6.70(7)
S(1)	0.0384(3)	0.42237(10)	0.4325(2)	7.08(7)
S(3)	0.6679(2)	0.10146(12)	0.4992(2)	6.69(7)
O(4)	-0.1333(5)	0.0211(3)	0.0033(5)	6.9(2)
O(2)	-0.0041(6)	0.0748(3)	0.4878(5)	6.7(2)
O(3)	0.1190(6)	-0.0505(3)	0.2675(5)	7.0(2)
O(1)	-0.2626(6)	0.1523(3)	0.1996(6)	8.1(2)
O(5)	-0.2771(6)	-0.0404(3)	0.3012(6)	8.0(2)
C(4)	-0.1150(7)	0.0300(4)	0.0958(7)	4.9(2)
C(2)	-0.0339(7)	0.0637(3)	0.3963(7)	4.6(2)
C(3)	0.0427(7)	-0.0144(4)	0.2601(6)	4.4(2)
C(1)	-0.1940(8)	0.1109(4)	0.2208(7)	5.0(2)
C(5)	-0.2017(8)	-0.0096(4)	0.2781(7)	5.5(2)
C(11)	0.0479(6)	0.2247(3)	0.2801(6)	4.0(2)
C(12)	0.0244(7)	0.2354(4)	0.3845(6)	4.8(2)
C(13)	0.0221(8)	0.2954(3)	0.4284(6)	5.2(2)
C(14)	0.0435(7)	0.3487(3)	0.3682(7)	4.7(2)
C(15)	0.0632(9)	0.3383(4)	0.2634(7)	7.0(3)
C(16)	0.0654(9)	0.2778(4)	0.2211(7)	6.9(3)
C(17)	0.0798(9)	0.4769(4)	0.3341(8)	7.4(3)
C(21)	0.0822(7)	0.1493(3)	0.0458(6)	4.1(2)
C(22)	0.1853(7)	0.1370(4)	-0.0022(6)	4.6(2)
C(23)	0.1851(7)	0.1514(4)	-0.1112(6)	4.8(2)
C(24)	0.0799(7)	0.1769(4)	-0.1774(6)	4.6(2)
C(25)	-0.0242(7)	0.1867(4)	-0.1332(6)	5.1(2)
C(26)	-0.0229(7)	0.1735(3)	-0.0236(6)	4.6(2)
C(27)	0.2260(8)	0.1946(5)	-0.3405(7)	7.5(3)
C(31)	0.2696(6)	0.1151(3)	0.3034(6)	4.0(2)
C(32)	0.3029(7)	0.0774(4)	0.3938(7)	5.2(2)
C(33)	0.4224(8)	0.0746(4)	0.4536(7)	5.4(2)
C(34)	0.5139(7)	0.1107(4)	0.4215(6)	4.3(2)
C(35)	0.4844(7)	0.1482(4)	0.3308(7)	5.8(2)
C(36)	0.3619(7)	0.1529(4)	0.2733(6)	5.2(2)
C(37)	0.7354(8)	0.1768(4)	0.4881(8)	7.6(3)

Table A2.18: Bond lengths (Å) and angles (°) for (p-$CH_3SC_6H_4$)$_3$SnMn(CO)$_5$.

Sn-C(21)	2.145(7)	Sn-C(11)	2.156(7)
Sn-C(31)	2.171(7)	Sn-Mn	2.6596(12)
Mn-C(1)	1.827(8)	Mn-C(5)	1.832(9)
Mn-C(2)	1.849(9)	Mn-C(4)	1.856(9)
Mn-C(3)	1.867(8)	S(2)-C(24)	1.777(7)
S(2)-C(27)	1.789(9)	S(1)-C(14)	1.758(8)
S(1)-C(17)	1.796(9)	S(3)-C(37)	1.779(10)
S(3)-C(34)	1.782(7)	O(4)-C(4)	1.133(8)
O(2)-C(2)	1.133(9)	O(3)-C(3)	1.125(8)
O(1)-C(1)	1.153(9)	O(5)-C(5)	1.133(9)
C(11)-C(16)	1.375(10)	C(11)-C(12)	1.376(10)
C(12)-C(13)	1.386(10)	C(12)-H(12)	0.93
C(13)-C(14)	1.396(10)	C(13)-H(13)	0.93
C(14)-C(15)	1.365(10)	C(15)-C(16)	1.386(11)
C(15)-H(15)	0.93	C(16)-H(16)	0.93
C(17)-H(17A)	0.96	C(17)-H(17B)	0.96
C(17)-H(17C)	0.96	C(21)-C(26)	1.392(9)
C(21)-C(22)	1.399(10)	C(22)-C(23)	1.375(10)
C(22)-H(22)	0.93	C(23)-C(24)	1.386(10)
C(23)-H(23)	0.93	C(24)-C(25)	1.372(10)
C(25)-C(26)	1.373(10)	C(25)-H(25)	0.93
C(26)-H(26)	0.93	C(27)-H(27A)	0.96
C(27)-H(27B)	0.96	C(27)-H(27C)	0.96
C(31)-C(32)	1.361(10)	C(31)-C(36)	1.397(10)
C(32)-C(33)	1.374(10)	C(32)-H(32)	0.93
C(33)-C(34)	1.380(10)	C(33)-H(33)	0.93
C(34)-C(35)	1.358(10)	C(35)-C(36)	1.394(10)
C(35)-H(35)	0.93	C(36)-H(36)	0.93
C(37)-H(37A)	0.96	C(37)-H(37B)	0.96
C(37)-H(37C)	0.96		

C(21)-Sn-C(11)	103.6(3)	C(21)-Sn-C(31)	108.4(3)
C(11)-Sn-C(31)	100.9(3)	C(21)-Sn-Mn	112.8(2)
C(11)-Sn-Mn	114.8(2)	C(31)-Sn-Mn	115.1(2)
C(1)-Mn-C(5)	93.2(4)	C(1)-Mn-C(2)	94.3(3)
C(5)-Mn-C(2)	90.9(3)	C(1)-Mn-C(4)	88.3(3)
C(5)-Mn-C(4)	95.6(3)	C(2)-Mn-C(4)	172.9(3)
C(1)-Mn-C(3)	170.7(3)	C(5)-Mn-C(3)	95.3(4)
C(2)-Mn-C(3)	89.2(3)	C(4)-Mn-C(3)	87.2(3)
C(1)-Mn-Sn	83.5(2)	C(5)-Mn-Sn	174.4(3)
C(2)-Mn-Sn	84.9(2)	C(4)-Mn-Sn	88.9(2)
C(3)-Mn-Sn	88.3(2)	C(24)-S(2)-C(27)	104.8(4)
C(14)-S(1)-C(17)	103.7(4)	C(37)-S(3)-C(34)	103.0(4)
O(4)-C(4)-Mn	179.4(6)	O(2)-C(2)-Mn	179.4(8)
O(3)-C(3)-Mn	179.8(8)	O(1)-C(1)-Mn	177.1(7)
O(5)-C(5)-Mn	175.4(8)	C(16)-C(11)-C(12)	115.3(7)
C(16)-C(11)-Sn	120.4(6)	C(12)-C(11)-Sn	123.8(5)
C(11)-C(12)-C(13)	122.4(7)	C(11)-C(12)-H(12)	118.8
C(13)-C(12)-H(12)	118.8	C(12)-C(13)-C(14)	121.4(7)
C(12)-C(13)-H(13)	119.3	C(14)-C(13)-H(13)	119.3
C(15)-C(14)-C(13)	116.3(7)	C(15)-C(14)-S(1)	126.4(6)

C(13)-C(14)-S(1)	117.3(6)	C(14)-C(15)-C(16)	121.4(8)
C(14)-C(15)-H(15)	119.3	C(16)-C(15)-H(15)	119.3
C(11)-C(16)-C(15)	123.2(8)	C(11)-C(16)-H(16)	118.4
C(15)-C(16)-H(16)	118.4	S(1)-C(17)-H(17A)	109.5
S(1)-C(17)-H(17B)	109.5	H(17A)-C(17)-H(17B)	109.5
S(1)-C(17)-H(17C)	109.5	H(17A)-C(17)-H(17C)	109.5
H(17B)-C(17)-H(17C)	109.5	C(26)-C(21)-C(22)	116.8(6)
C(26)-C(21)-Sn	120.0(5)	C(22)-C(21)-Sn	123.3(5)
C(23)-C(22)-C(21)	121.5(7)	C(23)-C(22)-H(22)	119.3
C(21)-C(22)-H(22)	119.3	C(22)-C(23)-C(24)	120.2(7)
C(22)-C(23)-H(23)	119.9	C(24)-C(23)-H(23)	119.9
C(25)-C(24)-C(23)	119.2(7)	C(25)-C(24)-S(2)	116.8(6)
C(23)-C(24)-S(2)	124.1(6)	C(24)-C(25)-C(26)	120.5(7)
C(24)-C(25)-H(25)	119.7	C(26)-C(25)-H(25)	119.7
C(25)-C(26)-C(21)	121.7(7)	C(25)-C(26)-H(26)	119.1
C(21)-C(26)-H(26)	119.1	S(2)-C(27)-H(27A)	109.5
S(2)-C(27)-H(27B)	109.5(3)	H(27A)-C(27)-H(27B)	109.5
S(2)-C(27)-H(27C)	109.5	H(27A)-C(27)-H(27C)	109.5
H(27B)-C(27)-H(27C)	109.5	C(32)-C(31)-C(36)	117.5(7)
C(32)-C(31)-Sn	125.2(6)	C(36)-C(31)-Sn	116.5(5)
C(31)-C(32)-C(33)	122.6(8)	C(31)-C(32)-H(32)	118.7
C(33)-C(32)-H(32)	118.7(5)	C(32)-C(33)-C(34)	119.6(7)
C(32)-C(33)-H(33)	120.2	C(34)-C(33)-H(33)	120.2
C(35)-C(34)-C(33)	119.4(7)	C(35)-C(34)-S(3)	123.7(6)
C(33)-C(34)-S(3)	116.8(6)	C(34)-C(35)-C(36)	120.7(8)
C(34)-C(35)-H(35)	119.6	C(36)-C(35)-H(35)	119.6
C(35)-C(36)-C(31)	120.0(7)	C(35)-C(36)-H(36)	120.0
C(31)-C(36)-H(36)	120.0	S(3)-C(37)-H(37A)	109.5
S(3)-C(37)-H(37B)	109.5	H(37A)-C(37)-H(37B)	109.5
S(3)-C(37)-H(37C)	109.5	H(37A)-C(37)-H(37C)	109.5
H(37B)-C(37)-H(37C)	109.5		

Table A2.19: Torsion angles (in degrees) for $(p\text{-}CH_3SC_6H_4)_3SnMn(CO)_5$.

C(21)-Sn-Mn-C(1)	-82.2(3)	C(11)-Sn-Mn-C(1)	36.2(3)
C(31)-Sn-Mn-C(1)	152.8(3)	C(21)-Sn-Mn-C(5)	-136(3)
C(11)-Sn-Mn-C(5)	-18(3)	C(31)-Sn-Mn-C(5)	98(3)
C(21)-Sn-Mn-C(2)	-177.1(3)	C(11)-Sn-Mn-C(2)	-58.8(3)
C(31)-Sn-Mn-C(2)	57.8(3)	C(21)-Sn-Mn-C(4)	6.3(3)
C(11)-Sn-Mn-C(4)	124.6(3)	C(31)-Sn-Mn-C(4)	-118.8(3)
C(21)-Sn-Mn-C(3)	93.5(3)	C(11)-Sn-Mn-C(3)	-148.1(3)
C(31)-Sn-Mn-C(3)	-31.5(3)	C(21)-Sn-C(11)-C(16)	-16.6(7)
C(31)-Sn-C(11)-C(16)	95.6(7)	Mn-Sn-C(11)-C(16)	-140.0(6)
C(21)-Sn-C(11)-C(12)	171.7(6)	C(31)-Sn-C(11)-C(12)	-76.1(7)
Mn-Sn-C(11)-C(12)	48.3(7)	C(16)-C(11)-C(12)-C(13)	-1.8(12)
Sn-C(11)-C(12)-C(13)	170.3(6)	C(11)-C(12)-C(13)-C(14)	0.2(13)
C(12)-C(13)-C(14)-C(15)	1.7(12)	C(12)-C(13)-C(14)-S(1)	-179.9(6)
C(17)-S(1)-C(14)-C(15)	-5.4(9)	C(17)-S(1)-C(14)-C(13)	176.4(7)
C(13)-C(14)-C(15)-C(16)	-1.9(14)	S(1)-C(14)-C(15)-C(16)	179.9(7)
C(12)-C(11)-C(16)-C(15)	1.7(13)	Sn-C(11)-C(16)-C(15)	-170.7(8)
C(14)-C(15)-C(16)-C(11)	0(2)	C(11)-Sn-C(21)-C(26)	-61.1(6)
C(31)-Sn-C(21)-C(26)	-167.7(6)	Mn-Sn-C(21)-C(26)	63.7(6)
C(11)-Sn-C(21)-C(22)	118.9(6)	C(31)-Sn-C(21)-C(22)	12.3(7)
Mn-Sn-C(21)-C(22)	-116.3(6)	C(26)-C(21)-C(22)-C(23)	3.4(11)
Sn-C(21)-C(22)-C(23)	-176.6(6)	C(21)-C(22)-C(23)-C(24)	-2.0(12)
C(22)-C(23)-C(24)-C(25)	-1.0(11)	C(22)-C(23)-C(24)-S(2)	179.5(6)
C(27)-S(2)-C(24)-C(25)	168.5(6)	C(27)-S(2)-C(24)-C(23)	-12.0(8)
C(23)-C(24)-C(25)-C(26)	2.4(12)	S(2)-C(24)-C(25)-C(26)	-178.1(6)
C(24)-C(25)-C(26)-C(21)	-0.9(12)	C(22)-C(21)-C(26)-C(25)	-2.0(11)
Sn-C(21)-C(26)-C(25)	178.0(6)	C(21)-Sn-C(31)-C(32)	-149.4(6)
C(11)-Sn-C(31)-C(32)	102.2(7)	Mn-Sn-C(31)-C(32)	-22.0(7)
C(21)-Sn-C(31)-C(36)	40.7(6)	C(11)-Sn-C(31)-C(36)	-67.7(6)
Mn-Sn-C(31)-C(36)	168.1(5)	C(36)-C(31)-C(32)-C(33)	-1.3(12)
Sn-C(31)-C(32)-C(33)	-171.1(6)	C(31)-C(32)-C(33)-C(34)	-0.6(13)
C(32)-C(33)-C(34)-C(35)	-0.4(12)	C(32)-C(33)-C(34)-S(3)	-176.9(6)
C(37)-S(3)-C(34)-C(35)	33.2(8)	C(37)-S(3)-C(34)-C(33)	-150.5(6)
C(33)-C(34)-C(35)-C(36)	3.3(12)	S(3)-C(34)-C(35)-C(36)	179.5(6)
C(34)-C(35)-C(36)-C(31)	-5.1(13)	C(32)-C(31)-C(36)-C(35)	4.0(12)
Sn-C(31)-C(36)-C(35)	174.7(6)		

Table A2.20: Anisotropic thermal factors (10^2 Å^2) for $(p\text{-}CH_3SC_6H_4)_3SnMn(CO)_5$.

	U_{11}	U_{22}	U_{33}	U_{12}	U_{13}	U_{23}
Sn	3.47(3)	3.93(3)	3.77(3)	0.41(3)	0.61(2)	-0.02(3)
Mn	3.51(6)	3.77(6)	4.44(7)	-0.05(5)	0.76(5)	-0.06(5)
S(2)	6.9(2)	9.3(2)	3.63(12)	0.74(11)	0.33(11)	-1.51(14)
S(1)	9.6(2)	4.55(13)	7.5(2)	-1.27(12)	2.7(2)	-0.68(13)
S(3)	4.04(13)	7.8(2)	7.6(2)	0.11(13)	-0.59(11)	0.82(12)
O(4)	6.3(4)	8.5(5)	5.3(4)	-1.2(3)	0.0(3)	0.4(3)
O(2)	9.2(5)	5.9(4)	4.5(4)	-0.8(3)	0.6(3)	-0.7(3)
O(3)	5.9(4)	6.1(4)	8.5(5)	0.0(3)	0.4(3)	1.9(3)
O(1)	6.4(4)	8.0(5)	10.1(5)	0.6(4)	2.0(4)	3.2(4)
O(5)	6.5(4)	6.4(4)	11.6(6)	0.5(4)	3.3(4)	-1.8(4)
C(4)	4.1(5)	4.5(5)	6.0(6)	-0.3(4)	0.5(4)	-0.1(4)
C(2)	4.3(5)	3.6(4)	6.0(6)	-0.2(4)	1.3(4)	0.0(4)
C(3)	4.2(5)	4.0(5)	4.8(5)	-0.6(4)	0.7(4)	-0.1(4)
C(1)	4.8(5)	4.2(5)	6.1(5)	-0.3(4)	1.5(4)	0.1(4)
C(5)	5.2(6)	5.2(5)	6.2(6)	-0.8(4)	1.3(4)	-1.4(4)
C(11)	3.6(4)	4.0(4)	4.7(5)	0.1(4)	1.3(3)	-0.2(3)
C(12)	6.2(5)	4.8(5)	3.5(4)	0.8(4)	1.1(4)	-1.0(4)
C(13)	8.5(6)	3.6(5)	3.8(4)	0.2(4)	1.7(4)	-0.1(4)
C(14)	4.5(5)	4.1(5)	5.6(5)	0.0(4)	1.2(4)	-0.5(4)
C(15)	11.3(8)	4.9(5)	6.3(6)	1.2(5)	5.0(6)	-0.5(5)
C(16)	9.7(8)	6.4(6)	5.5(5)	0.0(5)	4.1(5)	0.1(6)
C(17)	8.7(7)	3.4(5)	10.2(8)	0.2(5)	2.3(6)	-0.4(5)
C(21)	4.8(5)	3.8(4)	3.6(4)	0.7(3)	0.6(4)	-0.3(4)
C(22)	4.4(4)	4.7(5)	4.5(4)	0.3(4)	0.3(3)	0.7(4)
C(23)	4.6(5)	5.9(5)	4.1(4)	-0.6(4)	1.1(4)	-0.5(4)
C(24)	5.4(5)	4.6(5)	3.9(4)	-0.2(4)	0.7(4)	-1.8(4)
C(25)	4.4(5)	6.3(6)	4.2(5)	1.0(4)	-0.2(4)	-0.1(4)
C(26)	3.9(4)	5.3(5)	4.7(5)	0.8(4)	1.0(4)	0.3(4)
C(27)	7.7(7)	9.7(8)	5.6(6)	1.5(5)	2.8(5)	-0.4(6)
C(31)	3.1(4)	3.8(4)	4.9(4)	0.7(3)	0.6(3)	0.3(3)
C(32)	4.5(5)	4.6(5)	6.4(6)	1.0(4)	1.0(4)	0.1(4)
C(33)	4.9(5)	5.1(5)	6.0(6)	1.6(4)	0.4(4)	0.6(4)
C(34)	3.6(4)	5.1(5)	3.9(4)	-0.3(4)	0.4(3)	0.8(4)
C(35)	4.4(5)	6.6(6)	6.4(6)	0.2(4)	1.2(4)	-1.4(4)
C(36)	4.8(5)	5.8(5)	4.8(5)	0.9(4)	0.3(4)	-0.2(4)
C(37)	4.6(5)	9.1(7)	8.9(7)	-3.8(6)	0.9(5)	-1.0(5)

Structural Analysis of

Tris(*p*-fluorophenyl)tin(pentacarbonyl)manganese(I)

$(p\text{-}FC_6H_4)_3SnMn(CO)_5$

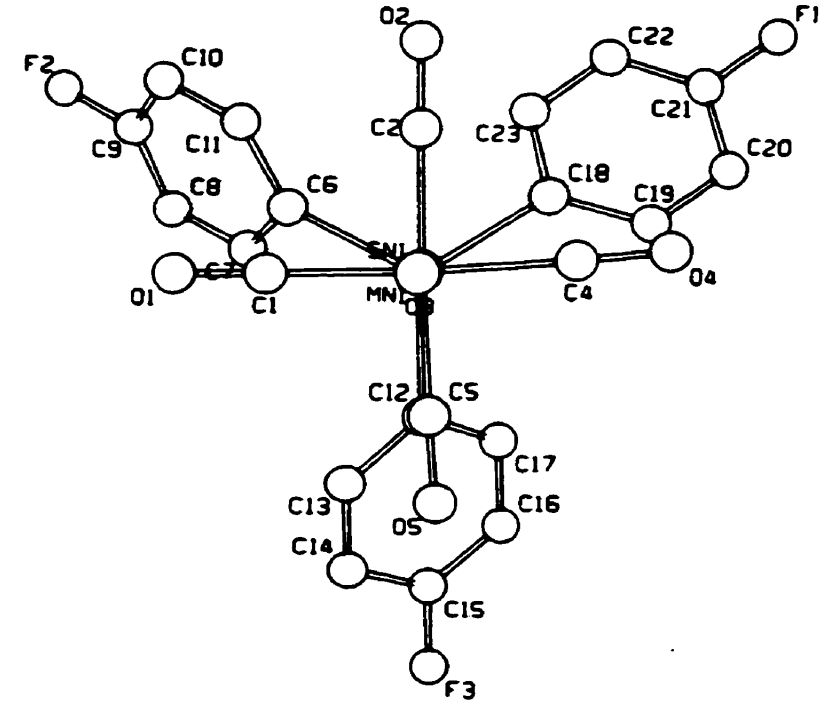

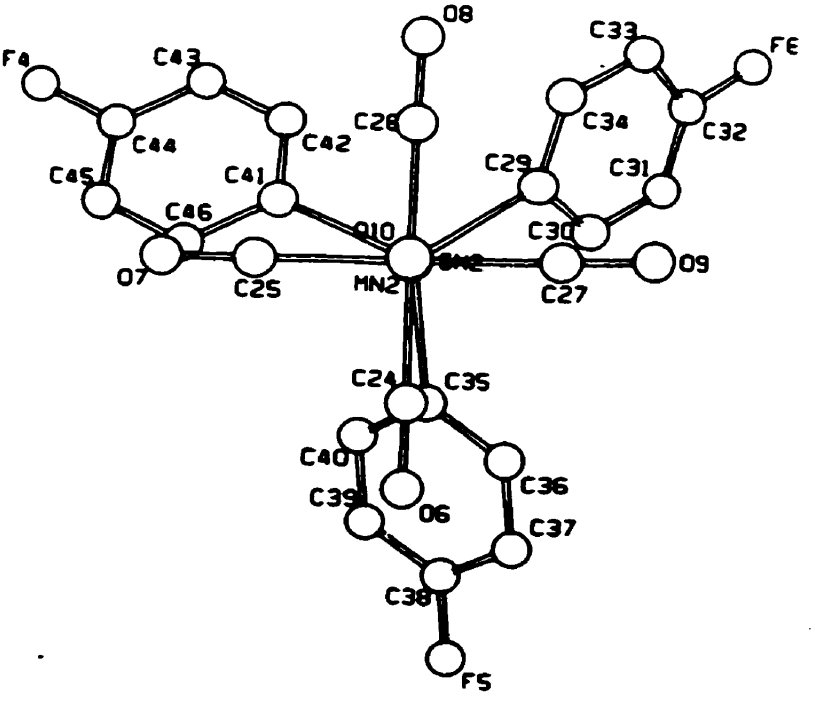

Crystal data for $(p\text{-}FC_6H_4)_3SnMn(CO)_5$

Empirical Formula: C23 H12 O5 Sn Mn F3

Space group: Triclinic, P 1

Cell dimensions:

a = 10.636 (5)Å

b = 11.450 (3)Å

c = 21.992 (7)Å

α = 83.20 (3)°

β = 78.30 (4)°

γ = 63.03 (2)°

Volume = 2336 (2)Å^3

FW = 598.96

Z = 4

D_{calc} = 1.703 g / cm^3

F(000) = 1168

Mo Kα radiation

λ = 0.7093 Å

Cell parameters from 19 reflections

2θ = 25 – 30°

μ = 1.664 mm^{-1}

T = 295 (2) °K

Colourless block

0.52 × 0.35 × 0.12 mm

Data collection

Rigaku AFC –6S diffractometer

ω / 2θ scans

Absorption correction: *Psi scans*

T_{min} = 0.45, T_{max} = 0.66

16582 measured reflections

8291 independent reflections

5383 observed reflections [$I > 2\sigma(I)$]

R_{int} = 0.079

θ_{max} = 50.0°

h = -12 → 12

k = -13 → 13

l = -26 → 26

3 standard reflections were monitored every 250 reflections

Intensity decay: 1.5 %

Structure was solved by the heavy atom method.

Refinement

Refinement on F^2	596 parameters
$R(F^2 > 2\sigma(F^2)) = 0.0518$	H atoms riding,
$wR(F^2) = 0.0997$	C–H = 0.93 Å
GoF = 1.101	$(\Delta/\sigma) = 0.004$
90 atoms	$\Delta\rho_{max} = 0.524$ e/Å^3
8291 reflections	$\Delta\rho_{min} = -0.550$ e/Å^3

where

$R = \Sigma(Fo-Fc) / \Sigma Fo$

$wR = [\Sigma(w(Fo-Fc)^2) / \Sigma wFo^2]^{1/2}$

GoF = [Σ(w(Fo-Fc)^2) / (No. of refins - No. of params.)

Table A2.21: Fractional atomic coordinates and equivalent isotropic displacement parameters (10^2 Å) for $(p\text{-}FC_6H_4)_3SnMn(CO)_5$.

	x	y	z	U_{eq}
Sn(1)	0.23022(5)	0.15580(4)	0.42670(2)	4.48(2)
Mn(1)	0.01555(12)	0.30811(10)	0.36677(5)	5.36(3)
F(1)	0.4238(6)	-0.4490(4)	0.4314(2)	10.4(2)
F(2)	0.1179(6)	0.2843(5)	0.7063(2)	9.9(2)
F(3)	0.7811(5)	0.1967(5)	0.2854(3)	10.2(2)
O(1)	-0.0778(7)	0.0982(6)	0.4046(3)	10.4(2)
O(2)	0.2075(8)	0.1532(7)	0.2573(3)	11.0(2)
O(3)	0.1574(7)	0.4830(6)	0.3298(4)	12.8(3)
O(4)	-0.1300(7)	0.4442(6)	0.4869(3)	10.7(2)
O(5)	-0.2306(6)	0.4753(6)	0.3040(3)	8.4(2)
C(1)	-0.0440(8)	0.1785(8)	0.3910(4)	7.2(2)
C(2)	0.1318(10)	0.2120(8)	0.2997(4)	7.3(2)
C(3)	0.1038(9)	0.4168(8)	0.3450(5)	7.8(3)
C(4)	-0.0752(9)	0.3910(7)	0.4408(4)	7.1(2)
C(5)	-0.1350(9)	0.4112(7)	0.3274(4)	6.1(2)
C(11)	0.2891(7)	-0.0500(6)	0.4265(3)	4.6(2)
C(12)	0.3271(7)	-0.1264(6)	0.4797(4)	5.6(2)
C(13)	0.3732(8)	-0.2605(7)	0.4813(4)	6.3(2)
C(14)	0.3780(9)	-0.3170(7)	0.4301(4)	6.2(2)
C(15)	0.3394(9)	-0.2477(8)	0.3766(4)	7.6(2)
C(16)	0.2941(8)	-0.1141(7)	0.3763(4)	6.7(2)
C(21)	0.1912(8)	0.1992(6)	0.5228(3)	4.8(2)
C(22)	0.0774(8)	0.1922(7)	0.5639(4)	6.1(2)
C(23)	0.0512(9)	0.2200(8)	0.6264(4)	6.9(2)
C(24)	0.1411(10)	0.2572(7)	0.6450(4)	6.7(2)
C(25)	0.2547(9)	0.2646(7)	0.6078(4)	6.2(2)
C(26)	0.2806(8)	0.2351(6)	0.5459(4)	5.8(2)
C(31)	0.4227(7)	0.1710(6)	0.3832(3)	4.5(2)
C(32)	0.4382(8)	0.2832(7)	0.3820(3)	5.7(2)
C(33)	0.5589(8)	0.2938(7)	0.3491(3)	6.1(2)
C(34)	0.6635(8)	0.1874(7)	0.3177(4)	6.3(2)
C(35)	0.6528(8)	0.0745(7)	0.3177(4)	7.1(2)
C(36)	0.5312(8)	0.0671(6)	0.3504(3)	5.6(2)
Sn(2)	0.19062(5)	0.15305(5)	0.90706(2)	5.06(2)
Mn(2)	0.29780(12)	0.32074(10)	0.85987(5)	5.48(3)
F(4)	-0.2884(5)	0.1854(5)	0.7706(2)	10.1(2)
F(5)	-0.0620(6)	0.2676(5)	1.1875(2)	11.5(2)
F(6)	0.6062(8)	-0.4463(5)	0.9090(4)	17.8(3)
O(6)	0.0186(6)	0.4824(6)	0.8167(3)	8.9(2)
O(7)	0.4104(7)	0.1698(6)	0.7452(3)	9.6(2)
O(8)	0.5562(7)	0.1237(7)	0.9087(3)	10.7(2)
O(9)	0.1799(9)	0.4564(6)	0.9806(3)	11.8(3)
O(10)	0.4208(7)	0.5036(7)	0.8061(4)	11.1(2)
C(6)	0.1239(9)	0.4196(8)	0.8337(4)	6.6(2)
C(7)	0.3649(9)	0.2269(8)	0.7891(4)	6.7(2)
C(8)	0.4569(10)	0.1996(9)	0.8908(4)	7.1(2)
C(9)	0.2244(10)	0.4031(8)	0.9354(4)	8.0(3)
C(10)	0.3746(9)	0.4341(9)	0.8263(4)	7.4(2)
C(41)	0.0251(7)	0.1637(7)	0.8616(3)	4.9(2)

C(42)	0.0454(8)	0.0637(7)	0.8267(3)	5.7(2)
C(43)	-0.0576(9)	0.0696(8)	0.7958(4)	6.9(2)
C(44)	-0.1851(9)	0.1788(9)	0.8012(4)	7.1(2)
C(45)	-0.2120(8)	0.2808(8)	0.8351(4)	7.3(2)
C(46)	-0.1064(8)	0.2730(8)	0.8663(4)	6.6(2)
C(51)	0.1042(8)	0.1863(6)	1.0042(3)	5.2(2)
C(52)	0.1882(9)	0.1865(7)	1.0438(4)	6.8(2)
C(53)	0.1337(11)	0.2133(9)	1.1065(4)	8.4(3)
C(54)	-0.0037(12)	0.2385(8)	1.1265(4)	7.6(3)
C(55)	-0.0920(10)	0.2377(8)	1.0893(4)	7.8(3)
C(56)	-0.0357(9)	0.2112(7)	1.0274(4)	6.6(2)
C(61)	0.3430(8)	-0.0509(7)	0.9045(4)	6.1(2)
C(62)	0.3455(9)	-0.1268(8)	0.9575(4)	8.0(3)
C(63)	0.4341(12)	-0.2602(9)	0.9596(5)	10.2(3)
C(64)	0.5208(12)	-0.3143(10)	0.9081(7)	11.0(4)
C(65)	0.5236(12)	-0.2483(11)	0.8529(6)	11.7(4)
C(66)	0.4328(9)	-0.1114(9)	0.8515(5)	9.4(3)

Table A2.22: Bond lengths (Å) and angles (°) for $(p\text{-}FC_6H_4)_3SnMn(CO)_5$.

Sn(1)-C(21)	2.143(7)	Sn(1)-C(11)	2.147(6)
Sn(1)-C(31)	2.151(7)	Sn(1)-Mn(1)	2.656(2)
Mn(1)-C(5)	1.820(8)	Mn(1)-C(2)	1.823(9)
Mn(1)-C(4)	1.838(9)	Mn(1)-C(3)	1.842(9)
Mn(1)-C(1)	1.848(9)	F(1)-C(14)	1.360(8)
F(2)-C(24)	1.366(8)	F(3)-C(34)	1.350(8)
O(1)-C(1)	1.120(9)	O(2)-C(2)	1.150(9)
O(3)-C(3)	1.126(9)	O(4)-C(4)	1.151(9)
O(5)-C(5)	1.133(8)	C(11)-C(16)	1.375(9)
C(11)-C(12)	1.389(9)	C(12)-C(13)	1.382(9)
C(12)-H(12)	0.93	C(13)-C(14)	1.343(10)
C(13)-H(13)	0.93	C(14)-C(15)	1.366(10)
C(15)-C(16)	1.379(9)	C(15)-H(15)	0.93
C(16)-H(16)	0.93	C(21)-C(22)	1.384(9)
C(21)-C(26)	1.390(9)	C(22)-C(23)	1.391(10)
C(22)-H(22)	0.93	C(23)-C(24)	1.354(11)
C(23)-H(23)	0.93	C(24)-C(25)	1.346(11)
C(25)-C(26)	1.384(9)	C(25)-H(25)	0.93
C(26)-H(26)	0.93	C(31)-C(32)	1.364(9)
C(31)-C(36)	1.374(9)	C(32)-C(33)	1.390(9)
C(32)-H(32)	0.93	C(33)-C(34)	1.363(9)
C(33)-H(33)	0.93	C(34)-C(35)	1.348(10)
C(35)-C(36)	1.380(10)	C(35)-H(35)	0.93
C(36)-H(36)	0.93		
Sn(2)-C(41)	2.145(7)	Sn(2)-C(51)	2.153(7)
Sn(2)-C(61)	2.155(7)	Sn(2)-Mn(2)	2.664(2)
Mn(2)-C(7)	1.826(8)	Mn(2)-C(8)	1.834(9)
Mn(2)-C(10)	1.841(9)	Mn(2)-C(6)	1.847(9)
Mn(2)-C(9)	1.852(10)	F(4)-C(44)	1.370(8)
F(5)-C(54)	1.370(9)	F(6)-C(64)	1.366(10)
O(6)-C(6)	1.134(8)	O(7)-C(7)	1.126(8)
O(8)-C(8)	1.131(9)	O(9)-C(9)	1.131(9)
O(10)-C(10)	1.120(9)	C(41)-C(42)	1.366(9)
C(41)-C(46)	1.385(9)	C(42)-C(43)	1.374(10)
C(42)-H(42)	0.93	C(43)-C(44)	1.360(10)
C(43)-H(43)	0.93	C(44)-C(45)	1.348(10)
C(45)-C(46)	1.395(10)	C(45)-H(45)	0.93
C(46)-H(46)	0.93	C(51)-C(52)	1.368(10)
C(51)-C(56)	1.377(10)	C(52)-C(53)	1.396(10)
C(52)-H(25)	0.93	C(53)-C(54)	1.342(12)
C(53)-H(53)	0.93	C(54)-C(55)	1.369(11)
C(55)-C(56)	1.382(10)	C(55)-H(55)	0.93
C(56)-H(56)	0.93	C(61)-C(62)	1.366(11)
C(61)-C(66)	1.376(11)	C(62)-C(63)	1.385(11)
C(62)-H(62)	0.93	C(63)-C(64)	1.319(14)
C(63)-H(63)	0.93	C(64)-C(65)	1.35(2)
C(65)-C(66)	1.421(12)	C(65)-H(65)	0.93
C(66)-H(66)	0.93		
C(21)-Sn(1)-C(11)	104.8(3)	C(21)-Sn(1)-C(31)	107.8(3)

C(11)-Sn(1)-C(31)	104.0(2)	C(21)-Sn(1)-Mn(1)	114.1(2)
C(11)-Sn(1)-Mn(1)	114.8(2)	C(31)-Sn(1)-Mn(1)	110.5(2)
C(5)-Mn(1)-C(2)	96.4(4)	C(5)-Mn(1)-C(4)	93.1(4)
C(2)-Mn(1)-C(4)	170.4(4)	C(5)-Mn(1)-C(3)	93.8(3)
C(2)-Mn(1)-C(3)	87.1(4)	C(4)-Mn(1)-C(3)	91.0(4)
C(5)-Mn(1)-C(1)	95.1(3)	C(2)-Mn(1)-C(1)	89.0(4)
C(4)-Mn(1)-C(1)	91.5(4)	C(3)-Mn(1)-C(1)	170.6(3)
C(5)-Mn(1)-Sn(1)	178.4(2)	C(2)-Mn(1)-Sn(1)	84.5(3)
C(4)-Mn(1)-Sn(1)	86.0(2)	C(3)-Mn(1)-Sn(1)	87.6(2)
C(1)-Mn(1)-Sn(1)	83.6(3)	O(1)-C(1)-Mn(1)	178.4(8)
O(2)-C(2)-Mn(1)	178.1(9)	O(3)-C(3)-Mn(1)	177.9(10)
O(4)-C(4)-Mn(1)	178.4(9)	O(5)-C(5)-Mn(1)	178.5(7)
C(16)-C(11)-C(12)	116.4(6)	C(16)-C(11)-Sn(1)	124.5(5)
C(12)-C(11)-Sn(1)	119.1(5)	C(13)-C(12)-C(11)	121.7(7)
C(13)-C(12)-H(12)	119.2	C(11)-C(12)-H(12)	119.2
C(14)-C(13)-C(12)	118.7(7)	C(14)-C(13)-H(13)	120.7
C(12)-C(13)-H(13)	120.7	C(13)-C(14)-F(1)	118.8(7)
C(13)-C(14)-C(15)	122.9(7)	F(1)-C(14)-C(15)	118.3(7)
C(14)-C(15)-C(16)	117.2(7)	C(14)-C(15)-H(15)	121.4
C(16)-C(15)-H(15)	121.4	C(11)-C(16)-C(15)	123.2(7)
C(11)-C(16)-H(16)	118.4	C(15)-C(16)-H(16)	118.4
C(22)-C(21)-C(26)	117.8(7)	C(22)-C(21)-Sn(1)	121.6(5)
C(26)-C(21)-Sn(1)	120.7(5)	C(21)-C(22)-C(23)	122.0(7)
C(21)-C(22)-H(22)	119.0	C(23)-C(22)-H(22)	119.0
C(24)-C(23)-C(22)	116.7(8)	C(24)-C(23)-H(23)	121.6
C(22)-C(23)-H(23)	121.6	C(25)-C(24)-C(23)	124.4(8)
C(25)-C(24)-F(2)	117.9(8)	C(23)-C(24)-F(2)	117.7(8)
C(24)-C(25)-C(26)	118.3(8)	C(24)-C(25)-H(25)	120.8
C(26)-C(25)-H(25)	120.8	C(25)-C(26)-C(21)	120.8(7)
C(25)-C(26)-H(26)	119.6	C(21)-C(26)-H(26)	119.6
C(32)-C(31)-C(36)	117.7(6)	C(32)-C(31)-Sn(1)	123.1(5)
C(36)-C(31)-Sn(1)	118.9(5)	C(31)-C(32)-C(33)	121.9(7)
C(31)-C(32)-H(32)	119.0	C(33)-C(32)-H(32)	119.0
C(34)-C(33)-C(32)	117.8(7)	C(34)-C(33)-H(33)	121.1
C(32)-C(33)-H(33)	121.1	C(35)-C(34)-F(3)	119.5(7)
C(35)-C(34)-C(33)	122.3(7)	F(3)-C(34)-C(33)	118.3(7)
C(34)-C(35)-C(36)	118.6(7)	C(34)-C(35)-H(35)	120.7
C(36)-C(35)-H(35)	120.7	C(31)-C(36)-C(35)	121.6(7)
C(31)-C(36)-H(36)	119.2	C(35)-C(36)-H(36)	119.2

C(41)-Sn(2)-C(51)	107.8(3)	C(41)-Sn(2)-C(61)	104.6(3)
C(51)-Sn(2)-C(61)	104.0(3)	C(41)-Sn(2)-Mn(2)	113.8(2)
C(51)-Sn(2)-Mn(2)	110.5(2)	C(61)-Sn(2)-Mn(2)	115.3(2)
C(7)-Mn(2)-C(8)	88.3(4)	C(7)-Mn(2)-C(10)	92.6(4)
C(8)-Mn(2)-C(10)	96.0(4)	C(7)-Mn(2)-C(6)	90.2(4)
C(8)-Mn(2)-C(6)	169.0(4)	C(10)-Mn(2)-C(6)	94.9(4)
C(7)-Mn(2)-C(9)	174.3(4)	C(8)-Mn(2)-C(9)	90.3(4)
C(10)-Mn(2)-C(9)	93.1(4)	C(6)-Mn(2)-C(9)	90.1(4)
C(7)-Mn(2)-Sn(2)	86.5(3)	C(8)-Mn(2)-Sn(2)	83.5(3)
C(10)-Mn(2)-Sn(2)	178.9(3)	C(6)-Mn(2)-Sn(2)	85.6(2)
C(9)-Mn(2)-Sn(2)	87.9(3)	O(6)-C(6)-Mn(2)	178.1(8)
O(7)-C(7)-Mn(2)	177.6(8)	O(8)-C(8)-Mn(2)	178.5(8)
O(9)-C(9)-Mn(2)	178.1(8)	O(10)-C(10)-Mn(2)	179.6(8)

C(42)-C(41)-C(46)	117.3(7)	C(42)-C(41)-Sn(2)	121.5(5)
C(46)-C(41)-Sn(2)	121.2(5)	C(41)-C(42)-C(43)	122.6(7)
C(41)-C(42)-H(42)	118.7	C(43)-C(42)-H(42)	118.7
C(44)-C(43)-C(42)	118.4(8)	C(44)-C(43)-H(43)	120.8
C(42)-C(43)-H(43)	120.8	C(45)-C(44)-C(43)	122.0(8)
C(45)-C(44)-F(4)	119.3(8)	C(43)-C(44)-F(4)	118.7(8)
C(44)-C(45)-C(46)	118.9(7)	C(44)-C(45)-H(45)	120.6
C(46)-C(45)-H(45)	120.6	C(41)-C(46)-C(45)	120.8(7)
C(41)-C(46)-H(46)	119.6	C(45)-C(46)-H(46)	119.6
C(52)-C(51)-C(56)	119.0(7)	C(52)-C(51)-Sn(2)	119.6(6)
C(56)-C(51)-Sn(2)	121.4(6)	C(51)-C(52)-C(53)	121.0(8)
C(51)-C(52)-H(25)	119.5	C(53)-C(52)-H(25)	119.5
C(54)-C(53)-C(52)	117.6(9)	C(54)-C(53)-H(53)	121.2
C(52)-C(53)-H(53)	121.2	C(53)-C(54)-C(55)	123.9(8)
C(53)-C(54)-F(5)	119.4(10)	C(55)-C(54)-F(5)	116.7(9)
C(54)-C(55)-C(56)	117.5(8)	C(54)-C(55)-H(55)	121.3
C(56)-C(55)-H(55)	121.3	C(51)-C(56)-C(55)	121.0(8)
C(51)-C(56)-H(56)	119.5	C(55)-C(56)-H(56)	119.5
C(62)-C(61)-C(66)	117.7(8)	C(62)-C(61)-Sn(2)	118.6(6)
C(66)-C(61)-Sn(2)	123.6(7)	C(61)-C(62)-C(63)	122.7(9)
C(61)-C(62)-H(62)	118.6	C(63)-C(62)-H(62)	118.6
C(64)-C(63)-C(62)	117.9(10)	C(64)-C(63)-H(63)	121.1
C(62)-C(63)-H(63)	121.1	C(63)-C(64)-C(65)	123.8(10)
C(63)-C(64)-F(6)	118.5(12)	C(65)-C(64)-F(6)	117.5(11)
C(64)-C(65)-C(66)	117.7(10)	C(64)-C(65)-H(65)	121.1
C(66)-C(65)-H(65)	121.1	C(61)-C(66)-C(65)	120.1(10)
C(61)-C(66)-H(66)	119.9	C(65)-C(66)-H(66)	119.9

Table A2.23: Torsion angles (in degrees) for $(p\text{-}FC_6H_4)_3SnMn(CO)_5$.

C(21)-Sn(1)-Mn(1)-C(2)	179.7(3)	C(11)-Sn(1)-Mn(1)-C(2)	-59.3(3)
C(31)-Sn(1)-Mn(1)-C(2)	58.0(3)	C(21)-Sn(1)-Mn(1)-C(4)	1.2(3)
C(11)-Sn(1)-Mn(1)-C(4)	122.3(3)	C(31)-Sn(1)-Mn(1)-C(4)	-120.4(3)
C(21)-Sn(1)-Mn(1)-C(3)	92.4(4)	C(11)-Sn(1)-Mn(1)-C(3)	-146.6(4)
C(31)-Sn(1)-Mn(1)-C(3)	-29.3(3)	C(21)-Sn(1)-Mn(1)-C(1)	-90.8(3)
C(11)-Sn(1)-Mn(1)-C(1)	30.3(3)	C(31)-Sn(1)-Mn(1)-C(1)	147.6(3)
C(21)-Sn(1)-C(11)-C(16)	165.6(6)	C(31)-Sn(1)-C(11)-C(16)	-81.3(7)
Mn(1)-Sn(1)-C(11)-C(16)	39.6(7)	C(21)-Sn(1)-C(11)-C(12)	-15.3(6)
C(31)-Sn(1)-C(11)-C(12)	97.8(6)	Mn(1)-Sn(1)-C(11)-C(12)	-141.3(5)
C(16)-C(11)-C(12)-C(13)	2.6(11)	Sn(1)-C(11)-C(12)-C(13)	-176.5(5)
C(11)-C(12)-C(13)-C(14)	-1.5(12)	C(12)-C(13)-C(14)-F(1)	179.7(7)
C(12)-C(13)-C(14)-C(15)	0.1(13)	C(13)-C(14)-C(15)-C(16)	0.1(13)
F(1)-C(14)-C(15)-C(16)	-179.6(7)	C(12)-C(11)-C(16)-C(15)	-2.6(12)
Sn(1)-C(11)-C(16)-C(15)	176.6(6)	C(14)-C(15)-C(16)-C(11)	1.3(13)
C(11)-Sn(1)-C(21)-C(22)	-66.9(6)	C(31)-Sn(1)-C(21)-C(22)	-177.3(5)
Mn(1)-Sn(1)-C(21)-C(22)	59.6(6)	C(11)-Sn(1)-C(21)-C(26)	112.8(5)
C(31)-Sn(1)-C(21)-C(26)	2.4(6)	Mn(1)-Sn(1)-C(21)-C(26)	-120.7(5)
C(26)-C(21)-C(22)-C(23)	0.1(10)	Sn(1)-C(21)-C(22)-C(23)	179.9(5)
C(21)-C(22)-C(23)-C(24)	1.4(11)	C(22)-C(23)-C(24)-C(25)	-2.2(12)
C(22)-C(23)-C(24)-F(2)	-179.7(6)	C(23)-C(24)-C(25)-C(26)	1.4(12)
F(2)-C(24)-C(25)-C(26)	178.9(6)	C(24)-C(25)-C(26)-C(21)	0.3(10)
C(22)-C(21)-C(26)-C(25)	-1.0(10)	Sn(1)-C(21)-C(26)-C(25)	179.3(5)
C(21)-Sn(1)-C(31)-C(32)	-59.2(6)	C(11)-Sn(1)-C(31)-C(32)	-170.2(6)
Mn(1)-Sn(1)-C(31)-C(32)	66.0(6)	C(21)-Sn(1)-C(31)-C(36)	126.5(5)
C(11)-Sn(1)-C(31)-C(36)	15.5(6)	Mn(1)-Sn(1)-C(31)-C(36)	-108.2(5)
C(36)-C(31)-C(32)-C(33)	-0.1(11)	Sn(1)-C(31)-C(32)-C(33)	-174.5(6)
C(31)-C(32)-C(33)-C(34)	-0.1(12)	C(32)-C(33)-C(34)-C(35)	0.0(12)
C(32)-C(33)-C(34)-F(3)	179.8(7)	F(3)-C(34)-C(35)-C(36)	-179.4(7)
C(33)-C(34)-C(35)-C(36)	0.4(13)	C(32)-C(31)-C(36)-C(35)	0.5(11)
Sn(1)-C(31)-C(36)-C(35)	175.1(6)	C(34)-C(35)-C(36)-C(31)	-0.7(12)
C(41)-Sn(2)-Mn(2)-C(7)	-65.5(3)	C(51)-Sn(2)-Mn(2)-C(7)	172.9(3)
C(61)-Sn(2)-Mn(2)-C(7)	55.3(3)	C(41)-Sn(2)-Mn(2)-C(8)	-154.2(3)
C(51)-Sn(2)-Mn(2)-C(8)	84.2(3)	C(61)-Sn(2)-Mn(2)-C(8)	-33.4(4)
C(41)-Sn(2)-Mn(2)-C(6)	24.9(3)	C(51)-Sn(2)-Mn(2)-C(6)	-96.6(3)
C(61)-Sn(2)-Mn(2)-C(6)	145.8(3)	C(41)-Sn(2)-Mn(2)-C(9)	115.2(4)
C(51)-Sn(2)-Mn(2)-C(9)	-6.3(4)	C(61)-Sn(2)-Mn(2)-C(9)	-123.9(4)
C(51)-Sn(2)-C(41)-C(42)	-125.3(6)	C(61)-Sn(2)-C(41)-C(42)	-15.0(7)
Mn(2)-Sn(2)-C(41)-C(42)	111.7(6)	C(51)-Sn(2)-C(41)-C(46)	55.2(6)
C(61)-Sn(2)-C(41)-C(46)	165.5(6)	Mn(2)-Sn(2)-C(41)-C(46)	-67.8(6)
C(46)-C(41)-C(42)-C(43)	1.2(11)	Sn(2)-C(41)-C(42)-C(43)	-178.3(6)
C(41)-C(42)-C(43)-C(44)	-0.9(12)	C(42)-C(43)-C(44)-C(45)	0.8(13)
C(42)-C(43)-C(44)-F(4)	180.0(7)	C(43)-C(44)-C(45)-C(46)	-1.0(14)
F(4)-C(44)-C(45)-C(46)	179.8(7)	C(42)-C(41)-C(46)-C(45)	-1.4(11)
Sn(2)-C(41)-C(46)-C(45)	178.1(6)	C(44)-C(45)-C(46)-C(41)	1.3(13)
C(41)-Sn(2)-C(51)-C(52)	-179.0(5)	C(61)-Sn(2)-C(51)-C(52)	70.3(6)
Mn(2)-Sn(2)-C(51)-C(52)	-54.0(6)	C(41)-Sn(2)-C(51)-C(56)	-0.9(6)
C(61)-Sn(2)-C(51)-C(56)	-111.6(6)	Mn(2)-Sn(2)-C(51)-C(56)	124.1(5)
C(56)-C(51)-C(52)-C(53)	-0.9(11)	Sn(2)-C(51)-C(52)-C(53)	177.2(6)
C(51)-C(52)-C(53)-C(54)	0.1(12)	C(52)-C(53)-C(54)-C(55)	0.9(13)
C(52)-C(53)-C(54)-F(5)	-178.8(7)	C(53)-C(54)-C(55)-C(56)	-1.0(13)
F(5)-C(54)-C(55)-C(56)	178.7(7)	C(52)-C(51)-C(56)-C(55)	0.8(11)

Sn(2)-C(51)-C(56)-C(55)	-177.3(6)	C(54)-C(55)-C(56)-C(51)	0.1(12)
C(41)-Sn(2)-C(61)-C(62)	-103.2(7)	C(51)-Sn(2)-C(61)-C(62)	9.8(7)
Mn(2)-Sn(2)-C(61)-C(62)	131.0(6)	C(41)-Sn(2)-C(61)-C(66)	72.7(7)
C(51)-Sn(2)-C(61)-C(66)	-174.2(7)	Mn(2)-Sn(2)-C(61)-C(66)	-53.0(8)
C(66)-C(61)-C(62)-C(63)	0.2(13)	Sn(2)-C(61)-C(62)-C(63)	176.4(7)
C(61)-C(62)-C(63)-C(64)	1(2)	C(62)-C(63)-C(64)-C(65)	-3(2)
C(62)-C(63)-C(64)-F(6)	-178.3(9)	C(63)-C(64)-C(65)-C(66)	4(2)
F(6)-C(64)-C(65)-C(66)	178.7(9)	C(62)-C(61)-C(66)-C(65)	0.1(13)
Sn(2)-C(61)-C(66)-C(65)	-175.8(7)	C(64)-C(65)-C(66)-C(61)	-2(2)

Table A2.24: Anisotropic thermal factors (10^2 Å^2) for (p-$FC_6H_4)_3SnMn(CO)_5$.

	U_{11}	U_{22}	U_{33}	U_{12}	U_{13}	U_{23}
Sn(1)	5.22(3)	3.80(3)	4.43(3)	-0.29(2)	-0.68(2)	-2.01(2)
Mn(1)	5.71(7)	4.80(6)	5.61(7)	0.55(5)	-1.26(6)	-2.40(5)
F(1)	14.6(5)	4.0(3)	11.8(4)	-0.7(3)	-2.4(4)	-3.1(3)
F(2)	12.3(4)	12.2(4)	4.1(3)	-1.6(3)	-1.2(3)	-4.4(3)
F(3)	7.8(3)	10.3(4)	12.5(5)	-2.1(3)	3.0(3)	-5.5(3)
O(1)	9.0(5)	8.1(4)	15.7(7)	2.6(4)	-1.6(4)	-6.0(4)
O(2)	13.3(6)	11.8(6)	5.2(4)	-1.1(4)	-0.4(4)	-3.3(5)
O(3)	9.4(5)	7.1(4)	23.5(9)	3.9(5)	-4.9(5)	-5.2(4)
O(4)	12.2(6)	7.6(4)	7.4(5)	-1.6(4)	-0.7(4)	-0.2(4)
O(5)	8.2(4)	7.8(4)	9.7(5)	2.0(3)	-4.1(4)	-3.4(3)
C(1)	5.2(5)	6.1(5)	9.6(7)	0.0(5)	-0.7(5)	-2.2(4)
C(2)	10.3(7)	7.5(6)	4.3(5)	0.8(4)	-2.2(5)	-3.9(5)
C(3)	5.7(5)	4.6(5)	13.3(9)	1.2(5)	-3.6(5)	-2.0(4)
C(4)	7.6(6)	4.8(5)	7.0(6)	1.1(4)	-1.9(5)	-1.1(4)
C(5)	7.1(6)	5.8(5)	6.5(5)	1.2(4)	-2.2(5)	-3.7(4)
C(11)	5.7(4)	2.9(3)	5.4(5)	-0.5(3)	-0.6(4)	-2.2(3)
C(12)	6.6(5)	4.1(4)	6.0(5)	-0.6(4)	-0.6(4)	-2.3(4)
C(13)	8.1(6)	4.8(5)	6.2(5)	0.8(4)	-1.6(4)	-3.0(4)
C(14)	8.5(6)	4.0(4)	6.4(6)	-0.7(4)	-1.3(5)	-2.8(4)
C(15)	10.6(7)	5.6(5)	7.2(6)	-2.1(4)	-1.1(5)	-3.7(5)
C(16)	8.6(6)	4.4(4)	7.4(6)	0.0(4)	-2.2(5)	-2.8(4)
C(21)	5.3(5)	4.0(4)	4.8(5)	0.3(3)	-1.0(4)	-1.8(3)
C(22)	7.4(6)	6.1(5)	5.4(5)	-0.2(4)	-1.8(4)	-3.1(4)
C(23)	7.8(6)	7.5(6)	5.0(5)	0.1(4)	-0.2(5)	-3.5(5)
C(24)	8.4(6)	5.5(5)	4.1(5)	-1.0(4)	-0.9(5)	-1.1(5)
C(25)	7.7(6)	6.1(5)	4.8(5)	-0.8(4)	-2.3(5)	-2.3(4)
C(26)	5.9(5)	5.3(4)	5.8(5)	0.3(4)	-0.4(4)	-2.5(4)
C(31)	5.1(4)	4.0(4)	3.9(4)	-0.3(3)	-0.5(3)	-1.6(3)
C(32)	5.7(5)	5.1(4)	6.0(5)	-1.3(4)	0.3(4)	-2.4(4)

C(33)	6.8(5)	6.0(5)	6.9(5)	-0.9(4)	-0.2(4)	-4.1(4)
C(34)	5.5(5)	5.8(5)	7.3(6)	-0.7(4)	0.5(4)	-2.8(4)
C(35)	5.7(5)	5.1(5)	8.8(6)	-1.4(4)	0.7(5)	-1.4(4)
C(36)	6.2(5)	4.2(4)	6.4(5)	-0.3(4)	-0.5(4)	-2.6(4)
Sn(2)	5.03(3)	4.76(3)	4.83(3)	-0.61(2)	-0.73(3)	-1.62(2)
Mn(2)	5.82(7)	5.75(7)	5.03(7)	-0.05(5)	-1.35(6)	-2.54(6)
F(4)	8.6(4)	13.4(5)	9.9(4)	-1.3(3)	-4.4(3)	-4.8(3)
F(5)	16.0(5)	11.8(4)	5.6(3)	-1.0(3)	1.9(3)	-6.6(4)
F(6)	16.9(6)	6.0(4)	24.5(9)	-4.0(4)	-7.7(6)	2.7(4)
O(6)	6.4(4)	7.6(4)	11.6(5)	0.8(4)	-3.2(4)	-1.8(3)
O(7)	10.3(5)	11.2(5)	6.1(4)	-2.1(4)	-0.2(4)	-3.7(4)
O(8)	8.8(5)	11.1(5)	11.8(6)	2.1(4)	-5.7(5)	-3.0(4)
O(9)	19.6(8)	7.4(4)	7.7(5)	-2.4(4)	-1.1(5)	-5.4(5)
O(10)	10.1(5)	10.1(5)	16.1(7)	3.7(5)	-4.0(5)	-7.2(4)
C(6)	6.6(6)	6.2(5)	7.3(6)	0.6(4)	-1.2(5)	-3.1(5)
C(7)	7.2(6)	8.1(6)	3.6(5)	-1.0(4)	-0.2(4)	-2.5(5)
C(8)	7.8(6)	9.4(7)	5.7(5)	0.5(5)	-2.7(5)	-4.9(5)
C(9)	10.7(7)	5.3(5)	8.2(7)	-0.5(5)	-1.8(6)	-3.4(5)
C(10)	6.4(6)	7.8(6)	8.7(7)	0.6(5)	-2.2(5)	-3.7(5)
C(41)	4.8(4)	5.5(4)	4.3(4)	-0.3(3)	-0.4(3)	-2.4(4)
C(42)	6.0(5)	5.7(5)	5.7(5)	-0.8(4)	-1.1(4)	-2.5(4)
C(43)	7.8(6)	6.3(5)	7.3(6)	-0.8(4)	-1.4(5)	-3.6(5)
C(44)	6.4(6)	8.1(6)	7.2(6)	-0.4(5)	-1.8(5)	-3.3(5)
C(45)	5.2(5)	6.7(5)	9.0(7)	-1.9(5)	-1.1(5)	-1.4(4)
C(46)	5.4(5)	7.0(5)	7.8(6)	-1.7(4)	-1.6(4)	-2.5(4)
C(51)	5.6(5)	4.7(4)	4.4(4)	-0.4(3)	-0.1(4)	-1.7(4)
C(52)	7.6(6)	7.5(6)	4.6(5)	-0.3(4)	-0.8(4)	-2.9(5)
C(53)	9.3(7)	10.3(7)	5.3(6)	0.7(5)	-0.9(5)	-4.5(6)
C(54)	12.3(9)	6.4(5)	3.8(5)	-0.3(4)	0.2(6)	-4.5(6)
C(55)	7.8(6)	6.8(6)	7.1(7)	-0.1(5)	1.5(5)	-2.8(5)
C(56)	7.1(6)	7.0(5)	5.5(5)	-0.3(4)	-0.6(5)	-3.1(5)
C(61)	5.8(5)	4.9(4)	7.1(6)	-1.1(4)	-1.5(4)	-1.6(4)
C(62)	9.8(7)	5.3(5)	7.9(7)	-1.3(5)	-3.3(6)	-1.5(5)
C(63)	13.4(9)	5.9(6)	10.6(9)	0.4(6)	-5.5(8)	-2.4(6)
C(64)	9.6(8)	7.0(7)	13.0(11)	-3.6(7)	-4.1(8)	0.9(6)
C(65)	10.0(8)	9.6(9)	12.9(11)	-5.9(8)	0.4(8)	-1.8(7)
C(66)	8.1(7)	6.6(6)	10.8(8)	-2.2(5)	0.9(6)	-1.4(5)

Structural Analysis of

Tris(*p*-chlorophenyl)tin(pentacarbonyl)manganese(I)

$(p\text{-}ClC_6H_4)_3SnMn(CO)_5$

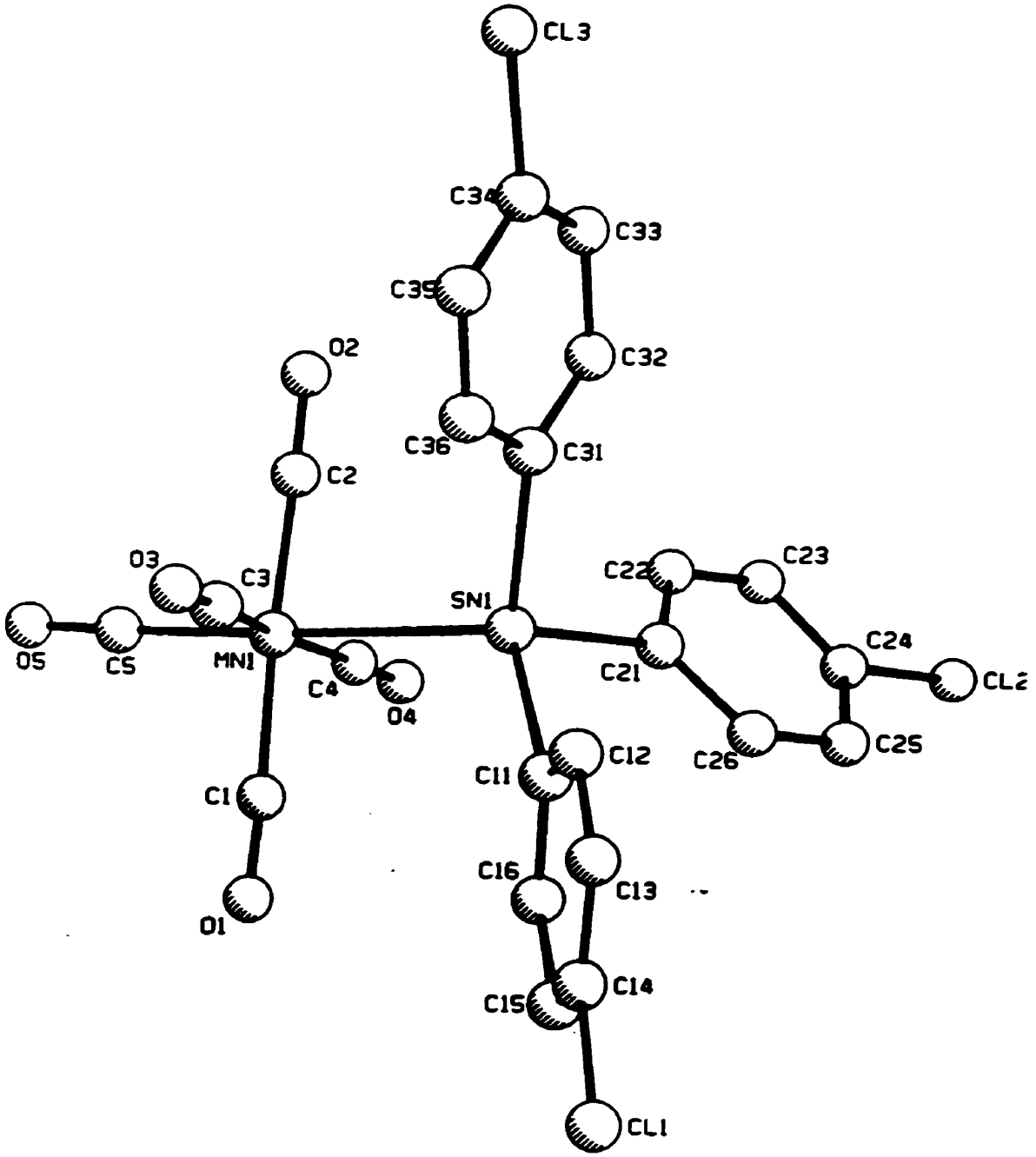

Crystal data for $(p\text{-}ClC_6H_4)_3SnMn(CO)_5$

Empirical Formula: C23 H12 O5 Sn Mn Cl3

Space group: Monoclinic, $P2_1/c$

Cell dimensions:

$a = 9.918\ (2)$Å

$b = 22.940\ (4)$Å

$c = 11.718\ (2)$Å

$\alpha = 90°$

$\beta = 109.78\ (1)°$

$\gamma = 90°$

Volume = 2508.8 (8)Å^3

FW = 648.31

Z = 4

$D_{calc} = 1.716$ g / cm^3

F(000) = 1264

Mo Kα radiation

$\lambda = 0.7093$ Å

Cell parameters from 23 reflections

$2\theta = 32 - 35°$

$\mu = 1.849$ mm^{-1}

T = 295 (2) °K

Colourless plate

0.51 × 0.49 × 0.09 mm

Data collection

Rigaku AFC –6S diffractometer

ω / 2θ scans

Absorption correction: *Psi scans*

$T_{min} = 0.33$, $T_{max} = 0.62$

8805 measured reflections

4412 independent reflections

3381 observed reflections [$I > 2\sigma(I)$]

$R_{int} = 0.062$

$\theta_{max} = 50.0°$

$h = -12 \rightarrow 12$

$k = 0 \rightarrow 27$

$l = -14 \rightarrow 14$

3 standard reflections were monitored every 250 reflections

Intensity decay: 11 %

Structure was solved by the heavy atom method.

Refinement

Refinement on F^2	299 parameters
$R(F^2 > 2\sigma(F^2)) = 0.0474$	H atoms riding,
$wR(F^2) = 0.1192$	C–H = 0.93 Å
GoF = 1.068	$(\Delta/\sigma) = -0.003$
45 atoms	$\Delta\rho_{max} = 0.958$ e/Å^3
4412 reflections	$\Delta\rho_{min} = -0.626$ e/Å^3

where

$R = \Sigma(Fo-Fc) / \Sigma Fo$

$wR = [\Sigma(w(Fo-Fc)^2) / \Sigma wFo^2]^{1/2}$

GoF = [Σ(w(Fo-Fc)^2) / (No. of refins - No. of params.)

Table A2.25: Fractional atomic coordinates and equivalent isotropic displacement parameters (10^2 Å) for $(p\text{-}ClC_6H_4)_3SnMn(CO)_5$.

	x	y	z	U_{eq}
Sn(1)	0.42518(5)	0.10504(2)	0.22113(4)	3.78(2)
Mn(1)	0.30610(12)	-0.00134(5)	0.18687(9)	4.61(3)
Cl(3)	1.0595(3)	0.09955(14)	0.6622(2)	10.14(9)
Cl(2)	0.5287(3)	0.22257(11)	-0.2636(2)	7.58(7)
Cl(1)	-0.0830(3)	0.24978(14)	0.3540(3)	10.11(9)
O(3)	0.5955(8)	-0.0564(3)	0.2847(6)	9.9(2)
O(1)	0.0254(7)	0.0600(3)	0.1078(9)	12.5(3)
O(2)	0.3196(10)	0.0139(3)	0.4423(6)	11.1(3)
O(4)	0.3241(9)	0.0022(3)	-0.0605(6)	10.8(3)
O(5)	0.1574(10)	-0.1148(3)	0.1410(7)	10.8(3)
C(3)	0.4859(10)	-0.0335(4)	0.2465(8)	6.5(2)
C(1)	0.1353(9)	0.0370(4)	0.1367(9)	7.6(3)
C(2)	0.3154(10)	0.0084(4)	0.3453(8)	6.9(2)
C(4)	0.3172(10)	0.0019(4)	0.0347(8)	6.6(2)
C(5)	0.2176(10)	-0.0721(4)	0.1613(8)	7.3(2)
C(11)	0.2790(7)	0.1591(3)	0.2724(6)	4.0(2)
C(12)	0.1780(8)	0.1927(3)	0.1849(7)	5.4(2)
C(13)	0.0673(8)	0.2207(3)	0.2101(7)	6.0(2)
C(14)	0.0585(8)	0.2169(3)	0.3236(8)	5.7(2)
C(15)	0.1588(9)	0.1866(4)	0.4129(7)	6.0(2)
C(16)	0.2671(8)	0.1579(3)	0.3869(6)	5.5(2)
C(21)	0.4548(7)	0.1422(3)	0.0635(5)	3.80(14)
C(22)	0.3457(8)	0.1497(3)	-0.0451(6)	4.7(2)
C(23)	0.3653(8)	0.1753(3)	-0.1463(6)	4.9(2)
C(24)	0.5003(8)	0.1918(3)	-0.1366(6)	4.6(2)
C(25)	0.6135(8)	0.1868(3)	-0.0309(7)	5.2(2)
C(26)	0.5908(7)	0.1622(3)	0.0692(6)	4.8(2)
C(31)	0.6321(7)	0.1073(4)	0.3612(6)	5.1(2)
C(32)	0.6576(8)	0.1398(3)	0.4662(6)	4.9(2)
C(33)	0.7891(8)	0.1380(4)	0.5578(7)	5.9(2)
C(34)	0.8955(8)	0.1054(4)	0.5439(7)	6.0(2)
C(35)	0.8773(8)	0.0727(4)	0.4406(7)	6.2(2)
C(36)	0.7454(8)	0.0754(4)	0.3494(7)	5.6(2)

Table A2.26: Bond lengths (Å) and angles (°) for $(p\text{-}ClC_6H_4)_3SnMn(CO)_5$.

Sn(1)-C(11)	2.142(6)	Sn(1)-C(21)	2.143(6)
Sn(1)-C(31)	2.151(7)	Sn(1)-Mn(1)	2.6814(12)
Mn(1)-C(1)	1.821(10)	Mn(1)-C(5)	1.821(10)
Mn(1)-C(4)	1.824(9)	Mn(1)-C(3)	1.836(9)
Mn(1)-C(2)	1.841(8)	Cl(3)-C(34)	1.749(7)
Cl(2)-C(24)	1.753(7)	Cl(1)-C(14)	1.734(7)
O(3)-C(3)	1.152(10)	O(1)-C(1)	1.153(10)
O(2)-C(2)	1.130(9)	O(4)-C(4)	1.141(9)
O(5)-C(5)	1.130(10)	C(11)-C(16)	1.386(9)
C(11)-C(12)	1.398(9)	C(12)-C(13)	1.387(10)
C(12)-H(12)	0.93	C(13)-C(14)	1.365(11)
C(13)-H(13)	0.93	C(14)-C(15)	1.365(11)
C(15)-C(16)	1.379(10)	C(15)-H(15)	0.93
C(16)-H(16)	0.93	C(21)-C(22)	1.374(9)
C(21)-C(26)	1.404(9)	C(22)-C(23)	1.393(9)
C(22)-H(22)	0.93	C(23)-C(24)	1.360(10)
C(23)-H(23)	0.93	C(24)-C(25)	1.366(10)
C(25)-C(26)	1.387(9)	C(25)-H(25)	0.93
C(26)-H(26)	0.93	C(31)-C(36)	1.387(10)
C(31)-C(32)	1.387(10)	C(32)-C(33)	1.382(10)
C(32)-H(32)	0.93	C(33)-C(34)	1.348(11)
C(33)-H(33)	0.93	C(34)-C(35)	1.383(11)
C(35)-C(36)	1.382(10)	C(35)-H(35)	0.93
C(36)-H(36)	0.93		

C(11)-Sn(1)-C(21)	108.3(2)	C(11)-Sn(1)-C(31)	109.5(3)
C(21)-Sn(1)-C(31)	105.9(3)	C(11)-Sn(1)-Mn(1)	105.2(2)
C(21)-Sn(1)-Mn(1)	114.5(2)	C(31)-Sn(1)-Mn(1)	113.2(2)
C(1)-Mn(1)-C(5)	91.9(4)	C(1)-Mn(1)-C(4)	91.3(4)
C(5)-Mn(1)-C(4)	93.4(4)	C(1)-Mn(1)-C(3)	174.3(4)
C(5)-Mn(1)-C(3)	93.2(4)	C(4)-Mn(1)-C(3)	90.9(4)
C(1)-Mn(1)-C(2)	89.5(4)	C(5)-Mn(1)-C(2)	97.5(4)
C(4)-Mn(1)-C(2)	169.0(4)	C(3)-Mn(1)-C(2)	87.4(4)
C(1)-Mn(1)-Sn(1)	85.6(3)	C(5)-Mn(1)-Sn(1)	177.5(3)
C(4)-Mn(1)-Sn(1)	86.6(3)	C(3)-Mn(1)-Sn(1)	89.3(3)
C(2)-Mn(1)-Sn(1)	82.5(3)	O(3)-C(3)-Mn(1)	176.5(9)
O(1)-C(1)-Mn(1)	177.4(10)	O(2)-C(2)-Mn(1)	179.2(9)
O(4)-C(4)-Mn(1)	178.1(8)	O(5)-C(5)-Mn(1)	176.6(10)
C(16)-C(11)-C(12)	116.5(6)	C(16)-C(11)-Sn(1)	123.2(5)
C(12)-C(11)-Sn(1)	119.9(5)	C(13)-C(12)-C(11)	121.5(7)
C(13)-C(12)-H(12)	119.3	C(11)-C(12)-H(12)	119.3
C(14)-C(13)-C(12)	119.6(7)	C(14)-C(13)-H(13)	120.2
C(12)-C(13)-H(13)	120.2	C(13)-C(14)-C(15)	120.7(7)
C(13)-C(14)-Cl(1)	119.7(6)	C(15)-C(14)-Cl(1)	119.7(6)
C(14)-C(15)-C(16)	119.6(7)	C(14)-C(15)-H(15)	120.2
C(16)-C(15)-H(15)	120.2	C(15)-C(16)-C(11)	122.2(7)
C(15)-C(16)-H(16)	118.9	C(11)-C(16)-H(16)	118.9
C(22)-C(21)-C(26)	116.4(6)	C(22)-C(21)-Sn(1)	123.7(5)
C(26)-C(21)-Sn(1)	119.9(5)	C(21)-C(22)-C(23)	123.3(7)
C(21)-C(22)-H(22)	118.4	C(23)-C(22)-H(22)	118.4
C(24)-C(23)-C(22)	117.6(6)	C(24)-C(23)-H(23)	121.2

C(22)-C(23)-H(23)	121.2	C(23)-C(24)-C(25)	122.4(6)
C(23)-C(24)-Cl(2)	118.5(5)	C(25)-C(24)-Cl(2)	119.0(6)
C(24)-C(25)-C(26)	118.8(6)	C(24)-C(25)-H(25)	120.6
C(26)-C(25)-H(25)	120.6	C(25)-C(26)-C(21)	121.4(6)
C(25)-C(26)-H(26)	119.3	C(21)-C(26)-H(26)	119.3
C(36)-C(31)-C(32)	117.5(6)	C(36)-C(31)-Sn(1)	120.5(5)
C(32)-C(31)-Sn(1)	122.0(5)	C(33)-C(32)-C(31)	120.9(7)
C(33)-C(32)-H(32)	119.5	C(31)-C(32)-H(32)	119.5
C(34)-C(33)-C(32)	119.6(7)	C(34)-C(33)-H(33)	120.2
C(32)-C(33)-H(33)	120.2	C(33)-C(34)-C(35)	122.2(7)
C(33)-C(34)-Cl(3)	120.2(6)	C(35)-C(34)-Cl(3)	117.5(7)
C(36)-C(35)-C(34)	117.4(7)	C(36)-C(35)-H(35)	121.3
C(34)-C(35)-H(35)	121.3	C(35)-C(36)-C(31)	122.3(7)
C(35)-C(36)-H(36)	118.9	C(31)-C(36)-H(36)	118.9

Table A2.27: Torsion angles (in degrees) for $(p\text{-}ClC_6H_4)_3SnMn(CO)_5$.

C(11)-Sn(1)-Mn(1)-C(1)	32.3(4)	C(21)-Sn(1)-Mn(1)-C(1)	-86.5(4)
C(31)-Sn(1)-Mn(1)-C(1)	151.9(4)	C(11)-Sn(1)-Mn(1)-C(4)	123.9(3)
C(21)-Sn(1)-Mn(1)-C(4)	5.0(4)	C(31)-Sn(1)-Mn(1)-C(4)	-116.6(4)
C(11)-Sn(1)-Mn(1)-C(3)	-145.2(3)	C(21)-Sn(1)-Mn(1)-C(3)	96.0(3)
C(31)-Sn(1)-Mn(1)-C(3)	-25.6(3)	C(11)-Sn(1)-Mn(1)-C(2)	-57.7(4)
C(21)-Sn(1)-Mn(1)-C(2)	-176.6(4)	C(31)-Sn(1)-Mn(1)-C(2)	61.8(4)
C(21)-Sn(1)-C(11)-C(16)	-161.0(6)	C(31)-Sn(1)-C(11)-C(16)	-45.9(6)
Mn(1)-Sn(1)-C(11)-C(16)	76.1(6)	C(21)-Sn(1)-C(11)-C(12)	26.7(6)
C(31)-Sn(1)-C(11)-C(12)	141.7(6)	Mn(1)-Sn(1)-C(11)-C(12)	-96.2(5)
C(16)-C(11)-C(12)-C(13)	-3.4(11)	Sn(1)-C(11)-C(12)-C(13)	169.5(6)
C(11)-C(12)-C(13)-C(14)	1.8(12)	C(12)-C(13)-C(14)-C(15)	1.2(13)
C(12)-C(13)-C(14)-Cl(1)	-177.8(6)	C(13)-C(14)-C(15)-C(16)	-2.3(13)
Cl(1)-C(14)-C(15)-C(16)	176.7(6)	C(14)-C(15)-C(16)-C(11)	0.6(13)
C(12)-C(11)-C(16)-C(15)	2.2(11)	Sn(1)-C(11)-C(16)-C(15)	-170.4(6)
C(11)-Sn(1)-C(21)-C(22)	-61.1(6)	C(31)-Sn(1)-C(21)-C(22)	-178.5(6)
Mn(1)-Sn(1)-C(21)-C(22)	56.0(6)	C(11)-Sn(1)-C(21)-C(26)	116.9(5)
C(31)-Sn(1)-C(21)-C(26)	-0.5(6)	Mn(1)-Sn(1)-C(21)-C(26)	-126.0(5)
C(26)-C(21)-C(22)-C(23)	0.3(10)	Sn(1)-C(21)-C(22)-C(23)	178.4(5)
C(21)-C(22)-C(23)-C(24)	2.0(11)	C(22)-C(23)-C(24)-C(25)	-3.3(11)
C(22)-C(23)-C(24)-Cl(2)	178.6(5)	C(23)-C(24)-C(25)-C(26)	2.2(11)
Cl(2)-C(24)-C(25)-C(26)	-179.7(6)	C(24)-C(25)-C(26)-C(21)	0.3(11)
C(22)-C(21)-C(26)-C(25)	-1.5(10)	Sn(1)-C(21)-C(26)-C(25)	-179.6(6)
C(11)-Sn(1)-C(31)-C(36)	179.7(6)	C(21)-Sn(1)-C(31)-C(36)	-63.7(7)
Mn(1)-Sn(1)-C(31)-C(36)	62.6(6)	C(11)-Sn(1)-C(31)-C(32)	0.2(7)
C(21)-Sn(1)-C(31)-C(32)	116.8(6)	Mn(1)-Sn(1)-C(31)-C(32)	-116.9(6)
C(36)-C(31)-C(32)-C(33)	-3.2(11)	Sn(1)-C(31)-C(32)-C(33)	176.3(6)
C(31)-C(32)-C(33)-C(34)	1.8(12)	C(32)-C(33)-C(34)-C(35)	-0.9(13)
C(32)-C(33)-C(34)-Cl(3)	-176.6(6)	C(33)-C(34)-C(35)-C(36)	1.4(13)
Cl(3)-C(34)-C(35)-C(36)	177.2(6)	C(34)-C(35)-C(36)-C(31)	-3.0(13)
C(32)-C(31)-C(36)-C(35)	3.9(12)	Sn(1)-C(31)-C(36)-C(35)	-175.7(6)

Table A2.28: Anisotropic thermal factors (10^2 Å^2) for (p-$ClC_6H_4)_3SnMn(CO)_5$.

	U_{11}	U_{22}	U_{33}	U_{12}	U_{13}	U_{23}
Sn(1)	3.59(3)	4.19(3)	3.30(2)	-0.02(2)	0.83(2)	0.10(2)
Mn(1)	5.25(7)	4.17(6)	4.23(6)	-0.02(5)	1.39(5)	-0.33(5)
Cl(3)	5.25(13)	13.9(3)	8.0(2)	0.9(2)	-2.12(11)	-1.1(2)
Cl(2)	8.4(2)	8.9(2)	6.35(13)	2.65(12)	3.67(11)	0.11(12)
Cl(1)	9.6(2)	10.7(2)	12.0(2)	1.2(2)	6.3(2)	5.1(2)
O(3)	8.5(5)	9.2(5)	10.6(6)	-0.2(4)	1.1(4)	3.2(4)
O(1)	5.4(4)	9.7(6)	18.3(8)	-3.3(6)	-1.4(5)	0.8(4)
O(2)	20.1(9)	8.7(5)	6.7(4)	-0.4(4)	7.4(5)	-2.1(5)
O(4)	16.8(8)	11.2(6)	4.8(4)	-1.6(4)	4.3(4)	-3.8(5)
O(5)	15.8(8)	6.6(5)	10.8(6)	-1.6(4)	5.5(5)	-4.8(5)
C(3)	7.3(6)	4.8(5)	6.5(5)	-1.1(4)	1.3(4)	0.9(4)
C(1)	4.8(5)	7.9(7)	8.8(6)	-1.4(5)	0.8(5)	-1.4(5)
C(2)	10.2(7)	5.6(5)	5.7(5)	0.4(4)	3.7(5)	-0.5(5)
C(4)	8.3(6)	5.4(5)	5.4(5)	-0.9(4)	1.4(4)	-1.8(4)
C(5)	8.2(6)	7.6(7)	6.7(6)	0.1(5)	3.1(5)	-1.0(5)
C(11)	4.3(4)	2.8(3)	4.7(4)	-0.2(3)	1.4(3)	0.1(3)
C(12)	6.0(5)	5.7(5)	4.5(4)	0.3(3)	1.7(3)	1.2(4)
C(13)	5.9(5)	5.0(5)	6.8(5)	1.0(4)	1.8(4)	1.7(4)
C(14)	5.5(5)	4.4(4)	7.6(5)	-0.2(4)	2.9(4)	0.9(4)
C(15)	7.3(5)	6.0(5)	5.6(5)	0.3(4)	3.4(4)	0.8(4)
C(16)	5.0(4)	6.6(5)	4.6(4)	0.2(4)	1.3(3)	1.0(4)
C(21)	4.9(4)	3.2(3)	3.1(3)	-0.2(3)	1.2(3)	-0.4(3)
C(22)	4.6(4)	5.0(4)	4.3(4)	0.3(3)	1.4(3)	-0.5(3)
C(23)	5.2(4)	5.0(4)	4.0(4)	0.7(3)	0.7(3)	-0.2(3)
C(24)	5.9(4)	3.6(4)	4.5(4)	0.8(3)	2.1(3)	0.2(3)
C(25)	4.5(4)	5.8(5)	5.7(4)	0.1(4)	2.3(3)	-0.7(3)
C(26)	3.7(4)	6.0(5)	4.3(4)	0.0(3)	0.9(3)	-0.3(3)
C(31)	3.7(4)	7.4(5)	3.7(3)	0.5(4)	0.8(3)	0.0(4)
C(32)	5.0(4)	4.3(4)	4.9(4)	-0.4(3)	1.1(3)	-0.3(3)
C(33)	5.8(5)	6.9(5)	4.1(4)	-0.9(4)	0.3(4)	-1.3(4)
C(34)	3.9(4)	7.0(5)	5.3(4)	0.5(4)	-0.7(3)	-1.5(4)
C(35)	4.2(4)	7.1(6)	6.8(5)	0.2(4)	1.2(4)	0.7(4)
C(36)	4.9(4)	6.7(5)	5.0(4)	-0.9(4)	1.2(3)	0.0(4)

APPENDIX III

Crystal Structures of

trans-Dibromo- and *trans*-Dichloro-

bis(tribenzylphosphine)nickel(II) Complexes

Structural Data for

trans-Dibromobis(tribenzylphosphine)nickel(II)

trans- $Br_2[(PhCH_2)_3P]_2Ni$

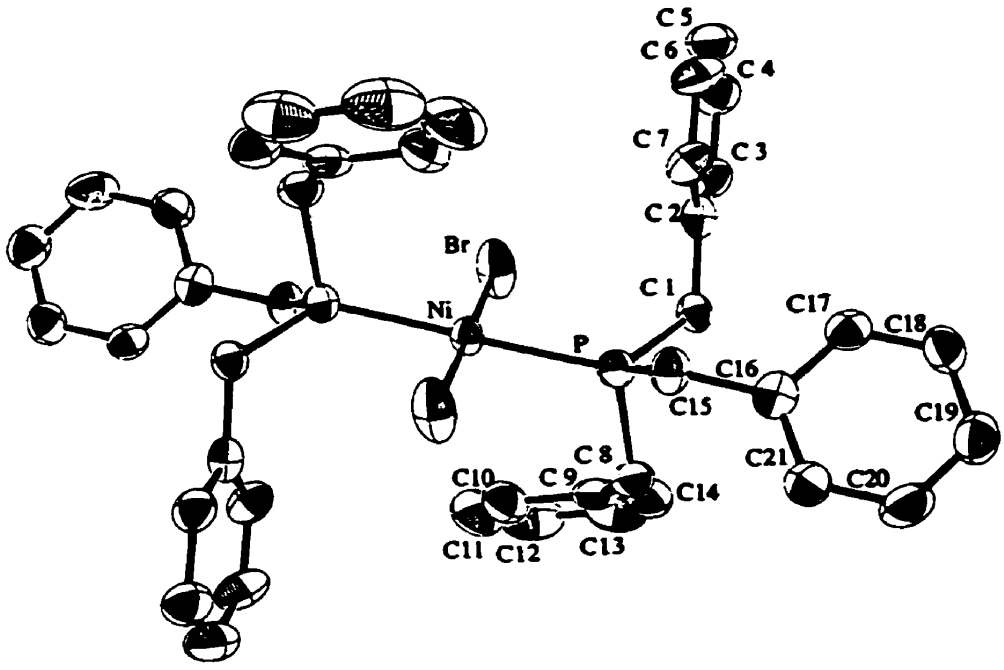

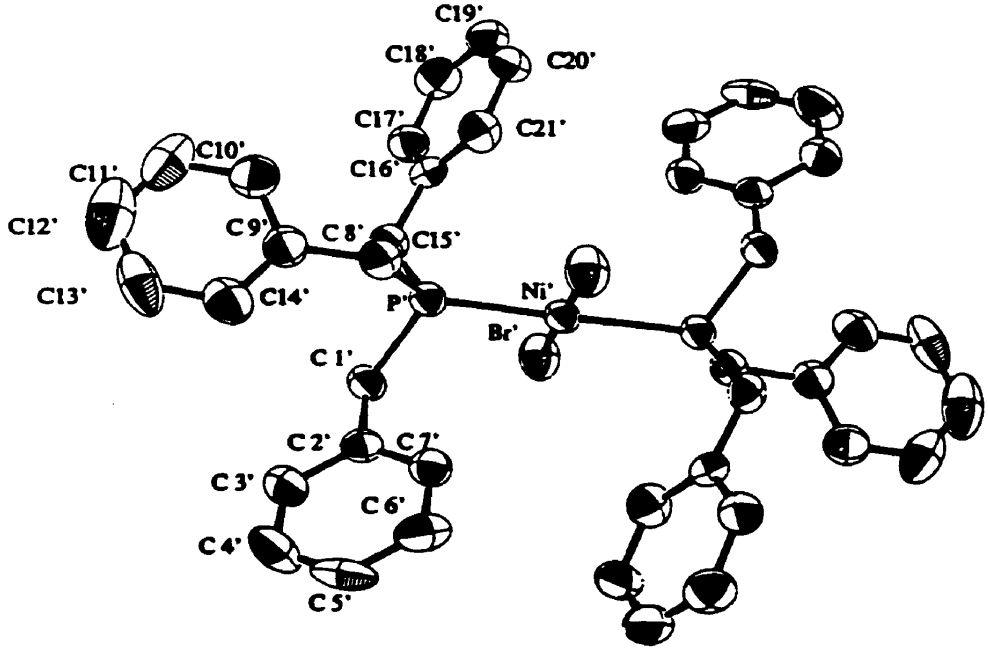

Crystallographic data for *trans*-$Br_2[(PhCH_2)_3P]_2Ni$

Empirical Formula: C42 H42 Br2 P2 Ni

Space group: Triclinic, P 1

Cell dimensions:

a = 10.497 (4)Å

b = 10.538 (4)Å

c = 19.556 (9)Å

α = 84.58 (4)°

β = 76.42 (3)°

γ = 63.33 (2)°

Volume = 1878.9 (12)Å^3

FW = 827.25

Z = 2

D_{calc} = 1.462 g / cm^3

F(000) = 844

Mo Kα radiation

λ = 0.70930 Å

Cell parameters from 25 reflections

2θ = 30 - 35°

μ = 2.74 mm^{-1}

T = 295 (2) °K

brown plate

0.40 × 0.20 × 0.20 mm

Data collection

Rigaku AFC –6S diffractometer

ω / 2θ scans

Absorption correction: 4 *psi scan*

T_{min} = 0.398, T_{max} = 0.550

5246 measured reflections

4925 independent reflections

3147 observed reflections [$I > 2.5\sigma(I)$]

R_{int} = 0.071

θ_{max} = 22.5°

h = -9 → 11

k = 0 → 11

l = -20 → 21

standard intensities remained constant throughout the course of collection

Average decrease: 0.7 %

Structure was solved by direct methods followed by a difference map.

Refinement

Refinement on F	428 parameters
$R(F > 2.5\sigma F = 0.038$	H atoms riding,
$wR(F) = 0.033$	C–H = 0.93 to 0.97 Å
GoF = 1.33	$(\Delta/\sigma) = 0.077$
90 atoms	$\Delta\rho_{max} = 0.47$ e/Å^3
3147 reflections	$\Delta\rho_{min} = -0.53$ e/Å^3

where

$$R = \Sigma(Fo-Fc) / \Sigma Fo$$

$$wR = [\Sigma(w(Fo-Fc)^2) / \Sigma[w(Fo)^2]]^{1/2}$$

$$GoF = [\Sigma(w(Fo-Fc)^2) / (\text{No. of refins - No. of params.})]^{1/2}$$

Table A3.1: Fractional atomic coordinates and equivalent isotropic displacement parameters (10^2 Å) for *trans*-$Br_2[(PhCH_2)_3P]_2Ni$.

	x	y	z	U_{eq}
Ni	0	0	0	2.38(6)
Br	0.14119(8)	-0.17076(8)	0.06757(4)	4.86(4)
P	0.16331(17)	0.08799(17)	-0.03033(8)	2.55(9)
C 1	0.3465 (6)	-0.0179 (6)	-0.0140 (3)	2.7 (3)
C 2	0.4354 (6)	-0.1674 (6)	-0.0451 (3)	2.9 (4)
C 3	0.5256 (7)	-0.2720 (6)	-0.0057 (3)	3.3 (4)
C 4	0.6121 (7)	-0.4100 (6)	-0.0317 (3)	4.0 (4)
C 5	0.6099 (7)	-0.4459 (6)	-0.0977 (3)	4.4 (4)
C 6	0.5208 (8)	-0.3434 (6)	-0.1367 (3)	4.2 (4)
C 7	0.4329 (7)	-0.2063 (6)	-0.1107 (3)	3.5 (4)
C 8	0.1000 (7)	0.2497 (6)	0.0220 (3)	3.3 (4)
C 9	0.0658 (7)	0.2289 (6)	0.1010 (3)	3.3 (4)
C10	-0.0610 (7)	0.2167 (7)	0.1334 (3)	4.2 (4)
C11	-0.0910 (8)	0.1957 (8)	0.2053 (4)	6.2 (5)
C12	0.0016 (9)	0.1889 (7)	0.2463 (3)	6.0 (6)
C13	0.1277 (8)	0.2007 (7)	0.2148 (4)	5.5 (5)
C14	0.1604 (7)	0.2201 (7)	0.1420 (3)	4.2 (4)
C15	0.1887 (6)	0.1562 (6)	-0.1210 (3)	3.1 (4)
C16	0.3009 (6)	0.2152 (6)	-0.1417 (3)	2.9 (4)
C17	0.4504 (6)	0.1272 (6)	-0.1635 (3)	3.0 (4)
C18	0.5507 (7)	0.1808 (7)	-0.1846 (3)	3.8 (4)
C19	0.5042 (7)	0.3270 (7)	-0.1852 (3)	4.1 (4)
C20	0.3584 (8)	0.4152 (6)	-0.1634 (3)	4.6 (5)
C21	0.2573 (7)	0.3605 (6)	-0.1422 (3)	3.9 (4)
Ni'	1	0	1/2	2.94(7)
Br'	1.07239(8)	0.16497(7)	0.44050(4)	4.73(4)
P'	0.76927(19)	0.17335(18)	0.51805(9)	3.13(10)
C 1'	0.7075 (7)	0.2556 (6)	0.4375 (3)	3.5 (4)
C 2'	0.6772 (7)	0.1686 (6)	0.3922 (3)	3.4 (4)
C 3'	0.5589 (7)	0.2385 (7)	0.3595 (3)	4.7 (4)
C 4'	0.5242 (8)	0.1637 (9)	0.3181 (4)	6.5 (5)
C 5'	0.6088 (8)	0.0195 (8)	0.3077 (3)	5.4 (5)
C 6'	0.7265 (8)	-0.0485 (7)	0.3380 (3)	4.8 (5)
C 7'	0.7609 (7)	0.0240 (6)	0.3807 (3)	3.7 (4)
C 8'	0.6228 (7)	0.1278 (6)	0.5678 (3)	3.6 (4)
C 9'	0.4683 (7)	0.2439 (7)	0.5803 (3)	4.1 (4)
C10'	0.4156 (8)	0.3328 (7)	0.6389 (3)	5.0 (5)
C11'	0.2703 (8)	0.4363 (7)	0.6528 (4)	6.3 (5)
C12'	0.1789 (8)	0.4504 (8)	0.6108 (5)	7.6 (6)
C13'	0.2315 (8)	0.3617 (8)	0.5533 (4)	6.3 (5)
C14'	0.3753 (7)	0.2580 (7)	0.5377 (3)	4.9 (5)
C15'	0.7415 (7)	0.3352 (6)	0.5597 (3)	3.5 (4)
C16'	0.7991 (6)	0.3253 (6)	0.6251 (3)	3.1 (4)
C17'	0.8021 (7)	0.4462 (7)	0.6465 (3)	4.1 (4)
C18'	0.8471 (8)	0.4454 (7)	0.7079 (4)	4.8 (5)
C19'	0.8897 (7)	0.3267 (7)	0.7488 (3)	4.7 (5)
C20'	0.8882 (7)	0.2062 (7)	0.7282 (3)	4.4 (4)
C21'	0.8419 (7)	0.2054 (6)	0.6673 (3)	4.0 (4)

Table A3.2: Bond lengths (Å) and angles (in degrees) for *trans*-$Br_2[(PhCH_2)_3P]_2Ni$.

Ni-Br	2.2928(12)	Ni'-Br'	2.3114(11)
Ni-Brb	2.2928(12)	Ni'-Br'b	2.3114(11)
Ni-P	2.2352(18)	Ni'-P'	2.2530(19)
Ni-Pb	2.2352(18)	Ni'-P'b	2.2530(19)
P-C1	1.827(6)	P'-C1'	1.836(6)
P-C8	1.840(6)	P'-C8'	1.847(7)
P-C15	1.856(6)	P'-C15'	1.833(6)
C1-C2	1.522(8)	C1'-C2'	1.507(9)
C2-C3	1.396(8)	C2'-C3'	1.399(9)
C2-C7	1.392(8)	C2'-C7'	1.384(8)
C3-C4	1.391(8)	C3'-C4'	1.388(10)
C4-C5	1.387(9)	C4'-C5'	1.379(11)
C5-C6	1.377(9)	C5'-C6'	1.364(10)
C6-C7	1.385(9)	C6'-C7'	1.386(9)
C8-C9	1.521(8)	C8'-C9'	1.509(9)
C9-C10	1.389(9)	C9'-C10'	1.391(9)
C9-C14	1.384(9)	C9'-C14'	1.378(9)
C10-C11	1.387(9)	C10'-C11'	1.399(10)
C11-C12	1.372(11)	C11'-C12'	1.355(12)
C12-C13	1.377(11)	C12'-C13'	1.373(12)
C13-C14	1.403(9)	C13'-C14'	1.390(10)
C15-C16	1.524(8)	C15'-C16'	1.514(8)
C16-C17	1.400(8)	C16'-C17'	1.394(9)
C16-C21	1.387(8)	C16'-C21'	1.396(8)
C17-C18	1.372(9)	C17'-C18'	1.387(9)
C18-C19	1.391(9)	C18'-C19'	1.372(10)
C19-C20	1.371(9)	C19'-C20'	1.376(10)
C20-C21	1.389(9)	C20'-C21'	1.389(9)
Br-Ni-Brb	179.9	Br'-Ni'-Br'b	180.0
Br-Ni-P	91.53(5)	Br'-Ni'-P'	87.37(6)
Br-Ni-Pb	88.47(5)	Br'-Ni'-P'b	92.63(6)
Brb-Ni-P	88.47(5)	Br'b-Ni'-P'	92.63(6)
Brb-Ni-Pb	91.53(5)	Br'b-Ni'-P'b	87.37(6)
P-Ni-Pb	180.0	P'-Ni'-P'b	180.0
Ni-P-C1	118.75(20)	Ni'-P'-C1'	114.62(21)
Ni-P-C8	109.41(21)	Ni'-P'-C8'	117.52(20)
Ni-P-C15	117.15(20)	Ni'-P'-C15'	114.69(21)
C1-P-C8	101.9(3)	C1'-P'-C8'	104.3(3)
C1-P-C15	106.1(3)	C1'-P'-C15'	97.3(3)
C8-P-C15	101.0(3)	C8'-P'-C15'	106.0(3)
P-C1-C2	118.9(4)	P'-C1'-C2'	117.2(4)
C1-C2-C3	118.1(5)	C1'-C2'-C3'	118.0(5)
C1-C2-C7	124.0(5)	C1'-C2'-C7'	123.6(5)
C3-C2-C7	117.8(5)	C3'-C2'-C7'	118.3(6)
C2-C3-C4	121.1(5)	C2'-C3'-C4'	120.7(6)
C3-C4-C5	120.2(6)	C3'-C4'-C5'	119.9(6)
C4-C5-C6	119.1(6)	C4'-C5'-C6'	119.7(6)
C5-C6-C7	121.0(6)	C5'-C6'-C7'	121.2(6)
C2-C7-C6	120.9(5)	C2'-C7'-C6'	120.2(6)
P-C8-C9	114.0(4)	P'-C8'-C9'	117.6(4)

C8-C9-C10	120.4(5)	C8'-C9'-C10'	119.2(6)
C8-C9-C14	120.9(6)	C8'-C9'-C14'	121.5(6)
C10-C9-C14	118.7(6)	C10'-C9'-C14'	119.2(6)
C9-C10-C11	120.3(6)	C9'-C10'-C11'	119.6(7)
C10-C11-C12	121.1(7)	C10'-C11'-C12'	121.2(7)
C11-C12-C13	119.1(6)	C11'-C12'-C13'	118.8(7)
C12-C13-C14	120.4(6)	C12'-C13'-C14'	121.6(7)
C9-C14-C13	120.4(6)	C9'-C14'-C13'	119.6(7)
P-C15-C16	117.0(4)	P'-C15'-C16'	120.1(4)
C15-C16-C17	122.2(5)	C15'-C16'-C17'	117.8(5)
C15-C16-C21	120.7(5)	C15'-C16'-C21'	124.1(5)
C17-C16-C21	117.1(5)	C17'-C16'-C21'	117.9(5)
C16-C17-C18	122.1(5)	C16'-C17'-C18'	120.3(6)
C17-C18-C19	119.8(6)	C17'-C18'-C19'	121.3(6)
C18-C19-C20	119.2(6)	C18'-C19'-C20'	119.1(6)
C19-C20-C21	120.8(6)	C19'-C20'-C21'	120.4(6)
C16-C21-C20	121.1(6)	C16'-C21'-C20'	120.9(6)

Table A3.3: Torsion angles (in degrees) for *trans*-$Br_2[(PhCH_2)_3P]_2Ni$.

Br-Ni-P-C(1)	14.6(2)	Br-Ni-P-C(8)	-101.7(3)
Br-Ni-P-C(15)	144.2(3)	Bra-Ni-P-C(1)	-165.4(3)
Bra-Ni-P-C(8)	78.3(2)	Bra-Ni-P-C(15)	-35.8(2)
Br-Ni-Pa-C(1)a	165.4(3)	Br-Ni-Pa-C(8)a	-78.3(2)
Br-Ni-Pa-C(15)a	35.8(2)	Bra-Ni-Pa-C(1)a	-14.6(2)
Bra-Ni-Pa-C(8)a	101.7(3)	Bra-Ni-Pa-C(15)a	-144.2(3)
Ni-P-C(1)-C(2)	56.2(4)	C(8)-P-C(1)-C(2)	176.4(6)
C(15)-P-C(1)-C(2)	-78.3(5)	Ni-P-C(8)-C(9)	54.7(4)
C(1)-P-C(8)-C(9)	-71.9(5)	C(15)-P-C(8)-C(9)	178.9(6)
Ni-P-C(15)-C(16)	-179.6(6)	C(1)-P-C(15)-C(16)	-44.3(4)
C(8)-P-C(15)-C(16)	61.7(5)	P-C(1)-C(2)-C(3)	-144.0(8)
P-C(1)-C(2)-C(7)	36.2(4)	C(1)-C(2)-C(3)-C(4)	-178.6(9)
C(7)-C(2)-C(3)-C(4)	1.2(5)	C(1)-C(2)-C(7)-C(6)	177.7(10)
C(3)-C(2)-C(7)-C(6)	-2.0(5)	C(2)-C(3)-C(4)-C(5)	0.0(5)
C(3)-C(4)-C(5)-C(6)	-0.2(5)	C(4)-C(5)-C(6)-C(7)	-0.7(5)
C(5)-C(6)-C(7)-C(2)	1.8(5)	P-C(8)-C(9)-C(10)	-75.1(6)
P-C(8)-C(9)-C(14)	104.2(7)	C(8)-C(9)-C(10)-C(11)	179.0(10)
C(14)-C(9)-C(10)-C(11)	-0.2(5)	C(8)-C(9)-C(14)-C(13)	-179.9(10)
C(10)-C(9)-C(14)-C(13)	-0.6(5)	C(9)-C(10)-C(11)-C(12)	1.2(5)
C(10)-C(11)-C(12)-C(13)	-1.2(5)	C(11)-C(12)-C(13)-C(14)	0.3(5)
C(12)-C(13)-C(14)-C(9)	0.6(5)	P-C(15)-C(16)-C(17)	81.8(6)
P-C(15)-C(16)-C(21)	-100.6(7)	C(15)-C(16)-C(17)-C(18)	177.6(9)
C(21)-C(16)-C(17)-C(18)	-0.1(5)	C(15)-C(16)-C(21)-C(20)	-177.7(10)
C(17)-C(16)-C(21)-C(20)	0.0(5)	C(16)-C(17)-C(18)-C(19)	-0.5(5)
C(17)-C(18)-C(19)-C(20)	1.2(5)	C(18)-C(19)-C(20)-C(21)	-1.3(5)
C(19)-C(20)-C(21)-C(16)	0.7(5)	Ni-Pa-C(1)a-C(2)a	-56.2(4)

Br'-Ni'-P'-C(1)'	57.0(2)	Br'-Ni'-P'-C(8)'	-179.9(3)
Br'-Ni'-P'-C(15)'	-54.4(2)	Br'b-Ni'-P'-C(1)'	-123.0(3)
Br'b-Ni'-P'-C(8)'	0.1(2)	Br'b-Ni'-P'-C(15)'	125.6(3)
Br'-Ni'-P'b-C(1)'b	123.0(3)	Br'-Ni'-P'b-C(8)'b	-0.1(2)
Br'-Ni'-P'b-C(15)'b	-125.6(3)	Br'b-Ni'-P'b-C(1)'b	-57.0(2)
Br'b-Ni'-P'b-C(8)'b	179.9(3)	Br'b-Ni'-P'b-C(15)'b	54.4(2)
Ni'-P'-C(1)'-C(2)'	72.3(4)	C(8)'-P'-C(1)'-C(2)'	-57.6(5)
C(15)'-P'-C(1)'-C(2)'	-166.2(7)	Ni'-P'-C(8)'-C(9)'	179.7(6)
C(1)'-P'-C(8)'-C(9)'	-52.2(5)	C(15)'-P'-C(8)'-C(9)'	50.0(5)
Ni'-P'-C(15)'-C(16)'	-48.8(4)	C(1)'-P'-C(15)'-C(16)'	-170.2(7)
C(8)'-P'-C(15)'-C(16)'	82.6(5)	P'-C(1)'-C(2)'-C(3)'	142.4(8)
P'-C(1)'-C(2)'-C(7)'	-38.3(4)	C(1)'-C(2)'-C(3)'-C(4)'	-179.0(10)
C(7)'-C(2)'-C(3)'-C(4)'	1.7(5)	C(1)'-C(2)'-C(7)'-C(6)'	-179.7(10)
C(3)'-C(2)'-C(7)'-C(6)'	-0.4(5)	C(2)'-C(3)'-C(4)'-C(5)'	-1.4(5)
C(3)'-C(4)'-C(5)'-C(6)'	-0.3(5)	C(4)'-C(5)'-C(6)'-C(7)'	1.6(5)
C(5)'-C(6)'-C(7)'-C(2)'	-1.3(5)	P'-C(8)'-C(9)'-C(10)'	-87.2(7)
P'-C(8)'-C(9)'-C(14)'	97.1(7)	C(8)'-C(9)'-C(10)'-C(11)'	-176.9(11)
C(14)'-C(9)'-C(10)'-C(11)'	-1.1(5)	C(8)'-C(9)'-C(14)'-C(13)'	176.6(11)
C(10)'-C(9)'-C(14)'-C(13)'	0.9(5)	C(9)'-C(10)'-C(11)'-C(12)'	1.0(5)
C(10)'-C(11)'-C(12)'-C(13)'	-0.6(5)	C(11)'-C(12)'-C(13)'-C(14)'	0.4(5)
C(12)'-C(13)'-C(14)'-C(9)'	-0.5(5)	P'-C(15)'-C(16)'-C(17)'	167.2(8)
P'-C(15)'-C(16)'-C(21)'	-16.4(4)	C(15)'-C(16)'-C(17)'-C(18)'	176.9(10)
C(21)'-C(16)'-C(17)'-C(18)'	0.2(5)	C(15)'-C(16)'-C(21)'-C(20)'	-177.4(10)
C(17)'-C(16)'-C(21)'-C(20)'	-1.0(5)	C(16)'-C(17)'-C(18)'-C(19)'	0.1(5)
C(17)'-C(18)'-C(19)'-C(20)'	0.3(5)	C(18)'-C(19)'-C(20)'-C(21)'	-1.0(5)
C(19)'-C(20)'-C(21)'-C(16)'	1.4(5)	Ni'-P'b-C(1)'b C(2)'b	-72.3(4)

Table A3.4: Anisotropic thermal factors (10^2 Å^2) for *trans*-$Br_2[(PhCH_2)_3P]_2Ni$.

	U_{11}	U_{22}	U_{33}	U_{12}	U_{13}	U_{23}
Ni	2.63(7)	3.20(7)	3.28(7)	-1.27(6)	-1.03(6)	0.66(5)
Br	3.99(4)	7.21(5)	7.39(5)	-2.72(4)	-2.57(4)	4.23(4)
P	3.00(10)	3.55(10)	3.25(10)	-1.48(9)	-0.82(8)	0.17(8)
C 1	3.1 (4)	4.1 (4)	3.1 (4)	-1.7 (3)	-0.8 (3)	0.0 (3)
C 2	3.4 (4)	4.7 (4)	3.6 (4)	-2.3 (3)	-1.0 (3)	0.6 (3)
C 3	4.5 (4)	4.2 (4)	4.5 (4)	-2.1 (4)	-1.6 (4)	-0.1 (3)
C 4	5.3 (5)	3.9 (4)	6.0 (5)	-2.0 (4)	-1.7 (4)	0.6 (4)
C 5	6.5 (5)	4.0 (4)	5.7 (5)	-2.0 (4)	-0.5 (4)	-0.8 (4)
C 6	8.0 (6)	4.4 (4)	4.4 (4)	-3.4 (4)	-1.1 (4)	-0.8 (3)
C 7	5.7 (5)	4.1 (4)	4.4 (4)	-2.7 (4)	-2.0 (4)	0.7 (3)
C 8	4.5 (4)	3.2 (4)	4.5 (4)	-1.6 (3)	-0.6 (4)	-0.1 (3)
C 9	4.4 (4)	2.6 (4)	4.6 (4)	-1.0 (3)	-0.4 (3)	-0.5 (3)
C10	4.6 (5)	5.5 (5)	5.0 (5)	-1.8 (4)	-0.2 (4)	-1.0 (4)
C11	7.8 (6)	7.4 (6)	5.9 (5)	-2.8 (5)	2.3 (5)	-1.6 (4)
C12	10.7 (7)	6.8 (6)	3.3 (5)	-2.7 (5)	0.0 (4)	-1.0 (4)
C13	8.2 (6)	6.2 (5)	5.1 (5)	-1.5 (5)	-2.1 (5)	-0.7 (4)
C14	5.1 (5)	5.3 (5)	5.6 (5)	-1.9 (4)	-1.3 (4)	-1.7 (4)
C15	3.9 (4)	4.6 (4)	3.7 (4)	-2.3 (4)	-1.0 (3)	1.1 (3)
C16	4.5 (4)	4.8 (4)	2.5 (4)	-2.5 (4)	-1.2 (3)	0.6 (3)
C17	4.7 (4)	3.9 (4)	3.1 (4)	-2.0 (4)	-0.7 (3)	-0.5 (3)
C18	4.1 (4)	5.9 (5)	4.5 (4)	-2.7 (4)	0.6 (4)	-1.1 (4)
C19	5.6 (5)	6.2 (5)	4.7 (5)	-3.7 (4)	0.0 (4)	-0.2 (4)
C20	7.6 (6)	3.6 (4)	6.0 (5)	-2.8 (4)	-0.1 (4)	0.4 (4)
C21	4.4 (4)	3.8 (4)	5.7 (5)	-1.8 (4)	-0.1 (4)	0.5 (4)
Ni'	4.08(8)	3.40(7)	3.56(7)	-1.41(6)	-1.24(6)	0.40(6)
Br'	5.52(5)	4.47(5)	7.51(6)	-2.09(4)	-1.36(4)	1.59(4)
P'	4.33(12)	3.54(11)	3.87(11)	-1.49(9)	-1.22(9)	0.26(9)
C 1'	4.7 (4)	4.1 (4)	4.3 (4)	-1.5 (4)	-1.7 (4)	0.4 (3)
C 2'	4.4 (4)	5.3 (5)	3.0 (4)	-2.2 (4)	-0.4 (3)	0.7 (3)
C 3'	6.0 (5)	6.1 (5)	5.4 (5)	-1.5 (4)	-2.5 (4)	-0.6 (4)
C 4'	7.0 (6)	11.3 (7)	6.6 (6)	-3.1 (5)	-4.2 (5)	1.0 (5)
C 5'	9.9 (7)	10.5 (6)	3.0 (4)	-6.6 (6)	-2.2 (4)	-0.1 (4)
C 6'	8.3 (6)	6.1 (5)	3.9 (4)	-3.4 (5)	-0.6 (4)	-0.5 (4)
C 7'	5.3 (5)	4.4 (4)	4.4 (4)	-1.8 (4)	-1.5 (4)	-0.1 (3)
C 8'	4.5 (4)	4.7 (4)	4.8 (4)	-2.0 (4)	-1.3 (4)	0.2 (3)
C 9'	4.5 (5)	6.1 (5)	4.6 (5)	-2.5 (4)	-0.6 (4)	1.0 (4)
C10'	6.5 (5)	6.7 (5)	5.0 (5)	-2.7 (4)	-0.7 (4)	0.8 (4)
C11'	7.2 (6)	5.5 (5)	8.9 (6)	-2.2 (5)	1.7 (5)	-0.4 (5)
C12'	5.9 (6)	6.4 (6)	13.7 (8)	-1.9 (5)	0.2 (6)	3.7 (5)
C13'	5.6 (5)	8.5 (6)	10.8 (7)	-3.9 (5)	-3.8 (5)	5.7 (5)
C14'	5.9 (5)	7.8 (6)	5.6 (5)	-3.8 (5)	-1.5 (4)	2.4 (4)
C15'	4.9 (5)	3.2 (4)	5.1 (5)	-1.6 (4)	-1.3 (4)	0.3 (3)
C16'	4.0 (4)	4.2 (4)	3.3 (4)	-1.7 (3)	-0.2 (3)	-0.5 (3)
C17'	5.5 (5)	4.9 (5)	5.0 (5)	-2.0 (4)	-1.5 (4)	-0.2 (4)
C18'	6.5 (5)	6.6 (5)	6.2 (5)	-3.5 (4)	-1.5 (4)	-1.4 (4)
C19'	5.6 (5)	7.4 (6)	4.6 (5)	-2.5 (4)	-1.2 (4)	-0.8 (4)
C20'	5.4 (5)	7.1 (5)	4.0 (4)	-2.3 (4)	-1.5 (4)	0.6 (4)
C21'	5.6 (5)	4.1 (4)	5.8 (5)	-2.4 (4)	-1.5 (4)	0.4 (4)

Structural Data for

trans-Dichlorobis(tribenzylphosphine)nickel(II)

trans-$Cl_2[(PhCH_2)_3P]_2Ni$

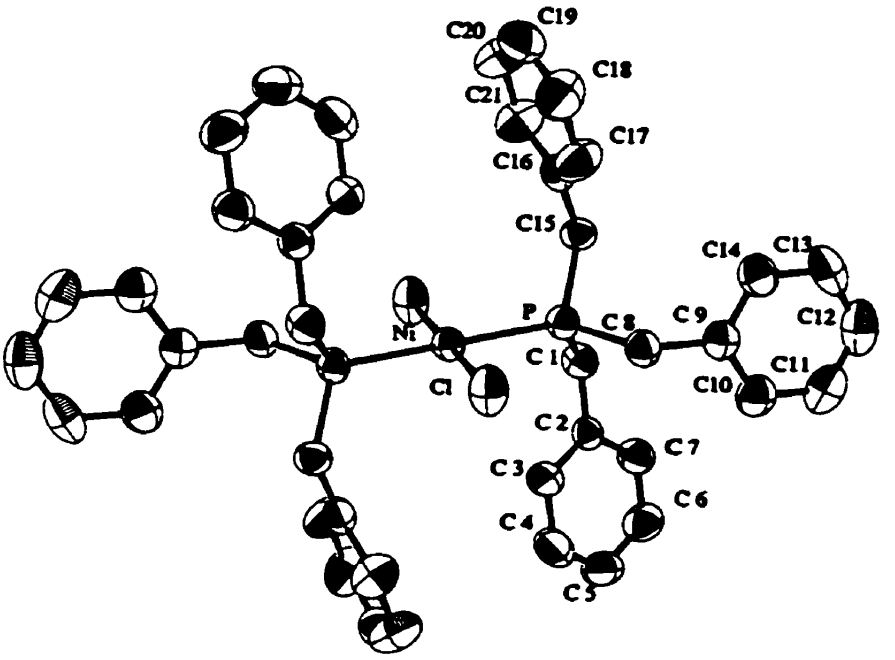

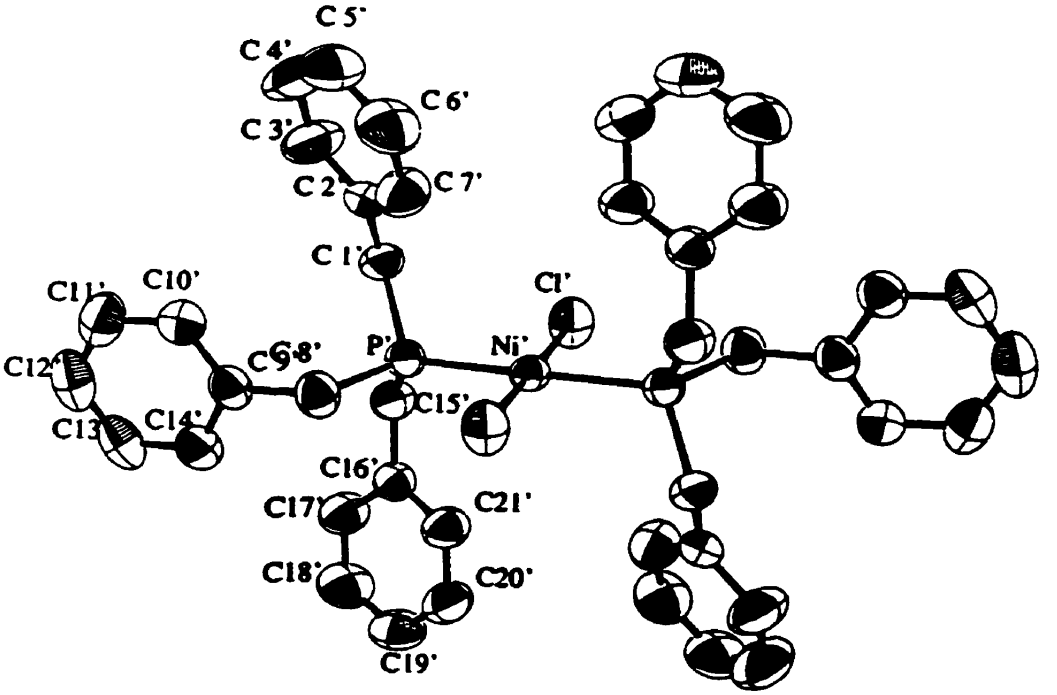

Crystallographic data for *trans*-$Cl_2[(PhCH_2)_3P]_2Ni$

Empirical Formula: C42 H42 Cl2 P2 Ni

Space group: Triclinic, P 1

Cell dimensions:

a = 9.505 (2)Å

b = 10.503 (2)Å

c = 18.876 (6)Å

α = 82.66 (2)°

β = 82.09 (2)°

γ = 88.15 (2)°

Volume = 1850.9 (8)Å^3

FW = 738.35

Z = 2

D_{calc} = 1.325 g / cm^3

F(000) = 774

Mo Kα radiation

λ = 0.70930 Å

Cell parameters from 25 reflections

2θ = 29 - 37°

μ = 0.78 mm^{-1}

T = 295 (2) °K

dark-red plate

0.50 → 0.33 → 0.17 mm

Data collection

Rigaku AFC –6S diffractometer

ω / 2θ scans

Absorption correction: *none*

T_{min} = 0, T_{max} = 1

5220 measured reflections

4866 independent reflections

3786 observed reflections [$I > 2.5\sigma(I)$]

R_{int} = 0.071

θ_{max} = 22.5°

h = -10 → 10

k = 0 → 11

l = -19 → 20

standard intensities remained constant throughout the course of collection

Average variation: 0.25 %

Structure was solved by direct methods followed by a difference map.

Refinement

Refinement on F	428 parameters
$R(F > 2.5\sigma F) = 0.037$	H atoms riding,
$wR(F) = 0.032$	C–H = 0.93 to 0.97 Å
GoF = 1.88	$(\Delta/\sigma) = 0.129$
90 atoms	$\Delta\rho_{max} = 0.19$ e/Å^3
3786 reflections	$\Delta\rho_{min} = -0.24$ e/Å^3

where

$R = \Sigma(Fo-Fc) / \Sigma Fo$

$wR = [\Sigma(w(Fo-Fc)^2) / \Sigma[w(Fo)^2]]^{1/2}$

$GoF = [\Sigma(w(Fo-Fc)^2) / (\text{No. of refins - No. of params.})]^{1/2}$

Table A3.5: Fractional atomic coordinates and equivalent isotropic displacement parameters (10^2 Å) for *trans*-$Cl_2[(PhCH_2)_3P]_2Ni$.

	x	y	z	U_{eq}
Ni	0	1/2	1/2	2.98(3)
Cl	0.10903(12)	0.45266(9)	0.39876(5)	4.93(5)
P	0.04020(11)	0.70890(9)	0.47000(5)	3.22(5)
C 1	-0.1214 (4)	0.8091 (3)	0.47315(19)	3.83(19)
C 2	-0.2180 (4)	0.8034 (3)	0.41691(18)	3.36(17)
C 3	-0.2495 (4)	0.6901 (3)	0.39266(20)	4.24(21)
C 4	-0.3455 (4)	0.6919 (4)	0.34327(21)	5.16(23)
C 5	-0.4106 (4)	0.8038 (4)	0.31816(20)	5.08(23)
C 6	-0.3782 (4)	0.9164 (4)	0.34212(21)	5.05(21)
C 7	-0.2835 (4)	0.9166 (3)	0.39124(20)	4.28(21)
C 8	0.1389 (4)	0.7571 (3)	0.38031(19)	3.88(19)
C 9	0.1555 (4)	0.8993 (3)	0.35642(19)	3.91(19)
C10	0.0695 (4)	0.9628 (4)	0.30893(20)	4.70(22)
C11	0.0873 (5)	1.0912 (4)	0.28406(22)	5.97(24)
C12	0.1911 (5)	1.1578 (4)	0.30712(22)	6.24(25)
C13	0.2772 (5)	1.0976 (4)	0.35406(23)	5.78(23)
C14	0.2610 (4)	0.9675 (4)	0.37875(20)	4.59(21)
C15	0.1235 (4)	0.7858 (3)	0.53548(18)	3.60(18)
C16	0.2509 (4)	0.7240 (3)	0.56584(18)	3.53(18)
C17	0.3717 (5)	0.6846 (4)	0.52549(21)	5.7 (3)
C18	0.4898 (4)	0.6369 (4)	0.55631(23)	6.18(25)
C19	0.4900 (5)	0.6284 (4)	0.62833(24)	5.88(25)
C20	0.3708 (5)	0.6667 (4)	0.67029(23)	6.6 (3)
C21	0.2532 (5)	0.7137 (4)	0.63899(21)	5.35(23)
Ni'	1	0	0	3.34(3)
Cl'	1.09961(12)	0.06704(11)	0.08398(5)	5.14(6)
P'	0.83168(11)	-0.08508(10)	0.08729(5)	3.67(5)
C 1'	0.8993 (4)	-0.1958 (3)	0.15862(19)	4.24(19)
C 2'	0.9565 (4)	-0.3260 (3)	0.14299(20)	4.23(19)
C 3'	0.9452 (5)	-0.4240 (4)	0.19973(25)	7.6 (3)
C 4'	1.0022 (6)	-0.5443 (4)	0.1890 (3)	9.7 (3)
C 5'	1.0682 (5)	-0.5685 (4)	0.1234 (3)	7.9 (3)
C 6'	1.0822 (5)	-0.4708 (4)	0.0680 (3)	7.1 (3)
C 7'	1.0256 (5)	-0.3508 (4)	0.07810(23)	6.00(25)
C 8'	0.6880 (4)	-0.1658 (4)	0.05622(20)	4.67(21)
C 9'	0.5707 (4)	-0.2248 (4)	0.11268(19)	4.25(21)
C10'	0.5797 (4)	-0.3506 (4)	0.14341(21)	5.05(21)
C11'	0.4657 (5)	-0.4063 (4)	0.18983(22)	6.02(24)
C12'	0.3439 (5)	-0.3358 (5)	0.20573(23)	6.6 (3)
C13'	0.3348 (4)	-0.2101 (4)	0.17647(23)	6.0 (3)
C14'	0.4467 (4)	-0.1539 (4)	0.12952(21)	4.99(23)

C15'	0.7457 (4)	0.0295 (4)	0.14594(19)	4.39(19)
C16'	0.6518 (4)	0.1334 (3)	0.11508(19)	4.06(19)
C17'	0.5266 (5)	0.1659 (4)	0.15470(22)	5.62(23)
C18'	0.4407 (5)	0.2650 (4)	0.12932(25)	6.8 (3)
C19'	0.4782 (5)	0.3338 (4)	0.06333(24)	6.2 (3)
C20'	0.6001 (5)	0.3010 (4)	0.02195(23)	6.11(25)
C21'	0.6862 (5)	0.2008 (4)	0.04747(22)	5.58(23)

Table A3.6: Bond lengths (Å) and angles (in degrees) for *trans*-$Cl_2[(PhCH_2)_3P]_2Ni$.

Ni-Cl	2.1534(12)	Ni'-Cl'	2.1556(12)
Ni-Cla	2.1534(12)	Ni'-Cl'b	2.1556(12)
Ni-P	2.2266(10)	Ni'-P'	2.2501(12)
Ni-Pa	2.2266(10)	Ni'-P'b	2.2501(12)
P-C(1)	1.832(4)	P'-C(1')	1.836(4)
P-C(8)	1.838(4)	P'-C(8')	1.830(4)
P-C(15)	1.836(4)	P'-C(15')	1.836(4)
C(1)-C(2)	1.503(5)	C(1')-C(2')	1.504(5)
C(2)-C(3)	1.385(5)	C(2')-C(3')	1.383(5)
C(2)-C(7)	1.387(5)	C(2')-C(7')	1.360(6)
C(3)-C(4)	1.389(6)	C(3')-C(4')	1.387(6)
C(4)-C(5)	1.372(6)	C(4')-C(5')	1.359(8)
C(5)-C(6)	1.377(6)	C(5')-C(6')	1.364(7)
C(6)-C(7)	1.378(6)	C(6')-C(7')	1.380(6)
C(8)-C(9)	1.511(5)	C(8')-C(9')	1.521(5)
C(9)-C(10)	1.389(5)	C(9')-C(10')	1.378(5)
C(9)-C(14)	1.391(5)	C(9')-C(14')	1.395(6)
C(10)-C(11)	1.378(5)	C(10')-C(11')	1.390(6)
C(11)-C(12)	1.375(7)	C(11')-C(12')	1.373(7)
C(12)-C(13)	1.370(7)	C(12')-C(13')	1.369(7)
C(13)-C(14)	1.393(5)	C(13')-C(14')	1.383(6)
C(15)-C(16)	1.504(5)	C(15')-C(16')	1.498(5)
C(16)-C(17)	1.371(5)	C(16')-C(17')	1.374(5)
C(16)-C(21)	1.374(5)	C(16')-C(21')	1.381(5)
C(17)-C(18)	1.385(6)	C(17')-C(18')	1.380(6)
C(18)-C(19)	1.351(6)	C(18')-C(19')	1.366(6)
C(19)-C(20)	1.370(7)	C(19')-C(20')	1.365(6)
C(20)-C(21)	1.383(6)	C(20')-C(21')	1.390(6)
Cl-Ni-Cla	180.0	Cl'-Ni'-Cl'b	180.0
Cl-Ni-P	92.71(4)	Cl'-Ni'-P'	87.19(5)
Cl-Ni-Pa	87.29(4)	Cl'-Ni'-P'b	92.81(5)
P-Ni-Pa	180.0	P'-Ni'-P'b	180.0
Ni-P-C(1)	113.94(12)	Ni'-P'-C(1')	114.63(13)
Ni-P-C(8)	116.52(12)	Ni'-P'-C(8')	115.41(13)
Ni-P-C(15)	115.05(12)	Ni'-P'-C(15')	114.55(13)
C(1)-P-C(8)	104.81(17)	C(1')-P'-C(8')	107.53(18)
C(1)-P-C(15)	96.64(16)	C(1')-P'-C(15')	96.65(17)
C(8)-P-C(15)	107.65(17)	C(8')-P'-C(15')	106.18(18)
P-C(1)-C(2)	118.86(24)	P'-C(1')-C(2')	119.9(3)
C(1)-C(2)-C(3)	123.0(3)	C(1')-C(2')-C(3')	117.4(3)
C(1)-C(2)-C(7)	117.9(3)	C(1')-C(2')-C(7')	124.1(3)
C(3)-C(2)-C(7)	119.0(3)	C(3')-C(2')-C(7')	118.4(4)
C(2)-C(3)-C(4)	119.6(3)	C(2')-C(3')-C(4')	119.6(4)
C(3)-C(4)-C(5)	121.4(3)	C(3')-C(4')-C(5')	121.3(4)
C(4)-C(5)-C(6)	118.8(4)	C(4')-C(5')-C(6')	118.9(4)
C(5)-C(6)-C(7)	120.7(4)	C(5')-C(6')-C(7')	120.2(4)
C(2)-C(7)-C(6)	120.6(3)	C(2')-C(7')-C(6')	121.5(4)
P-C(8)-C(9)	117.18(25)	P'-C(8')-C(9')	117.9(3)
C(8)-C(9)-C(10)	120.3(3)	C(8')-C(9')-C(10')	121.2(3)
C(8)-C(9)-C(14)	120.8(3)	C(8')-C(9')-C(14')	119.4(3)

C(10)-C(9)-C(14)	118.9(3)	C(10')-C(9')-C(14')	119.2(4)
C(9)-C(10)-C(11)	121.1(4)	C(9')-C(10')-C(11')	120.2(4)
C(10)-C(11)-C(12)	119.5(4)	C(10')-C(11')-C(12')	120.1(4)
C(11)-C(12)-C(13)	120.7(4)	C(11')-C(12')-C(13')	120.1(4)
C(12)-C(13)-C(14)	120.2(4)	C(12')-C(13')-C(14')	120.4(4)
C(9)-C(14)-C(13)	119.7(4)	C(9')-C(14')-C(13')	119.9(4)
P-C(15)-C(16)	120.07(24)	P'-C(15')-C(16')	118.9(3)
C(15)-C(16)-C(17)	124.9(3)	C(15')-C(16')-C(17')	120.0(3)
C(15)-C(16)-C(21)	118.7(3)	C(15')-C(16')-C(21')	122.6(3)
C(17)-C(16)-C(21)	116.2(4)	C(17')-C(16')-C(21')	117.3(3)
C(16)-C(17)-C(18)	122.2(4)	C(16')-C(17')-C(18')	121.6(4)
C(17)-C(18)-C(19)	120.5(4)	C(17')-C(18')-C(19')	120.5(4)
C(18)-C(19)-C(20)	118.8(4)	C(18')-C(19')-C(20')	119.1(4)
C(19)-C(20)-C(21)	120.2(4)	C(19')-C(20')-C(21')	120.3(4)
C(16)-C(21)-C(20)	122.0(4)	C(16')-C(21')-C(20')	121.1(4)

Table A3.7: Torsion angles (in degrees) for *trans*-$Cl_2[(Ph_2CH_2)_3P]_2Ni$.

Cl-Ni-P-C(1)	122.6(1)	Cl-Ni-P-C(8)	0.3(1)
Cl-Ni-P-C(15)	-127.1(1)	Cla-Ni-P-C(1)	-57.4(1)
Cla-Ni-P-C(8)	-179.7(1)	Cla-Ni-P-C(15)	52.9(1)
Cl-Ni-Pa-C(1)a	57.4 (1)	Cl-Ni-Pa-C(8)a	179.7(1)
Cl-Ni-Pa-C(15)a	-52.9(1)	P-Ni-Pa-C(1)a	-102.2(1)
P-Ni-Pa-C(8)a	20.0(1)	P-Ni-Pa-C(15)a	147.4(1)
Cla-Ni-Pa-C(1)a	-122.6(1)	Cla-Ni-Pa-C(8)a	-0.3(1)
Cla-Ni-Pa-C(15)a	127.1(1)	Ni-P-C(1)-C(2)	-70.9(2)
C(8)-P-C(1)-C(2)	57.7(2)	C(15)-P-C(1)-C(2)	167.9(3)
Ni-P-C(8)-C(9)	174.6(3)	C(1)-P-C(8)-C(9)	47.6(2)
C(15)-P-C(8)-C(9)	-54.5(2)	Ni-P-C(15)-C(16)	47.5(2)
C(1)-P-C(15)-C(16)	167.8(3)	C(8)-P-C(15)-C(16)	-84.3(3)
P-C(1)-C(2)-C(3)	40.6(2)	P-C(1)-C(2)-C(7)	-142.8(4)
C(1)-C(2)-C(3)-C(4)	176.7(5)	C(7)-C(2)-C(3)-C(4)	0.1(2)
C(1)-C(2)-C(7)-C(6)	-177.0(5)	C(3)-C(2)-C(7)-C(6)	-0.3(2)
C(2)-C(3)-C(4)-C(5)	-0.4(2)	C(3)-C(4)-C(5)-C(6)	0.8(2)
C(4)-C(5)-C(6)-C(7)	-0.9(3)	C(5)-C(6)-C(7)-C(2)	0.7(2)
P-C(8)-C(9)-C(10)	-101.2(4)	P-C(8)-C(9)-C(14)	81.9(3)
C(8)-C(9)-C(10)-C(11)	-177.1(5)	C(14)-C(9)-C(10)-C(11)	-0.1(3)
C(8)-C(9)-C(14)-C(13)	177.9(5)	C(10)-C(9)-C(14)-C(13)	0.9(3)
C(9)-C(10)-C(11)-C(12)	-0.6(3)	C(10)-C(11)-C(12)-C(13)	0.4(3)
C(11)-C(12)-C(13)-C(14)	0.3(3)	C(12)-C(13)-C(14)-C(9)	-1.0(3)
P-C(15)-C(16)-C(17)	52.0(3)	P-C(15)-C(16)-C(21)	-133.0(4)
C(15)-C(16)-C(17)-C(18)	175.1(5)	C(21)-C(16)-C(17)-C(18)	0.0(3)

C(15)-C(16)-C(21)-C(20)	-175.2(5)	C(17)-C(16)-C(21)-C(20)	0.2(3)
C(16)-C(17)-C(18)-C(19)	-0.4(3)	C(17)-C(18)-C(19)-C(20)	0.5(3)
C(18)-C(19)-C(20)-C(21)	-0.4(3)	C(19)-C(20)-C(21)-C(16)	0.0(3)
Cl'-Ni'-P'-C(1)'	-55.7(1)	Cl'-Ni'-P'-C(8)'	178.5(2)
Cl'-Ni'-P'-C(15)'	54.7(1)	Cl'b-Ni'-P'-C(1)'	124.3(1)
Cl'b-Ni'-P'-C(8)'	-1.5(1)	Cl'b-Ni'-P'-C(15)'	-125.3(1)
Cl'-Ni'-P'b-C (1)'b	-124.3(1)	Cl'-Ni'-P'b-C(8)'b	1.5(1)
Cl'-Ni'-P'b-C(15)'b	125.3(1)	Cl'b-Ni'-P'b-C(1)'b	55.7(1)
Cl'b-Ni'-P'b-C(8)'b	-178.5(2)	Cl'b-Ni'-P'b-C(15)'b	-54.7(1)
Ni'-P'-C(1)'-C(2)'	-71.5(2)	C(8)'-P'-C(1)'-C(2)'	58.3(3)
C(15)'-P'-C(1)'-C(2)'	167.6(4)	Ni'-P'-C(8)'-C(9)'	-179.8(3)
C(1)'-P'-C(8)'-C(9)'	50.9(2)	C(15)'-P'-C(8)'-C(9)'	-51.7(2)
Ni'-P'-C(15)'-C(16)'	68.3(2)	C(1)'-P'-C(15)'-C(16)'	-170.7(4)
C(8)'-P'-C(15)'-C(16)'	-60.3(3)	P'-C(1)'-C(2)'-C(3)'	-151.1(5)
P'-C(1)'-C(2)'-C(7)'	33.1(2)	C(1)'-C(2)'-C(3)'-C(4)'	-177.0(6)
C(7)'-C(2)'-C(3)'-C(4)'	-0.9(3)	C(1)'-C(2)'-C(7)'-C(6)'	176.6(6)
C(3)'-C(2)'-C(7)'-C(6)'	0.8(3)	C(2)'-C(3)'-C(4)'-C(5)'	-0.6(3)
C(3)'-C(4)'-C(5)'-C(6)'	2.2(3)	C(4)'-C(5)'-C(6)'-C(7)'	-2.2(3)
C(5)'-C(6)'-C(7)'-C(2)'	0.8(3)	P'-C(8)'-C(9)'-C(10)'	-90.8(4)
P'-C(8)'-C(9)'-C(14)'	94.3(4)	C(8)'-C(9)'-C(10)'-C(11)'	-174.0(5)
C(14)'-C(9)'-C(10)'-C(11)'	0.9(3)	C(8)'-C(9)'-C(14)'-C(13)'	174.8(5)
C(10)'-C(9)'-C(14)'-C(13)'	-0.1(3)	C(9)'-C(10)'-C(11)'-C(12)'	-0.6(3)
C(10)'-C(11)'-C(12)'-C(13)'	-0.6(3)	C(11)'-C(12)'-C(13)'-C(14)'	1.4(3)
C(12)'-C(13)'-C(14)'-C(9)'	-1.0(3)	P'-C(15)'-C(16)'-C(17)'	139.1(4)
P'-C(15)'-C(16)'-C(21)'	-41.6(2)	C(15)'-C(16)'-C(17)'-C(18)'	177.0(6)
C(21)'-C(16)'-C(17)'-C(18)'	-2.2(3)	C(15)'-C(16)'-C(21)'-C(20)'	-176.7(5)
C(17)'-C(16)'-C(21)'-C(20)'	2.5(3)	C(16)'-C(17)'-C(18)'-C(19)'	0.1(3)
C(17)'-C(18)'-C(19)'-C(20)'	1.8(3)	C(18)'-C(19)'-C(20)'-C(21)'	-1.5(3)
C(19)'-C(20)'-C(21)'-C(16)'	-0.7(3)	Ni'-P'b-C(1)'b C(2)'b	71.5(2)

Table A3.8: Anisotropic thermal factors (10^2 Å^2) for *trans*-$Cl_2[(Ph_2CH_2)_3P]_2Ni$.

	U_{11}	U_{22}	U_{33}	U_{12}	U_{13}	U_{23}
Ni	4.13(4)	3.15(4)	4.01(4)	0.07(3)	-0.19(3)	-0.71(3)
Cl	8.56(9)	4.25(6)	5.33(7)	-0.20(6)	1.74(6)	-1.22(5)
P	4.70(7)	3.30(6)	4.23(6)	0.00(5)	-0.33(5)	-0.74(5)
C 1	5.2 (3)	3.51(22)	6.0 (3)	0.97(20)	-0.94(22)	-1.10(19)
C 2	4.35(24)	4.06(22)	4.13(23)	-0.38(19)	0.14(19)	-0.39(18)
C 3	6.3 (3)	4.36(24)	5.4 (3)	-0.46(22)	-0.71(23)	-0.54(20)
C 4	6.7 (3)	6.6 (3)	6.5 (3)	-1.98(25)	-0.5 (3)	-1.45(23)
C 5	5.3 (3)	9.1 (3)	4.9 (3)	-1.2 (3)	-0.91(23)	-0.58(23)
C 6	5.6 (3)	7.0 (3)	6.4 (3)	0.73(24)	-1.36(24)	0.37(23)
C 7	5.5 (3)	4.42(24)	6.4 (3)	0.23(21)	-1.10(23)	-0.65(20)
C 8	5.9 (3)	4.19(23)	4.52(24)	-0.63(21)	-0.08(21)	-0.63(18)
C 9	5.7 (3)	4.36(23)	4.47(24)	-0.16(21)	0.73(21)	-0.85(19)
C10	7.0 (3)	5.6 (3)	4.9 (3)	0.15(24)	0.19(23)	-0.58(21)
C11	9.6 (4)	6.3 (3)	6.0 (3)	1.5 (3)	0.6 (3)	0.35(23)
C12	10.7 (4)	4.4 (3)	7.3 (3)	-0.1 (3)	3.1 (3)	-0.22(23)
C13	7.7 (3)	5.5 (3)	8.3 (3)	-2.4 (3)	2.0 (3)	-2.04(24)
C14	5.7 (3)	5.5 (3)	5.9 (3)	-0.63(22)	0.57(23)	-0.68(21)
C15	5.2 (3)	4.10(22)	4.50(24)	-0.21(20)	-0.59(21)	-1.02(18)
C16	4.9 (3)	3.80(22)	4.73(24)	-0.75(19)	-0.52(20)	-0.45(18)
C17	6.2 (3)	9.9 (4)	5.2 (3)	0.6 (3)	-0.44(24)	0.20(25)
C18	4.9 (3)	9.9 (4)	7.7 (3)	0.5 (3)	0.5 (3)	0.9 (3)
C19	5.8 (3)	6.9 (3)	9.7 (4)	-1.2 (3)	-2.5 (3)	0.3 (3)
C20	9.9 (4)	9.7 (4)	6.1 (3)	1.7 (3)	-3.2 (3)	-0.8 (3)
C21	7.2 (3)	7.4 (3)	5.6 (3)	1.3 (3)	-1.0 (3)	-0.86(23)
Ni'	4.31(4)	4.36(4)	3.90(4)	0.35(4)	-0.40(4)	-0.37(3)
Cl'	6.81(8)	8.23(8)	4.68(7)	-1.84(7)	-0.78(6)	-1.06(6)
P'	4.44(7)	4.87(6)	4.42(6)	0.29(5)	-0.25(5)	-0.16(5)
C 1'	5.6 (3)	5.4 (3)	4.9 (3)	0.39(22)	-0.73(22)	0.56(20)
C 2'	4.1 (3)	5.6 (3)	6.2 (3)	0.39(21)	-1.14(22)	0.23(21)
C 3'	10.4 (4)	7.7 (3)	8.6 (4)	3.3 (3)	1.9 (3)	2.7 (3)
C 4'	12.2 (5)	7.4 (4)	14.6 (5)	3.0 (4)	1.6 (4)	4.0 (3)
C 5'	8.9 (4)	6.6 (3)	14.6 (5)	2.4 (3)	-2.1 (4)	-1.1 (3)
C 6'	8.3 (4)	8.7 (4)	10.0 (4)	1.8 (3)	0.0 (3)	-3.0 (3)
C 7'	8.3 (4)	5.9 (3)	8.0 (3)	0.8 (3)	0.5 (3)	-1.06(25)
C 8'	5.3 (3)	7.4 (3)	4.9 (3)	-0.91(24)	-0.53(22)	-0.44(22)
C 9'	4.6 (3)	6.9 (3)	4.7 (3)	-0.62(22)	-0.76(21)	-0.85(21)
C10'	6.1 (3)	6.5 (3)	6.6 (3)	-0.05(24)	-1.04(25)	-0.35(23)
C11'	8.8 (4)	7.6 (3)	6.4 (3)	-2.6 (3)	-1.2 (3)	0.30(25)
C12'	6.4 (3)	12.6 (4)	6.0 (3)	-3.7 (3)	0.2 (3)	-1.7 (3)
C13'	4.6 (3)	10.7 (4)	8.0 (3)	-0.5 (3)	-0.1 (3)	-2.7 (3)
C14'	5.6 (3)	7.2 (3)	6.4 (3)	-0.18(24)	-1.33(24)	-0.97(23)
C15'	5.8 (3)	5.8 (3)	4.7 (3)	0.98(22)	0.49(22)	-0.43(20)
C16'	5.0 (3)	5.00(25)	5.3 (3)	0.61(21)	-0.22(21)	-0.99(20)
C17'	7.1 (3)	6.8 (3)	6.7 (3)	1.9 (3)	0.7 (3)	-0.17(24)
C18'	7.5 (4)	8.7 (4)	9.1 (4)	3.1 (3)	0.4 (3)	-1.9 (3)
C19'	8.5 (4)	6.0 (3)	9.6 (4)	2.4 (3)	-2.5 (3)	-1.4 (3)
C20'	8.7 (4)	6.3 (3)	7.9 (3)	0.6 (3)	-1.4 (3)	0.67(25)
C21'	6.6 (3)	7.2 (3)	6.5 (3)	1.8 (3)	0.4 (3)	0.59(24)